3D PRINTABLE SHAPE MORPHING ARCHITECTURES VIA PROGRAMMABLE STRESS: ACTIVE ABSORBENTS, MECHANICAL ACTUATORS, HIERARCHICAL STRUCTURES, AND MICROCHANNELS WITH EMBEDDED CRYSTAL MORPHOLOGIES

A Dissertation

by

DUANDUAN HAN

Submitted to the Office of Graduate and Professional Studies of

Texas A&M University

in partial fulfillment of the requirements for the degree of

DOCTOR OF PHILOSOPHY

Chair of Committee, Victor Ugaz
Committee Members, Arul Jayaraman
Jodie Lutkenhaus
Zivko Nikolov
Head of Department, Arul Jayaraman

May 2020

Major Subject: Chemical Engineering

ABSTRACT

3D printing can manufacture polymer components with customized shapes and intricate structures easily without pre-made molds. When fabricated with responsive materials, smart 3D printed components experience shape morphing over time and display functionalities in response to external stimuli. However, due to an unfavorable combination of inaccessible printing systems and specially composited material mixtures employed in current studies, these smart components have yet to create sizable impact outside academic laboratories. This need was addressed by producing smart components using a commercially available fused deposition modeling printer and a single material, poly (lactic acid) (PLA), a biodegradable polyester with inherent shape memory properties, promising programmable and repeatable shape change in response to elevated temperatures. Combining the capillary force imposed by the microscale porous structures and the oleophilic surface properties of PLA produced rigid and reusable oil absorbents. Mathematical models were developed for the absorption behaviors as a guide to choose porous network architectures based on oil properties to maximize oil absorption efficiency. The commercialization potential of the absorbents was also explored.

Further examination of the 3D printed components revealed that thin samples warped when exposed to heat due to the release of printing generated-residual stresses. The correlation between warpage behaviors and printing parameters were assessed and implemented to develop a library of elements with programmable shape morphing features. By arranging these elements spatially, 2D structures capable of morphing into complex 3D topologies were produced. This was demonstrated by printing a sheet that morphed into a bio-inspired blooming lily displaying hierarchical structures.

3D printing facilitates the ease of producing customized parts, as demonstrated by development of a novel toolbox to manufacture microchannel devices in a lithography-free manner. In addition to enlisting 3D printing to produce customized assembly-ready channel covers, the advantage of enzymatic etching, thermal annealing, tape masking, and vacuum-aided bonding were also explored. The final product was a completely biodegradable assembled microchannel device with potential to perform bioanalysis. Furthermore, these research topics were utilized as a vehicle to engage undergraduate students in research activities and inspired a laboratory course providing hands-on experience for a conventional theory-only fluid mechanics course.

DEDICATION

To my parents who always believe in me.

ACKNOWLEDGEMENTS

I would like to show great appreciation to my advisor, Dr. Victor Ugaz for his invaluable supervision and support throughout my graduate program. I appreciate that he provided the freedom to try out new research projects in the scientific domains and opportunities to explore different aspects of professional domains (teaching, mentoring, and entrepreneurship). I also in debt to him for being a patient and influential mentor who helped me building skills not only in research, but also in writing and presenting.

I would like to express my sincere gratitude to my committee members, Professor Arul Jayaraman, Professor Jodie Lutkenhaus, and Professor Zivko Nikolov for their mentoring and guidance on the research.

I want to thank my seniors Dr. Jen-Huang Huang, who helped me establish my approach in research during early PhD years, and Dr. Aashish Priye, who helped me explore my view in research. I would also like to thank my group members, colleagues, and friends for their inspiration.

Finally, I would like to thank my parents for always believing in me. I could not have complete this work without their continuous encouragement and support.

NOMENCLATURE

3D	Three Dimension
AM	Additive Manufacturing
CAD	Computer Aided Design
FFF	Free Form Fabrication
FDM	Fused Deposition Modeling
PB	Prussian Blue
PLA	Poly (lactic acid)
PK	Proteinase K
PW	Prussian White
RP	Rapid prototyping
SEM	Scanning Electron Microscopy

CONTRIBUTORS AND FUNDING SOURCES

Contributors

This work was supervised by a dissertation committee consisting of Professor Victor Ugaz (committee chair), Professor Arul Jayaraman, and Professor Jodie Lutkenhaus of Department of Chemical Engineering, and Professor Zivko Nikolov of Department of Biological & Agricultural Engineering

All work conducted for the dissertation was completed by the student independently.

Funding Sources

Graduate study and this dissertation work were supported in part by National Science Foundation under Grant Number 1106005 and 1740388.

TABLE OF CONTENTS

LIST OF FIGURES

LIST OF TABLES

Table Page

CHAPTER I

INTRODUCTION AND LITERATURE REVIEW

1.1 Overview

3D printing, also known as additive manufacturing or rapid prototyping, has shown great potential to produce polymer-based components with intricate structures and customized shapes. Coupled with the spatial deposition of materials following predesigned specific patterns, these components display active and passive functionalities in response to external stimuli (e.g., light, magnetic field, moisture, and heat) and have great potential in various fields (e.g., drug delivery, medical implants, and soft robotics). However, customized printing systems (e.g., direct ink writing with external magnetic fields [1]) and specially composited materials (e.g., hydrogels embedded with metal nanoparticles [2]) present challenges to expand their applications outside academic laboratories.

My first research goal was to pave the way for accessible 3D printing of smart responsive components with customized intricate structures to become commonplace. My work utilized commercially available fused deposition modeling (FDM) printers and the inherent shape memory properties of poly (lactic acid) (PLA), a biodegradable commodity polymer from renewable sources. These PLA components experienced programmable shape morphing from two dimensions (2D) to three dimensions (3D) in response to elevated temperatures (Chapter IV). They functioned as either active rigid reusable oil absorbents to clean up oil spills (Chapter II) or actuators to perform mechanic tasks (Chapter III). A second project was to leverage 3D printing to facilitate a novel lithography-free toolbox for microchannel fabrication that overcame the high instruments and personnel cost barriers of the current governing approach that employed soft-

lithography (Chapter V). Additionally, I complemented my research experience with entrepreneurial (Chapter VI) and teaching activities (Chapter VII). I explored the commercialization potential of 3D printed reusable oil absorbents and took initiative to develop innovative laboratory sessions to supplement conventional fluid mechanics theory courses.

1.2 Oil absorbents

In 2010, the Deepwater Horizon oil spill cost 11 lives and released more than four million barrels of oil into the Gulf of Mexico.[3] It was considered the largest marine oil spill in petroleum industry history and endangered livelihoods and precious habitats. The overall financial cost to BP, the environment, and the US gulf coast economy was estimated to be $36.9 billion.[4] Within the first 10 weeks of the spill, 400 burnings were completed,[5] 1.5 million gallons of dispersants were spread, 27 million gallons of oily water were recovered by skimmers, and more than 700 kilometers of booms were deployed.[6]

These efforts included the four major cleanup solutions: in-situ burning, dispersants, skimmers, and absorbents (Table 1.1). Unfortunately, none of these approaches can solve an oil spill problem thoroughly. In-situ burning is burning spilled oil in the sea. This process transfers water pollution to atmosphere pollution [7] and cannot be applied to the heavy oil with a low vapor pressure. Dispersants (dispersing agents) break down oil into small droplets and remove oil from water surface. Nevertheless, dispersants inevitably introduce additional chemical products into water, which are harmful to humans, marine animals, and bacteria.[8, 9] Dispersants suppress the growth of natural oil-degrading bacteria [10] and reduce the self-cleaning abilities of the sea. Skimmers are mechanical

devices to recover spilled oil from the water surfaces without adding chemical hazards. However, they have a limited collecting and recovery efficiency due to the poor adherence of oil to the recovery surfaces. In addition, skimmers do not function effectively in rough and choppy water and other geographically challenging areas, such as sea surfaces covered by ice.[11] To address these drawbacks, oleophilic and hydrophobic absorbents have been studied as an environmentally-friendly and easily-adaptable approach to clean up oil spills. Common materials employed as absorbents are categorized into three groups: natural organic materials, natural inorganic materials, and synthetic materials (Table 1.2).

Table 1.1 Performance and applications of different cleanup approaches.

Approach	Working mechanism	Advantages	Disadvantages
In-situ burning	Ignites spilled oil by combustion of hydrocarbon vapors	Can quickly remove large amount of oil, produces no oily wastes	Consumes oil, transfers pollution from water to atmosphere as smoke and soot, not suitable for heavy oil with a low vapor pressure or thin oil layers (< 2mm) that could not sustain combustion
Dispersants	Use chemical reagents to break oil down into small droplets	Quick to deploy, can be used in strong currents, inhibit formation of emulsions	Introduce additional chemicals to water, not suitable for oil with a high viscosity
Skimmers	Physically remove oil from the surface of water with mechanical devices	Do not transfer pollution to air, do not add chemicals to the sea, produce no oily wastes	Not practical for high current situations, can be clogged by debris and ice
Absorbents	Absorption of oil into absorbents	Some absorbents are reusable, available in different shapes and sizes	Soft absorbents do not retain oil when handled, labor-intensive to deploy and collect after use, generate large amount of oily wastes

Table 1.2 Characteristics of different absorbent materials.

Material source	Advantages	Disadvantages
Nature organic materials	Degradable, suitable for immobilizing oil in areas rich with vegetation and wildlife, cost-effective	Material properties vary by batches, loose materials are hard to collect after use, may absorb water and sink
Nature inorganic materials	Cost-effective	Material properties vary by batches, may sink and hard to collect after use
Synthetic materials	High absorption capacity, available in different shapes and sizes	Non-degradable, soft, absorbed oil may be squeezed out during handling

Natural-sourced material absorbents are cost-effective and do not generate extra waste to the environment (Table 1.3). However, the quality tends to vary from batch to batch. The inconsistent quality affects the absorption performance greatly and makes it difficult to estimate the accurate amount of material needed for a spill. For example, the absorption capacity of human hairs varied from two to five grams of oil per gram of hair depending on the origin of the hair. [6] Some natural material absorbents absorb water and sink, so the amount of oil absorbed drops, and it is difficult to collect used absorbents after they sink. Multiple approaches were reported to enhance the oil absorption performance: increase the oleophilicity and decrease the hydrophilicity of natural material absorbents or increase the porosity of materials. [12-14] Unfortunately, these additional treatments all elevate the cost of absorbents and produce extra chemical wastes, which defy the advantages of using natural material absorbents in the first place. Therefore, synthetic materials have become mainstream absorbents because of their outstanding oil absorption capacity and uniformity between batches.

Table 1.3 Absorption performance of natural absorbents.

Material	Absorption capacity (g oil/g absorbent)	Reusability	Ref.
Loose human hair	Crude oil: 2.06 - 5.07, depending on origin of hair	3 cycles Extraction with solvent (n-hexane)	[6]
Cellulose fiber (freeze drying sponge)	Pump oil: 137	30 cycles Mechanical squeezing to desorb oil Porosity: 99.84%	[14]
Loose kapok	Diesel: 36.7	15 cycles Vacuum to desorb oil	[15]
Grounded walnut shell	Mineral oil: 0.3	Not reported	[16]
Untreated fly ash (aluminosilicate composition)	Paraffinic process oil: 0.14	Not reported	[12]
Untreated sawdust	Diesel: 5 Crude oil: 6.5 Gasoline: 3	Not reported	[13]

Currently available synthetic absorbents (Table 1.4) have different shapes (e.g., booms, socks, and pads) and are usually soft. They require intensive human power to deploy and collect after use, and then generate a large amount of material waste. Consequently they are mostly applied to large-scale spills to achieve economic efficiency and rarely used in small-scale spills (less than one gallon). These gallon-size spills happen on a daily basis due to recreational and commercial boat operations including fueling and bilge cleaning. For example, in Puget Sound, Washington, reported spills from recreational vessels added up to almost 6000 gallons in four years, and two-thirds of them were less than one gallon. [17] These small-scale spills add up to 150 million gallons, which are 20% of all oil spills worldwide, whereas large scale spills that attract worldwide attention only contribute 5%.[18] Sadly, these small-scale spills are largely ignored by responsible parties and

cleanup teams due to the inefficiency of deploying the current-generation of absorbent materials.

Another drawback of commercially-available absorbents is their soft texture. These absorbents deform under external mechanical forces. When collecting the used absorbents from water with a net, forces squeeze out absorbed oil and cause new oil contamination. Additionally, reusability of these absorbents and collecting of absorbed oil can only be achieved by squeezing out the absorbed oil to a designated collecting site. This dilemma identified a blank in the current absorbent varieties: a rigid absorbent that can sequester absorbed oil to ensure easy handling, and then release absorbed oil when specific environmental conditions are met: in response to external stimuli.

Table 1.4 Absorption performance of synthetic absorbents.

Material	Fabrication approach	Absorption capacity (g/g)	Reusability	Note	Ref.
Melamine	Sponge: dip-coating with graphene	Pump oil: 95	Not reusable: capacity drops more than 20% Mechanical squeezing to desorb oil		[19]
Melamine	Sponge: silanization	Mineral oil: 100.7 Diesel: 93.6	1,000 cycles Mechanical squeezing to desorb oil	Density: 8.10 mg/cm^3 Porosity: 99.48% Size: 2.5 x 2.5 x 2.5 cm^3	[20]
Polyurethane	Sponge: surface coated with metal nanoparticles	Lubrication oil: 13	Not reusable: capacity drops more than 20% Mechanical squeezing to desorb oil		[21]
Polyurethane	Sponge: surface coated with reduced graphene oxide	Diesel: 90	50 cycles Mechanical squeezing to desorb oil	Density: 8.80 mg/cm^3 Porosity: 99.29% Size: 2.5 x 2.5 x 2.5 cm^3	[22]
Polyurethane	Sponge: surface treated with silane coupling agents	Crude oil: 30 Gasoline: 39 Silicone oil: 27	200 cycles Mechanical squeezing to desorb oil	Sustain a large strain deformation (80%) under a relatively low stress (2 kPa)	[23]
Polydimethylsiloxane	Sponge: sugar-templated	Silicone oil: 4 Motor oil: 4	20 cycles Mechanical squeezing to desorb oil	Density: 0.18 - 0.75 g/cm^3 Elastic modulus: 0.00002 GPa	[24]

Table 1.4 Continued.

	Fabrication approach	**Absorption capacity (g/g)**	**Reusability**	**Note**	**Ref.**
Polydimethylsiloxane	Sponge: sugar-templated in p-xylene solution	Diesel: 12 Silicone oil: 8 Gasoline: 22	20 cycles Mechanical squeezing to desorb oil,	Density: 0.1 - 0.42 g/cm^3 Porosity: 43 - 83% Size: 1 x 1 x 1 cm^3	[25]
Poly (lactic acid)	Sponge: freeze-drying and surface modification with reduced graphene oxide	Diesel: 44 Mineral oil: 48	3 cycles Centrifugal force	Porosity: 98.27%	[26]
Graphene	Aerogel: use melamine formaldehyde microspheres as spacers to create porous structure	Diesel: 220	10 cycles Distillation to desorb oil	Density: 5 mg/cm^3 Porosity: 99.7%	[27]
Polyurethane	Sponge: sequential infiltration	Crude oil: 90 Silicone oil: 65	Reusability not reported Mechanical squeezing to desorb oil	Density: 22.5 mg/cm^3 Porosity: 98%	[28]
Butylacrylate, methyl-meth-acrylate, Nitraria seed	Resins made by grafting copolymerization with synthetic polymers	Diesel: 22 Gasoline: 21	6 cycles Immersion in solvent (butane)		[29]

1.3 Responsive materials

Responsive materials (Table 1.5, 1.6, 1.7), such as shape memory polymers,[30] [31] swellable hydrogels,[32, 33] and shape memory alloys,[34, 35] change between programed shapes when exposed to external stimuli including temperature,[36] light,[37] magnetic field,[38] and pneumatic actuation.[39] Their applications can be found in diverse areas, including biomedical devices,[40] flexible electronics,[41] and soft robotics.[42]

Living organisms have inspired responsive materials. For example, a composition material inspired by plant cells featured a soft acrylamide matrix embedded with stiff cellulose fibrils and displayed anisotropic swelling. Programmed alignment of this material via direct ink writing (DIW) generated complex flower morphologies (Fig. 1.1a).[32] The fibrils experienced shear-induced alignment during fabrication and consequently acquired anisotropic stiffness. Variance in swelling between two layers with different material alignments led to curvature. A resulting mathematical models quantified the variance and guided the design and verification of a library of simple curved surfaces, which were combined to generate a family of functional folding flower architectures, including orchid and calla lily.

Another bioinspired programmable material mimicked the instantaneous extension or retraction of conical papilla in *Octopus rubescens* for camouflage purposes (Fig. 1.1b).[39] The materials, fiber mesh (local connective structure) and silicone elastomer (stretchable connected component), were patterned in concentric circles through casting and laser cutting. Upon inflation, the elastomer inflated into a dome shape, and the mesh limited the circumferential stretch. By controlling the width and arrangement order of the mesh and

elastomer sections, the flat surfaces displayed non-symmetric and hierarchical shape morphing, which led to successful replication of natural shapes of a cactus plant.

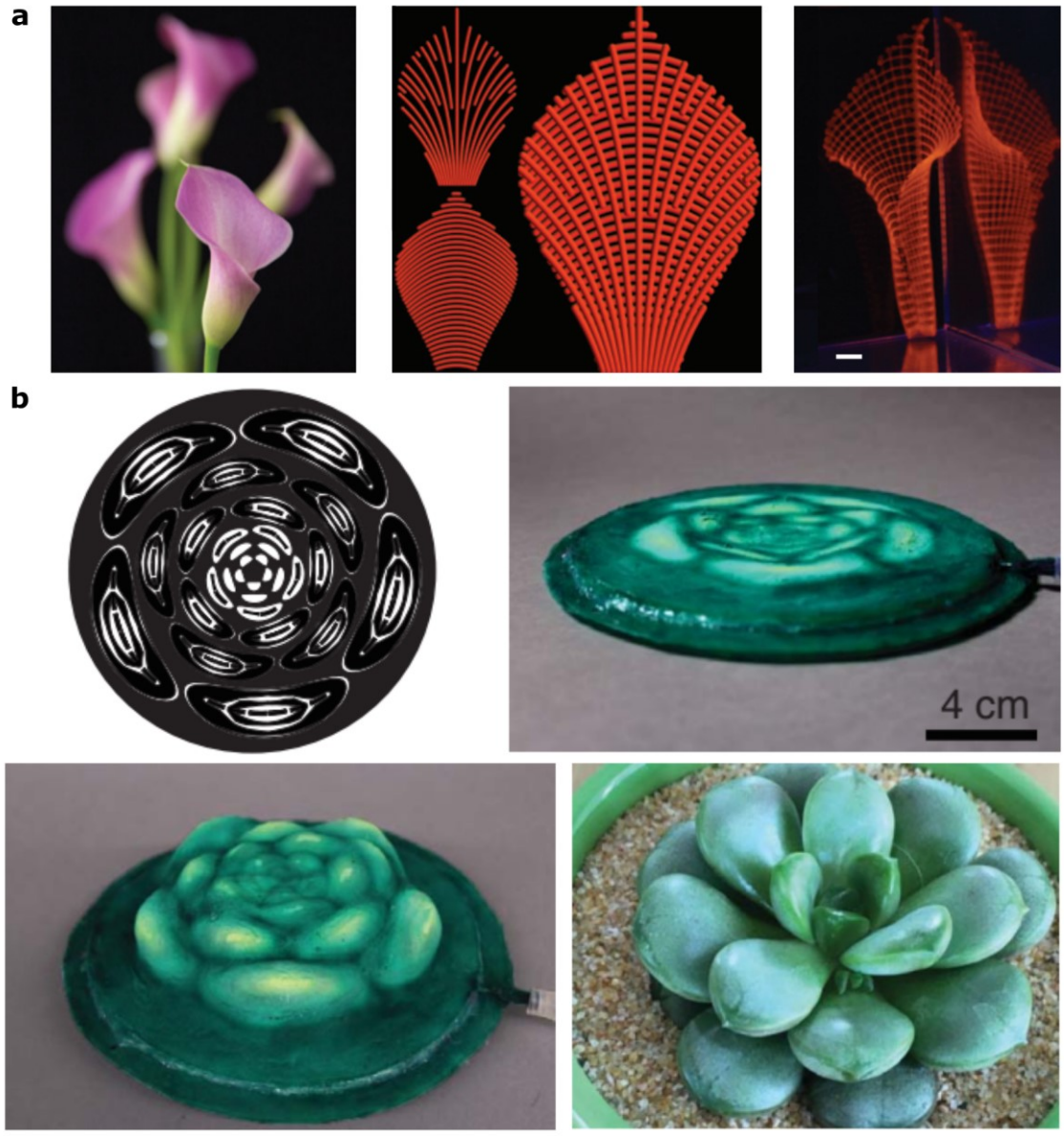

Fig. 1.1 Responsive material shape morphing process activated by hydration and inflation. (a) A complex flower morphology created through swelling of a hydrogel. From left to right: photo of a calla lily, printing path, and after-swelling morphology. Scale bar, 5 mm. Reprinted with permission.[32] **(b)** A circular shaped membrane inflated to programmed biomimetic shapes. From top left in clockwise order: mesh design, deflated surface, a digital photo of a cactus plant, and inflated surface mimicking the cactus. Reprinted with permission.[39]

Apart from mimicking a sophisticated shape, responsive materials can perform basic mechanical functions. Palleau and coworkers developed shape memory hydrogels that memorized the curvature generated during fabrication and can be tuned to a second curvature upon immersion in solvent (Fig. 1.2a).[1] The hydrogel was produced via ionoprinting, which used a copper anode to imprint cupric ions. The ions were distributed on hydrogel surfaces replicating the patterns of the anode. Ethanol induced swelling and contraction, and then offered a rapid and uniform bending of the hydrogel, mimicking the function of tweezers. A following rehydration step in water made the tweezers return to the original flat shape. Consequently, the tweezers picked up a small object in ethanol, and then released it in water.

Tuning the external stimuli enables responsive materials to perform more sophisticated motions (e.g., approaching a target at a desired speed). Kim and colleagues reported silicone rubber-based soft robots that can move and change shapes under the influence of controlled magnetic fields (Fig. 1.2b).[38] DIW produced soft robots with composite silicone rubbers containing non-magnetized NdFeB alloy particles. An external magnetic field was applied at the nozzle and controlled the orientation of NdFeB particles while printing, and thus magnetic polarities-dependent ferromagnetic domains were encoded in finished components. A second external magnetic field induced torques in ferromagnetic domains. Consequently, the 2D components buckled and formed 3D morphologies under stresses built up in these domains. By rotating the external magnetic field, a 2D six-branch shape formed a roll and carried a medicine tablet with it, and then rolled to a second location and released its cargo on-demand.

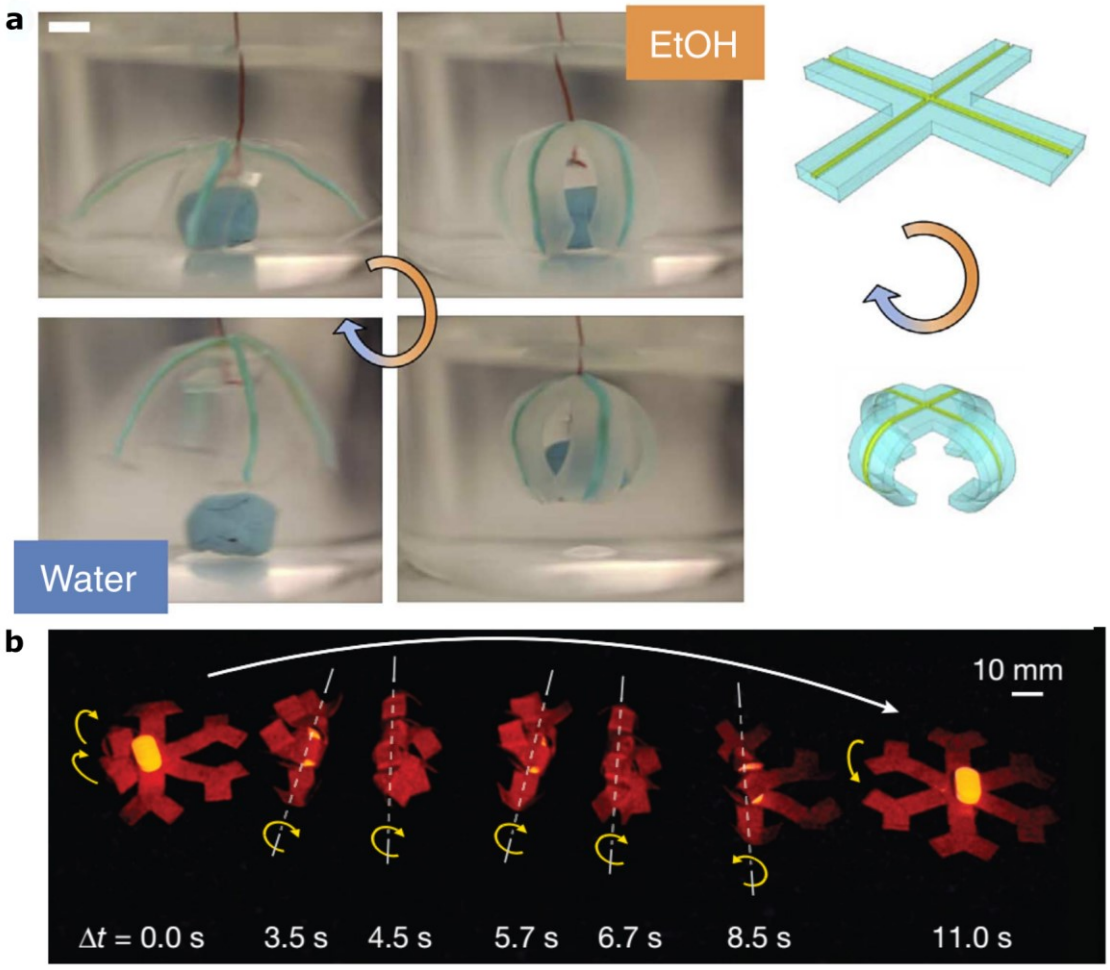

Fig. 1.2 Responsive material shape morphing process activated by ion concentration gradient and magnetic field. (a) An X-shaped gel with two ionoprinted perpendicular lines along each side of its appendages functioned as soft tweezers. It folded in ethanol solution and subsequently picked up a cube of PDMS weighted one gram and released it in water. Reprinted with permission.[1] **(b)** Under a rotating magnetic field, a six-branch 2D structure formed a roll and carried a small object. Reprinted with permission.[38]

Despite these successes, these designer smart materials have not been made available beyond academic settings for wide adaption due to the need for customized manufacturing tools, complex fabrication procedures, and specific compositions of materials. A key challenge continues to be a lack of an accessible fabrication platform where smart components can be made with commodity materials and commercially-available machines.

Table 1.5 Examples of elastomer smart materials.

Materials	Manufacturing approach	Activation method	Activation time	Overall part size	Smallest feature size	Ref.
Liquid crystal elastomer: composition 1: urethane acrylate oligomer, exo-1,7,7-trimethylbicyclo[2.2.1]hept-2-yl acrylate, a methacrylate oligomer, polyurethane resin; composition 2: isobornyl acrylate, urethane acrylate; silver nanoparticle ink	Multi-material inkjet printing, direct ink writing, UV curing, thermal curing	Temperature (Joule heating produced by the embedded conductive wires)	3 minutes	0.7 - 48 mm	0.5 mm	[43]
Liquid crystal elastomer: 1,4-bis-[4-(6-acryloyloxhexyloxy) benzoyloxy]-2-methylbenzene	Customized high operating temperature direct ink writing, UV curing	Temperature	1 minute	0.25 - 25 mm	100 μm	[44]
Liquid crystal elastomer: 1,4-bis-[4-(6-acryloyloxhexyloxy) benzoyloxy]-2-methylbenzene	Direct ink writing, UV curing	Temperature	1 minute	5 - 30 mm	Not reported	[45]

Table 1.5 Continued.

Materials	Manufacturing approach	Activation method	Activation time	Overall part size	Smallest feature size	Ref.
Liquid crystal elastomer: 1,4-bis-[4-(6-acryloyloxhexyloxy) benzoyloxy]-2-methylbenzene, 1,4-bis-[4-(3-acryloyloxhexyloxy) benzoyloxy]-2-methylbenzene	Point-by-point optical patterning	Temperature	Not reported	1 - 3 cm	Not reported	[46]
Silicone elastomer, non-woven mesh	Mold casting, laser cutting	Inflation	5 s	7.5 - 20 cm	5 mm	[39]
Silicone elastomer, magnetizable NdFeB microparticle	Magnetic field assisted direct ink writing, curing, removal of support materials	Magnetic field	1 - 10 s	1 - 10 cm	1 cm	[38]
Silicone elastomer, NdFeB microparticles (5 μm), aluminum powder	Mold casting, laser cutting	Magnetic field	5 s	5 - 10 mm	Not reported	[47]

Table 1.6 Examples of hydrogel smart materials.

Materials	Manufacturing approach	Activation method	Activation time	Overall part size	Smallest feature size	Ref.
Alginate-PNIPAAM ionic covalent entanglement hydrogel	Direct ink writing, UV curing, calcium chloride solution curing	Temperature	2 minutes	1 - 6 cm	250 µm (layer thickness)	[48]
PNIPAAM hydrogel	Customized projection micro-stereolithography	Temperature	3 - 45 minutes	1.6 - 3.6 mm	300 µm (layer thickness)	[49]
PNIPAAM hydrogel	Halftone gel lithography (solution casting and UV curing)	Temperature	Not reported	1 cm x 1cm	7 - 17 µm (sample thickness)	[50]
PNIPAAM hydrogel, poly(p-methylstyrene)	Patterned UV curing	Temperature	Not reported	10 - 15 cm	Not reported	[30]
Poly(sodium acrylate) hydrogel, cupric ion	Electric field assisted patterning of cupric ions onto hydrogel	Ionic concentration gradient	30 s	0.5 - 5 cm	100 µm	[1]

Table 1.6 Continued.

Materials	Manufacturing approach	Activation method	Activation time	Overall part size	Smallest feature size	Ref.
Gelatin-alumina hydrogel, PNIPAAM-alumina hydrogel	Magnetic field assisted gel curing stepwisely in plastic molds	Hydration	24 hours	0.5 - 7 cm	Not reported	[33]
Nanofibrillated cellulose, PNIPAAM hydrogel	Direct ink writing, UV curing	Hydration	5 - 25 min	1 - 5 cm	200 μm	[32]
Alginate hydrogel, Fe_3O_4 nanoparticle	Mold casting	Magnetic field	2 minutes	1 cm^3	Not reported	[2]
Gelatin hydrogel, Fe_3O_4 nanoparticle	Direct laser writing, mold casting	Magnetic field, temperature	3 minutes	5 – 50 μm	5 μm	[51]

Table 1.7 Examples of other smart materials.

Materials	Manufacturing approach	Activation method	Activation time	Overall part size	Smallest feature size	Ref.
Electrochemical polymer: polypyrrole, polyol-borate	Solution casting (electrochemical synthesis of polymer film)	Hydration	5 - 15 minutes	5 cm	15 μm (sample thickness)	[52]
Graphene oxide	Direct ink writing	Electricity	10 s	1 - 4 cm	200 μm (fabrication resolution)	[53]
Polyurethane acrylate oligomer, alumina platelet, fumed silica	Magnetic field aided direct ink writing	Chemical reagent (ethyl acetate)	30 minutes to 3.5 hours	3 cm	Not reported	[54]
Photocurable polymer: poly ethylene glycol diacrylate (PEGDA), Fe_3O_4 nanoparticle	Magnetic field assisted modulated UV photopatterning	Magnetic field	Not reported	100 - 500 μm	Not reported	[55]
Polystyrene	Desktop laser printer patterning with black toner	Temperature	5 - 10 s	0.5 - 2 mm	0.5 mm	[56]

1.4 Organization of dissertation

My research focus is novel fabrication approaches of polymer based elements, which include oil absorbents, shape memory mechanical parts, residual stresses induced shape morphing elements, and microfluidic channels. Chapters II to V document the scientific aspects of each topic, and chapters VI and VII describe the commercialization exploration and education application of these discoveries as in the professional domain (Fig. 1.3).

In Chapter II, I describe the process of designing and producing 3D printed, rigid, biodegradable, and reusable oil absorbents. I combined the capillary force imposed by the microscale porous structures and the hydrophobic/oleophilic surface properties of PLA to produce oil absorbents with minimal environmental footprints owing to their biodegradability and renewable starch-sourced nature. I also analyzed oil absorption behaviors and developed mathematical models that reflected the influence of absorbent porosity and fluid properties (viscosity and density). These models provide a guide to choose absorbent structures based on oil properties to maximize oil absorption efficiency.

In Chapter III, I report the design and fabrication of mechanical actuators that operate in principle of shape memory properties. I applied manual mechanical stretching to samples and studied the curvatures formed the recovery phase. These elements can function as a gripper to pick up items or form a self-tying knot.

In Chapter IV, I illustrate an accessible 3D printing approach to produce programmable responsive soft materials. Compared to other reported 3D printed smart materials, my approach required only commercially available supplies: off-the-shelf PLA filaments and a fused deposition modeling printer without customization. 3D printed samples warped when exposed to heat due to the release of internal stresses that were embedded in the parts

during the printing process. I assessed the correlation between warpage behaviors and printing parameters and produced a library of elements with programmable shape morphing features.

In Chapter V, I present a novel lithography-free microchannel fabrication approach using enzymatic etching. This procedure harnessed the advantage of enzymatic etching (creating microchannels with controllable depths through the highly selective enzyme/substrate reaction), thermal annealing (generating microscale crystal morphologies), tape masking (eliminating soft lithography operations to reduce cost and shorten production time), and vacuum-aided thermal bonding (ensuring bonding strength without comprising the channel dimension integrity). The final product was a completely biodegradable assembled microchannel device with potential to perform bioanalysis. This manufacturing procedure makes it possible to establish an accessible lithography-free toolbox for microchannel fabrication.

In Chapter VI, I share my journey of commercializing the oil absorbents and related products through setting up online store (Etsy platform) and entrepreneurial program (NSF I-Corps). From these entrepreneurial endeavors, I discovered the gap between laboratory experiment inventions and market viable products and learned the importance to adjust my business according to customers' opinions other than my assumptions.

In Chapter VII, I document four projects of embedding hands-on activities to engineering education: adding mini-lab experience to a core undergraduate fluidic mechanics theory course, training undergraduate researchers in 3D printed oil absorbent application study through Aggie Challenge, teaching basic physics principles (capillary action) with 3D printing demonstration at local science events, and developing accessible

hands-on activities enabled by 3D printing. Through these projects, I gained valuable experience in developing courses and hands-on activity modules, leading an undergraduate student research team, and communicating with colleagues with various backgrounds.

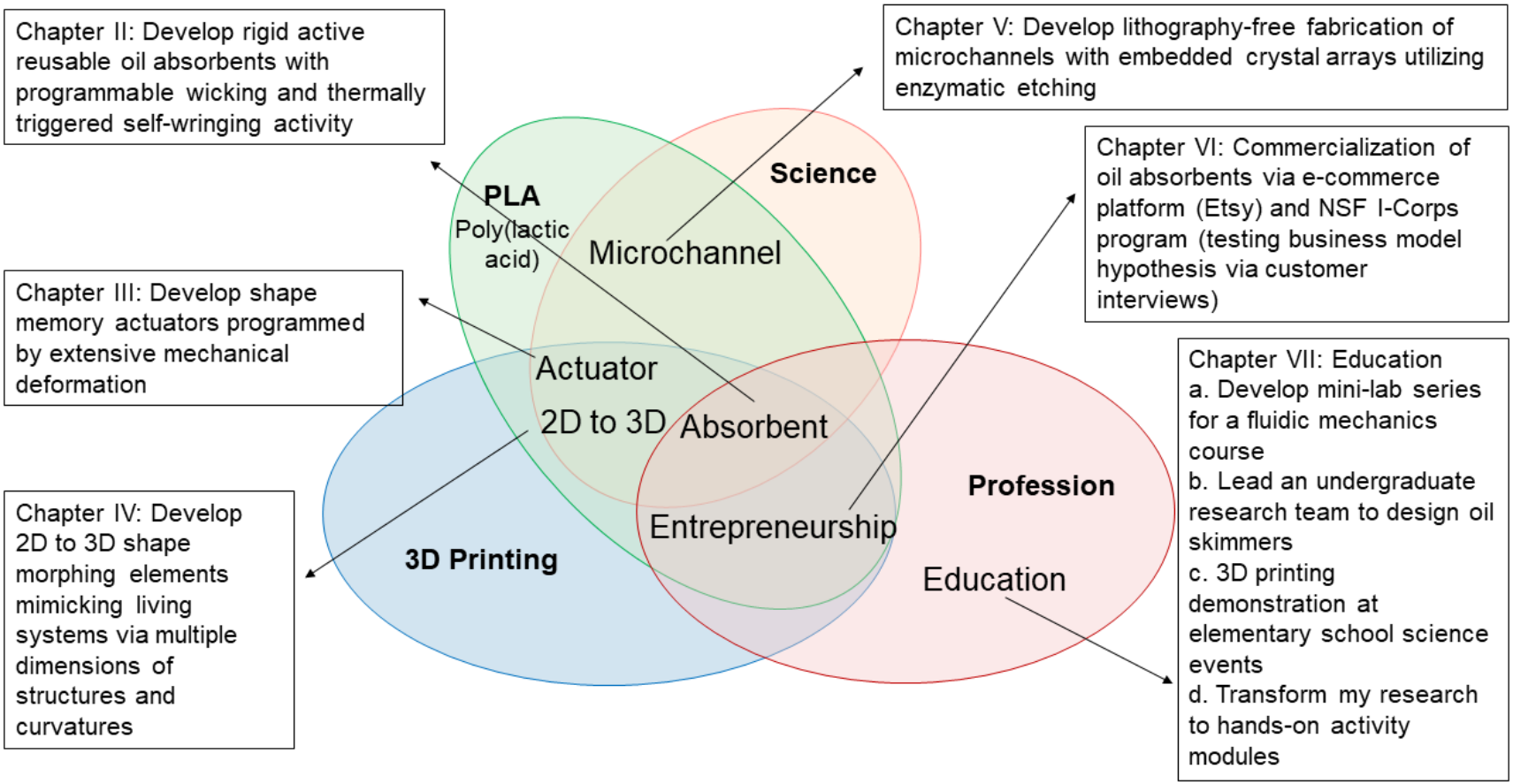

Fig. 1.3 Organization of dissertation.

CHAPTER II

BIODEGRADABLE REUSABLE 3D PRINTED OIL ABSORBENTS

2.1 Introduction

Remarkable progress in developing oil spill cleaning solutions has largely been driven by the pressing environmental challenges triggered by oil spill accidents that have occurred worldwide. Both physical and chemical methods have their limitations and present further environmental hazards. Among these approaches, new absorbent materials were discovered and developed [57-60] because of the untapped possibilities to increase absorption capacity, selectivity, and efficiency, reduce cost, and improve reusability.

However, these materials have three major drawbacks which limit their application in real-life spill scenarios. Firstly, many of these novelty materials are made of unrenewable polymers (e.g. melamine,[19, 20] polyurethane,[21-23, 28] and polydimethylsiloxane,[24, 25]). To achieve desired absorption performance, these materials require intensive chemical modification and specific treatments, which increase their environmental footprints. Secondly, the high absorption capacity (e.g., on the order of up to 90 times the initial absorbent weight [28]) raised the concern that whether the absorbents can stand the weight of absorbed oil and still maintained their shape and structure. Thirdly, these materials are usually sponge-based and achieve their reusability by mechanically squeezing out the absorbed oil. These absorbents are soft in nature and inevitably share the issue with other traditional soft absorbents (e.g., polypropylene pads and booms), which leak oil when being collected by nets from water surfaces. Reported experiments were usually carried out with a small absorbent sample (< 10 cm^3) that was handled gently with hands or tweezers, so the oil-retention in the absorbents was left unknown. Consequently, these

novel absorbent materials have yet to find their applications in real-life oil cleanup efforts. This chapter presents a 3D printed poly (lactic acid) (PLA) oil absorbent, which is produced from renewable source, requires no chemical modification, has rigid nature to retain absorbed oil, and is reusable because of self-wringing (shape memory) properties .

2.2 3D printed oil absorbent design

2.2.1 Sample manufacturing

Absorbents were produced using a Makergear M2 printer with a 0.35 mm diameter nozzle. Natural color PLA filaments (DeltaMaker 1.75mm, no dye added) were obtained in 1 kg spools and used as received. 3D models were created using OpenSCAD (version 2015.03) and exported as .stl files. These files were then imported into Simplify3D (version 4.0.1), a slicing software used to generate the g-code instructions that direct the printer to produce the designed object. General printing settings employed were extruder temperature of 210 °C, printing speed of 4,800 mm/min, and layer thickness of 0.2 mm. A raft was used for printing parts larger than 5 x 5 cm. The soda lime glass printing bed was covered with Kapton tape, and a thin layer of adhesive spray was applied to the tape surface to ensure that the printed parts adhere to the bed surface.

2.2.2 Absorption performance test

Oil absorption was characterized using samples of varying viscosity (Table 2.1) labeled with Oil Red O dye (Sigma-Aldrich Cat. No. O1391) at a ratio of 1:49 by volume. Oil absorption experiments were performed using parts printed with a 1 x 1 cm square cross-section and height of 4 cm embedding an infill of 30, 40, 50, or 60%. Absorption was characterized by acquiring video recordings of oil uptake upon placing the printed parts in a petri dish containing dyed oil. One frame per second was extracted from each video and

analyzed to obtain the meniscus height as s function of time, where the height was defined as the top of the oil meniscus after subtracting the initial oil level in the petri dish. At least three replicates of each absorption experiment were performed.

Table 2.1 Properties of oil samples used in absorption tests.

Oil sample	Oil type	Cat. No.	Viscosity (mPa s)	Density (kg/m^3)
A	Mineral oil	Sigma-Aldrich M1180	30.36	875
B	Mineral oil	Fisher BP 26291	26.40	830
C	Mineral oil	Sigma-Aldrich M5904	12.45	845
D	Silicone oil	Sigma-Aldrich 378321	9.30	930
E	Silicone oil	Sigma-Aldrich 317667	4.65	930

2.2.3 Physical principle

3D printed absorbents were produced by combining internal pore morphologies conducive to programmable wicking. Wicking in microporous networks is governed by the same phenomena that drive capillary rise in a single tube, in which the surface tension-induced pressure changes across a fluid meniscus. The net interfacial pressure, expressed by the Young-Laplace equation under the assumption of a hemispherical-shaped meniscus (equation 2.1), is balanced when the fluid in the capillary rises to an equilibrium height, h_{eq}, where θ is the contact angle, and R is the capillary radius (Fig. 2.1a) (equation 2.2).

$$\Delta p = \frac{2\sigma cos\theta}{R} \quad (2.1)$$

$$h_{eq} = \frac{2\sigma cos\theta}{\rho g R} \quad (2.2)$$

This framework was extended to consider absorbents produced using a commercial 3D printer with standard PLA filaments to readily enable manufacturing outside of dedicated

laboratory environments. Interconnected microporous networks were embedded within the void spaces between periodically spaced filaments printed in a woodpile configuration (i.e., layers whose orientation alternates by 90°, resembling a stack of logs; Fig. 2.1b). This architecture was selected because it can be easily produced using a standard rectilinear infill setting universally accessible in FDM slicing software packages. Porosity ∅ was controlled by selection of the infill percentage IF, representing the fraction of the part's cross-section occupied by printing material (∅ = 1 – IF). Infills considered in here ranged from 30 to 60%, corresponding to average void dimensions ranging from 979 to 303 μm, respectively. Other infills were not suitable for purpose of absorbents because the capillary driving force diminished at IF < 30%, and minimal interstitial space was available for fluid uptake at IF > 60%. A small infill structure had a large void space to increase oil uptake capacity. When the absorbent was saturated with oil, a 30% infill absorbent had the capacity of 1.88 g oil per gram of absorbent (Fisher BP 26021 oil). An absorbent with a higher infill of 40%, 50%, and 60% had the capacity of 1.28, 0.88, and 0.5 g of oil, respectively.

Capillary rise was quantified in printed bundles with 1 x 1 cm cross-section by obtaining video recordings of oil labeled with colored dye during wicking, from which the meniscus position as a function of time $h(t)$ and the equilibrium height h_{eq} were extracted (Fig. 2.1c). The dynamics of capillary rise can be elucidated by considering a momentum balance on fluid drawn into a single tube, yielding a differential equation of the form (equation 2.3), where μ is the fluid viscosity, σ is surface tension, and ρ is the fluid density.

$$\frac{2\sigma cos\theta}{R} = \frac{d(\rho h \frac{dh}{dt})}{dt} + \frac{8\mu h}{R^2}\frac{dh}{dt} + \rho g h \quad (2.3)$$

The inertial (first on the right hand side) term is associated with fluid entry into the tube, and can be neglected during the majority of capillary rise. Likewise, the gravity term (third on the right hand side) can be neglected during early stages of wicking where viscous effects dominate, yielding the Bell-Cameron-Lucas-Washburn equation (equation 2.4 and 2.5).[61-63]

$$\frac{2\sigma cos\theta}{R} = \frac{8\mu h}{R^2}\frac{dh}{dt} \quad (2.4)$$

$$h(t) = \sqrt{\frac{\sigma cos\theta R}{2\mu}}\sqrt{t} \quad (2.5)$$

The unknowns σ and θ are expressed in terms of h_{eq} subject to the assumption of equivalency between static and dynamic contact angles (equation 2.6).

$$\sigma cos\theta = \frac{2\mu h_{eq}^2}{Rt} \quad (2.6)$$

Combining equation 2.5 and 2.6 produces

$$h(t) = \sqrt{\frac{\rho g R^2 h_{eq}}{4\mu}}\sqrt{t} \quad (2.7)$$

This framework was applied to printed bundles by adopting R as a fitting parameter for $h(t)$ data obtained during the first 60% of capillary rise (when $h(t) < 0.6h_{eq}$) over an ensemble of four different infills (30, 40, 50, or 60%) and five different oil formulations (Fig. 2.1d). Define dimensionless time and height as follows [64, 65]:

$$t^* = \left(\frac{8\mu}{\rho R^2}\right)t \quad (2.8)$$

$$h^* = \left(\sqrt{\frac{32\mu^2}{\rho^2 g h_{eq}}}\right)h \quad (2.9)$$

When plotted in terms of $t^*$and h^*, the capillary rise in the printed bundles displayed a characteristic scaling, yielding a global parametric map that made it possible to rationally design absorbents that deliver a desired filling rate. Phenomena during later stages of wicking (when $0.6h_{eq} < h(t) < h_{eq}$) were captured by including the gravity term that was previously neglected in the single tube momentum balance and recasting the resulting differential equation in terms of the microporous network's permeability, K. [66, 67]

$$K = \frac{\emptyset R^2}{8} \quad (2.10)$$

This gravity-dependent model was applied to analyze capillary rise in absorbents with homogeneous infill using K as a fitting parameter, enabling the data to collapse onto a master curve when plotted in terms of dimensionless time, TN and height, HN (Fig. 2.1e).[67]

$$TN = \frac{R\rho^2 g^2 K}{2\emptyset\mu\sigma cos\theta} \quad (2.11)$$

$$HN = \frac{R\rho g}{2\sigma cos\theta} h \quad (2.12)$$

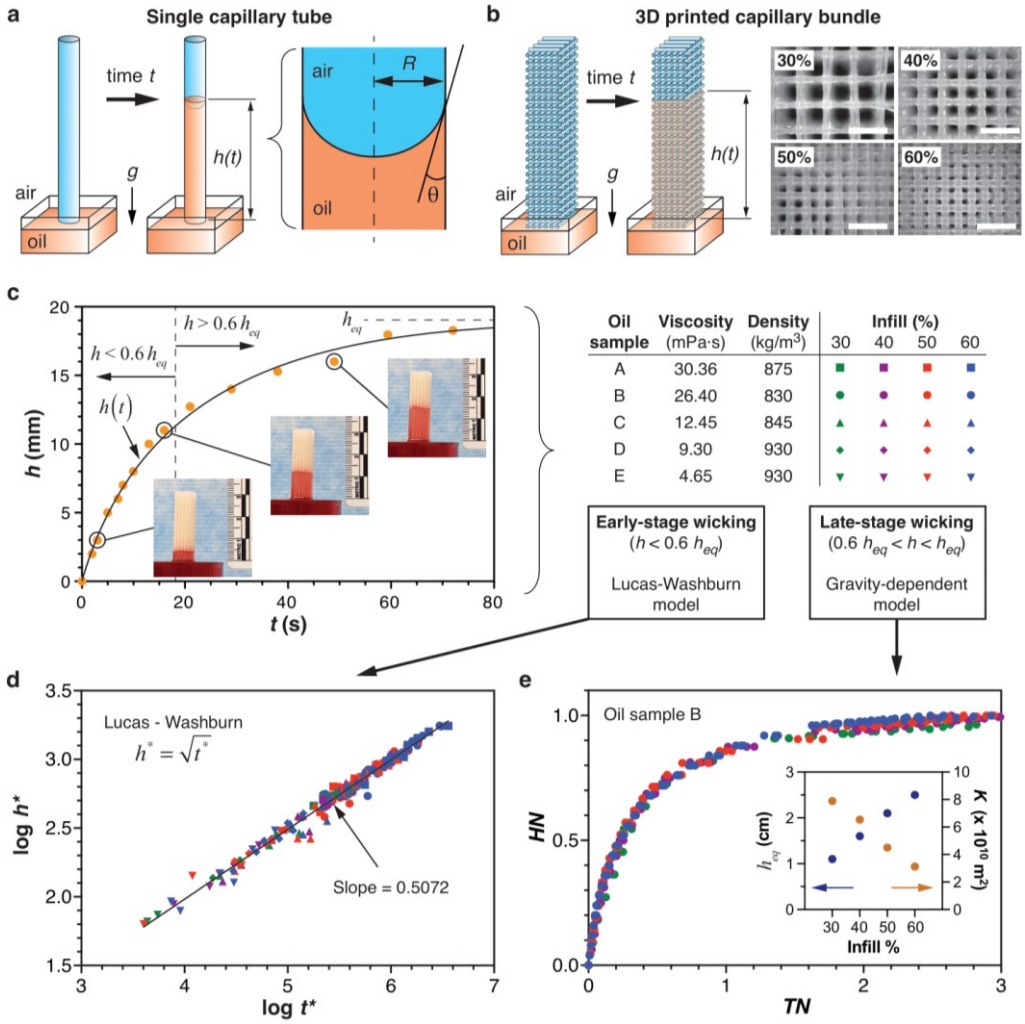

Fig. 2.1 Oil absorption in 3D printed capillary networks. (a) Vertical capillary rise in a single tube of radius R was driven by the surface tension-induced pressure change across a fluid meniscus of contact angle θ. **(b)** Analogous capillary wicking occurs in 3D printed networks. Internal void dimensions were determined by the embedded infill percentage. Infills of 30, 40, 50, and 60% were studied, corresponding to measured void dimensions of 979 ± 32, 619 ± 25, 466 ± 25, and 303 ± 20 μm, respectively (mean ± sd, n = 10). **(c)** Analysis of video recordings of capillary rise in 3D printed networks yielded evolution of the meniscus position as a function of time $h(t)$ and the equilibrium height h_{eq}. Data from the early stage ($h(t) < 0.6h_{eq}$) and late stage ($h(t) > 0.6h_{eq}$) of capillary wicking were analyzed separately across a range of oil viscosity and absorbent porosity (infill). **(d)** Early-stage wicking was captured by the Lucas-Washburn model, consistently displaying scaling across all oil samples and infills studied. **(e)** Late-stage wicking was captured by a gravity-dependent model that, when combined with h_{eq}, yielded the network's permeability K. The plots in **(d)** and **(e)** showed all data obtained from 3 independent replicates at each oil-infill combination, demonstrating universal scalings that enable printed networks to be rationally designed to achieve desired wicking performance.

3D printing makes it possible to manufacture absorbents containing porosity gradients that enhance the speed and capacity of oil uptake beyond levels attainable in conventional homogenous systems. Previous studies have shown that optimal capillary rise in single tubes occurs when cross-sectional dimensions decrease in the flow direction. [68] Therefore, absorbents were constructed embedding porosity gradients where infill increased with height from 30 to 60% in discrete increments and recorded wicking dynamics associated with the approach of $h(t)$ toward the equilibrium value h_{eq} (Fig. 2.2a). The gravity-dependent capillary rise model was applied piecewise within each zone of a constant infill, where the height of each zone was sized from $0.4h_{eq}$ to $0.8h_{eq}$ (e.g., in a $0.8h_{eq}$ design, the boundary between 30 and 40% infill zones is positioned at 80% of the equilibrium capillary rise height associated with the 30% infill layer, and so forth). This analysis revealed that absorbents embedding a porosity gradient consisting of infill segments of height $0.5h_{eq}$ attained 30% faster capillary rise (based on the time to reach h = 2 cm) with 20% greater capacity than homogenous absorbents composed of 60% infill, in agreement with experimental data (Fig. 2.2b). In this way, the capability to print precisely controlled spatial porosity distributions within an absorbent can be leveraged to design optimal pore morphologies tailored to the needs for a specific application.

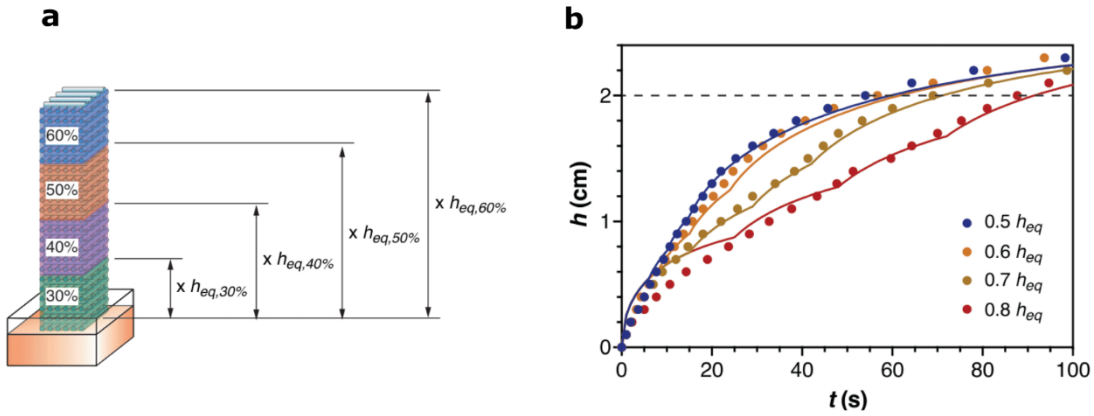

Fig 2.2 Absorbents with gradient porosity. (a) Porosity gradients enabled enhanced oil uptake. A vertical stepwise gradient from low (30% infill) to high (60% infill) is embedded, where each discrete infill zone is a fraction *x* of the equilibrium height that would have been achieved in an absorbent with homogenous porosity at that infill. **(b)** Wicking phenomena in absorbents with stepwise porosity gradients are captured by piecewise application of the gravity-dependent capillary rise model. The configuration in **(a)** consisting of infill segments of height $0.5h_{eq}$ absorbs oil 30% faster than an absorbent composed of homogenous 60% infill (based on the time to reach h = 2 cm).

2.3 Self-wringing absorbent

2.3.1 Self-wringing principle

The shape memory properties of PLA can be leveraged to embed spring element actuators that introduce thermally triggered self-wringing functionality, enabling recovery of collected oil so that the printed absorbents can be reused (Fig. 2.3a). A printed active absorbent is programmed by mechanical stretching at a temperature $T_{program}$ above the material's glass transition T_g (~ 60 °C for PLA [69, 70]) followed by cooling to ambient conditions to preserve the deformation (Fig. 2.3b, c). The programmed absorbent is then used to collect oil, after which it is heated above T_g to a dispensing temperature $T_{reocver}$, where shape memory recovery of the spring element compresses the surrounding absorbent and squeezes out the collected oil. In this way, the absorbent can be reused multiple times via application of sequential programming and recovery/dispensing cycles.

2.3.2 Active absorbent design and characterization

Small size active absorbents in Figs. 2.3a, b, c, and d were constructed by printing parts containing a 2.5 x 0.5 x 0.5 cm absorbent zone embedding an infill of 30, 40, 50, and 60% capped by 0.25 x 0.25 x 0.5 cm segments of 100% infill at each end to function as grips for mechanical stretching during programming. A spring element was embedded within the absorbent zone that consisted of a 0.05 x 0.95 x 0.5 cm cross-section at 100% infill in a zigzag shape with spring angles α of 15, 30, or 45°. The printed parts were first heated at $T_{program}$ in an oven, after which the parts were longitudinally stretched by hand using pliers and held in place until they cooled to room temperature. The programmed parts were placed in a petri dish filled with oil to permit absorption, after which they were heated at $T_{recover}$, where shape memory recovery of the spring element squeezed out the absorbed oil. Programming and recovery temperatures of 70, 80, 90, and 100 °C were investigated. Larger scale absorbents in Figs. 3e and f were produced in the same manner, but incorporating a 4 x 2 x 0.5 cm absorbent zone of 30% infill capped by 0.4 x 2 x 0.5 cm grip segments of 100% infill at each end and an embedded spring angle of 45° (0.05 x 0.95 x 0.5 cm cross-section at 100% infill). The printed parts were programmed via longitudinal stretching by hand using a canvas stretching tool ($T_{program}$ = 70 °C, and $T_{recover}$ = 80 °C). Oil absorption and recovery were quantified by weighing the parts before and after each programming and dispensing cycle.

2.3.3 Self-wringing performance

Self-wringing activity is governed by simultaneously maximizing (i) achievable deformation during programming ($\frac{L_{program}}{L_{print}}$) and (ii) recovery of the initially printed dimensions ($\frac{L_{program}-L_{recover}}{L_{recover}-L_{print}}$), suggesting a figure of merit based on the product of these

two ratios (L denotes the length of the printed part in the direction of mechanical stretching). The dependence of this figure of merit was experimentally evaluated on temperature, infill, and spring angle α over an ensemble of programming and recovery temperatures to obtain a map of the global design space, and selected 30% infill, α = 45°, $T_{program}$ = 70 °C, and $T_{recover}$ = 80 °C to achieve optimal self-wringing activity (Fig. 3d). These design parameters were adopted to construct larger scale 4 x 2 x 0.5 cm absorbents, and used them to quantify the mass of absorbed and dispensed oil across successive programming and recovery cycles (Fig. 3e). After initial priming, the printed absorbents consistently deliver oil recovery levels exceeding 90% after each cycle (Fig. 3f), indicating strong potential for sustained reuse.

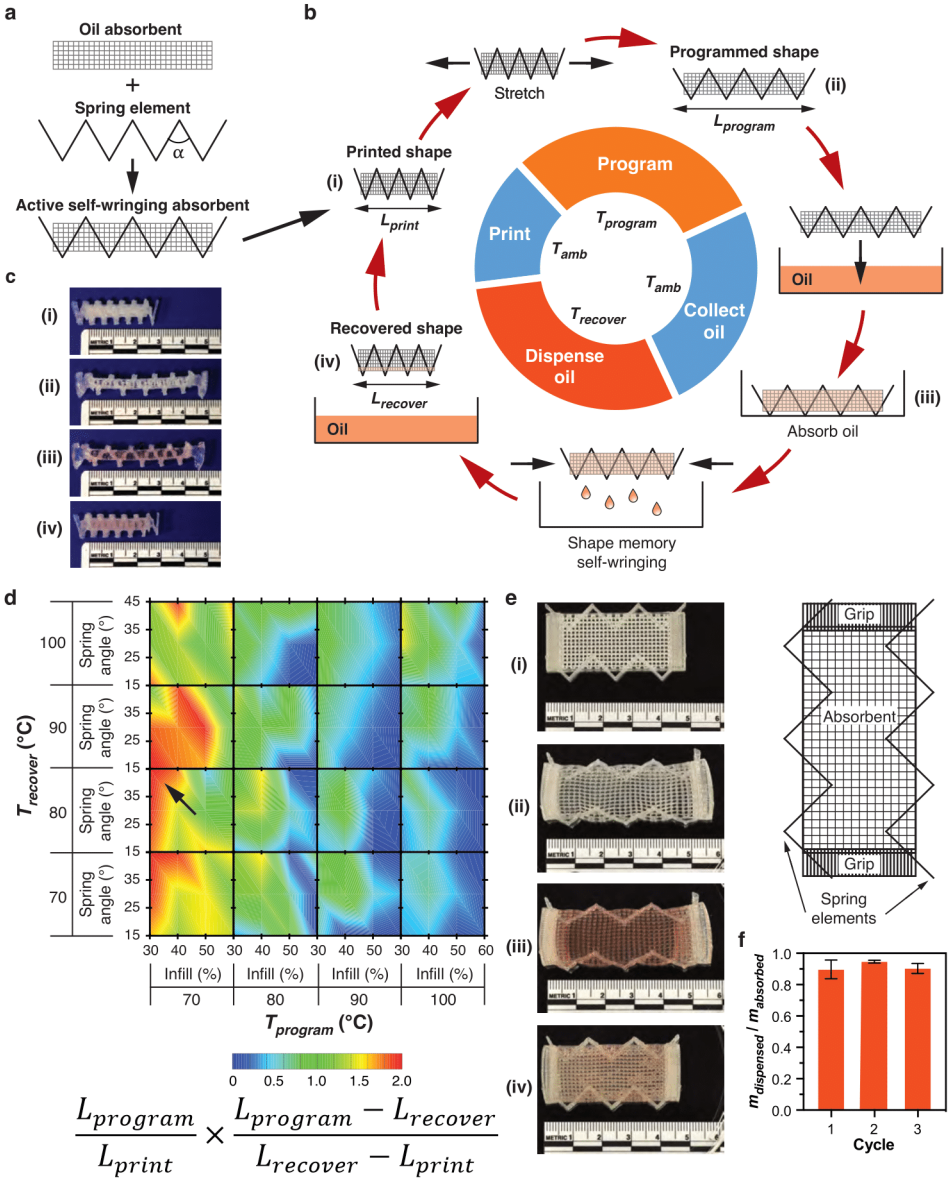

Fig 2.3 A 3D printed self-wringing oleophilic smart sponge. (a) Absorbents containing embedded zigzag-shaped spring elements enable self-wringing activity via the shape memory response of PLA. **(b)** After mechanical programming, absorbed oil is dispensed when the part shrinks back to its printed dimensions during recovery of the spring elements. **(c)** Programming and recovery are evaluated using small size test specimens. **(d)** Experiments performed over an ensemble of absorbent infill, spring angle, and programming/recovery temperatures reveal optimal conditions that simultaneously maximize deformations associated with programming and recovery (arrow). **(e)** Larger sized absorbents manufactured using the optimal design parameters established in **(d)** are used to evaluate performance across successive programming and recovery cycles. **(f)** Oil recovery levels exceeding 90% per cycle are achieved after initial priming.

2.3.4 Recycling oil through centrifugal force

In addition to removing absorbed oil through shape memory properties of PLA, centrifugal force can also be applied to collect absorbed oil and make the absorbents reusable. In each cycle, absorbents were placed in oil then centrifuged at 10,000 g (Eppendorf 5417R, USA) for 20 seconds. The absorbents' weights were measured before oil absorption, after oil absorption, and after centrifugation. To evaluate the reusability of the absorbents, absorption capacity was defined as the ratio between absorbed oil and oil absorbent without oil. The absorption capacity remained constant after five cycles (Fig. 2.4). The absorbent weight before oil absorption and after each centrifugation maintained at 0.3 g, which meant there was no oil left in the absorbent after centrifugation and 100% of absorbed oil was recovered from the absorbent. The absorbents maintained structural integrity and did not deform or break apart, which indicated reliable reusability and durability of these absorbents.

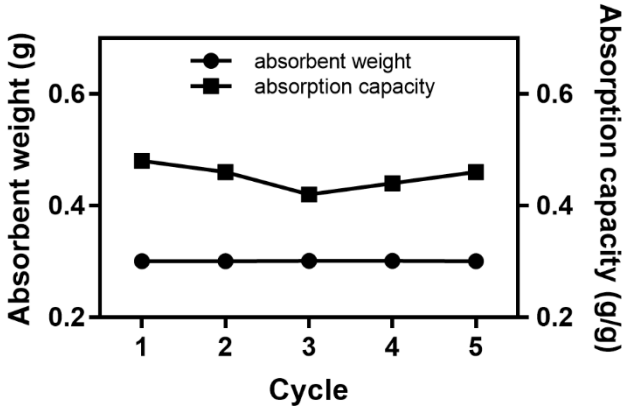

Fig. 2.4 Centrifugal extraction does not change oil absorption. Absorbent sample: cylinder shape absorbent (to fit in the centrifuge tube), 60% infill, diameter 3.5 mm, height 10 mm. Oil sample: mineral oil (Fisher BP26291).

2.5 Annealing treatment

My other research goal of studying PLA based microchannels (Chapter V) implemented annealing and etching as tools to control the PLA surface crystallography. Naturally, it inspired me to experiment with annealing and etching to tune the oil absorption performance of the absorbents. Absorbent samples were treated following three procedures: annealing, etching, or annealing followed by etching.

Cube-shaped (1 x 1 x 1 cm) absorbents were printed with 40% infill. The annealing process was to keep samples in the oven at various temperatures (70 °C and 80 °C) for different durations (30 minutes, one hour, and two hours). The etching process was to immerse samples in proteinase K (PK) enzyme solution (MW = 28.9 kDa, BP1700, Fisher Scientific, in 30 mM Tris-HCl buffer, pH 8.0, BP1758, Fisher Scientific) and kept in an incubator at 37 °C for 24, 48, or 72 hours. The samples were washed with deionized water, dried with pressurized air, and dried in an ambient environment (room temperature 25 °C) for one week. The samples were weighed before and after treatment. Then, the samples were placed in a petri dish filled with mineral oil (Fisher BP 26291) and weighed after samples were filled with oil. The time it took for the oil to be absorbed was also recorded.

PLA is a semi-crystalline polymer in which both amorphous regions and crystalline domains exist; however, the printed samples were amorphous. The printing process was a melting-and-rapid-cooling process: the nozzle deposited melted PLA filament at 210 °C to the printing surface or the previous layer. There was a fan (12V, 5 cm diameter) mounted 5 cm above the extruder, and it cooled the last printed layer rapidly. This rapid cooling process left no time for polymer chains to form crystal domains. Heat annealing increased crystallinity by allowing polymer chains to fold into crystal structures. Enzymatic etching

applied PK to selectively remove amorphous regions from PLA surfaces. Amorphous regions had loosely packed structures compared to crystal domains, so they were more vulnerable to enzyme attack.

Annealing and etching had minimum impact on absorption capacity. They did not change the void volume in absorbents to store oil, so the absorbed oil volume and weight remained unchanged. Annealing also had no effect on the absorbent weight. Etching had negligible effect on the absorbent weight and reduced the weight by 0.002 to 0.006 g, which only made up to less than 2% of the overall absorbent weight (0.35 to 0.71g). Samples with annealing treatment developed crystal domains, which were not easily degraded by PK, so the samples lost 0.002 g from the etching. In contrast, samples with no annealing treatment had only amorphous regions, which were subjected to interaction with PK, so the samples lost more mass (0.006 g). This difference in weight change agreed with the finding that PK degraded amorphous regions easier than crystal domains (more detail in section 5.5.1).

In terms of the absorption speed, both treatment slowed down the absorption process (Fig. 2.5a) to different degrees. Annealing greatly prolonged the absorption process; higher annealing temperature and longer annealing time did not further change absorption behaviors. Enzymatic etching, when applied to amorphous samples, slowed down the absorption process. Longer etching time (72 hours compared with 24 hours) made the absorption process slower. When enzymatic etching was applied to annealed samples with both amorphous regions and crystal domains, it increased the speed of oil absorption compared to samples with only annealing treatment.

Contact angle with oil of different treated surface did not always predict the change in absorption speed after treatment (Fig. 2.5b). In one example, annealing treatment increased the contact angle, which indicated a slower absorption speed and agreed with the absorption test. In another example, enzymatic treatment decreased the contact angle, which suggested a faster absorption that were not observed. The underlying reason was the preparation method of PLA surfaces. Oil was absorbed by the 3D printed absorbent samples, so it could not form a droplet on the sample surface. The contact angle was measured by adding oil droplets to PLA substrates made via melting PLA filaments in an oven at 210°C. The substrates had a flat and smooth surface and did not absorb oil.

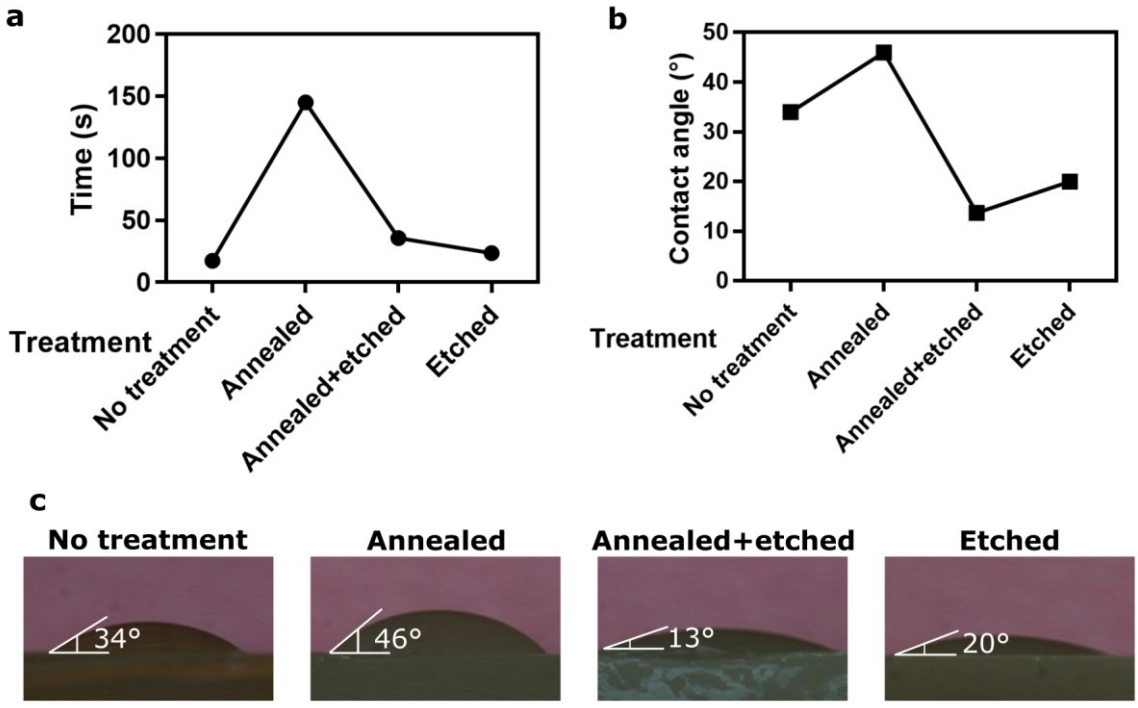

Fig. 2.5 Annealing and etching treatment affects contact angle and absorption rate. **(a)** Absorption time, the time it took for the oil to fill the absorbent cube. Sample: infill 40%, 1 x 1 x 1 cm. **(b)** Contact angle. The PLA substrate was produced by melting PLA filaments on a flat PDMS sheet. It was not feasible to measure the contact angle on filaments (could not provide a flat surface) or on absorbents (oil would be absorbed). Oil sample: mineral oil (Fisher BP26291). **(c)** Oil droplet (20 μL) on PLA substrate.

2.6 Hierarchical porosity control

The absorbent porosity is directly associated with the absorption performance, so increasing porosity will greatly improve absorption capacity. In addition to tuning the infill, filaments with a sacrificial phase that can be leached out offer another degree of freedom in controlling porosity. Sodium chloride (NaCl) was chosen as the sacrificial phase because it can be easily leached out with water.

NaCl (Sigma-Aldrich 221465) particles were first grounded with a coffee grinder (Mr. Coffee 12 Cup Electric Coffee Grinder) and screened with a metal mesh (pore size 200 μm). NaCl particles smaller than 200 μm were collected. Screened NaCl particles were mixed with PLA pellets (MW = 1.04 x 10^5 g/mol, NatureWorks grade 3051D and 3052D; Jamplast Inc., US) at a weight ratio of 20%:80% and 50%:50%. The mixture was fed to a filament maker (Filabot Wee, Filabot) and extruded at 180 °C with a 3 mm nozzle. The extruded filament fell freely into a water bath at room temperature. The filament diameter was controlled by the nozzle size and the distance of free falling before being quenched by the water bath. The filament segment with a diameter between 1.5 and 1.8 mm was collected and dried. Pure PLA filaments were produced from PLA pellets in the same manner. Filaments with 50% NaCl clogged the filament maker extruder, and 20% NaCl composition guaranteed smooth extruding of filaments, which were used in following tests.

The 20% NaCl filament was fed into a Makergear 3D printer (Makergear M2) and printed at nozzle temperature of 210 °C, and cubes (1 x 1 x 1 cm) with 40% infill were printed. NaCl filament cubes and filaments were leached by water in a plastic cup for 72 hours on a magnetic stirring plate at room temperature. Sample weight change was measured after being air-dried in fume hoods for one week. Morphological characterization

of the cubes and filaments was performed by scanning electron microscopy (SEM) (JEOL JSM-7500F). All specimens were pre-coated with a 3 nm conductive layer. The micrographs were taken at an accelerating voltage of 1 keV at different magnifications.

Optical microscope images demonstrated that NaCl particles were distributed through filaments, both on surfaces and inside filaments (Fig. 2.6a). Less than 1% weight loss of NaCl filament cubes was observed after 24 hours of leaching in water. Pure PLA filaments have smooth surfaces (Fig. 2.6b, c), and NaCl particles increased the roughness of filaments (Fig. 2.6d, e). The water leaching process dissolved NaCl particles on the surface and smoothened the surface (Fig. 2.6f, g). However, there was no pore visible on the filaments after leaching. A possible explanation is that the NaCl particles were embedded in PLA, so they did not have direct contact with water and no means to dissolve in water. The weight loss observed probably came from hydrolysis of PLA. These findings point to the need for a procedure to enhance decomposition of PLA to increase contact between water and NaCl particles, thus improving the leaching effect. One promising tool is to introduce enzymatic etching to increase PLA surface degradation, then expose more NaCl particles to water.

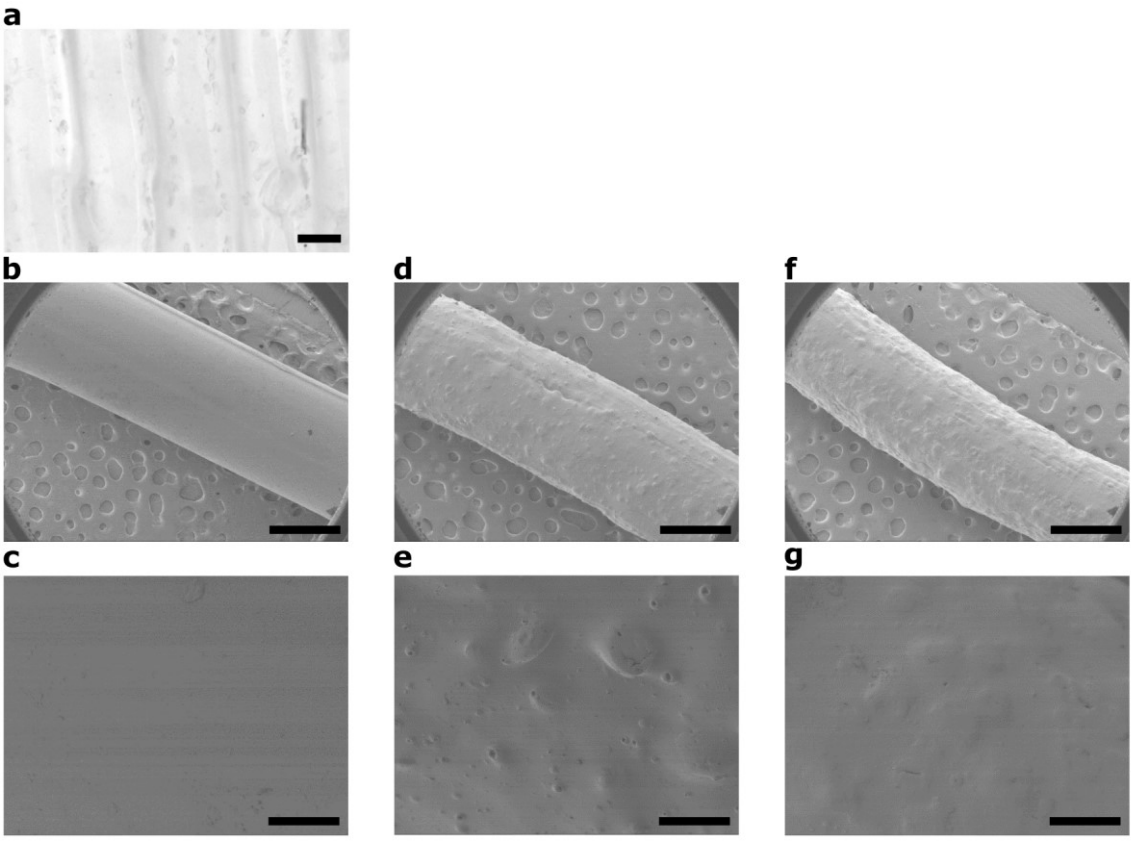

Fig. 2.6 Surface morphologies of NaCl filaments before and after leaching. (a) 20% NaCl filament. **(b)(c)** Pure PLA. **(d)(e)** 20% NaCl filament. **(f)(g)** 20% NaCl filament, after 72 hours leaching in water. Scale bar, **(b)(d)(f)** 1 mm, **(a)(c)(e)(g)** 100 μm.

2.6 Applications

2.6.3 Assembled absorbents

3D printing can construct rigid absorbents of arbitrary bulk size and shape from a library of interlocking parts with customizable internal morphologies (Fig. 2.7). This approach eliminated the need for printing large size objects, which require industrial scale printers and have inevitable structural defects during to warpage. It also adds another degree of freedom to absorbent design, so different internal structures co-exist in one absorbent to accommodate specific oil sequestration need.

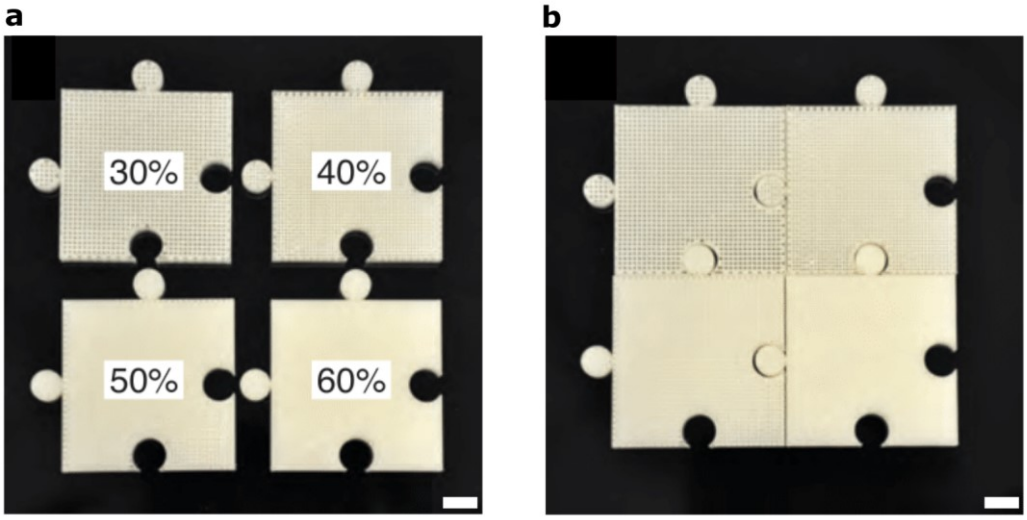

Fig. 2.7 Absorbents of arbitrary size can be manufactured where spatially varying properties are achieved via physical assembly from a library of individual interlocking puzzle piece-shaped parts. (a) Individual pieces of different infills. Each piece is 5 x 5 x 1 cm, with 1 cm diameter circular interlocking tessellations. **(b)** Interlocked pieces create a larger part with tailored absorbent properties. Scale bar, 1 cm.

2.6.4 Oil spill cleanup autonomous robot (OSCAR)

Oil spill cleanup autonomous robot (OSCAR) was designed to support rapid remediation using an autonomous robotic skimmers by providing superior uptake, selectivity, and ease of deployment (Fig. 2.8). It was configured from a Solar Breeze pool skimmer (Solar Pool Technologies, US). On-demand configurability provided absorbents that fit the dimension of the collecting tray. The skimmer was deployed on water surface and moved through the water surfaces powered by solar energy. In the meantime, oil/water mixture flew through the collecting tray, and oil was absorbed. The rigid absorbents did not deform during retrieval handling and retained the absorbed oil. OSCAR collected 50 mL of motor oil in 15 minutes.

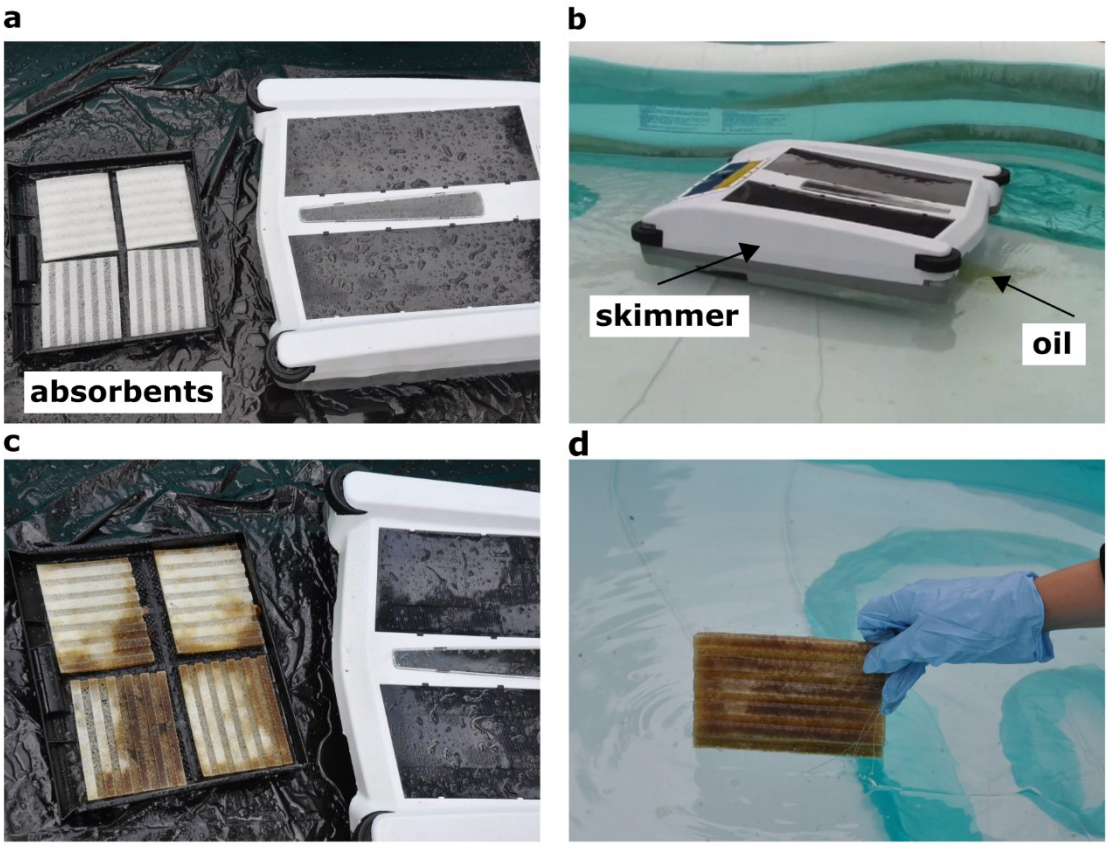

Fig. 2.8 Oil skimmer skimmed through water surfaces and collected oil in embedded absorbents. (a) Four 14 x 11 x 0.5 cm printed absorbents are loaded inside a robotic skimmer. **(b)** The skimmer was deployed for oil cleanup. The inflation pool used here was 2 x 2 x 0.2 m. **(c)** Oil was collected by the absorbents. **(d)** Used absorbents can be easily handled without releasing the absorbed oil.

2.7 Conclusions

This section presented the first-ever 3D printed oil absorbents that elegantly addressed drawbacks of conventional industry-standard polypropylene absorbents. Unlike the soft oil pads and booms, these absorbents were rigid and to be easily handled without releasing the absorbed oil. They were to be disposed of without added environmental contamination by virtue of the biodegradability and starch-based nature of PLA. 3D printing made it possible to produce active absorbents in an on-demand manner that can be highly customized to suit the needs for a specific application (e.g. gallon-size spills, mixture of oil with different

viscosities and densities). Components were produced in virtually any shape and size while simultaneously embedding spatially variable internal microporous architectures that enable selective collection and sequestration of absorbed oil and hydrocarbons. The shape memory properties of PLA led to self-wringing absorbents with the ability to collect the absorbed oil, which recycled oil and made the absorbents reusable simultaneously.

CHAPTER III

SHAPE MEMORY ACTUATORS

3.1 Introduction

The shape memory properties characterized in self-wringing absorbents can be applied more broadly to establish a library of printed mechanical actuators. Similar to the self-wringing mechanisms, an actuator precursor is printed in its permanent shape, then heated and stretched manually to its temporary shape, which was locked in during cooling. Depending on the strain, samples might be able to recover to the permanent shape or form a curvature. This shape recovery process inspired two actuators: a gripper to pick up an object and a self-tying knot.

3.2 Gripper

In a self-wringing absorbent, a spring layer was embedded within a support layer, the absorbent capillary network, and the absorbent recovery to its printed permanent shape upon recovery. In contrary to this design, a bimorph architecture recovered to a programmed curvature, in which a spring layer (Fig. 3.1a) was printed on top of a support layer (Fig. 3.1b). The spring layer was 1 mm thick, and the support layer was also 1 mm thick and composed of 100% fill oriented in the direction of spring extension (Fig. 3.1a). Upon recovery after programming by mechanical stretching, the part experienced a bending deformation with curvature oriented either toward the support layer (Fig. 3.1c) or the spring layer (Fig. 3.1d). The achievable curvature was tuned by adjusting the spring angle and strain produced by stretching (Fig. 3.1e). Although the strip was stretched, the two branches in each zigzag repeating unit of the spring were either compressed or stretched depending on the spring angle; C and C_1 denoted the length of the spring branch

before and after the strip was stretched. Strain was defined as $(L1 - L)/L$, in which L and $L1$ denoted the length of the strip before and after stretching. For a spring with a small spring angle (e.g., 5°) and experienced a small strain (e.g., strain = 2), the spring branch was compressed ($C1/C < 1$). For a spring with a large spring angle (e.g., 15°) and experienced a large strain (e.g., strain = 5), spring branch was stretched ($C1/C > 1$). The compression ($C1/C < 1$) or stretching ($C1/C > 1$) of each branch played a key role in the orientation of the bending deformation during the recovery phase. The strip bent toward the support layer if the branches were compressed ($C1/C < 1$) and bent toward the spring layer if the branches were stretched ($C1/C > 1$). For example, a sample with 5° spring had compressed branches and bent toward the support layer (Fig. 3.1c), and a sample with 15° spring had stretched branches and bent toward the spring layer (Fig. 3.1d).

More mass in the spring layer made the spring more rigid and was better able to deform the support layer. Taking a 1 cm long bimorph structure as example, a 5° spring layer , 15° spring layer, and a support layer weighed 0.08 g, 0.04 g, and 0.12 g. A 5° spring layer made up for 40% of the overall weight of the bimorph structure, while a 15° spring layer was accounted for 25%. Additionally, the 5° spring layer embedded more spring units per unit length. For example, a 1 cm long bimorph structure embedded four spring units whereas a 15° spring layer embedded two spring units. Therefore, the larger mass and greater number of spring units per length in the 5° spring layer made it the preferred configuration in gripper designs to maximize the achievable gripping force.

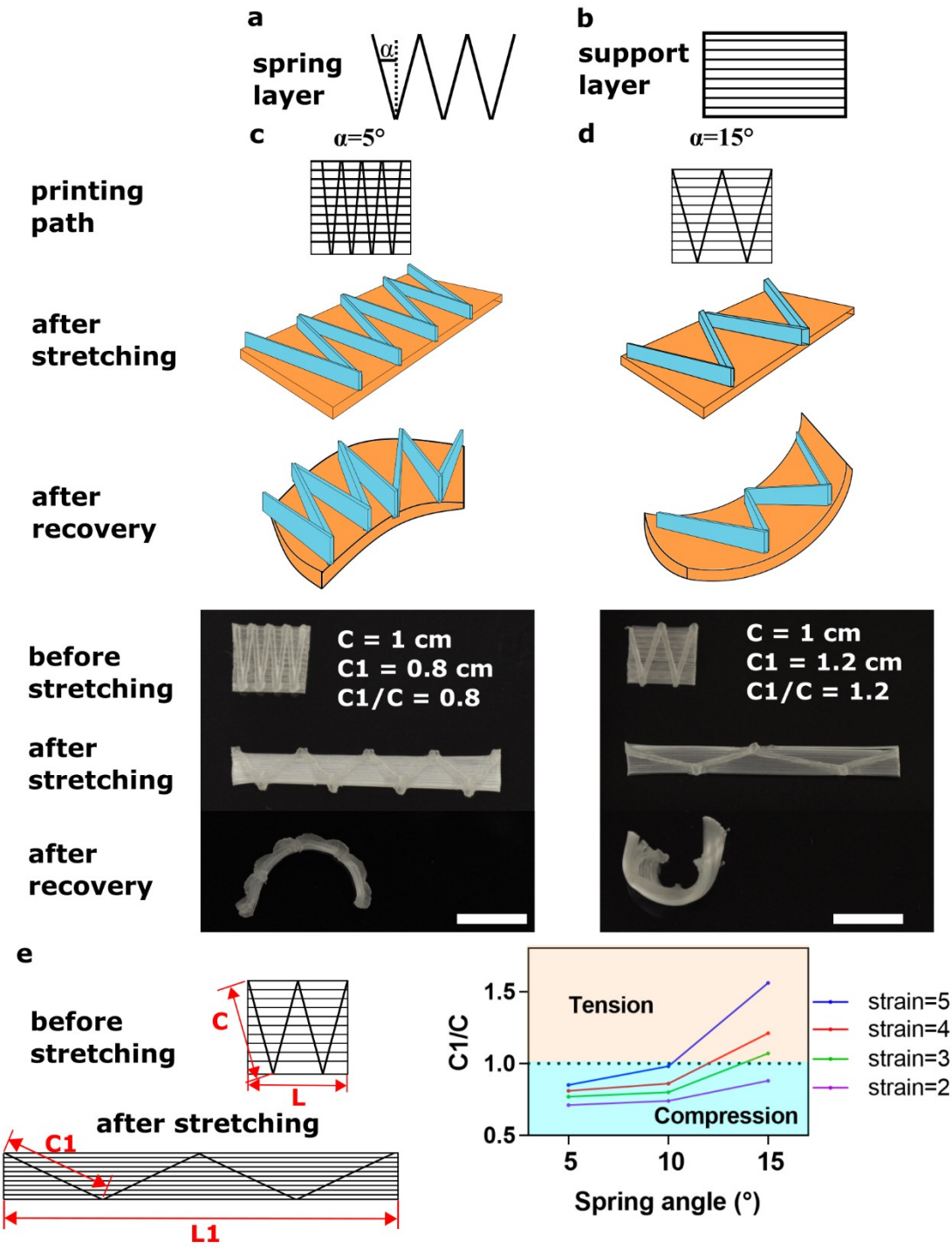

Fig. 3.1 3D printable shape memory mechanical actuators and effects of the spring angle. (a)(b) Printing path of a bimorph structure. (a) Top spring layer. (b) Bottom support layer. **(c)(d)** Spring angle determined the curvature direction. **(c)** 5°. Sample bent towards the support layer. **(d)** 15°. Sample bent towards the spring layer. **(e)** Spring unit dimension change after stretching at different strains. A larger spring angle and a larger strain both increased the spring branch length (larger $C1$). Scale bar, 1 cm.

Two thermally triggered grippers were constructed leveraging the bending behaviors of 5° spring bimorph structures. A strip-shape gripper wrapping around an object upon heating (Fig. 3.2). Multiple 3D printed finger-shaped elements, each containing a bimorph actuation segment, operated in a synchronized manner to mimic the gripping capability of a hand (Fig. 3.3). Each "finger" element had three parts: two solid ends and the middle bimorph structure. Pliers held at the solid ends when stretching the samples, so the bimorph section was stretched properly and not pressed. The solid end was 1 cm wide and did not fit the slit opened around the edge of the palm part. One solid end was cut off, so the stretched bimorph section could be inserted into the palm part. The other solid end was saved to provide a large surface area to secure the object being gripped.

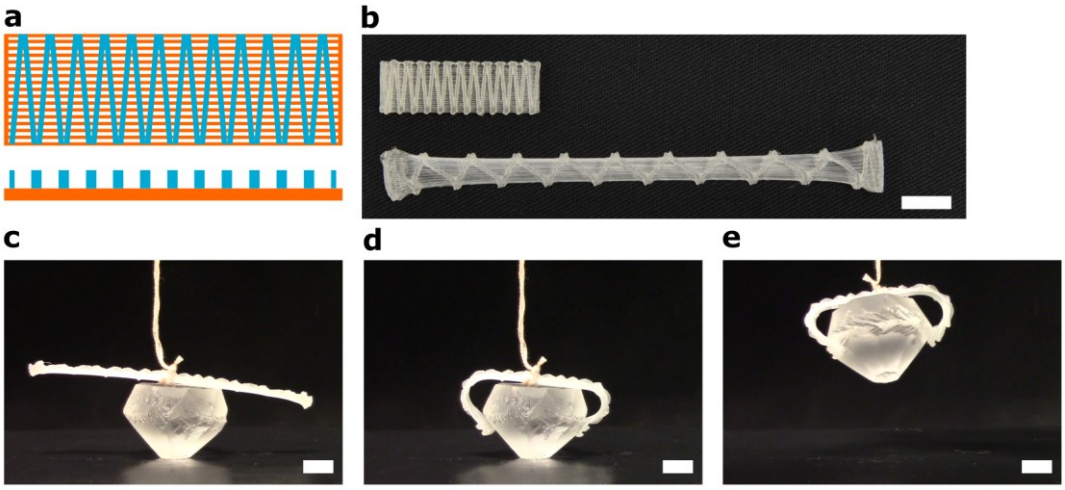

Fig. 3.2 A two-digit gripper was capable of wrapping around and picking up an object upon heating. (a) Printing path and sample side view. Spring layer: blue. Support layer: orange. **(b)** Top: printed sample, 3 cm x 1 cm x 0.2 cm. Spring angle 5°. The support layer and spring layer were both 0.1 cm thick. Bottom: stretched sample. The sample was heated in an oven at 80 °C for one minute, then stretched to 10.5 cm. The spring section was stretched to 3.5 to 4 times of the printed length. **(c)** Attached a piece of cotton string to the gripper, then placed the gripper on the object made of PDMS. The object was placed on a hotplate, with temperature setting at 220 °C. The temperature of air around the gripper was 80 °C. **(d)** After 50s, both end of the gripper curled and wrapped around the object. Used pressurized air to cool the gripper and hardened it. **(e)** Pulled the string attached to the gripper, and the gripper picked up the object, which weighted 20g. Scale bar, 1 cm.

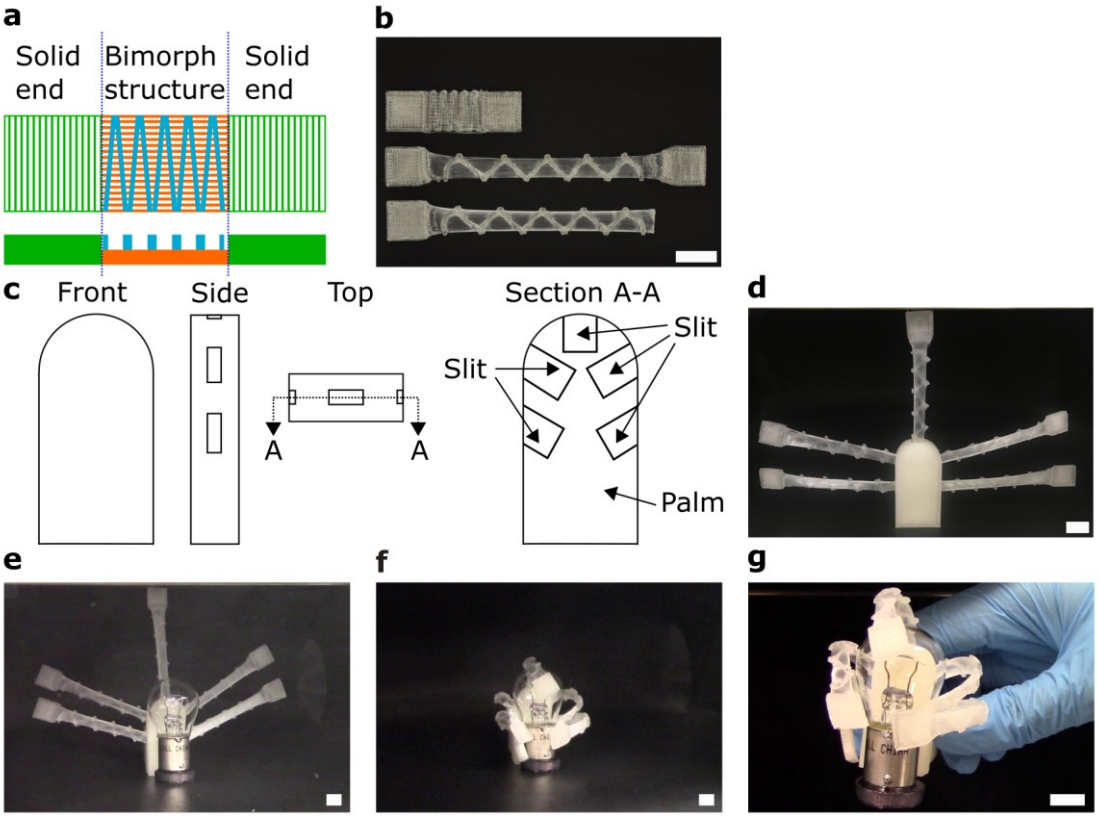

Fig. 3.3 A hand-shape gripper wrapped around and picked up a delicate object (light bulb) in response to elevated temperature. (a) Printing path of the finger-shape element and sample side view. Spring layer: blue. Support layer: oragne. Solid end: green. **(b)** Top: printed sample. Two solid ends: 1 cm x 1 cm x 0.2 cm, 90°/0°, 100% infill. Spring layer: 1.5 cm x 1 cm x 0.2 cm. Spring angle 5°.The support layer and spring layer were both 0.1 cm thick. Middle: stretched sample. The sample was heated in an oven at 80 °C for one minute, then the spring section was stretched to 5.8 cm. Bottom: cropped sample. **(c)** From left to right: front, side, top, and section view of the palm. The section views showed five slits for fingers. **(d)** Assembled hand-shape gripper. The five finger-shape element shared the same design. **(e)** The assembled gripper and a light bulb were placed in an oven set at 80 °C. **(f)** After 60s, all five finger-shape element curled and wrapped around the light bulb. Used pressurized air to cool the gripper and hardened it. **(g)** Lifted the assembled the gripper from the oven. The gripper picked up the light bulb without breaking it. Scale bar, 1 cm.

3.3 Self-tying knot

The bending deformation of the bimorph structure inspired the idea of a self-tying knot. The goal was to tie an overhand knot by mimicking the hand-tying steps. The procedure to tie an overhand knot with hands is as follows: arrange the two ends of a piece

of string in parallel; cross the two ends to form a loop; pass one end through the loop; and pull the two ends to fasten the knot. To repeat these steps, the stretched strip would follow these steps. Step 1, the middle of the strip curls and brings the two ends to a parallel arrangement, and the deformed sample had the shape of a hairpin. Step 2, the two ends crossed, curled, and formed a loop. Step 3, one end entered the loop thus formed a knot. Step 4, both ends continued to curl to tighten the knot. These steps inspired a three-part design: three segments with bimorph structures with different thicknesses, two solid joints, and two solid ends (Fig. 3.8 a, b).

Each bimorph segment had two layers, a spring layer and a support layer. Both layers in the left and right segment were 0.12 cm thick (0.24 cm total thickness), and both layers in the middle segment were 0.08 cm thick (0.16 cm total thickness). The thickness controlled the responsive behaviors of curling: the response time increased with increasing sample thickness (Fig. 3.4). A thicker sample had a greater mass, hence required a larger amount of thermal energy to deform, so longer time was needed. A thin sample (0.08 cm both layers, 0.16 cm total thickness) started to curl after five seconds, and a thicker sample (0.12 cm both layers, 0.24 cm total thickness) required 10 seconds before it started to curl. The middle segment was 0.16 cm thick, so it curled first and arranged the left and right segments in parallel. Because the left and right segments were 0.24 cm thick, so they would not curl until they were in parallel arrangement. The delay of the curling of the left

and right segment allowed the formation of the hair pin status (Fig. 3.8e).

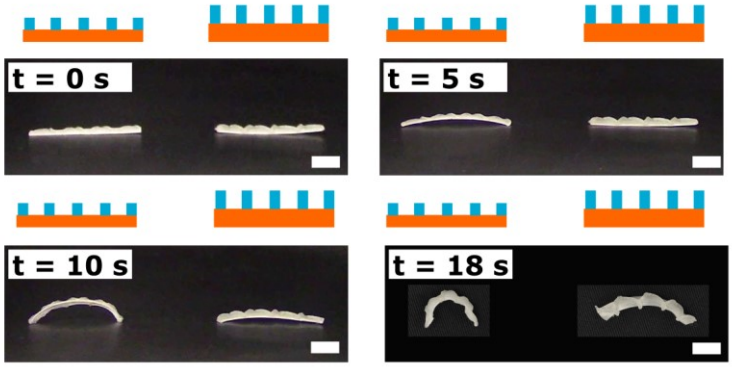

Fig. 3.4 Bimorph element curling response time was determined by the sample thickness. Left: 0.08 cm both layers, 0.16 cm total thickness. Right: 0.12 cm both layers, 0.24 cm total thickness. The thinner sample started to curl earlier than the thicker sample.

The sequential curling of bimorph segments to form a hairpin arrangement was critical to the formation of the knot, so each segment was expected to curl independently without interference from other segments. This expectation presented a challenge for a proper way to connect these segments: connect via both the spring layer and support layer, connect via the support layer, or connect via straight solid joints or at an angle. Connecting via both the spring layer and support layer created overlapped springs (Fig. 3.5), which remained connected after stretching, and led to a sharp curve after recovery. Connecting via the support layer eliminated the overlapped springs. The support layer of three segments were stretched as one extended long piece (approximately 5 cm), which increased the chance of delamination (layer separation) (Fig. 3.6) and disrupted the curling. This design also increased the possibilities of uneven stretching of the middle segment, which led to unusual curling behavior (e.g., curled towards the spring layer). In conclusion, connecting the bimorph segments through either the support layer or the spring layer affected the formation of the hairpin arrangement. Adding a pair of solid joints addressed this issue:

bimorph segments were separated from each other and joined by the solid joints. These joints could be arranged vertically or at an angle. The slanted solid joint (15°) created a wide area with only a joint and a support layer (Fig. 3.7), with no spring layer. This arrangement had the similar effect of a 0.08 cm thin layer, which may curl earlier than the middle segment and interrupted the curling sequence. Vertical solid joints were the optimal choices, as they occupied minimal space and still kept the segment separated.

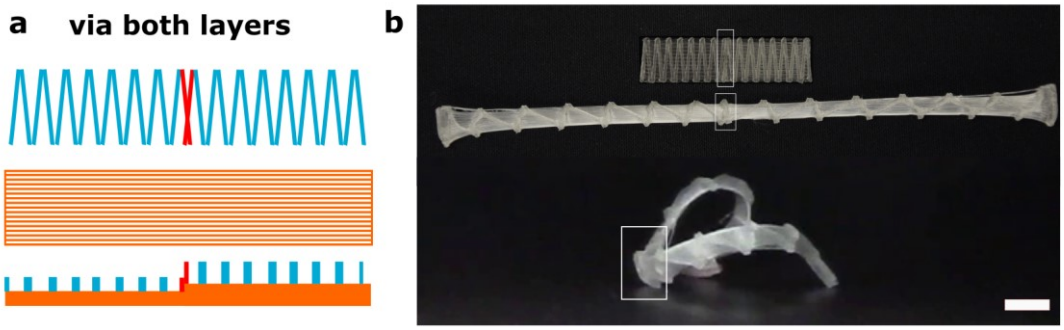

Fig. 3.5 Connecting bimorph segments via both spring and support layer. This sample was to evaluate the curling behaviors of overlapped springs, so it had two segments, not a completed design for a knot. **(a)** Printing path of both layers and side view. Spring layer: blue. Support layer: orange. Overlapped spring: red. **(b)** Top: printed sample. Middle: stretched sample. Bottom: recovered sample. White box highlighted overlapped spring. In the recovered sample, the overlapped springs led to this sharp curve.

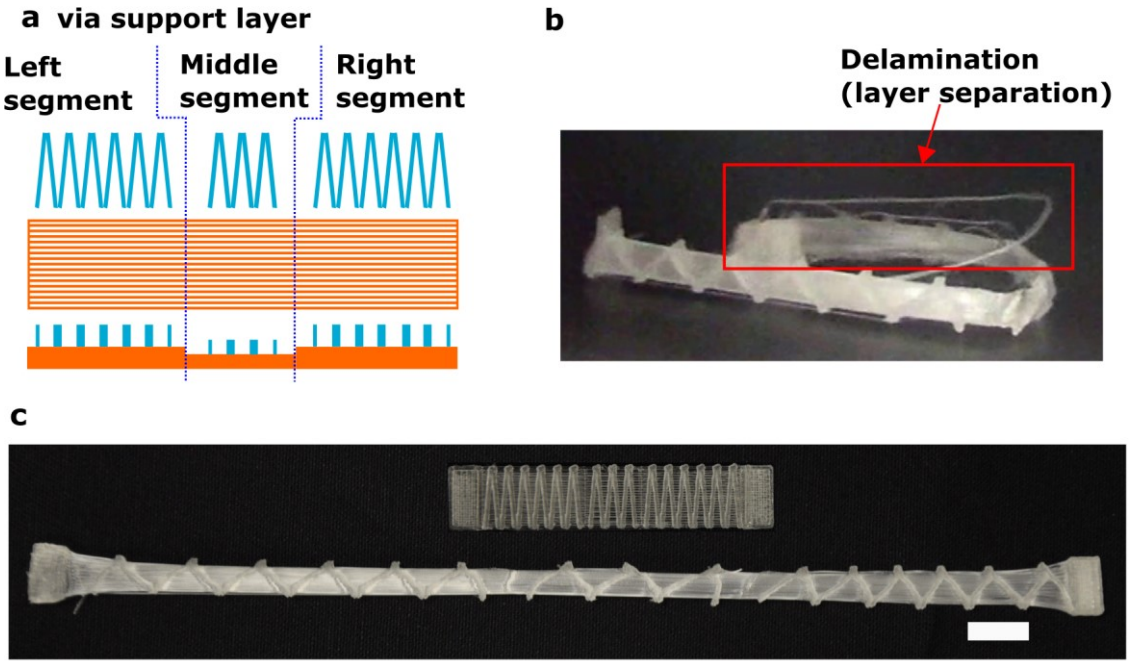

Fig. 3.6 Connecting bimorph segments via the support layer. (a) Printing path of both layers and side view. Spring layer: blue. Support layer: orange. Solid ends were not shown. **(b)** Recovered sample. The delamination made the right segment curled faster than the middle segment, so the sample was not able to form a hairpin arrangement. **(c)** Top: printed sample. Bottom: stretched sample.

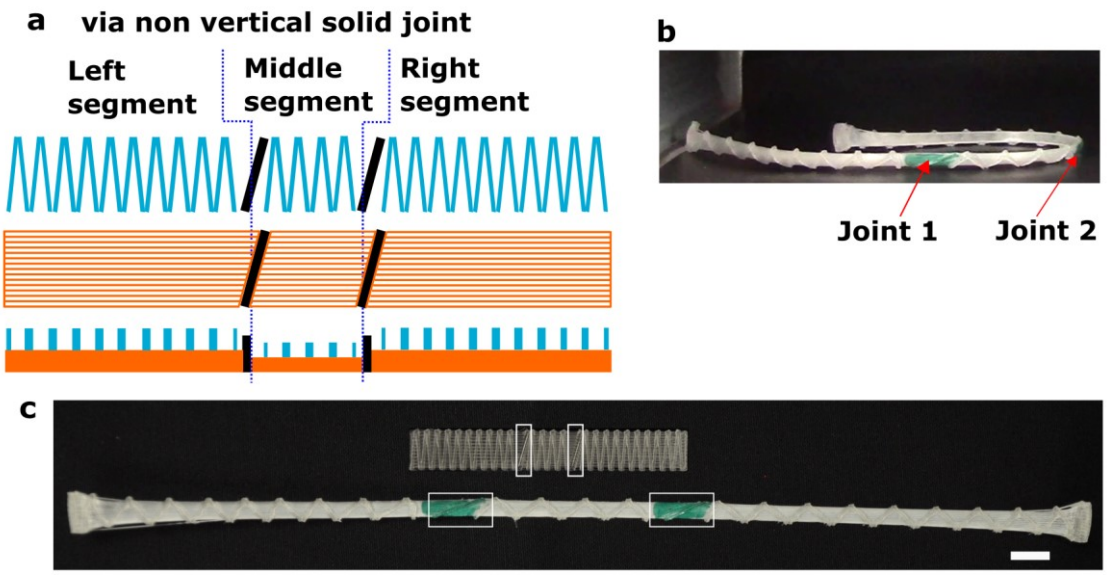

Fig. 3.7 Connecting bimorph segments via non vertical solid joint. (a) Printing path of both layers and side view. Spring layer: blue. Support layer: orange. Solid ends were not shown. **(b)** Recovered sample. The thin segment near the joint 2 curled earlier than the middle segment (between joint 1 and 2), so the sample was not able to form a hairpin arrangement. **(c)** Top: printed sample. Bottom: stretched sample. White box highlighted the joints.

The solid ends were to be gripped by pliers during stretching, so the spring segments were properly stretched without being pressed flat by pliers. The solid ends were cut off, because they had no further role in forming a knot. The strip was heated at 80 °C for two minutes and stretched with pliers (Fig. 3.8c), cooled and then the strip was placed in an oven at 80 °C.

A stretched strip followed the aforementioned four steps to form a knot. Step 1, the middle segment was thinner than the other two segments, so it bent first and brought the left and right segments to a parallel status (Fig. 3.8e). At this point, the deformed sample had the shape of a hairpin. Step 2 left and right segments crossed, curled, and formed a loop (Fig. 3.8f). Step 3, one segment entered the loop thus formed a knot (Fig. 3.8g). Step 4, both left and right segment continued to curl to tighten the knot (Fig. 3.8h).

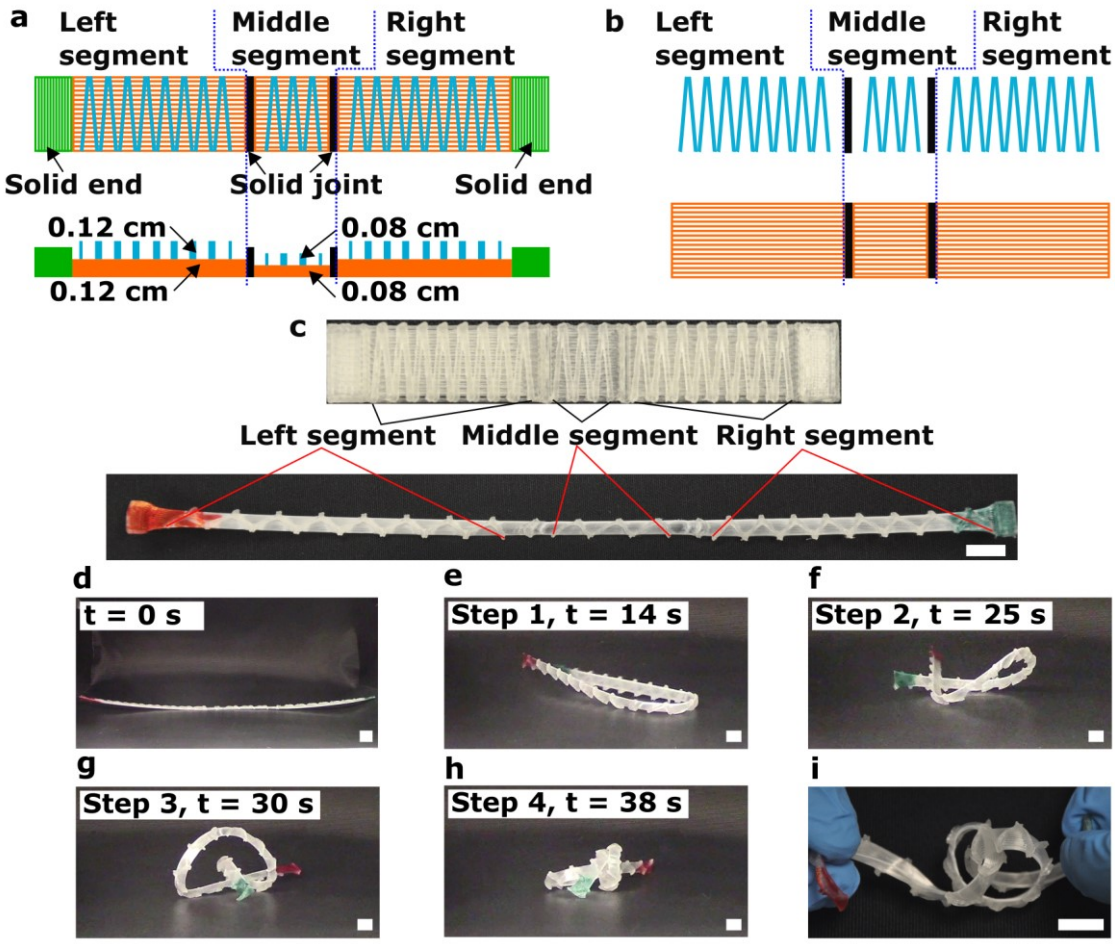

Fig. 3.8 A self-tying knot strip formed curvatures mimicking the process of tying an overhand knot. (a) Sample before stretching. Top: Printing path. Bottom: side view, showing the segment thickness difference. Solid end: 0.5 x 1 x 0.2 cm, 100% infill. Solid joint: 0.1 x 1 x 0.2 cm, 100% infill. Left and right segment: 2.2 x 1 x 0.2 cm. Spring layer: 0.1 cm thick, 5° spring angle. Support layer: 0.1 cm thick, 100% infill. Middle segment: 1 x 1 x 0.16 cm. Spring layer: 0.08 cm thick, 5° spring angle. Support layer: 0.08 cm thick, 100% infill. Spring layer: blue. Support layer: orange. Solid end: green. Solid joint: black. **(b)** Top: spring layer printing path. Bottom: support layer printing path, segments were separated by solid joints. **(c)** Top: printed sample. Bottom: stretched sample. The sample was heated in an oven at 80 °C for two minutes, then stretched. Used pliers to hold the solid ends, so the spring part was stretched properly and not pressed. Cut off both solid ends. The photo showed the ends before they were cut off. Both ends of the strip were colored to track their movements in video recordings. **(d) - (i)** The strip formed a knot due to curvatures formed during the recovery process. **(d)** Placed the stretched stripe in the oven set at 80 °C. **(e)** Step 1. After 14s, the middle segment curled, and the left and right segment aligned in parallel and formed a hairpin shape. **(f)** Step 2. After 25s, both left and right segment curled and formed a loop. **(g)** Step 3. After 30s, one segment (right segment, colored green) continued to curl and entered the loop then completed a knot. **(h)** Step 4. After 38s, both left and right segment continued to curl and tightened the knot. **(i)** Pulling both ends of knot showing the completed overhand knot. Scale bar, 1 cm.

Manual stretching of the strip inevitably introduced the inconsistent stretched features, which made the strip unable to accomplish the first three steps described above (failures at step 4 were not observed). Failures at step 1 were failing to form a hairpin arrangement. When the left or right segment was not sufficiently stretched, it curled faster than the middle section, so the strip could not formed a hairpin (Fig. 3.9a). Failures at step 2 happened when the middle section was not evenly stretched, skewed toward one direction and twisted, so the left and right segment could not cross to form a loop (Fig. 3.9b). Failures at step 3 were always resulted from a small loop formed by the left and right segment, so neither segment could enter the loop and completed a knot (Fig. 3.9c).

An earlier study demonstrated a surgical suture fiber made from multiblockcopolymers that tightened at elevated temperature.[71] However, this self-fastening knot required the knot to be made by hands. My self-tying knot design eliminates manual intervention completely and is able to complete both the knot formation and fastening steps in sequence by leveraging strategic arrangement of bimorph segments and other supplementary structures (solid ends and joints).

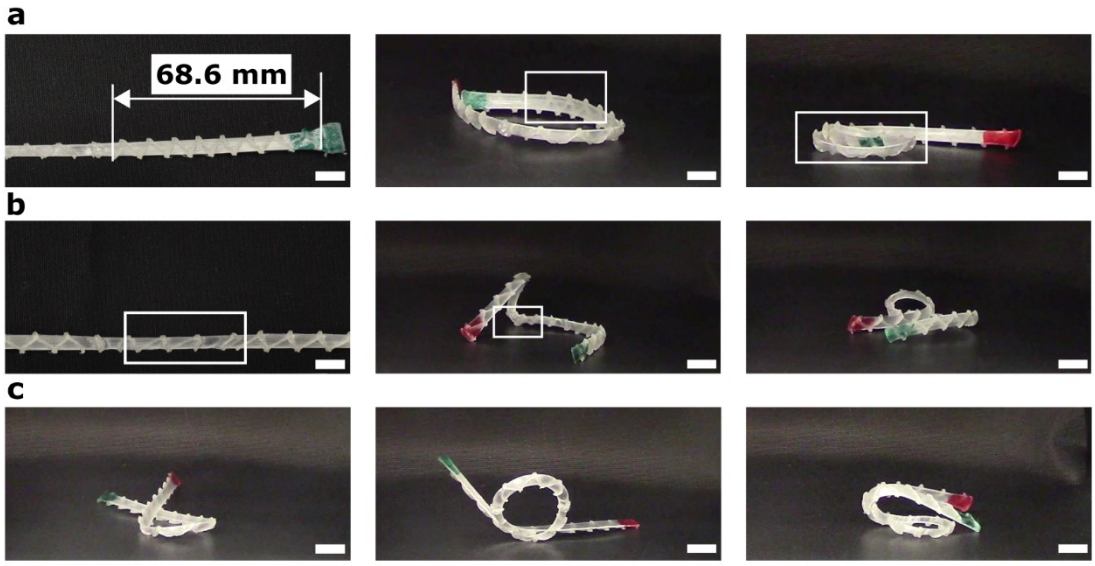

Fig. 3.9 The self-tying process may fail at different steps. (a) Failure at step 1. The highlighted green end segment was expected to be stretched to 8 cm. It was not properly stretched and only reached the length of 6.86 cm. Then it curled earlier than the middle segment, so the strip could not form a hairpin shape. This segment further curled into a spiral without interaction with the red end segment. **(b)** Failure at step 2. The middle section was not evenly stretched, so it twisted the direction of the left and right segments, which could not form a loop. **(c)** Failure at step 3. The two segments formed a loop, then the green end segment failed to enter the loop to form a knot.

3.4 Conclusions

This chapter presented mechanical actuators combining the shape memory properties of PLA and intricate structures created by 3D printing. The shape programming process was accomplished by stretching samples using a pair of pliers and did not require additional mechanical devices, which made the production of these actuators possible virtually in any laboratory settings. Mechanical stretching controlled the recovery curvatures, which have been applied to develop mechanical actuators that can pick up object as a gripper or tie a knot without manual intervention.

CHAPTER IV

2D TO 3D SHAPE MORPHING VIA EMBEDDING PROGRAMMED INTERNAL STRESS

4.1 Introduction

Existing methods to product shape-morphing elements [1, 32, 38, 39] are not available for wide adaptions outside academic settings owing to their needs for customized manufacturing tools, complex fabrication procedures, and specific compositions of multiple materials. Here, I present commercially available 3D printing (FDM) of domains with prescribed internal stresses in planar 2D PLA substrates that enable fast and programmable transformations into a desired 3D shape via heat actuation.

4.2 Shape transformation characterization

4.2.1 Overview

Shrinkage and warpage occur in the production of injection molded parts with controlled size and shape.[72-74] These shape deformations are caused by residual stresses that are generated during and after the molding process. Similarly, the filament extrusion process in FDM embeds residual stresses in a similar manner. The thermoplastic in the extruder is heated at its melting point and is in an amorphous random-coil state. Upon extrusion, the polymer is sheared and elongated, and then solidifies (cooled to room temperature) rapidly before the molecules are able to re-attain an equilibrium state. Flow-induced residual stresses are therefore embedded, which are released upon re-heating the part above its glass transition temperature. Consequently, the printed parts shrink and/or warp. Shrinkage and warpage are pronounced in amorphous polymers and can be tuned by increasing crystallinity. [75] When the shrinkage is uniform, the printed parts simply

become smaller and remain flat. In contrast, non-uniform shrinkage leads to sample warpage.

Shrinking and warping behaviors are controlled by internal factors and external factors. Internal factors refer to material properties, such as molecular weight, glass transition temperature, and thermal conductivity, which are constants in my work because PLA was chosen as the material of interest. External factors will be discussed here, including printing parameters such as printing speed, infill pattern, and sample dimension. To be noted, the layer thickness setting of the printer was set to 0.1 mm for samples used in this chapter.

4.2.2 Residual stress induced birefringence

Residual stresses make the polymer optically anisotropic and cause birefringence that allows light to be transmitted through crossed polarizers.[76] To quantify birefringence induced by residual stresses, test samples were made with various printing speeds (2400, 4800, 7200, or 9600 mm/min) and examined under crossed polarizers (Fig. 4.1). The color difference represented the different levels of residual stresses generated by the printing process.

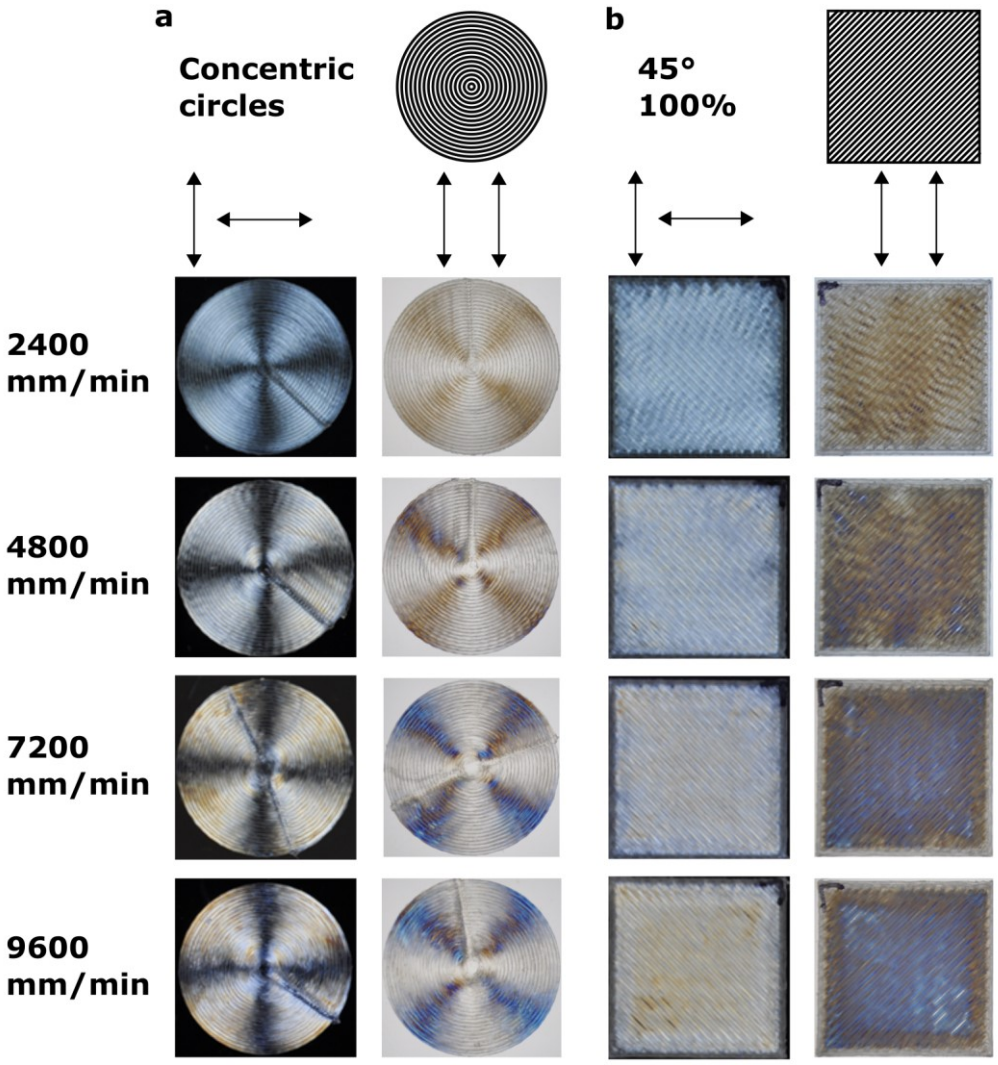

Fig. 4.1 Printed samples with straight lines or concentric circles printing path displayed birefringence patterns when observed with a pair of polarizers. Samples were printed with different printing speeds: 2400, 4800, 7200, or 9600 mm/min. **(a)** Infill pattern: concentric circles. Sample dimension: diameter 20 cm, thickness 0.8 mm. **(b)** Infill pattern: 45°, 100% infill. Sample dimension: 20 x 20 x 0.8 mm.

4.2.3 Printing speed

To quantitatively present the influence of the printing speed on residual stresses, PLA strips (10 x 5 x 0.8 mm, Fig. 4.2b) were printed at different speeds (2400, 4800, 7200, or 9600 mm/min) with 100%, 0° infill (longwise infill, Fig. 4.2a). The samples were placed in an oven at 80 °C or 100 °C for one minute and shrank in length (Fig. 4.2c).

The deformation process was recorded in videos. One frame per second was extracted from each video and analyzed to obtain the sample length as a function of time. The original length was $L0$, and the length after shrinking was $L1$. The strain was calculated from $(L0 - L1)/L0$ and plotted along time. The contracted strain increased with the printing speed (Fig. 4.2d) and heating temperature (Fig. 4.2e).

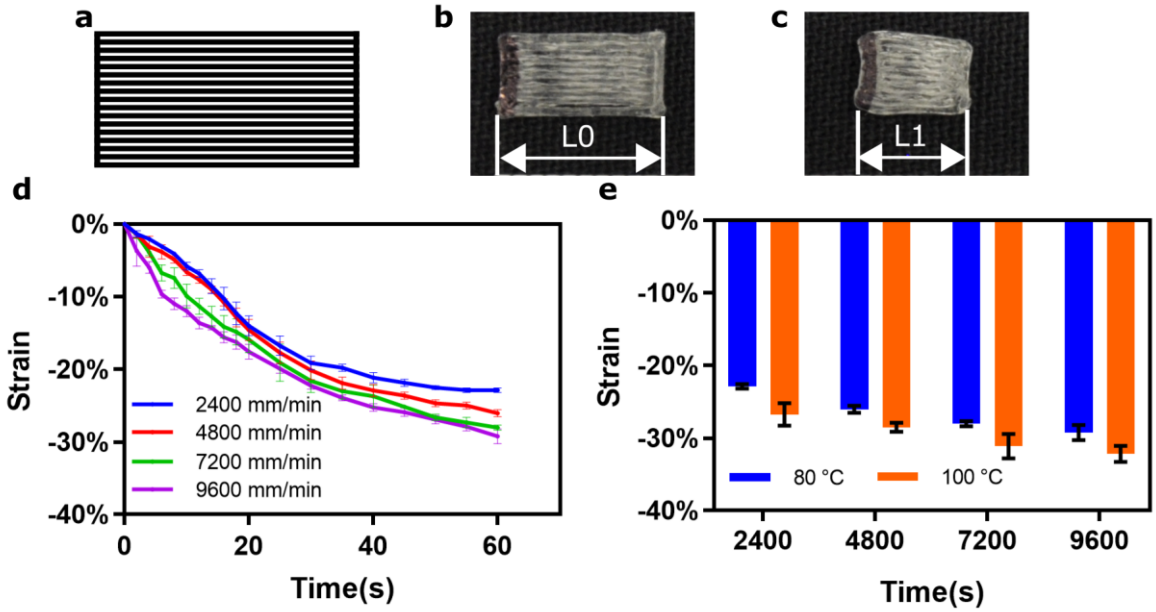

Fig. 4.2 Strip-shaped samples shrank in length at elevated temperature. (a) Printing path. The infill is 100%, 0°. **(b)** Sample before heating in its original length $L0$ = 10 mm. **(c)** Sample before heating in its original length $L1$ = 6.6 mm. This sample was printed at 9600 mm/min and heated at 80 °C for one minute. **(d)** Strain of samples printed with different speeds increased over time. **(e)** Strain of samples printed with different speeds and heated at 80 or 100 °C for one minute.

4.2.4 Bilayer structure

Square samples (2 x 2 cm) had a bilayer structure (Fig 4.3a). The top layer had 40%, 60%, 80%, or 100%, 45° and -45° rectilinear infill (Fig. 4.3b); the bottom layer had 100%, 90° infill (Fig. 4.3c). Both layers had the same thickness with each layer measuring 0.4 or 0.6 mm. The samples were printed at 2400, 4800, 7200, or 9600 mm/min. After being heated at 80 °C for one minute, the squares warped toward the top layer and formed an arc

shape, which was matched to part of a circle. The radius of the arc, R and the degree of curvature, φ were measured to quantitatively define the arc (Fig. 4.3d). Smaller top layer infill, higher printing speed, and smaller sample thickness decreased R and increased φ (Fig. 4.3e, f). Samples made 100% top layer infill/2400 mm/min printing speed condition rendered a shallow dome shape (large radius, small degree of curvature), while samples made with 40% top layer infill/ 9600 mm/min printing speed condition led to a complete roll (small radius, large degree of curvature). Regardless of the top layer infill, 1.2 mm thick (0.6 mm per layer) made at 9600 mm/min warped into a shallower dome shape compared to samples of 0.8 mm thickness (Fig. 4.4).

The arrangement of three segments of bilayer structures in order produced a wavy band upon warping. Each segment had a 40%, 45° and -45° rectilinear top layer and a 100%, 90° infill bottom layer, and warped to a roll independently towards the top layer. Three connected segments formed a wavy shape.

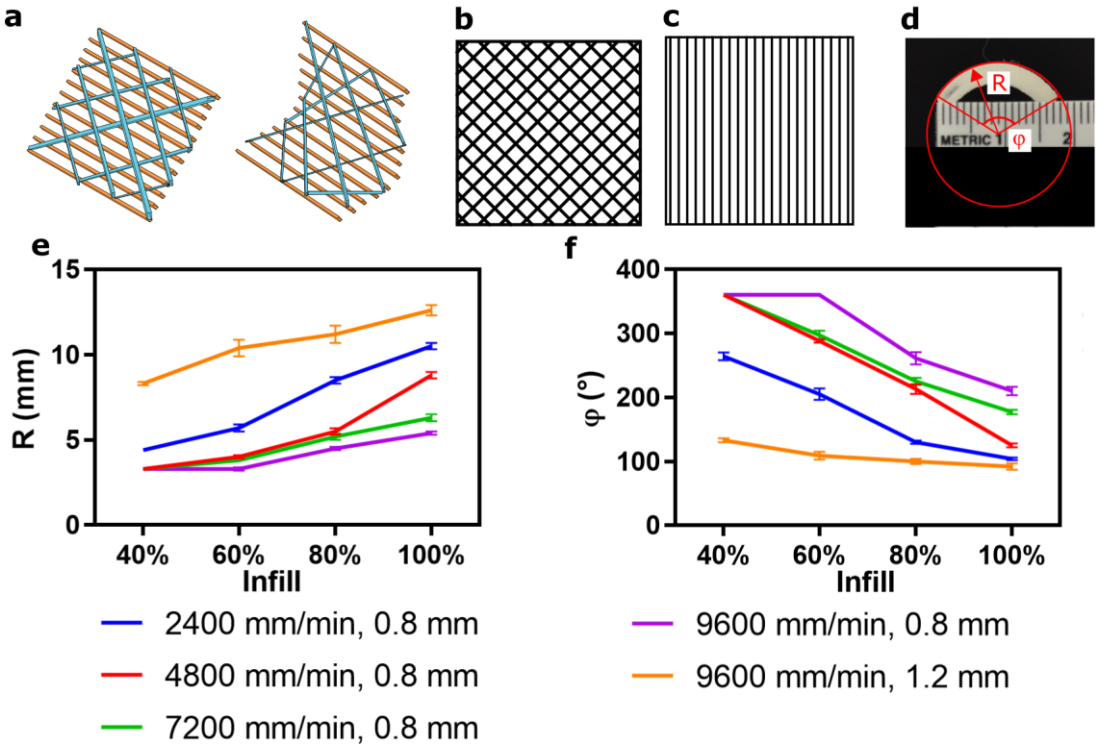

Fig. 4.3 Bilayer square samples warped to an arc shape. (a) Bilayer squares. Left: as printed. Right: after warping. **(b)** Printing path of top layer: 45° and -45°, 40% to 100%. **(c)** Printing path of bottom layer: 90°, 100%. **(d)** Deformed sample in an arc shape, characterized by the radius of the arc R and degree of the curvature φ. **(e)** The radius of the arc R increased as infill increased, printing speed decreased, or sample thickness increased. **(f)** Degree of the curvature φ decreased as infill increased, printing speed decreased, or sample thickness increased.

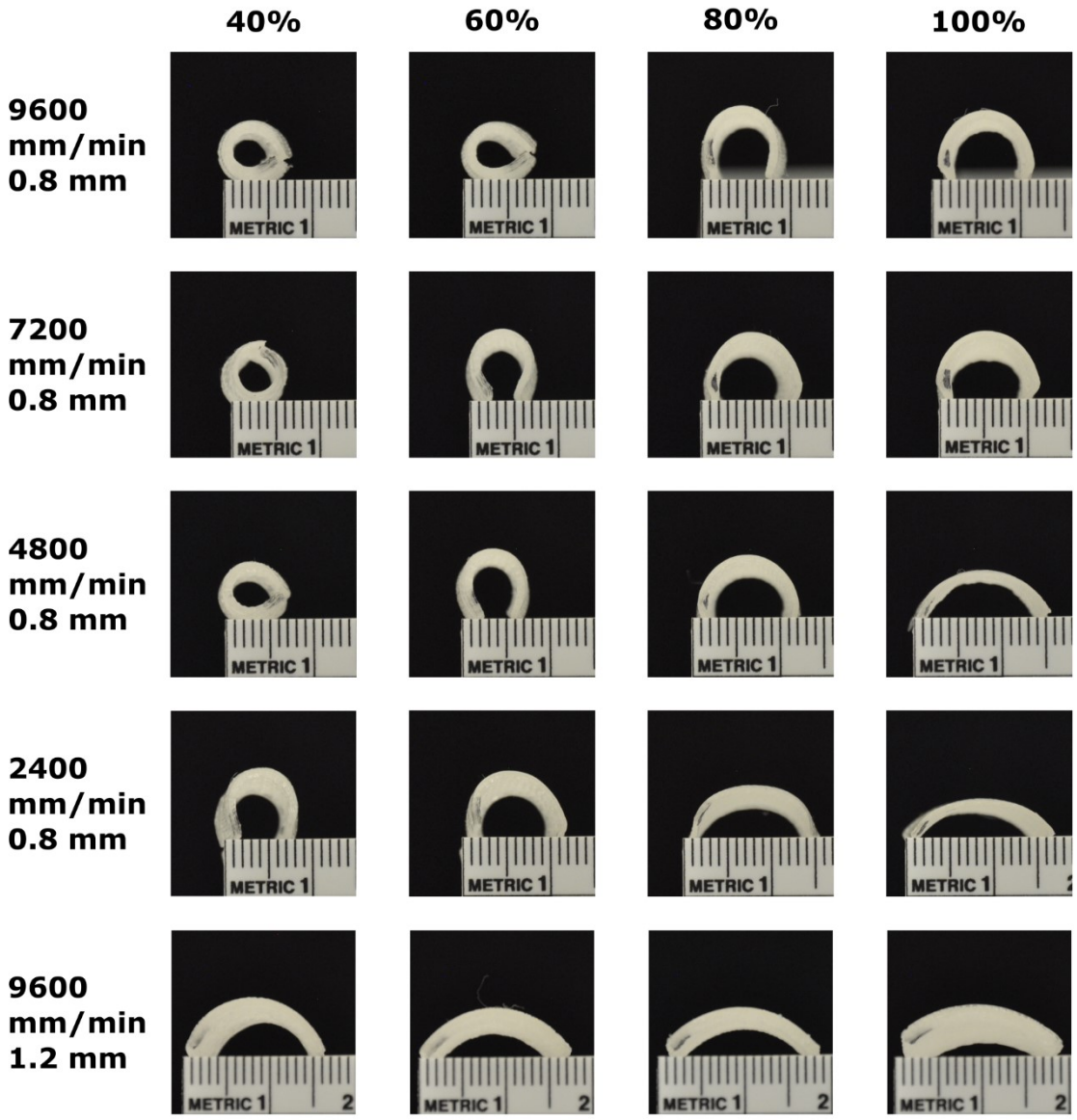

Fig. 4.4 A complete matrix of warped samples of different top layer infills, printing speeds, and thicknesses. Smaller top layer infill, higher printing speed, and smaller sample thickness decreased R and increased φ.

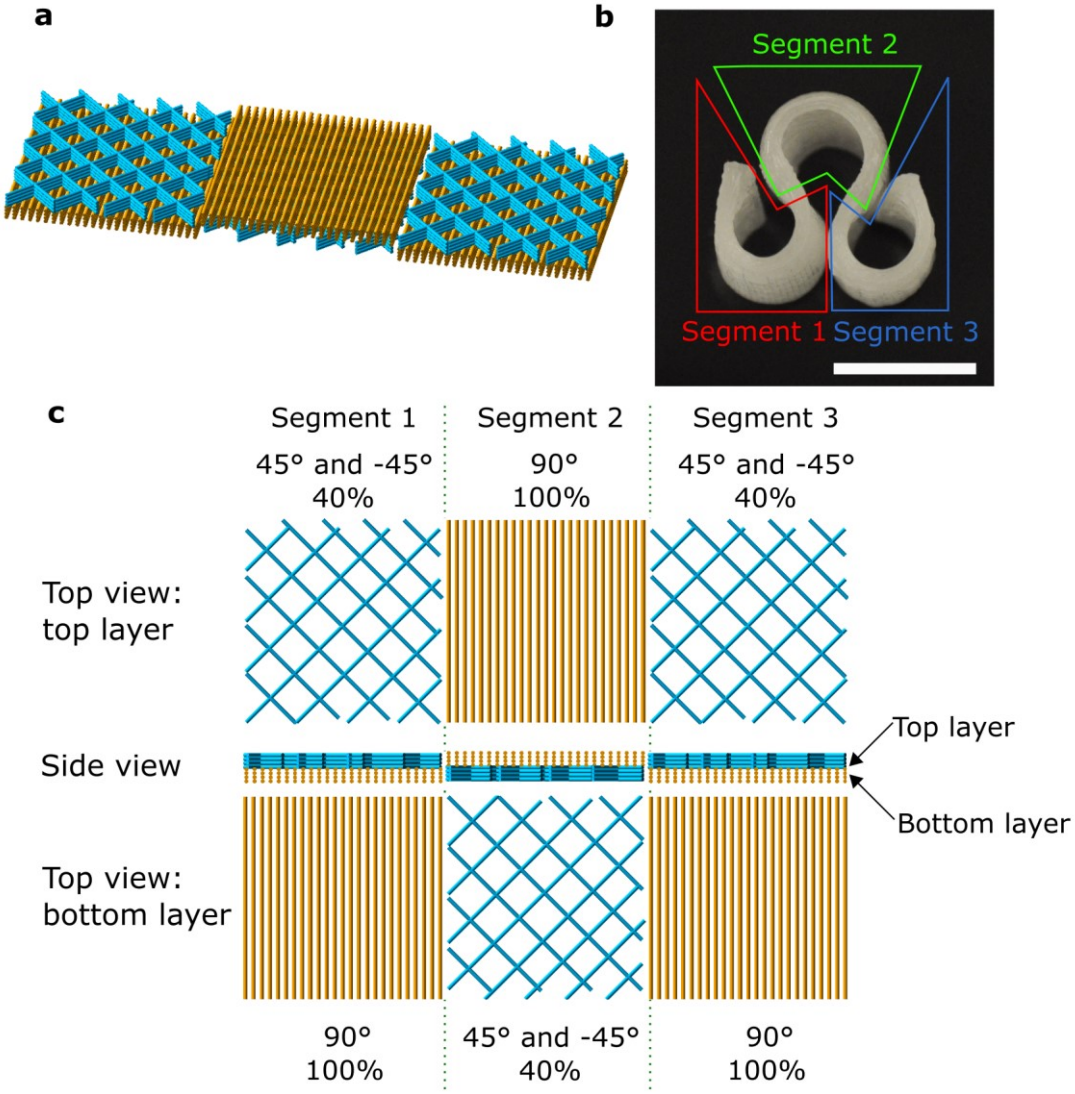

Fig. 4.5 A sample consisted of three bilayer segments warped to a wavy band shape upon heating. (a) Diagonal view of printing path. Three squares connected together with alternating patterns. **(b)** Each segment formed a roll and warped independently. **(c)** Side view and top view of printing path. Scale bar, 1 cm.

4.2.5 Concentric circles

Disk-shaped samples (diameter 20 mm, thickness 0.8 mm) were printed at 2400, 4800, 7200, or 9600 mm/min with a concentric circle infill pattern. After heating at 80 °C for one minute, each circle in the infill pattern contracted, reduced in radius, and pushed the adjacent inner circle towards the center of the disk. Eventually, the circles were pushed upwards, and the disk samples formed a dome shape (Fig. 4.6a). The dome shape was

characterized by measuring its height, *H* and radius, *R* (Fig. 4.6b). The printing speed formed a linear relationship with both *H* and *R*. Samples made with a faster printing speed contracted more and warped to a dome with a larger height and a smaller radius (Fig. 3.6c). The volume of the dome was constant regardless of the printing speed (481±1 mm^3).

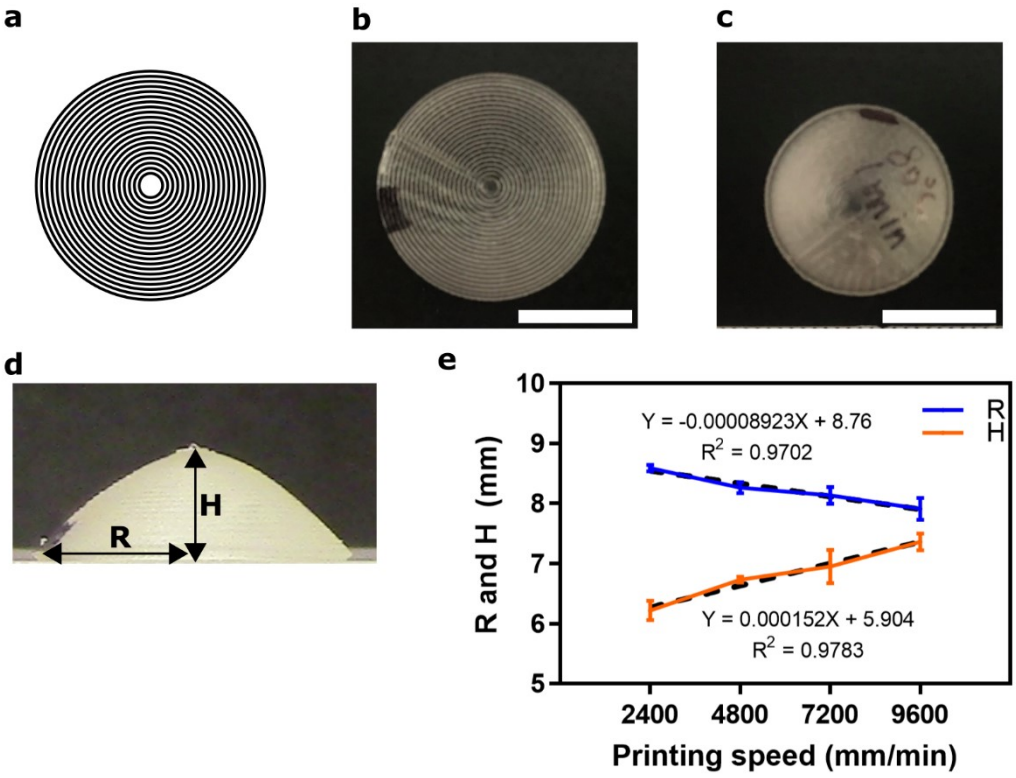

Fig. 4.6 Disk-shaped samples warped to a dome. (a) Printing path. **(b)** Printed sample. **(c)** Warped sample. Sample size: diameter 20 mm, thickness 0.8 mm. **(d)** Side view of a warped sample, showing the height and radius. **(e)** Height and radius comparison of samples with different printing speeds. Scale bar, 1 cm

4.2.6 Wavy edges

A circular edge was added to the concentric circle samples to present wavy edges (Fig. 4.7a, b). Two measurements were taken to quantify the waviness: maximum amplitude, *H* and wavelength, *L* (Fig. 4.7c). Three parameters were tested: the number of compartments in edges, thickness of the edges, and printing speed. The printing speed did not affect the wavy features. One possible explanation was that the edge infill was as short as 0.5 cm, so

the flow-induced residual stresses were not dominant. The number of compartments did not influence the wave maximum amplitude but affected the wavelength. The wavelength in 12-compartment samples were slightly longer and less consistent than the one in four-compartment samples (Fig. 4.7d). The edge thickness played a critical role in determining the wave features. Thin edges (0.2 mm thick) had eight to 12 waves, while thick edges (0.4 mm thick) produced three to five waves. Consequently, waves in thin edges had a smaller maximum amplitude and shorter wavelength compared to those in thick edges (Fig. 4.7e, f).

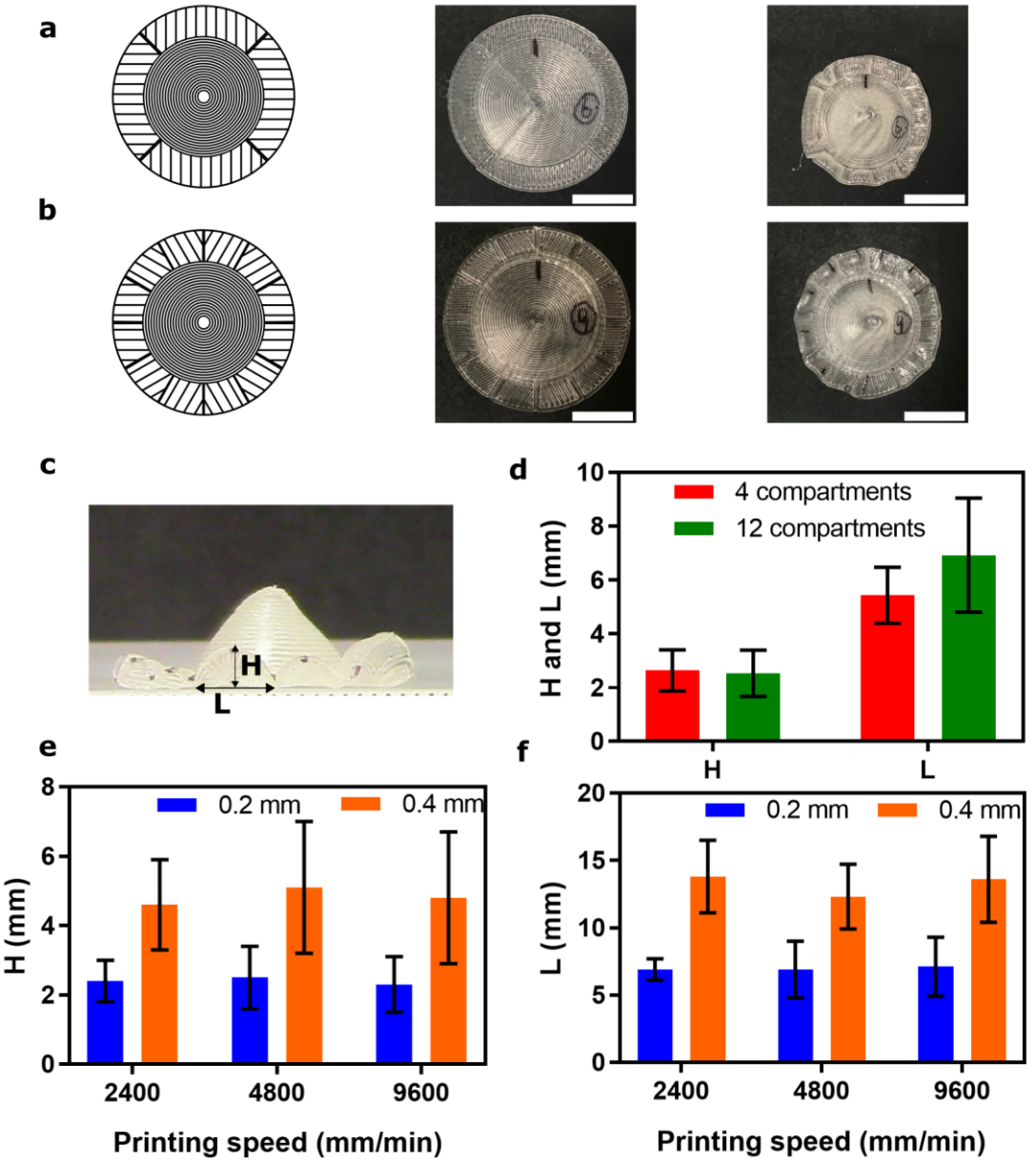

Fig. 4.7 Narrow edges transformed to wrinkled and wavy features upon heating. (a) 4-compartment sample. From left to right: printing path, printed sample, warped sample. Diameter 30 mm, diameter of the center 20 mm, center thickness 0.4 mm, edge thickness 0.2 mm. **(b)** 12-compartment sample. From left to right: printing path, printed sample, warped sample. Diameter 30 mm, diameter of the center 20 mm, center thickness 0.4 mm, edge thickness 0.2 mm. **(c)** Side view a warped sample, showing the wave maximum amplitude and length. **(d)** Wave maximum amplitude and length comparison for samples with different numbers of compartments. Printing speed: 4800 mm/min. Center thickness: 0.4 mm, edge thickness: 0.2 mm. **(e)** Wave maximum amplitude comparison of samples with different edge parameters. **(f)** Wave length comparison of samples with different edge parameters. **(e)(f)** Center thickness 0.4 mm, 12 compartments.

4.3 Application: replication of natural morphologies

Formation of curved topologies in the petals of flowering plants is of interest because they embed multiple levels of curvatures that are challenging to replicate.[77, 78]. For example, a lily (*Lilium orientalis*) has six petals (which are, botanically speaking, three inner petals and three outer sepals) (Fig. 4.8a, b) that share the following three features: outward bending, wrinkled edges (Fig. 4.8c), and a curved midrib (Fig. 4.8d). These curved surfaces emerge from a 2D surface as the plant grows. Moreover, they are difficult to reproduce using conventional fabrication methods (e.g., FDM requires the use of sacrificial support materials). These challenges can be overcome by using residual stresses to morph a 2D surface into a 3D surface upon heating.

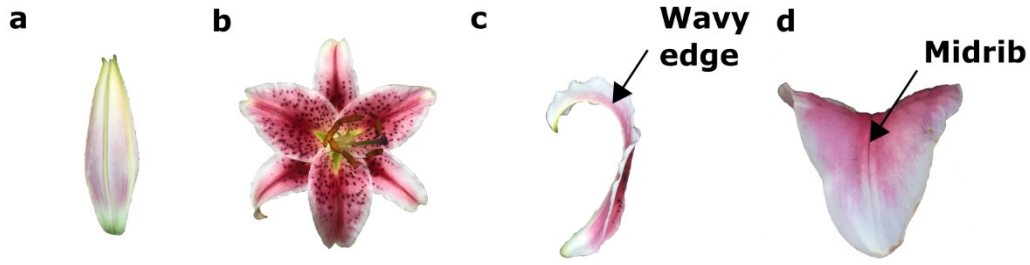

Fig. 4.8 Petals of a bloomed lily (*Lilium orientalis*) displayed features of wavy edges and a midrib. (a) A bud. **(b)** A fully bloomed lily. **(c)** A petal side view showing wavy edges. **(d)** A petal front view showing the midrib.

To demonstrate this, an artificial petal was constructed consisting of three parts: a stub, a center, and an edge (Fig. 4.9a). The stub had a 100% infill and connected the petal to a base with six slots arranged in two circles (Fig. 4.9c) to mimic the arrangement of petals (Fig. 4.9b). The center and the edge were designed to mimic the midrib and curvy edges.

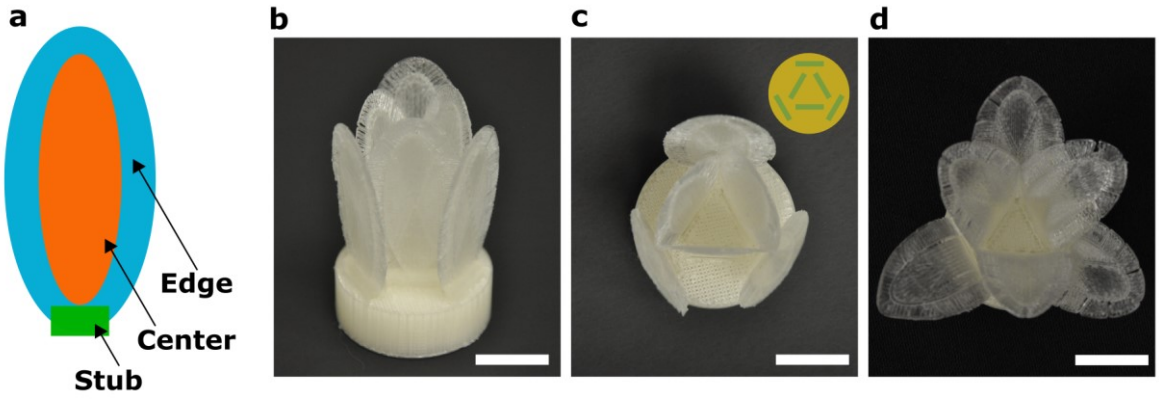

Fig. 4.9 Assembled shape morphing structures resembling bloomed lily morphologies. **(a)** Each petal consists of three parts: a stub, a center, and an edge. **(b)** Side view of an assembled lily. **(c)** Top view of an assembled lily. Inset: CAD model of the base. **(d)** A bloomed lily. Scale bar, 1 cm.

The center was expected to bend outward, so it had a bilayer structure: a 0.6 mm thick top layer and a 0.2 mm thick bottom layer. The bottom layer had a 100% infill aligned lengthwise (0°) and acted as a support and faced outwards (away from the central axis of the flower). The top layer had three designs (Fig. 4.10a, b, and c). The 0° design had a 100% infill along the long edge of the petal (0° infill, Fig. 4.10a) and created a simple curved feature without the midrib. The 90° design had a 100% infill along the short edge (90°, Fig. 4.10b) of the petal and generated a curved feature plus a lump at the center of the petal. The 90°/0° design consisted of four sections with a 100% infill aligned either lengthwise or crosswise (Fig. 4.10c). Each compartment formed a curved surface individually. This design was chosen because it presented the closest resemblance of the midrib of a real petal.

The edge was expected to create the effect of wavy edges and had two parameters: thickness and number of compartments. The edge functioned in the same way as edges of concentric circles discussed in section 4.2.6, in which thinner edges with more compartments produced waves with more variations in wavelength and height. Similarly,

the 8-compartment samples formed waves with less variation (Fig. 4.10d) than the 16-compartment samples (Fig. 4.10e). The 0.2 mm thick edge (Fig. 4.10f) produced more variation in the wavelength and height compared to the 0.4 mm thick edge (Fig. 4.10g). Consequently, 16-compartment and 0.2 mm edges were used in the final design of the petal, as this combination produced wavy edges that looked more natural (small nonuniform waves). The assembly of six petals deformed into the status resembling a blooming lily upon heating at 80 °C after two minutes (Fig. 4.9d).

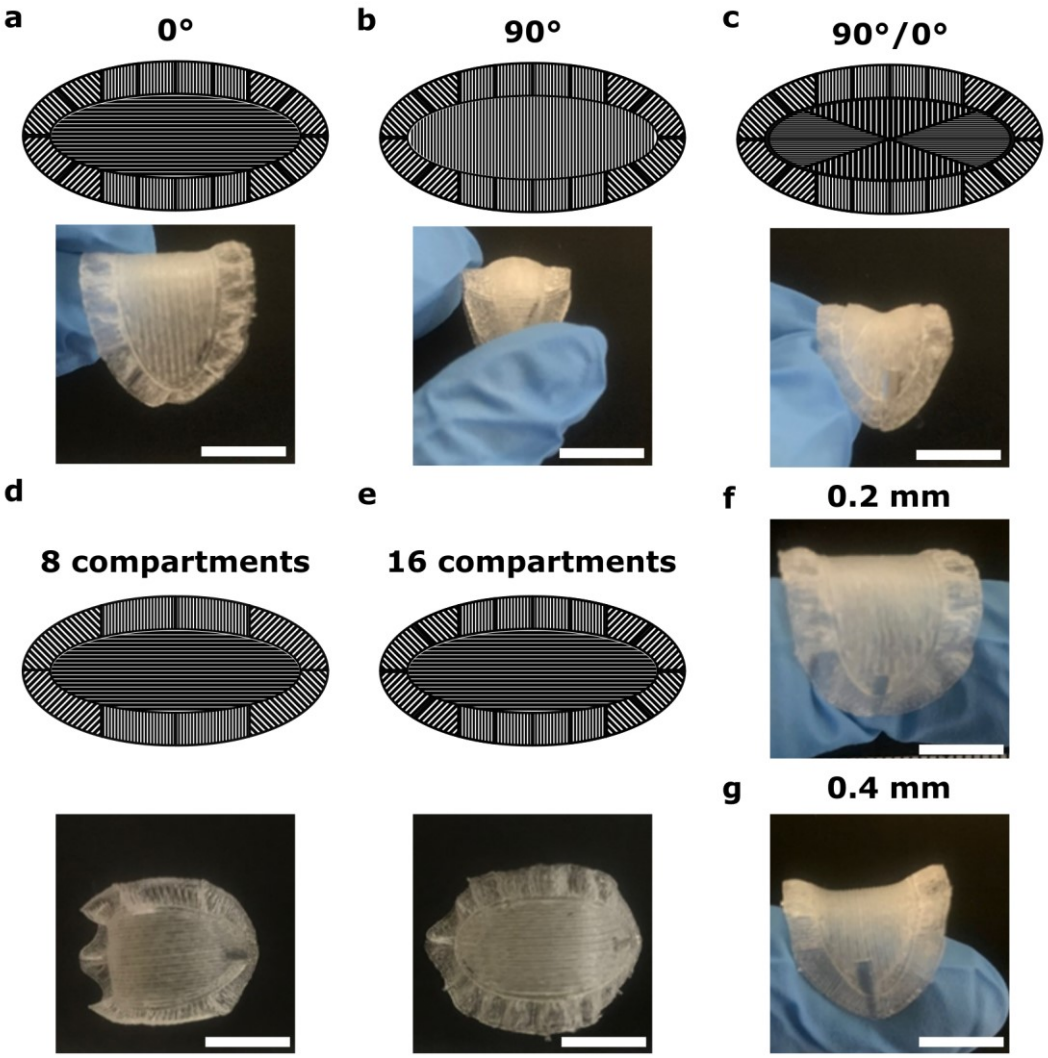

Fig. 4.10 Shape morphing structures replicating hierarchical structures of a flower petal. (a) (b) (c) Printing path and warped surface of petal designs with different center patterns. **(a)** 0°. **(b)** 90°. **(c)** 90°/0°. **(d) (e)** Printing path and warped surface of petal designs with different edge patterns. Center pattern: 0°. Edge thickness: 0.2 mm. **(d)** 8 compartments. **(e)** 16 compartments. **(f) (g)**Warped surface of petal designs with different edge thickness. Center pattern: 0°. 16 compartments. **(f)** 0.2 mm. **(g)** 0.4 mm. Scale bar, 1 cm.

4.4 Conclusions

This chapter presented a simple and accessible approach to produce responsive materials via commercially available FDM with single material PLA. This process eliminated the need for customized 3D printing technologies and specific composited material that were employed in other soft material studies and suggested potential for

widespread adoption of soft mechanical systems beyond laboratory settings. Internal stresses were embedded in PLA components through prescribed deposition of filaments. By characterizing the release of internal stresses upon exposing to a temperature above the glass transition point, planar 2D surfaces with designed infill patterns were able to actuate into programmed 3D morphologies. This controllable and programmable shape morphing enabled construction of a library of active components. Arrangement of these components mimicked hierarchical structures found in living systems (e.g., lily), which were challenging to replicate artificially owing to their unique complexity.

CHAPTER V

LITHOGRAPHY-FREE FABRICATION OF PLA MICROFLUIDIC DEVICES WITH EMBEDDED MICROSCALE CRYSTAL MORPHOLOGIES VIA ENZYMATIC MACHINING AND 3D PRINTING AIDED ASSEMBLY

5.1 Introduction

Flow behavior at the microscale is significantly different than at the macroscale and inspire numerous studies for its momentum, heat, and mass transfer principles. These findings lead to a need for microfluidic components with accurate dimensions produced in an accessible and effective way. Polymers are strong material candidates for microfluidics devices due to their wide range of properties (mechanical, optical, and chemical), low price, and adaptation to a myriad of fabrication approaches, among which soft lithography is prevalent. However, soft lithography is typically carried out in cleanroom facilities and requires dedicated instruments (e.g., plasma cleaner, spin coater) and personnel training for cleanroom operation. An alternative fabrication approach to overcome these challenges is enzymatic etching. Here first presents a review of biodegradable polymers and enzymatic degradation pathways. Next, a lithography-free approach (Fig. 5.1) to manufacture biodegradable PLA-based microfluidic devices with embedded crystal structures through enzymatic etching, vacuum aided bonding, and 3D printing is introduce

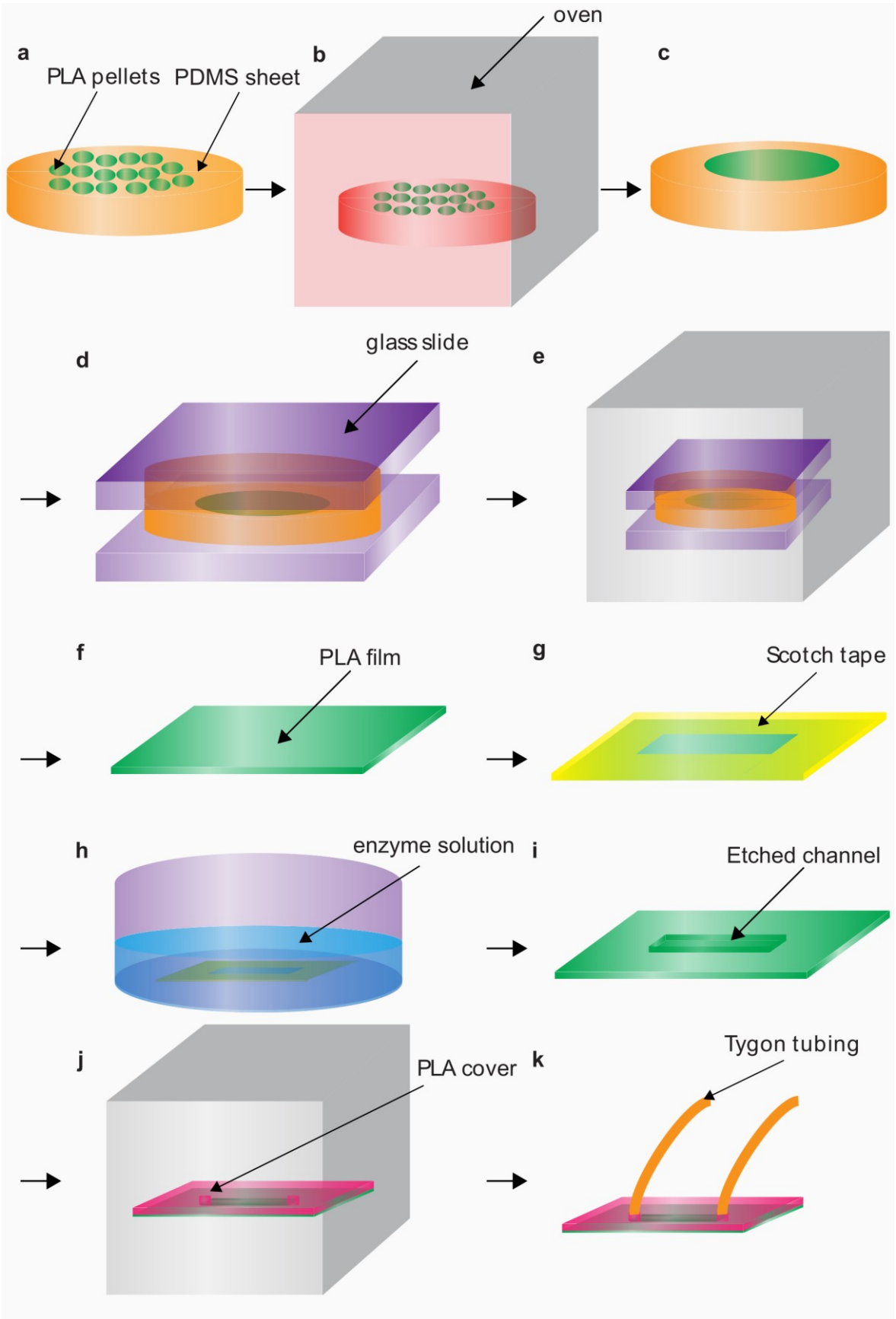
a
PLA pellets
PDMS sheet
b
oven
c
d
glass slide
e
f
PLA film
g
Scotch tape
h
enzyme solution
i
Etched channel
j
PLA cover
k
Tygon tubing

Fig. 5.1 Overview of a lithography-free fabrication procedure of PLA microchannels with embedded microscale crystal morphologies via enzymatic etching, vacuum aided bonding, and 3D printing aided assembly. (a) PLA pellets were placed on a PDMS sheet and weighed. **(b)** Pellets were melted in an oven at 180 °C for 90 minutes. **(c)** Pellets melted and formed a thin layer of molten polymer. **(d)** Another piece of PDMS was placed on top of the melted polymer. Square glass slides were used to sandwich the PDMS sheets and the melted PLA. The whole assembly was secured with binder clips. **(e)** The assembly was heated in an oven at 180 °C for 30 minutes. **(f)** The melted PLA was pressed into a flat and thin film (thickness1 mm). **(g)** The film was wrapped with Scotch tape, and a rectangular shaped area in the center was left uncovered by the tape. This unwrapped area was to be etched. **(h)** The wrapped film was etched in proteinase K aqueous solution at 37 °C for several hours. **(i)** After etching, the tape was removed, and the etched part became a channel on the film surface. **(j)** The film with the etched channel and a 3D printed flat PLA piece with ports were stacked and sealed in a plastic pouch through vacuum. The sealed pouch was heated in an oven at 80 °C for 15 minutes. **(k)** Tygon tubes were inserted in the ports of the cover. Then the ports were sealed with the epoxy glue.

5.2 Biodegradable polymer

Biodegradable polymers refer to a group of polymers that fragment, degrade, and/or lose mechanical properties through chemical decomposition when exposed to enzymes secreted by living organisms, primarily bacteria and fungi, and occasionally mammal organs.[79, 80] Their degradability has inspired applications that include reducing packaging waste,[81-83] increasing biocompatibility of medical devices (e.g., wound dressing, medical implants),[84, 85] and optimizing crop yield and pest control in agriculture.[86, 87] Major groups of biodegradable polymers include polyesters, polyamides, and polysaccharides. This chapter focuses on polyesters that including PLA.

5.2.1 Poly (lactic acid) (PLA)

PLA was first synthesized through polycondensation of lactic acid by Théophile-Jules Pelouze in 1845.[88] In current industrial productions, the PLA synthesis process has three steps: (1) fermentation of corn or sugar feedstocks to yield lactic acid, (2) thermal and catalytical conversion of lactic acid to lactide, and (3) ring-opening polymerization of lactide to PLA.[89, 90]

The structure of monomer lactic acid is similar to alanine. Alanine-alanine linkages are easily cleaved by proteinase K (PK), a serine protease. Consequently, the ester bonds in PLA are susceptible to etching by PK. In the early 1980s, PK was reported for the first time as an effective degradation agent for PLA,[91] leading PLA to be intensively studied as a biodegradable polymer ever since.[92-95] The etching process starts when PK contacts the PLA surface. The formation of enzyme-substrate complexation accelerates surface reactions and yields small molecules of PLA fragments, which are hydrolyzed then released into the bulk enzyme solution along with the dissociated PK.

The contact between PK and the PLA surface triggers the enzymatic degradation process, and PLA crystal structure affects the degradation rate. PLA crystallinity is determined by the monomer optical form and thermal history. PLA monomers exist in two optical forms: L-lactide and D-lactide. Poly L- lactide (PLLA) is semi-crystalline, and poly D-lactide (PDLA) is amorphous. PLLA has a melting point of 175 °C [92] and a glass transition temperature of approximately 65 °C (ranging from 55 to 67 °C).[69, 70] Amorphous PLLA develops crystal domains under isothermal crystallization between 80 °C and 130 °C. During the etching process of semi-crystalline PLLA, PK has a propensity to degrade amorphous regions more efficiently than crystal domains. The decrease in the degree of crystallinity from 50% to 0% yielded a ten-fold increase in the material degradation rate.[96] Consequently, PK becomes an attractive agent for the design of microscale crystal morphologies on PLA substrates through selectively removing amorphous regions.

5.2.2 Poly (butylene adipate) (PBA) and copolymer

PBA and its copolymers have been degraded by enzymes secreted by microorganisms.

There are three main factors contributing to the various enzymatic degradation behaviors: (1) the polymorphic crystal structures of PBA, (2) the structure and composition of the copolymer, and (3) the properties of enzymes.

The first parameter that affects degradation rate is the crystal structures of PBA, which are determined by the temperature of isothermal crystallization from molten status.[97] PBA forms α crystals (flat-on lamellars) and ß crystals (edge-on crystals) at temperatures above 32 °C and below 27 °C, respectively. In mixed crystal structures, higher α crystal composition corresponded to a faster biodegradation rate under the effect of *Pseudomas sp*., a commercially available lipase.[98]

Another contributor to degradation efficiency is the aromatic components in PBA copolymer. In general, aromatic components slowed down the degradation process because of their rigid backbones. In poly butylene adipate-butylene terephthalate (P(BA-co-BT)), the benzyl group in butylene terephthalate enhanced degradation by decreasing the lamellar thickness and crystallinity. In contrast, rigid backbones in the benzyl group protected substrates from enzymes and reduced degradation. The combination of these two contrary effects yielded a low degradation rate expressed in weight loss.[99] A similar result was also reported by U. Witt and coworkers [100] in 1997 with an enzyme secreted from microorganisms that grew on BTA films (copolyester of 1,4-butanediol, dimenthyl adipate, and dimenthyl terephthalate). The degradation rate of the BTA films dropped from 10 to 5 μm/week when terephthalic acid mole percentage increased by 17%.

Enzyme properties also affect degradation behaviors. In addition to the aforementioned lipase from *Pseudomonas sp.* (PsL), lipases from *Thermobifida fusca* (TfH) and *Aspergillus oryzae* (AoL) were also capable of degrading PBTA (polyester of 1.4-

butanediol, dimenthyl terephthalate, and adipic acid) by breaking the ester bond. TfH was proven to be the most efficient by reaching 100% ester cleavage by cutting ester bonds and dissolving detached esters, compared to 40% achieved by PsL and AoL. [101]

5.2.3 Poly(ethylene terephthalate) (PET)

Interest in PET has intensified over the last couple of decades owing to the need for accelerating the decomposition of PET-based disposable products (e.g., plastic bottles, utensils, plastic with code number 1 in the ASTM International Resin Identification Coding System).[102] As an aromatic polyester with rigid backbones, PET has been traditionally considered inert in response to a biological attack. However, three major groups of enzymes have shown potential in degrading PET, including lipase,[103-105] cutinase,[106] and hydrolase.[107] Furthermore, an induction process successfully developed enzymes from *Penicillium funiculosum* [108] and *Thermobifida fusca*.[103]

Same as the PK/PLA pair, the activity of these enzymes showed selectivity toward the PET crystallinity. Biaxially oriented PET films (35% crystallinity) and low crystallinity PET films (7% crystallinity) were incubated with cutinases from *Humilica insolens* (Hic) at 70 °C, *Pseudomonas mendocina* (PmC) at 50°C, and *Fusurium solani* (FsC) at 40 °C.[106] HiC, PmC, and FsC showed a 25, 10, and 6 fold increase of activity, respectively, when reacted to low crystallinity PET. Vertommen *et al.* observed a lower hydrolytic activity of FsC on semi-crystalline PET (48% crystallinity) compared to the activity on the amorphous substrate (4% crystallinity).[109]

5.2.4 Polycaprolactone (PCL)

The study of PCL degradability dates back to the early 1970s.[110] PCL is degradable in soil, and a wide variety of microorganisms capable of degrading PCL have been

isolated,[111] including bacteria [112, 113] and fungi.[114-121] Enzymes capable of degrading PCL include cutinases and lipases. Interestingly and in contrast, lipases from *Candida antartica* [122] and *Candida rugosa* [123] aided PCL synthesis.

PCL crystallinity affects the degradation rate.[124-126] Low crystallinity amorphous regions are degraded prior to the degradation of high crystallinity crystal domains. Amorphous regions with loosely packed polymer chains are more vulnerable to enzyme degradation. The effect of crystallinity overrode that of the molecular weight, as samples with a high molecular weight (35,000 g/mol) and low crystallinity (60.5%) were degraded faster than samples with a low molecular weight (18,600 g/mol) and high crystallinity (75.5%).[125]

5.3 Enzymatic etching to create microscale features

Polymers are strong material candidates for microfluidic devices because of their wide range of mechanical, thermal, and optical properties to choose from and their simple manufacturing procedures compared to glass and silicon.[127, 128] The fabrication methods can be broadly classified into two major subgroups (Table 5.1) based on the presence of a template: replicating from a master template (e.g., hot embossing,[129, 130] injection molding,[131, 132] and soft lithography,[133, 134]) and no-template direct machining (e.g., laser ablation [135, 136] and X-ray lithography [137, 138]). However, these approaches pose challenges as they require critical operation conditions (e.g., high temperature to melt polymer), expensive instruments, intensive training (e.g., qualification to work in cleanroom facilities), and corrosive/toxic reagents (e.g., photoresist, hydrofluoric acid). To address these drawbacks, enzymatic etching of biodegradable polymers emerges as a novel fabrication approach of intense interest. Enzymatic etching is

performed in mild conditions in a regular laboratory environment, and the required enzyme is extracted from bacteria/fungi or produced via gene engineering. Further exploration of the enzyme-polymer reactions proves that polymer crystallinity and compositions as well as enzyme species and concentrations controlled the degradation behaviors. Additionally, the use of an inhibitor and/or a recovery agent introduces a new degree of freedom in controlling degradation processes.

Table 5.1 Comparison of different fabrication approaches for polymer microfluidic devices.

Technology	Advantages	Disadvantages
Hot embossing	A rapid process, usually under two minutes; suitable for mass production; a large range of material choices; available for mass production; metal stamps have a long lifetime	Operate at a relatively high temperature to soften the polymer; could not create 3D structures; long cycle time of heating and cooling steps (approximately 10 minutes)
Injection molding	Can create 3D structures; pre-formed elements can be embedded into the final product; suitable for mass production; large range of material choices; metal molds have a long lifetime	High startup cost of the machine; need premade metal molds, metal molds are hard to modify
Soft lithography	Silicone stamps are reusable; elastomer-based final products can bond easily with other plastic or glass substrates to make a sealed device; elastomer-based final products can serve as casting molds for other materials; can create 3D multilayer devices	Requires cleanroom facility to fabricate silicone stamps; high cost and limited device throughput; mainly used in academic settings
X-ray lithography	Product surfaces are smooth; can create high aspect ratio structures; no use of chemicals	High cost; mainly for academic settings
Laser ablation	Minimal heat transfer and no damage to the areas surrounding the spot under laser focus; no premade pattern or mold required; no use of chemicals	Product surfaces are usually rough and have debris that requires additional cleaning; not suitable for surface-sensitive applications because the ablation process changes the surface chemistry

Table 5.2 Degradation rate of different enzyme and polymer substrate pairs.

Enzyme	Polymer	Condition	Degradation rate	Ref.
PK	PLA	Enzyme concentration: 2 μM Temperature: 37 °C Enzyme solution flew pass the surface of the substrate	2 μm/h	[139]
PK	PLA	30 μL of enzyme solution (1 mg/mL) was dropped on substrate surface	600 nm/h	[140]
Depolymerase	BTA(copolyester of 1,4-butanediol, dimenthyl adipate, and dimenthyl terephthalate)		5 - 10 μm/week or 30 - 60 nm/h	[100]
Hydrolase	PET	Temperature: 37 °C	17 μm/week or 0.1 μm/h	[107]
Lipase from *Pseudomonas sp.*	PCL	Enzyme concentration: 1 mg/mL	110 nm/h, erosion of substrate stopped after one hour of contact	[140]

Enzyme etching, as a fabrication tool, has a high yield, high selectivity of substrates, and mild operation conditions, compared to traditional actinic radiation and synthetic chemicals etching.[141] When using an enzyme as an etchant to create microscale and nanoscale features on polymer surfaces, the key challenge is to control the contact between enzyme and substrate regarding location and duration. The development of scanning probe microscopy addressed this issue elegantly. In 1998, via an atomic force microscope (AFM), phospholipase A_2 was first used as an etching tool to create nanoscale channels on dipalmitoylphosphatidylcholine.[142] Later, trypsin was delivered via an AFM cantilever-controlled nanopipets to dried bovine serum albumin (BSA) films.[143] Trypsin etched

holes on the BSA film surface, and the enzyme volume and concentration determined the dimension of the holes. The same group later created nanochannels by using AFM to control nanopipets.[144] This AFM-based method was further developed into dip pen lithography (DPL) (Fig. 5.2a),[145, 146] which is capable of creating patterns on peptides,[147] lipids,[148] polymers,[149] and other substrates.[150] However, the use of AFM increased the fabrication cost and limited its throughput. Then, microcontact printing (μCP) presented a new solution by using pre-structured PDMS stamps to apply ink and create patterns on surfaces, though it is limited by the availability of pre-made patterns (Fig. 5.2b).[151, 152] Polymer pen lithography (PPL) [153-155] combines the advantages of AFM and μCP, using PDMS soft tips to replace AFM tips (Fig. 5.2c). PPL largely reduces the operation cost as the PDMS tips are cheaper, more durable, and can produce complicated patterns with high resolution. In addition to function as enzyme carriers, PDMS molds were also explored as template to control the contact between polymer surface and flowing enzyme streams (Fig. 5.2d).[139, 156]

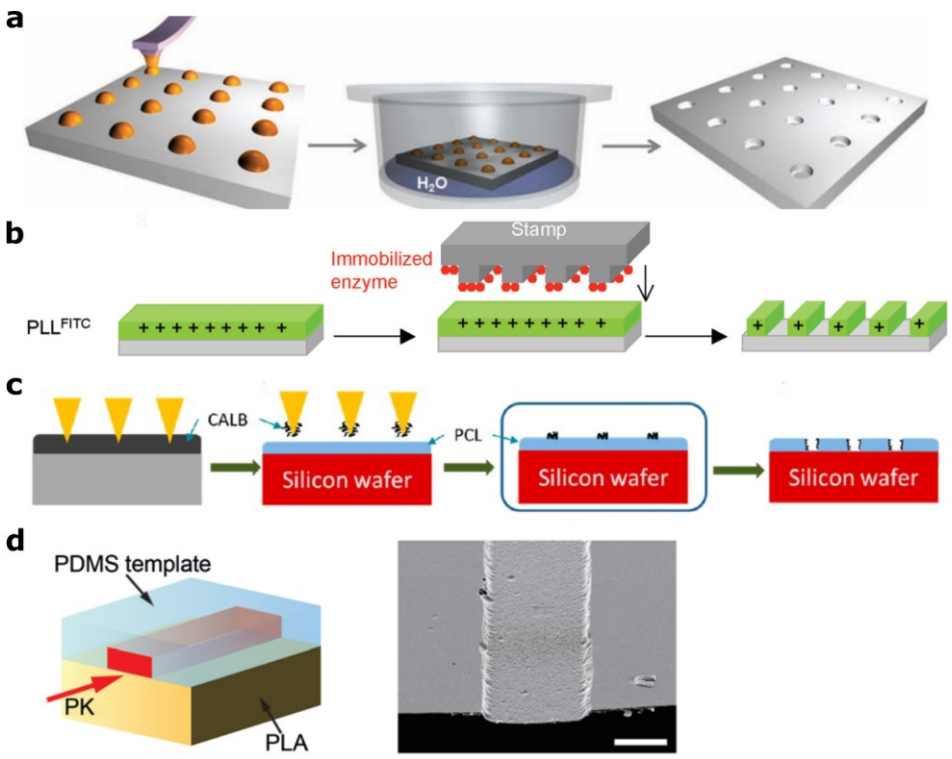

Fig. 5.2 Schematic illustrations of four enzymatic etching processes. (a) The process of patterning PK on PLLA film by agarose-assisted DPL. Enzyme solution was applied to PLLA film surfaces through DPL; the patterned film was incubated; the film obtained biodegraded nanopatterns with arrays of holes (depth 10 - 20 nm, diameter 500 - 1500 nm). Reprinted with permission.[146] **(b)** Enzymatic patterning of PLL films by trypsin using μCP. A thin layer of PLL film was adsorbed on a silicon substrate; a trypsin grafted PDMS stamp with strip patterns contacted the PLL film; trypsin degraded PLL and the PLL film displayed replication of the template pattern. Reprinted with permission.[152] **(c)** The process of etching patterns on PCL films with CALB enzyme via PPL. CALB was loaded on the pen array; the pen deposited the enzyme on the PCL film supported by a silicon wafer; the patterned film was incubated; the film developed the pattern. The etching rate was 20 nm/min, and the smallest feature was under 1 μm. Reprinted with permission.[155] **(d)** PK solution (enzyme) was were directed through a soft lithography fabricated PDMS template. The PLA surface that had direct contact with PK was subjected to enzymatic degradation, which imprinted a replica of the flow path onto the PLA surface. The characteristic etching rate was 2 μm/h. Scale bar, 200 μm. Reprinted with permission.[139]

Although these successes showed great potential is using enzymatic etching to create microscale and nanoscale features, cleanroom facilities or advanced microscopy are always applied, which required dedicated instruments and personnel to be employed at each step.

There is a need for developing a lithography-free approach to perform enzymatic etching in regular laboratory settings.

5.4 Lithography-free fabrication procedure

5.4.1 PLA substrate preparation

PLA resin pellets (MW = 1.04 x 10^5 g/mol, Nature Works grade 3051D and 3052D; Jamplast Inc.) were weighed (1.5 g), spread onto a PDMS sheet, and heated at 180 °C for 90 minutes under vacuum. Another PDMS sheet was placed on top of the film. The two PDMS sheets and the film were sandwiched with two square glass plates and secured with four binder clips. The entire assembly was heated for 30 minutes at 180°C to press the molten PLA into a thin (approximately 1 mm), nearly round film. The PDMS sheets were easily separated from the PLA and also produced a PLA film with smooth surfaces.

5.4.2 Lithography-free fabrication

Scotch tape (3M, Catalog No. 810) was used to wrap the film. A rectangular area was left unwrapped in the middle and exposed to enzymatic etching. The wrapped film was immersed and incubated at 37 °C for several hours in proteinase K solution (proteinase K, MW = 28.9 kDa, BP1700, Fisher Scientific in 30 mM Tris-HCl buffer, pH 8.0, BP1758, Fisher Scientific, enzyme concentration 6.92 μM = 0.2 mg/mL). After etching, the tape was peeled off, and the PLA surfaces were cleaned with isopropanol. The film was rinsed with deionized water and dried with the pressured air. SEM (JEOL JSM-6400) images showed that the edge of the channel defined by the tape was clear and sharp (Fig. 5.3a). This lithography-free rapid prototyping method eliminated the need for cleanroom facilities and intensive training. Designing, fabricating, and testing of polymer-based microfluidic devices were easy to accomplish in a regular laboratory setting.

Adhesive vinyl sheets with cuts and slits also functioned as etching templates and created etched areas with clear and shape profiles. The vinyl patterns used were purchased from a craft store and had a resolution of 1 mm and simple letter patterns. A desktop size industrial grade vinyl cutter can produce cuts with customized patterns and achieve a resolution of 12.5 μm. A cutter of this grade costs around $2000 (e.g., Roland CAMM-1 GS-24 Desktop Cutter), which is significantly lower than the cost to use cleanroom facilities to create PDMS templates in soft lithography. In addition, a hobby-level vinyl cutter offers a cheaper alternative that costs around $150 (e.g., Silhouette Portrait 2) and can reach a resolution of 25 μm.

5.4.3 Vacuum aided bonding and 3D printed channel cover

The enzymatic etching resulted in open channels that must be covered to create enclosed channels. The first attempt was to bond the cover and the channel chip via thermal fusion bonding. A flat PLA sheet was placed on the channel chip. The two pieces were heated at 80 °C for 15 minutes in the oven. This temperature was slightly higher than the glass transition temperature of PLA (55 to 67 °C [69, 70]) and softened the material without inducing heat annealing and crystal formation. It was also significantly lower than the PLA melting point (175°C) [92] and avoided deformation of the channel. The area around the channel was gently pressed together with fingers to secure the sealing. The entanglement of polymer chains bonded two PLA pieces. The bonding strength was affected by the manual pressing process. Excess pressing made the channel collapse, which led to blockage of the channel. Inadequate pressing did not provide enough bonding strength, which resulted in leaking. The small dimension of the channel made it hard to avoid the channel part in the center while still covering all areas around the channel.

Accidental pressing on the channel may deform the channel too much and render it blocked. The successful rate was even lower because the surface contaminants (e.g., dust) might interfere with the bonding process. Surface defects like pits or uneven areas also interfered with the bonding process and caused failure.

Another challenge was to create ports for the channel cover, which was a flat piece of PLA made by melting PLA pellets on a smooth PDMS sheet. This cover was easy to produce and guaranteed that the whole device remained biodegradable. The ports for inserting tubes were created on the flat PLA piece with a press drill. However, the drilling process left debris on the cover, which may result in the aforementioned faulty bonding and leakage. Furthermore, the area around the port cracked unexpectedly during or after drilling and leaving the cover unusable.

To address these challenges and produce reliable microchannel devices, 3D printing (FDM) and vacuum aided bonding was enlisted. 3D printing was used to manufacture customized channel covers with ports (Fig. 5.3b). The cover was a thin block (2 mm thick) with two ports. The dimension of the block and positions of the ports were customized through computer aided design (CAD) to match each channel chip. Consequently, because the drilling of the ports was eliminated, the problems with debris and cracks were also avoided. The robustness of 3D printing enabled the rapid customization of channel covers.

With channel covers ready, vacuum aided bonding was explored next. The vacuum process applied a uniform pressure across the substrate and completely avoided the inconsistent pressing with hands, thus creating enclosed channels with a bonding strength exceeding the thermal fusion bonding approach. The process was performed using a commercial food vacuum sealer (FoodSaver V2480). The PLA channel piece and a 3D

printed cover were rinsed with isopropanol and dried with pressurized air. The two pieces were stacked and placed in a plastic pouch, which was vacuumed and sealed with the sealer (Fig. 5.3c). The sealed pouch was kept in the oven for 15 minutes at 80 °C. Then, the pouch was allowed to cool to room temperature and cut open to retrieve the PLA samples. The sealed PLA pieces were ready for tube assembly. A piece Tygon tube (Small parts Inc., 0.03 inch I.D., 0.09 inch O.D.) of 5 cm long was inserted into each of two access ports. Then the ports were sealed with the epoxy glue (Loctite epoxy plastic bonder). Water (0.01 ml/min) was injected into the channel through the tube for five minutes, and no leakage occurred. More than 70% of all channels were sealed without the channels being blocked. The enclosed channels were tested with water again after two months of bonding. The bonding strength remained the same, indicating a long shelf-life of the device (Fig. 5.3d, e). This vacuum aided bonding approach was also economically viable with minimum instrument investment. Instead of a vacuum pump, a commercial food vacuum sealer was capable of providing enough pressure in a short time (15 seconds). Compared with a vacuum pump, the food vacuum sealer was easily affordable (approximately $100), required low maintenance and operated quietly while the vacuum pump generated loud noise.

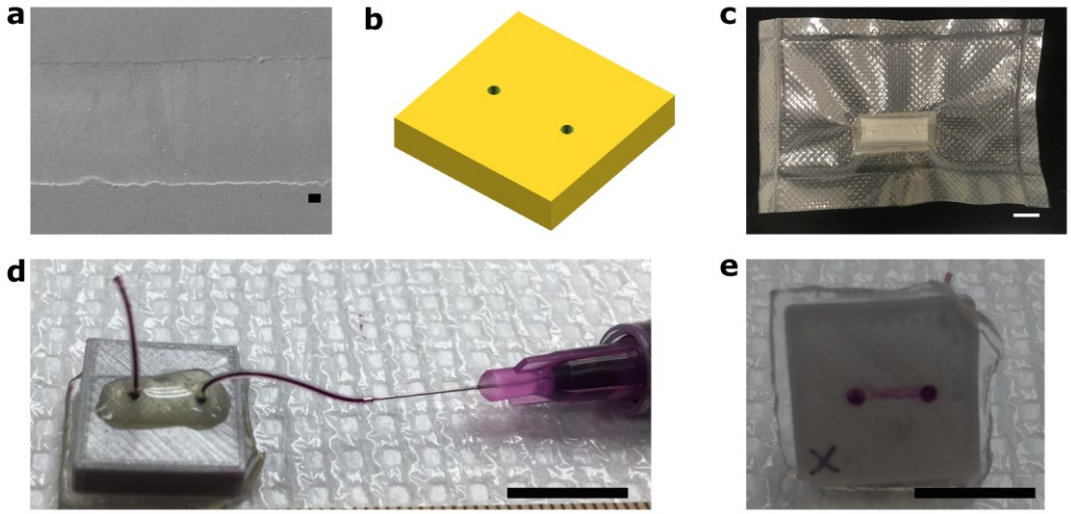

Fig. 5.3 Assembled microchannel device with a 3D printed cover. (a) Top view of etched amorphous substrate inside a microchannel. Scotch tape was used as the mask to template this channel, followed by etching for six hours at 37 °C in Petri dish. **(b)** CAD model of a channel cover: one thin block with two ports. **(c)** Channel piece and 3D printed cover were sealed in a vacuum bag. **(d)** An assembled microchannel with a 3D printed cover. Water was injected into the channel through the tube with a syringe. **(e)** The channel was filled with water (dyed magenta). **(a)** Scale bar, 100 μm. **(c) (d) (e)** Scale bar, 1 cm.

5.5 Fabrication of microchannel with embedded crystal post arrays

In the conventional microchip-based liquid chromatography, the main practical challenge is to retain the stationary phase inside the chip and at the desired position during both the packing and testing process.[157] However, current solutions, such as tapered capillary,[158] frits,[159] bottle neck geometries,[160] and weirs,[161] have either a high fabrication cost or a low separation efficiency. There is a need for creating microchannels with embedded structures to serve as barriers to keep the stationary phase in place.

Enzymatic etching elegantly solved this problem by packing the channel with crystal arrays while simultaneously fabricating the channel. Crystal domains were generated through isothermal crystallization and then revealed by enzymatic etching that selectively removed amorphous regions. These exposed crystal arrays were embedded in microchannels and acted as barriers to maintain the positions of a stationary phase.

5.5.1 Thermal annealing

Thermal treatments (annealing or quenching) were conducted by keeping the melted polymer at different temperatures then cooling them to room temperature. The binder clips were not removed until the films reached room temperature because early disassembly produced uneven films, which were not suitable for further etching and imaging.

Thermal annealing induced isothermal crystallization in PLA substrates. Melted samples were transferred to an oven and annealed at a low temperature between the glass transition temperature and melting point for several hours. The semi-crystalline substrates were etched with proteinase K aqueous solutions. Some substrates had only a microchannel size area exposed to the enzyme, while others were etched across the substrate surfaces. Crystallinity affected the etching rate significantly, and the estimated etching rate for amorphous regions was ten-fold of the rate for crystal domains.[162] Consequently, proteinase K selectively removed amorphous regions and revealed the crystal domains. The crystal domains showed dark outlines in microscope images (Zeiss Axiovert 200M), and Image J (NIH, version 1.52P) was used to calculate the area coverage (percentage of area covered by crystal domains) on sample surfaces. For film samples, images were acquired at 20 different evenly distributed locations on each sample. For channel samples, images of the entire channel surfaces were taken section by section. An average of the area coverage of crystal domains was obtained and plotted as a function of the annealing temperature.

In the PLA film samples, the area coverage increased from 20% to 56% as the annealing temperature increased from 90 °C to 140 °C. In the microchannel samples, the area coverage obtained after annealing ranged from 15% to 35%, which was much lower

than film samples (Fig. 5.4a). The difference of area coverage between film and microchannel samples were larger at a higher annealing temperature.

The differences in area coverage observed in the microchannels were explained in two ways. First, the channel sample image area (902 x 250 μm) was smaller than that on PLA films (902 x 902 μm), possibly limiting a sufficiently large ensemble of crystal domains to be counted. This hypothesis was proven to be unlikely by repeating the area coverage analysis in the PLA film images using the channel image size, which showed the same result as the large area size. A second and perhaps more likely explanation was that the defined channel width (100 - 250 μm) may inhibit large crystals from being revealed under enzymatic etching. The limitation of channel edges was predominant because the crystal spherulites grew larger at a higher annealing temperature. For example, annealing treatment at 90 °C generated an average spherulite diameter around 10 μm, and at 140 °C crystals grew until they impinged upon adjacent growing crystals and formed a larger crystal domain (> 1000 μm^2). The area coverage and annealing temperature followed a linear correlation and predicted that the area coverage dropped to zero for substrates annealed at 63.5 °C (Fig. 5.4b), which indicated the absence of crystal domains. The reported glass transition temperature of PLA ranged from 55 to 67 °C,[69, 70] depending on the composition and molecular weight of the polymer. The PLA resins used in this study did not form crystalline domains at an annealing temperature lower than 65 °C, which was close to the 63.5 °C prediction.

The effect of the cooling rate was also investigated. The first quenching process was to turn off the oven and let the samples cool to room temperature inside the oven. While the oven was well-insulated, it took seven hours to cool to room temperature, so the cooling

within the oven was slow. This cooling process allowed the mobilized polymer chains to form crystal structures. The second quenching process was to cool the melted samples at room temperature, and it took 30 minutes for the sample to cool to 25 °C. The seven-hour slow quenching process (Fig. 5.4c3, c4) provided a long time for polymer chains to form crystal domains and produced larger crystal spherulites that covered large areas. In comparison, the 30-minute fast quenching process (Fig. 5.4c1, c2) offered a short window for crystal forming and led to a few small spherulites. Rapid quenching processes below room temperature, either in an ice bath (0 °C), in a ultra-low temperature freezer (-80 °C), or in liquid nitrogen (-196 °C), all generated a larger area covered by crystals.

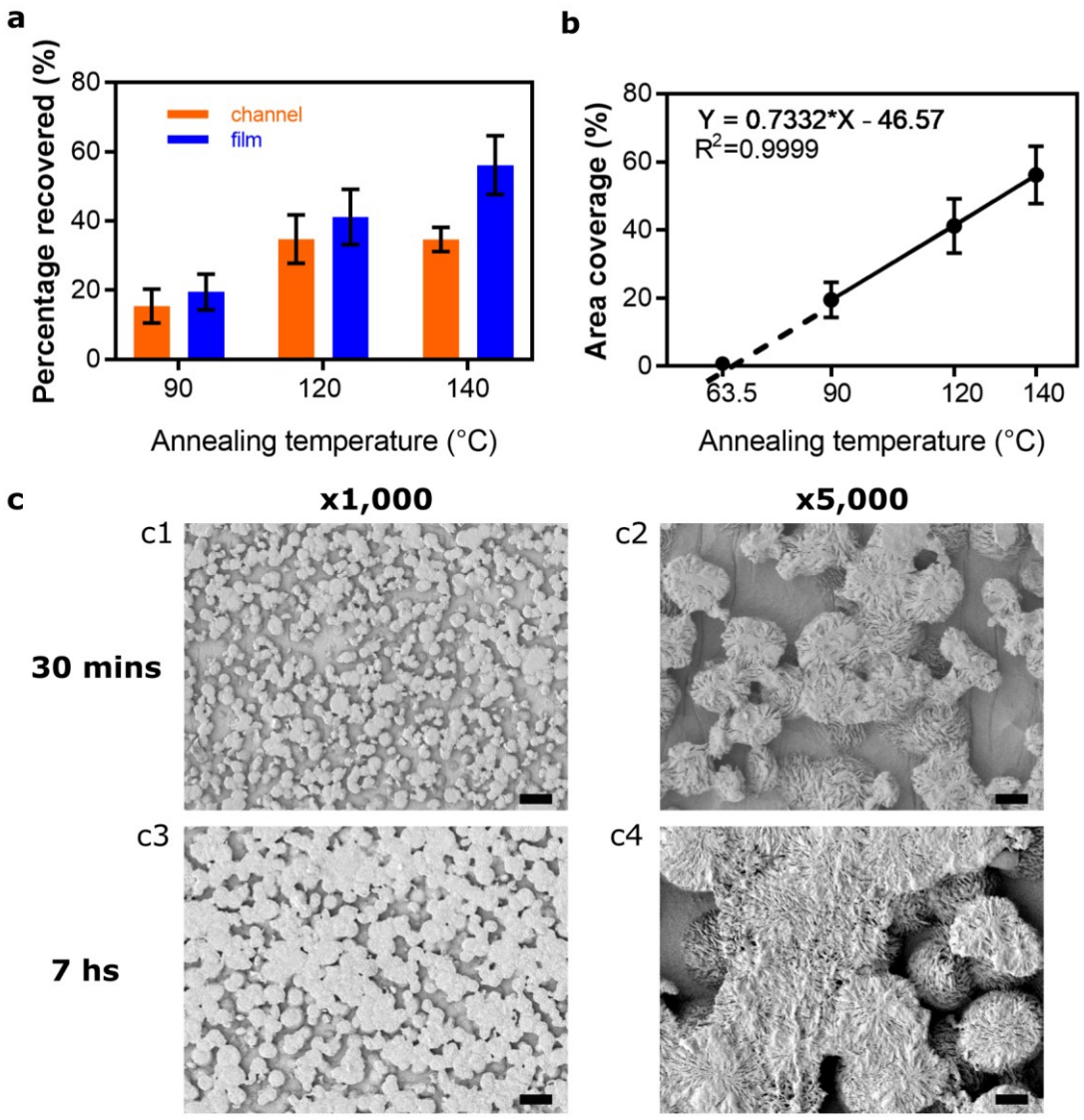

Fig. 5.4 Annealing and quenching temperature affected surface morphologies of PLA substrates. (a) Crystal domain area coverage at different annealing temperatures for film and microchannel samples. Film samples showed a higher crystal domain area coverage than microchannel samples. **(b)** The area coverage and the annealing temperature formed a linear relationship. **(c)** A slow quenching process generated large crystals. **(c1) (c2)** Quenching at room temperature. Quenching to room temperature took 30 minutes. **(c3) (c4)** Quenching in oven. Quenching to room temperature took seven hours. **(c1) (c3)** Scale bar, 10 μm; **(c2) (c4)** Scale bar, 1 μm.

5.5.2 Microchannels with embedded crystal post arrays

Next, the ability to control the PLA crystalline morphology was implemented to construct microchannels with embedded packing structures. Microchannels fabricated with

annealed substrates were photographed. Top-view SEM images showed that crystal structures were densely distributed throughout the entire channel in the 120 °C (Fig. 5.5b) and 140 °C (Fig. 5.5c) annealing conditions, while the 90 °C sample showed a sparse coverage of crystals (Fig. 5.5a). Side view images confirmed that the heights of the crystal domains were the same as the depth of the channel (Fig. 5.5d, e, f). The crystal structures fully spanned from the bottom to the top of the microchannel. In other words, the crystal structure reached the bottom of the cover when a plain PLA block was added on the top to create an enclosed channel.

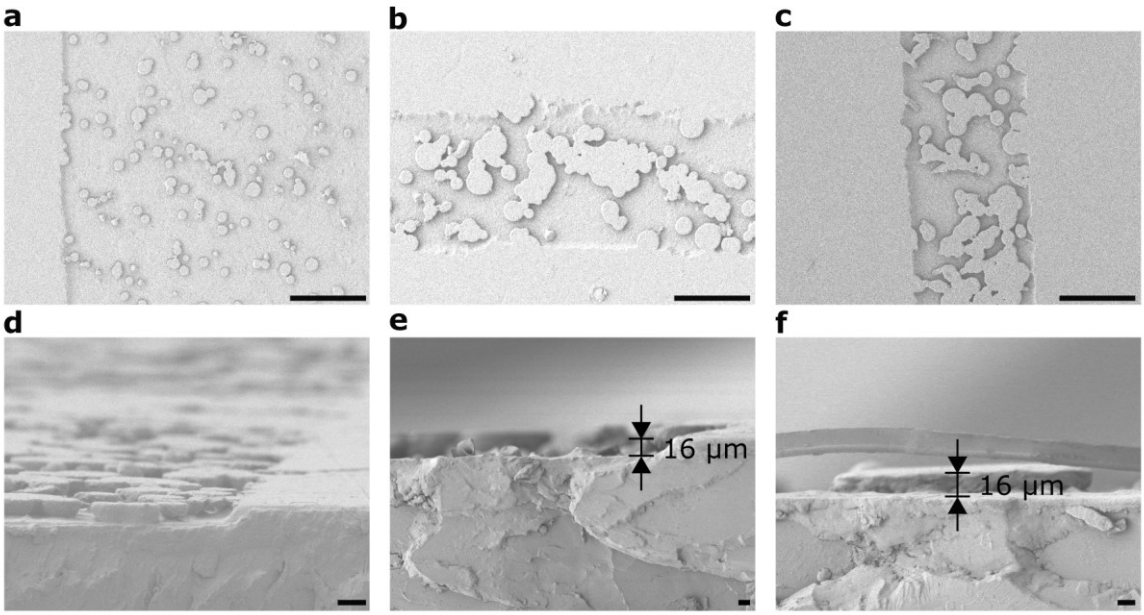

Fig. 5.5 Surface morphologies and crystal structures in etched channels. (a) (b) (c) Top view of channels etched after annealing at different temperatures. **(a)** 90 °C. **(b)** 120 °C. **(c)** 140 °C. Scale bar, 100 µm. **(d) (e) (f)** Side view of etched crystalline domains inside a microchannel. The side view image was obtained by mounting a fractured channel on a vertical sample holder. The channel chip was scored, kept in liquid nitrogen for 15 minutes, then broken into two pieces. The etching rate was 2 µm/h. **(d)** Samples were quenched to the room temperature in oven, followed by etching for four hours at 37 °C, 2 µL/min proteinase K flow rate. Scale bar, 100 µm. **(e) (f)** Samples were quenched to room temperature in an oven, followed by etching for eight hours at 37 °C. Scale bar, 10 µm. **(e)** Showing the channel depth as 16 µm. **(f)** Showing the crystal structure thickness as 16 µm, same as the channel depth. **(a) (b) (c) (d)** Scale bar, 100 µm. **(e) (f)** Scale bar, 10 µm.

5.6 Microchannel for biomolecule separation

Embedded crystal arrays are part of the microchannels, so they remain in design positions and can act as barriers to retaining a stationary phase that can adsorb biomolecules. ZnO and bovine serum albumin (BSA) were chosen as the stationery phase and the biomolecule. BSA adsorbed on ZnO nanoparticle surfaces and formed protein-nanoparticle complexes.[163] The adsorption dynamic between this pair was studied as followed. Various concentrations of BSA (Sigma-Aldrich A2153) solution were prepared by dissolving BSA powder in pH = 5 acetic acid/sodium acetate buffer (close to the BSA isoelectric point of 4.7 [163]). Different amounts of ZnO particles (Sigma-Aldrich A2153) and BSA solution were added in 15 mL conical tubes. The conical tube was shaken with a digital vortex mixer (speed 3000rpm, 15 seconds, Fisher 02215370) to guarantee the proper mix of BSA and ZnO nanoparticles. A small amount of the ZnO suspension (1 mL) was centrifuged at 10,000 G (9695 rpm, Eppendorf 5417R) for one minute. The protein concentration of the clear liquid was measured with a spectrophotometer (Fisher Nanodrop 1000). The adsorption data was fitted with both the Freundlich model and Langmuir model.

The Freundlich model was expressed as

$$C_2 = K_F * C_1^n \quad (5.1)$$

and in the linear form as

$$logC_2 = logK_F + nlogC_1 \quad (5.2)$$

The Langmuir model was expressed as

$$C_2 = \frac{mK_LC_1}{1+K_LC_1} \quad (5.3)$$

And in the linear form as

$$\frac{C_1}{C_2} = \frac{1}{m}C_1 + \frac{1}{mK_L} \quad (5.4)$$

The parameters were

C_1: free BSA in solution, mg/mL

C_2: BSA adsorbed on ZnO at equilibrium state, mg BSA /g ZnO

K_F, K_L, m, n: coefficients.

The Freundlich model fitted the data (Fig. 5.6a), and the parameters acquired from Fig. 5.6a were K_F as 380 and n as 1.032. The Langmuir model (Fig. 5.6b) did not fit the experiment data. These fittings suggested that BSA was adsorbed onto ZnO nanoparticles in a multilayer fashion rather than a monolayer one.

The next step tested the BSA adsorption on ZnO particles in microchannels. Nanoparticle suspensions were prepared by mixing 0.5 g of ZnO particles with 10 g of isopropanol (Fisher A451). The suspension was injected with a syringe pump (PHD 2000, Harvard Apparatus) into the channel at the rate of 0.005 mL/ min. The nanoparticles-packed channels were dried in a vacuum chamber at the room temperature for 24 hours. The BSA solution was injected into the channel with a 3 mL syringe. The injection was controlled manually, and only the Tygon tube of the inlet was filled (5 μL). Then the liquid in the Tygon tube was pushed into the channel with an empty syringe. Liquid passed through the channel and flew out of the outlet. The protein concentration of the liquid collected at the outlet was measured by a spectrophotometer.

The breakthrough curve showed that BSA concentration dropped after the protein solution passed through the channel, which indicated that a portion of BSA was adsorbed by the nanoparticles packed in the channel (Fig. 5.6c). These preliminary tests proved that the crystal arrays embedded-microchannels can host a stationary phase that can adsorb

biomolecules from aqueous solutions and offer great potentials to catalyze a revolution in the field of bioanalysis. Further exploration directions include testing other stationary phases/biomolecules combinations (e.g., silica/DNA) and establishing the platform of performing sequential biomolecule extraction tasks.

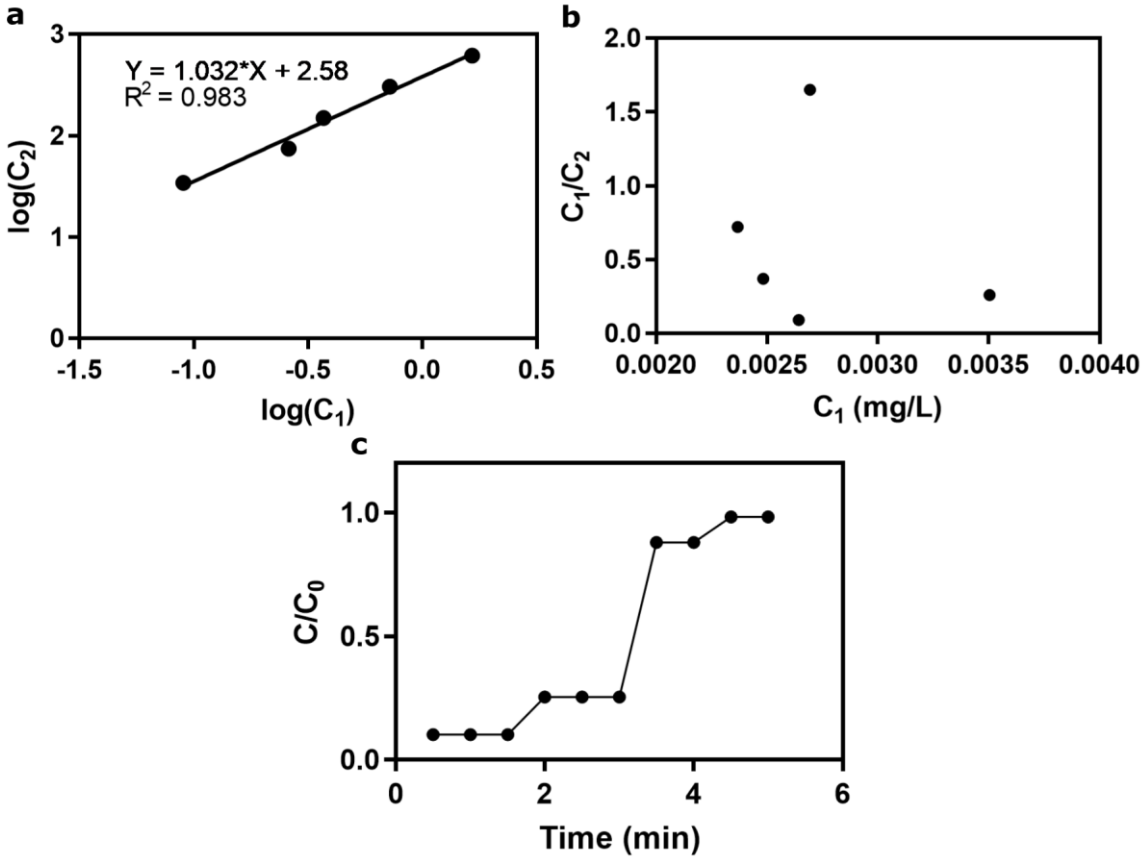

Fig. 5.6 BSA adsorption behaviors on ZnO nanoparticles. (a) Freundlich adsorption model fit. **(b)** Langmuir adsorption model fit. The data did not fit the model. (**c)** Breakthrough curve of BSA adsorption behavior on ZnO nanoparticles in microchannels BSA concentration: 1.65 mg/mL. C: protein concentration of droplets collected after passing through the channel, mg/mL. C_0: protein concentration before the liquid passing through the channel, mg/mL.

5.7 Other treatments to control surface morphologies

5.7.1 Solvent annealing

Solvent annealing was conducted in two ways: solvent vapor annealing and direct solvent annealing. For solvent vapor annealing, PLA samples were kept in a sealed chamber with a beaker that was filled with chloroform or acetone. The solvent evaporated at room temperature, and vapor filled the chamber. For direct solvent annealing, PLA samples were immersed in ethyl acetate or acetone. After six hours, the samples were removed from the solvent, dried, and imaged.

In previous studies, Lee *et. al.* used solvent annealing to direct crystal growth in thin films and suggested that crystal spherulites formed with solution deposition were characteristically different from those formed via thermal treatment.[164] Therefore, the possibility of solvent as an approach to modify crystal growth was explored. Chloroform and acetone were tested in solvent vapor annealing experiments. Chloroform annealing generated a rough surface, sharpened the edge of the crystallites already formed during thermal annealing, and created unique crystal morphologies, which were revealed by enzymatic etching (Fig. 5.7). Chloroform annealing created a shallow dip circling around crystal features (Fig. 5.7a) and unique crepe-like structures (Fig. 5.7b). Acetone vapor treatment showed minimal effect in altering the surface structures.

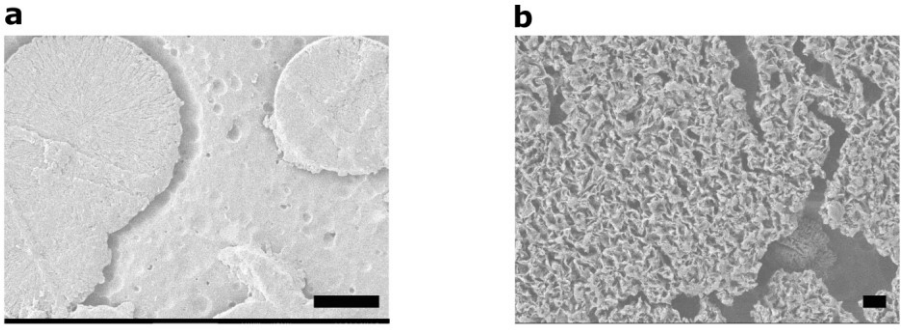

Fig. 5.7 SEM images of surface morphologies after chloroform solvent vapor annealing treatment. Heating annealing at 90 °C for 2 h, chloroform vapor annealing 6 h, proteinase K etching 2 h. **(a)** Scale bar, 10 μm. **(b)** Scale bar, 1 μm.

Ethyl acetate and acetone were tested for direct solvent annealing; PLA samples were immersed in solvents for various time durations. After treatment with either solvent, amorphous sample surfaces demonstrated hierarchical structures consisting of microscale pores. The surfaces turned from transparency to opaque, which suggested the formation of crystals. The polymer chains at the surface were able to rearrange into crystal domains after the solvent dissolved the surface of PLA samples. For ethyl acetate solvent annealing, after five minutes, sponge-like structures were observed on the surfaces (Fig. 5.8a, b). After 30 minutes, more pores were formed, and there were also thin film structures connecting multiple pores (Fig. 5.8c, d). After 60 minutes, thin film structures disappeared, and clusters of particles (5 μm diameter) covered the surfaces. Small pores (1 μm) were observed on these particles (Fig. 5.8e, f). After two hours of treatment, the solvent had dissolved further into the surface, and the morphologies remained similar (Fig. 5.8g, h). Acetone annealing was more effective in changing surface morphologies of the substrates. After five minutes, particle clusters were formed. (Fig. 5.9a, b, c). As annealing time became longer, the particle size remained the same, and more pores were observed on these particles (Fig. 5.9e, h, k, n). Round crystal structures were revealed after 30 minutes

of annealing (Fig. 5.9i, l, o).

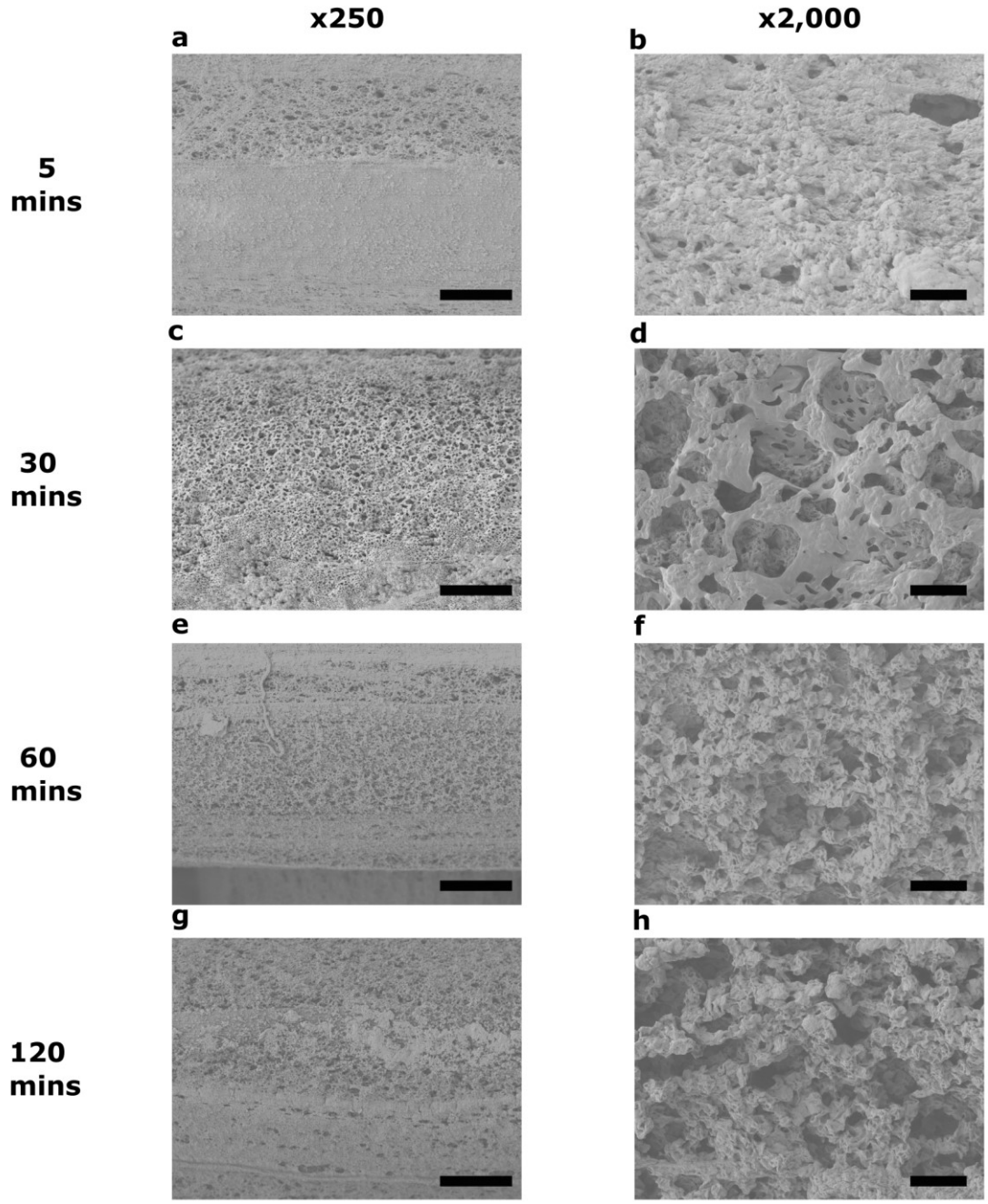

Fig. 5.8 SEM images of surface morphologies after ethyl acetate direct solvent annealing treatment of different time durations. (a) (b) 5 minutes. **(c) (d)** 30 minutes. **(e) (f)** 60 minutes. **(g) (h)** 120 minutes. **(a)(c) (e) (g)** Scale bar, 100 μm. **(b) (d) (f) (h)** Scale bar, 10 μm.

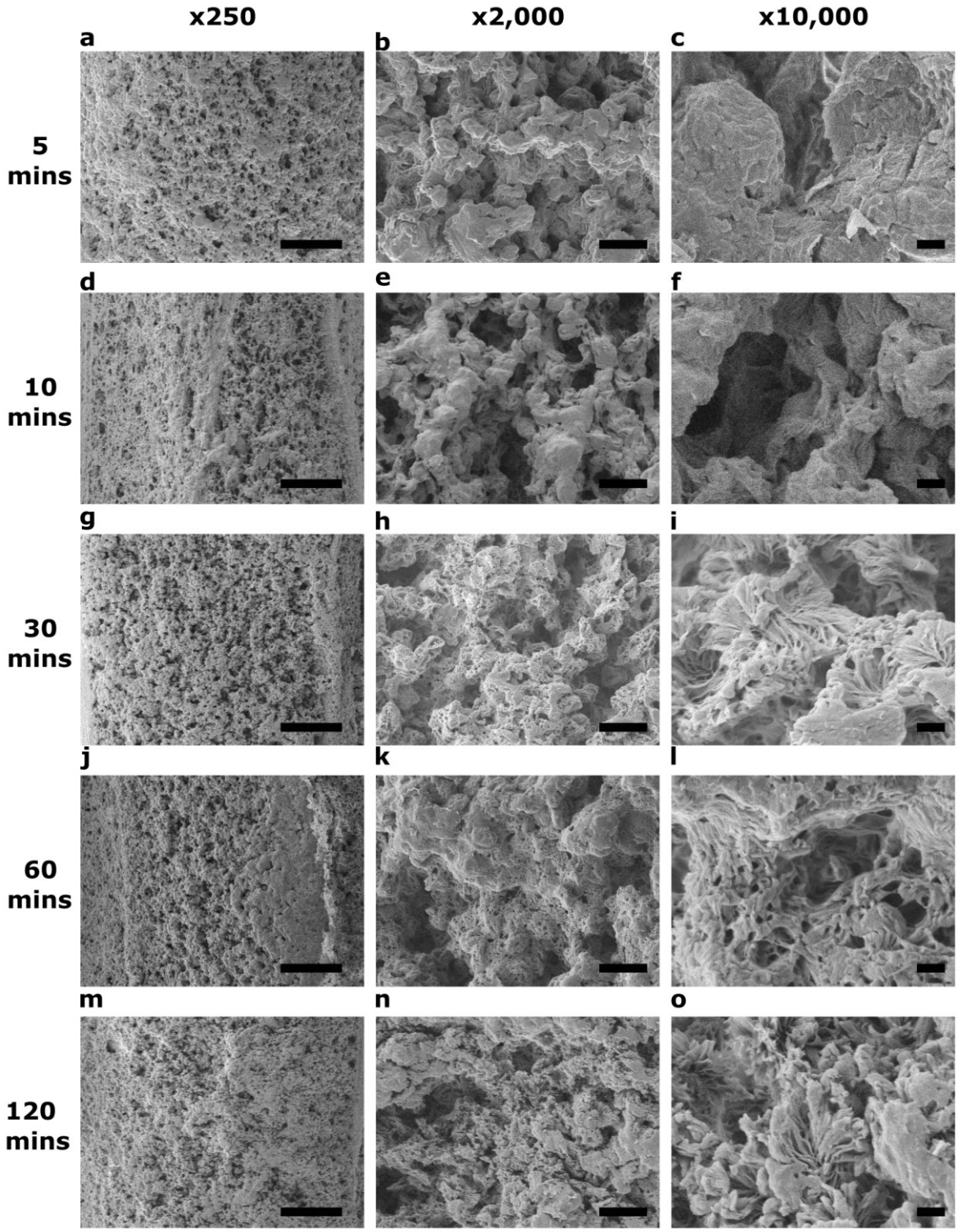

Fig. 5.9 SEM images of surface morphologies after acetone direct solvent annealing treatment of different time durations. (a)(b) (c) 5 minutes. **(d) (e) (f)** 10 minutes. **(g) (h) (i)** 30 minutes. **(j) (k) (l)** 60 minutes. **(m) (n) (o)** 120 minutes. **(a) (d) (g) (j) (m)** Scale bar, 100 μm. **(b) (e) (h) (k) (n)** Scale bar, 10 μm. **(c) (f) (i) (l) (o)** Scale bar, 1 μm.

5.7.2 Long term etching

Although the enzymatic etching rate decreased as crystallinity increased, it was possible to completely degrade crystal structures. Prolonged etching (up to 8.5 days/204 hours) were studied, and the enzyme solution was renewed after 60 hours and after 132 hours. After 60 hours, a dark area appeared in the center of these crystal structures (Fig. 5.10a) and the center started to crack (Fig. 5.10a3); it kept growing bigger until reaching the edge of the crystals after 132 hours (Fig. 5.10b) and the cracks grew larger (Fig. 5.10b3). Crystal structures also became thinner during this process. After 204 hours, the crystals were completely removed, and only shallow pits (Fig. 5.10c) were observed on the surface. The inside surface of pits were rough (Fig. 5.10c3).

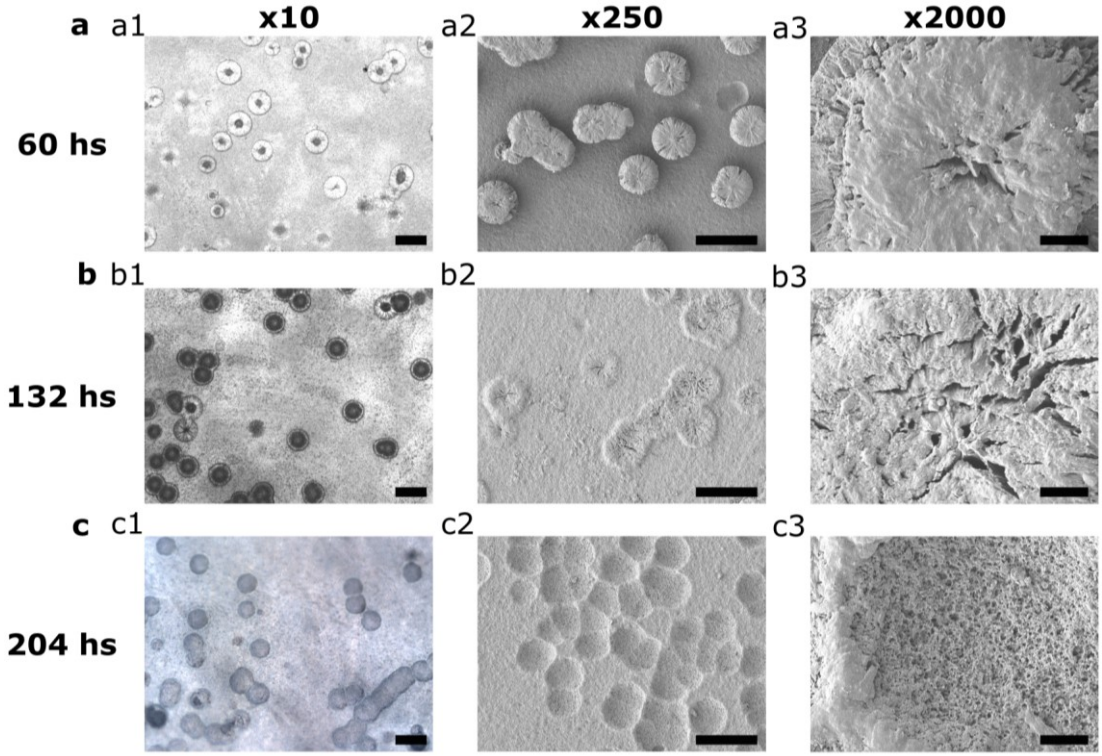

Fig. 5.10 Surface morphologies after long term etching. (a) 60 hours (2.5 days). **(b)** 132 hours (5.5 days). **(c)** 204 hours (8.5 days). **(a1) (b1) (c1)** Scale bar, 100 µm. **(a2) (b2) (c2)** Scale bar, 100 µm. **(a3) (b3) (c3)** Scale bar, 10 µm.

5.7.3 Base etching

PLA was applied in disposable utensil production because of its biodegradability and good flowability for molding. In industrial manufacturing, a drinking straw is made by extruding pellets through a metal die of a hollow tube shape. This extrusion process creates straws consisting of long fibers. Short pieces of PLA straws (2 cm long, EcoProduct, 7.75" Clear Wrapped Straw, EP-ST770) were immersed in drain cleaner solutions (Instant Power Hair and Grease Drain Cleaner, active ingredients: sodium hydroxide and potassium hydroxide) for 24 hours and air-dried. PLA straw became brittle, easy to tear apart, and developed porous surfaces. SEM images showed the fibers on straw surface detached from others (Fig. 5.11), thus weakening the straw.

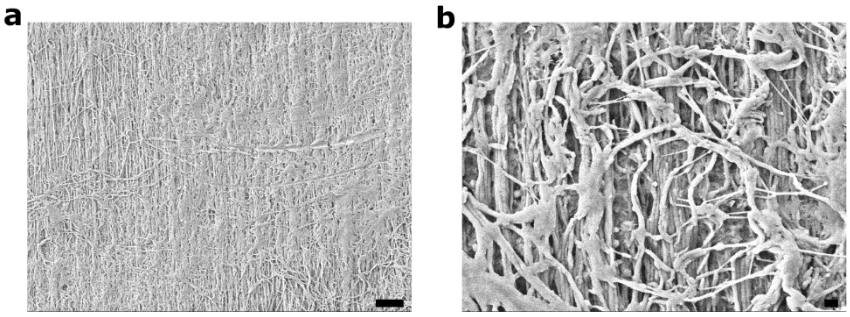

Fig. 5.11 PLA straw after 24 hours of base etching at 25 °C. (a) Scale bar, 10 μm. **(b)** Scale bar, 1 μm.

5.8 Conclusions

This chapter presented a novel procedure to fabricate polymer-based microchannel devices through enzymatic etching, 3D printing, and vacuum aided bonding. This approach eliminated the drawbacks of dedicated equipment and personnel requirements associated with conventional lithography-dominated manufacturing and presented a significant step forward to realize the vision of accessible microfluidics devices. This method harnessed

enzymatic etching as a tool to create microchannels of precise profiles. For substrates with tunable crystal morphologies generated by thermal or solvent annealing, the selectivity of enzymatic etching favored low crystallinity regions and led to microchannels with embedded crystal structures. These channels can serve as microchip-based liquid chromatography solutions because the crystal arrays can act as barriers to retain the stationary phase in place. This approach can be expanded across various biodegradable polymer and enzyme pairs, which constitute an untapped range of crystal morphologies and etching profile (rate and accuracy). The fast turnaround between designs enabled by 3D printing, coupled with minimized environmental impact owning to the renewably-sourced nature of PLA, paves a way to bring affordable and customizable microchannel devices to commonplace.

CHAPTER VI

COMMERCIALIZATION OF 3D PRINTED OIL ABSORBENTS AND RELATED PRODUCTS

6.1 Overview

The 3D printed oil absorbent was the first of its kind. Its rigid nature, biodegradability, reusability, and easiness of customization via 3D printing distinguished it from other commercial available and laboratory created absorbents. Additionally, these absorbents also inspired the creation of oil-loaded bracelets and diffusers, which expanded the application of absorbents from environmental and industrial cleaning to the territory of domestic products. Naturally, I wondered about the possibility of turning this invention to a product. I explored the commercialization possibility through both e-commerce (Etsy store) and funded entrepreneurial program (NSF I-Corps).

6.2 Design principle of bracelets and oil diffusers: oil encapsulation

In section 2.2.2, a porous increment of 10% was verified as a tool to optimize oil uptake rate. More dramatic changes in porosity were studied to encapsulate and sequester the absorbed fluid. A three-layer with different infills were printed in one sample (Fig. 6.1): the shell, the support rib, and the core had 100%, 10%, and 60% infill, respectively. The dense low porosity core was surrounded by a high porosity support rib (Fig. 6.1). The core had strong capillary forces, so that the absorbed oil was confined at discrete locations within the printed part.

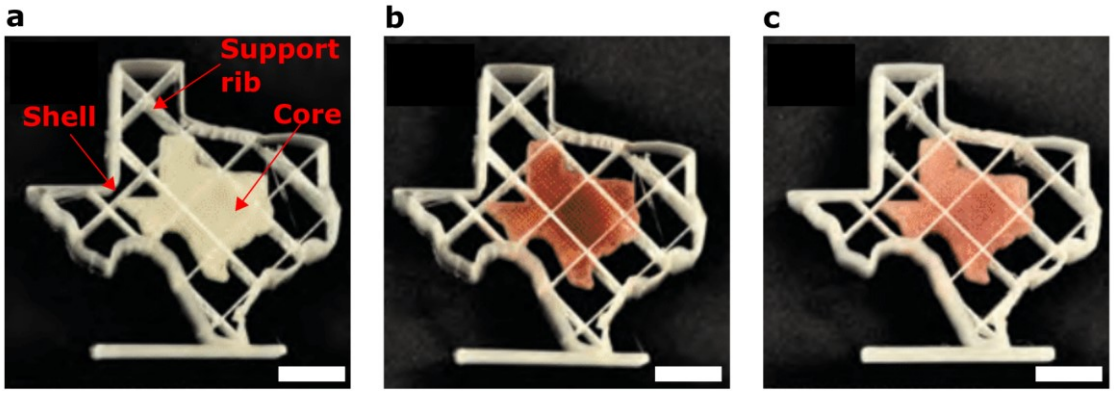

Fig. 6.1 Large step changes in porosity make it possible to sequester absorbed oil at prescribed locations. (a) Printed part. Core: 1 cm thickness, 60% infill. Support rib: 2 cm thickness, 10% infill. Shell: 2 cm thickness, 100% infill. **(b)** Oil confined in core immediately after uptake. **(c)** Oil remains confined in core over 3 years after uptake. Scale bar, 1cm.

This oil encapsulation and sequester in low porosity dense region was explained as follows. In these absorbents, the capillary force increased as the pore diameter decreased. On one hand, a low porosity/high infill structure had a stronger capillary force than a high porosity/low infill region, so it absorbed oil from the latter. On the other hand, a high porosity/low infill region did not take oil from a low porosity/high infill structure because its weaker capillary force. As shown in Fig 6.2c and d, oil was loaded to a high infill core (infill 80%), and no oil was absorbed into the surrounding low infill support (infill 20%). When oil was loaded to a low infill core (infill 20%), the high infill support (infill 80%) absorbed the oil from the core (Fig. 6.2a, b).This core-support structure was expanded to 3D structures consisting of a high infill core surrounded by a low infill support (Fig. 6.3). The large pore of the support layer allowed a pipet tip to reach the core, so oil was loaded directly into the core. The support layer did not absorb oil, remained oil-free, and served as a screen to separate the oil-soaked core from the environment, so this double-layer system was leak-free. The openings of the support layers also provided ample air flow to allow

contact with the oil. Volatile components evaporated and diffused into the surrounding atmosphere.

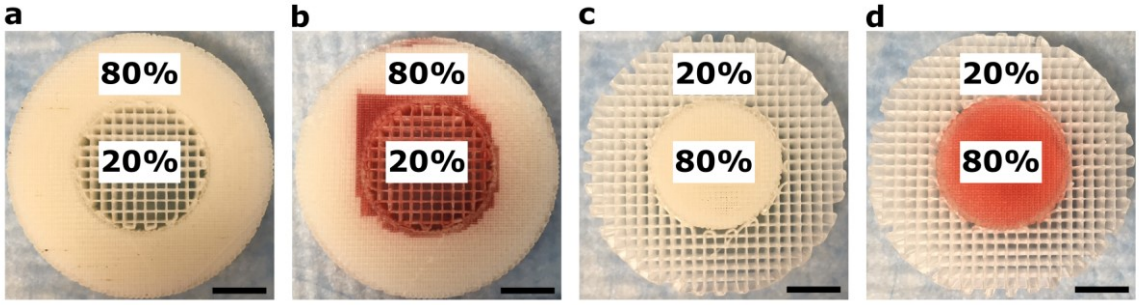

Fig. 6.2 2D Core-support double layer structures. (a) Before loading oil. **(b)** Oil was loaded into the core, then oil was absorbed to the support by stronger capillary forces. **(a) (b)** Core: 20% infill. Support: 80% infill. **(c)** Before loading oil. **(d)** Oil was loaded into the core, and the core retained the oil. No oil was absorbed into the support. **(c) (d)** Core: 80% infill. Support: 20% infill. Scale bar, 1 cm.

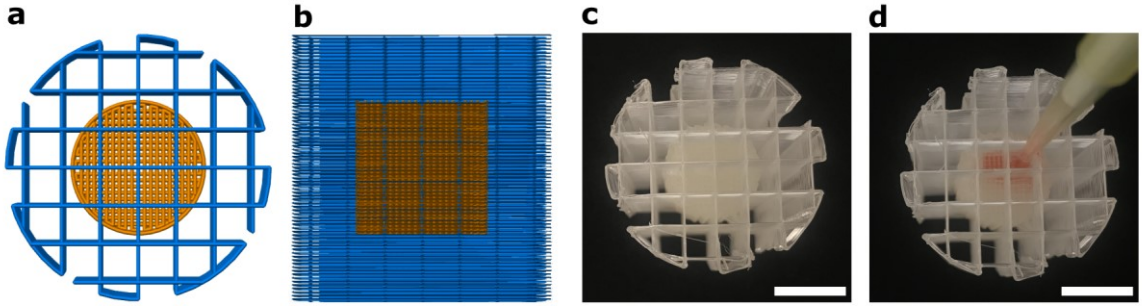

Fig. 6.3 3D Core-support double layer structures. (a) Top view. **(b)** Cross-section view. **(a) (b)** Orange: core, high infill, 60%. Blue: support, low infill, 10%. **(c)** Printed sample. The core was embedded in the support and had no contact with the environment. **(d)** Oil was loaded into the core. The pipet tip reached the core through pores of the support. Scale bar, 1cm.

6.3 Repellent loaded bracelets

7.3.1 PLA bracelets

Almost one in five (17%) of all infectious diseases are vector-borne diseases, which cause more than 700,000 deaths annually.[165] The mosquito is the best known vector and can carry and transmit malaria, dengue fever, and yellow fever. Zika virus is carried by

Aedes mosquitos and poses a global public health emergency after large outbreaks in French Polynesia and Brazil in 2013 and 2015, respectively.

However, many of these vector-borne diseases are preventable by avoiding insect bites. Various insect repellents have been commercially available for decades but are cumbersome to use. They are either sprayed on skin directly or soaked into a fabric bracelet worn by the user. The repellents usually contain natural (citronella) or synthetic (DEET, N, N-diethyl-meta-toluamide) mosquito repelling chemicals as active ingredients, which may cause skin irritation and stain clothes. The oil base in these repellents is also greasy and causes an unpleasant feeling especially in hot and humid weather when mosquitoes are active. Furthermore, perspiration dilutes the repellents and results in reduced effectiveness. Due to the limited amount of repellent that could be applied at a time, periodical reapplication is required throughout the day. These drawbacks point to a need for a safe, effective, and easy-to-use repellent releasing device.

The core-support rib-shell diffuser design was implemented in the bracelet format capable of retaining oil-based repellents in the core, delivering sustained release at higher doses than would be possible if the repellent were applied directly to the skin (Fig. 6.4). The bracelet eliminated the direct contact between the repellent and skin and guaranteed controllable and sustainable release of active ingredients for a long period of time. It offered a new avenue to help combat the spread of mosquito-borne infectious disease.

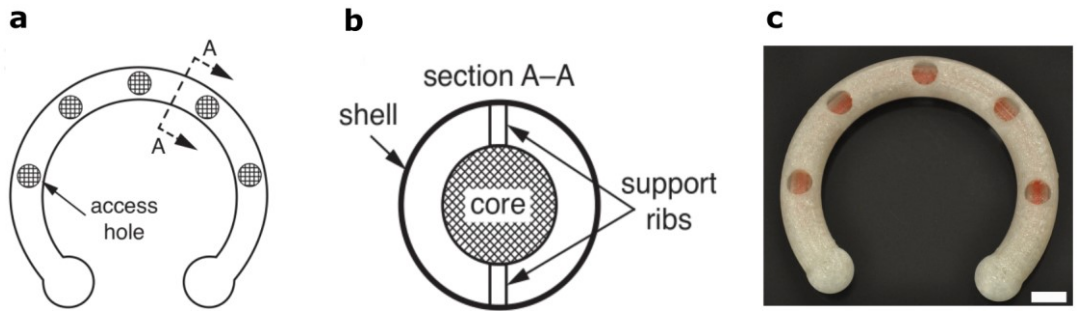

Fig. 6.4 A 3D printed PLA bracelet (5.5 cm inner diameter) loaded with dyed oil. (a) The bracelet was consisting of a low porosity inner core (0.6 cm diameter, 60% infill) connected to an outer shell (1 cm diameter, 100% infill) via highly porous support ribs (0.1 cm wide, 10% infill) enables long-term encapsulation of an oil-based mosquito repellent, eliminating the need for direct application to the skin. **(b)** Cross-section view showing the core-shell structure. **(c)** Printed bracelet. Access holes enable oil-based liquid to be loaded into the core using an eyedropper.

7.3.2 Flexible bracelets

To improve the wearability of the bracelets, a flexible thermoplastic polyurethane filament, PolyFlex TPU95, was used to print flexible bracelets. The soft and flexible nature of this filament improved users' wearing experience. PolyFlex featured a "Shore A" hardness of 90 to 95 A and had a large strain-to-failure of over 400%, It was also lighter in weight (1.17 g/cm^3) than PLA (1.25 g/cm^3). The PolyFlex bracelet deformed when pressed with hands and bounced back to the original shape once the pressure was released (Fig. 6.5). When squeezed by hands, the diameter of the bracelet increased 54%. This increased diameter was wider the palm, so the bracelet was slipped onto the wrist easily. Once the force was released, the bracelet bounced back to its original shape that had a similar diameter to the wrist, so the bracelet was secured on the wrist. This changing diameter elegantly solved the issue with PLA bracelet, which was either too small in diameter to put it on or too large in diameter then it slipped it off the wrist. Flexible bracelets shared the same design as regular rigid PLA bracelets, so the repellent retaining and releasing

performance remained the same. The deformation was also moderate, so no loaded oil was squeezed out of the bracelet.

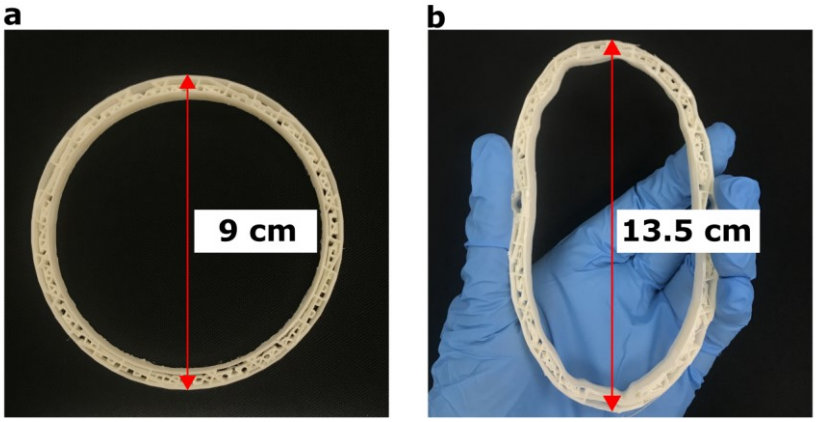

Fig. 6.5 A bracelet made with flexible filaments deformed under pressure and recovered its original shape when the pressure was released. (a) Bracelet without deformation. **(b)** Deformed bracelet. When pressed with hands, the bracelet deformed to an oval shape. Once the pressure was released, the bracelet bounced back to the original shape.

6.4 Etsy: setting up an online store

The successful development of repellent loaded bracelets encouraged me to share this creation with the general public as my solution to prevent Zika virus spread during its outbreak in the spring of 2015. With encouragement and help from my advisor, I launched an Etsy store in August 2015 introducing 3D printed repellent loaded bracelets and customizable oil diffusers to the online shopping community. The store also carried my other creations inspired by core-shell oil diffusers (Fig. 6.6).

Etsy is an online trading platform specializing in handmade products. It had 195.59 million US dollars annual revenue [166] and 19.81 million active buyers [167] in 2014, the year before the opening of my store. Its popularity brings both adventurous customers and seasoned competitors. The competitors were not my concern because I was confident that my products are unique comparing to other oil diffusers. However, the customers who

visited Etsy to purchase oil diffusers had not appreciated the creativity. I made only one sale and closed the store after four months. At the time of closing, the store acquired 116 shop views and 179 listing views from seven listed items.

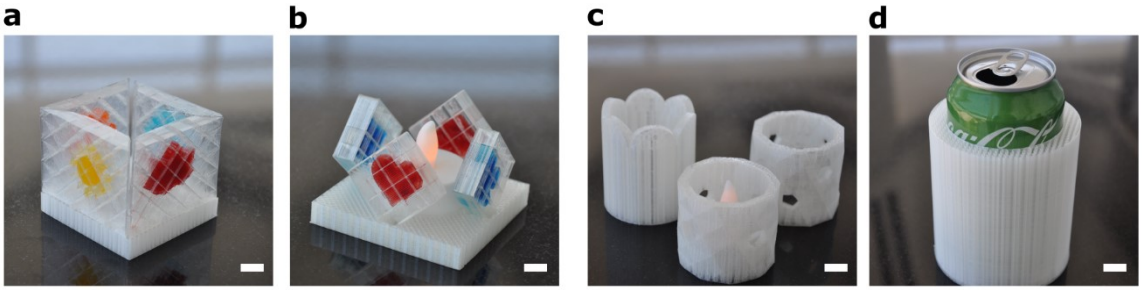

Fig. 6.6 Selected 3D printed home décor products listed on Etsy store. **(a) (b)** Candle holder with panels featuring embedded symbols that were filled with colored mineral oil. The symbol had a denser infill than the surrounding frame, so the absorbed oil did not infuse to the frame. The frame remained oil-free for easy handling. **(a)** Featured seasonal symbols (spring: flower, colored orange; summer: sun, colored yellow; fall: maple leaf, colored red; and winter: snowflake, colored blue). **(b)** Featured playing card suit symbols (heart, club, diamond, and spade). **(c)** Candle holders of different geometric shapes and housing LED candles. **(d)** 3D printed aluminum can sleeve. The sleeve wall was partially solid, and 20% of the volume had a scaffold-like structure. The void space was filled with air, which provided an insulation layer for the can. Scale bar, 1 cm.

Upon closing the shop in December 2015, I determined that the customers I reached through Etsy were not appropriate for my products. The customers did not appreciate the uniqueness of 3D printed bracelets and diffusers as I did as the creator. I greatly valued the efforts I invested in designing and producing these products, so I anticipated a high profit margin and listed the price too high. Then I assumed a boutique store specialized in designer products would attract the customers who could afford my products. In addition, handmade art trade shows in a metropolitan city or local art festivals might also have been a good idea. However, I did not further pursue the idea of commercialization due to time conflict with my research work. Additionally, my products displayed more features when handling in person, so online selling was not the best option for customers to carefully

examine my products. Selling at a physical location where customers can interact with the products in person would be a better fit.

6.5 I-Corps: entrepreneurial program to explore commercialization possibilities

After discovering that shape memory properties can make 3D printed absorbents reusable, I concluded that the 3D printed absorbents were capable of absorbing, releasing, and reabsorbing oil, which assured the reusability of the absorbents. I decided to present these absorbents as a product to meet the market need for oil absorbents suitable for small-scale spills (as previous discussed in section 1.2). Consequently, I planned to explore the commercialization of the 3D printed absorbents through the Innovation Corps program (I-Corps) funded by the National Science Foundation (NSF).

6.5.1 Program outline

The purpose of I-Corps program is to support the commercialization of technologies developed in university research laboratories by providing financial support and training in fundamental entrepreneurial skills to researchers to help them evaluate the translational potential of their inventions. Researchers as a team submit proposals, which are accepted year-around. The select teams join a cohort and attend eight weeks of training in entrepreneurial topics and participate in customer discoveries. The team reaches a conclusion of commercialization potential of its technology and has an extended three-month to continue customer discoveries.

6.5.2 Application phase and team composition

I-Corps program requires a team with three roles: an entrepreneurial lead, a technical lead investigator, and an industrial mentor. I, as the co-inventor of the 3D printed oil absorbents, was the driving force to investigate and evaluate the commercial potential of

this technology and served as the entrepreneurial lead. My committee chair, Dr. Victor Ugaz, is the co-inventor of this technology. As a faculty member, he served as the technical lead. Mr. John Adams was the industrial mentor. He is a Professional Engineer in chemical engineering with 30 years' experience in oil and gas industry and provided contacts in the industry and advice on the team's progress to transition the technology out of academic laboratories.

The program application required a one-page proposal and two interviews with the program director. My team was immediately admitted to the program (NSF award number 1645285) at the end of the first interview with the program director, which was a rare case. My team was thrilled by this achievement. During the program, each team was required to attend training workshops and online seminars, develop business models, conduct interviews, and present a final report. As the entrepreneurial lead, my responsibilities included leading the direction of this business endeavor, conducting all customer discovery interviews, and preparing presentations.

6.5.3 Program curriculum

The program has four phases: kickoff phase, customer discovery phase, closing phase, and extension phase. The two major activities were developing business model canvas and conducting customer interviews under the guidance of instructors and reading materials ("Business Model Generation"[168] and "The Startup Owner's Manual"[169]). Business model canvas (Fig. 6.7) is a visual chart with nine business model building blocks (business canvas elements) arranged in one page to help create new or update old business models. Each block is expected to be updated with information acquired from customer interviews. The canvas presents a business hypothesis that to be tested by customer

interviews. The target of these interviews is not limited to the traditional concept of a customer, who purchases and uses the product, but also includes people who are involved in producing and distributing them and even competitors. The interview target is chosen according to which business canvas element is to be filled or revised, so the business hypothesis is updated. Developing business model canvas and conducing customer interviews are intertwined and complemente each other in the common goal of delivering values to potential customers.

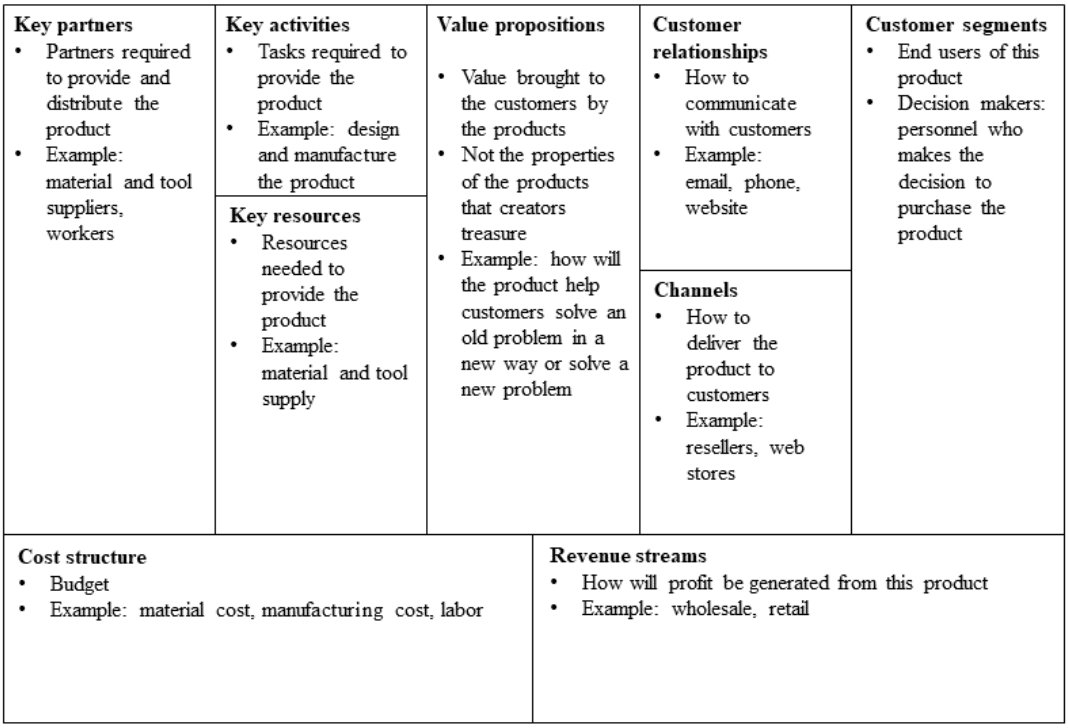

Fig. 6.7 Business model canvas template.

6.5.4 Kickoff phase

This first phase was a kickoff workshop. I-Corps program held the workshop multiple times per year at different locations. Given the schedule of team members, my team had to choose between Atlanta, Georgia in early April 2017 and San Diego, California in late April 2017. The determining factor was the accessibility to potential customers because the

program required the team to start customer interviews during this phase. My team chose San Diego because of its coastline environment, which is rich with marinas and oil spill cleaning needs.

The training workshop was a three-day event. Day 1 and day 2 consisted of lectures in the morning, meeting with potential customers (customer discovery) in the afternoon, and mandatory office hours with instructors at night. Every night, I had to prepare a presentation on that day's customer discovery for the next morning's workshop. Day 3 included only morning lectures. These three days were the most intensive section of the project because the schedule was packed with new topics (learning about entrepreneurial concepts), unfamiliar activities (searching for customers in a new city and introducing my research results to lay audiences), and challenging questions (from instructors at the workshop).

My presentation on Day 1 required a one-minute technical video to introduce my product and commercialization prospect. It was a video-version of an elevator speech and featured an appealing story line. The video was scripted in the following order: a challenging problem that greatly impacted the world (oil spill accidents), serious drawbacks of current solutions (shortcomings of oil absorbents on the market), my product as a new solution (a brief summary of the working mechanism of my product), and the advantages of my products compared to others (the process of my product at work). Because no previous zero experience in producing videos, I failed to explore the full potential of a video initially. The first draft was a slide show with my narrative, which delivered the story in a plain and boring manner. After collecting feedback from my team, I gave the video a face-lift in its second version by adding videos clips and background

music, which were the key difference between a video and a slide show. I included video clips to visualize the oil spill issue and labor-intensive process when using traditional soft absorbents; these built the stage where my products would debut. Then I presented a video clip of my absorbent manufacturing process resembling the style of science documentaries for the general public to bridge the gap between a scientific concept and an actual product. In the last scene, my product was shown functioning in a field test delivering the final message that my products were ready to solve problems.

Through this video and first business model canvas (Fig. 6.8), my team's first issue was identified. As a researcher, I focused on the features of my products, such as being reusable, biodegradable, and tailored to volume and composition of each individual oil spill accident. I listed the features of my absorbents as value propositions. Mistaking product features as value propositions was a common issue with all 20 teams in my cohort of the I-Corps program. These descriptions of features were adopted directly from my scientific journal manuscripts and suited the scientific community rather than industrial customers. Potential customers would like to see how my products could help them in solving a problem more efficiently (e.g., cleaning up oil spill ten times faster, saving 20% of cost, and requiring 50% less labor) or solving a problem that no other products could (e.g., cleaning up oil spill during bad weather or at geographically challenging areas like water surfaces covered with ice). Quickly, I updated the value propositions to "save material and labor cost in response to small-scale spills that happened at marinas."

The second issue was that I made assumptions about my customers' needs rather than listening to their opinions. For instance, I assumed my potential customers, marina operating managers, would like to have biodegradable oil absorbents that were

environmentally-friendly. However, after talking to three marina and fuel dock staff, I found out that there were no clear regulations requiring environmentally-friendly oil absorbing supplies, so they were not interested in this biodegradability feature. "Biodegradability" was just a jargon that distance me from my interviewees, so I decided not to discuss this feature in my following customer discovery.

6.5.5 Customer discovery phase

This phase was a six-week course, consisting of customer interviews, course material reading, and weekly online seminars to report progress to instructors. The course material each week covered different elements of the business model, except for value propositions and customer segments which were discussed in the kickoff phase. At the each seminar, I presented the new information acquired from customer interviews of the previous week and an updated business model canvas.

Immediately after returning from the workshop, I attended Offshore Technology Conference (OTC 2017) in Houston, TX. Through this exhibition, I identified potential key partners, for examples, manufacturers of oil concentration analyzers, which could verify the spill cleanup performance of our absorbents.

Then I returned to interview more marina staff at lakes near my location (College Station, TX) and invited them to talk about their experience with using pad and boom absorbents. I discovered that although marinas store oil absorbents on hand in case of spill, they do not use absorbents in a large amount. Also because of their limited usage of absorbent, they did not observe any drawbacks when using current available products. This finding inspired me to explore another customer segment, oil spill response contractors, which are widely available in the Houston area. One or multiple contractors are usually

called to a spill case by the responsible party or US Coast Guard depending on the spill size. A contractor uses both skimmers and absorbents to clean up, keeps a huge inventory of absorbents at any time, and receives truck-load of new supplies in response to a major spill (e.g. a medium size contractor spends $28,000 per year on absorbents and a contractor said he "*received absorbents in eighteen-wheelers.*") Amazed by the large amount of absorbents consumed, I asked if he would be interested in reusable absorbents to save material. His answer was no. Contractors add a surcharge to the disposal fee of used oil absorbents when charging their clients, so reusable absorbents may cut a contractors' profit. I was surprised by this response and concluded that different customer segments have their own views on a product. Being reusable to reduce material cost is not a value proposition to contractors.

I also attended the triennial International Oil Spill Conference (IOSC 2017), which expanded my interviewee scope to every link in the oil spill recovery business. One critical interview was with a sales representative from a polypropylene absorbent manufacturer. He described pad and sheet absorbents are ubiquitous among all manufacturing industry to clean up spill and collect leak, and they are often referred to as "industry paper towel." Then I realized that my absorbents have to compete with these mass-produced absorbents, and my absorbents would not be favored because of their price.

While researching about price of other absorbents, I visited several hardware stores and marine supply stores. On both occasions, I met boat owners who came to purchase absorbents to clean bilge water. Cleaning bilge water was a new concept as none of my team has any boating experience. A bilge is the lowest compartment of a boat and collects water in normal boat usage. The water has to be pumped out periodically to ensure safe

boat operation (e.g. too much bilge water may sink the boat). The water is often contaminated with oil, lubricant, and grease from bilge pumps, engines, or generators. Discharging of oily bilge water may result in fine. One boat owner suggested that our absorbents could serve as bilge water cleaners. This idea was innovative. First, rather than cleaning up oil spills, my products could be used as a prevention solution: preventing oil in bilge water from polluting the environment. Second, this new product application, bilge water cleaner, was not used widely like the absorbents. This product had a larger profit margin, which fit my team's product profile (a high-end product rather than a commodity product). This was the moment that my team's focus made a significant pivot (Fig. 6.9).

Another interviewee segment consisted of regulators (e.g. Environmental Protection Agency, US Coast Guard (USCG), Galveston Police Department) and training instructors (e.g. from Oil Spill Control Tactical and Operations Level training offered by Texas A&M University Engineering Extension Service). Interview sessions with two USCG members and the two instructors (who are former USCG members) all pointed out that Bakken crude oil and other shale oil are challenging for current available absorbents. I was excited about this finding. If my absorbents could absorb these oils, there will be a ready market without competitors. I decided to investigate these two oils in my future research plans.

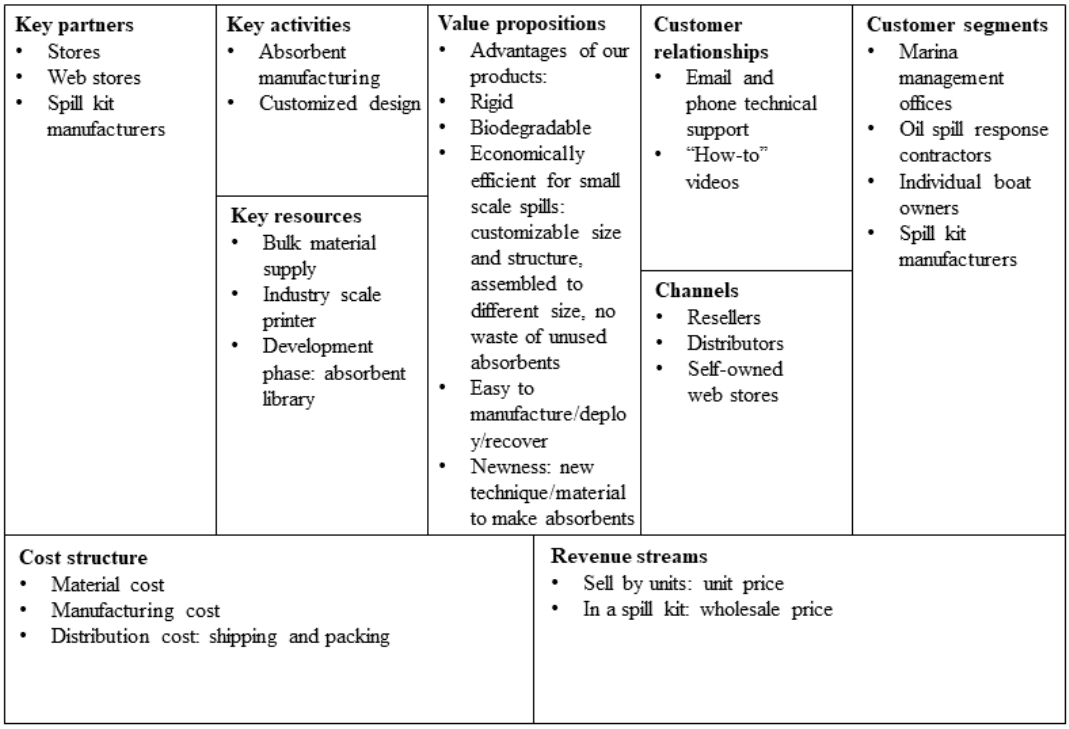

Fig. 6.8 Original business model canvas before the I-Corps training.

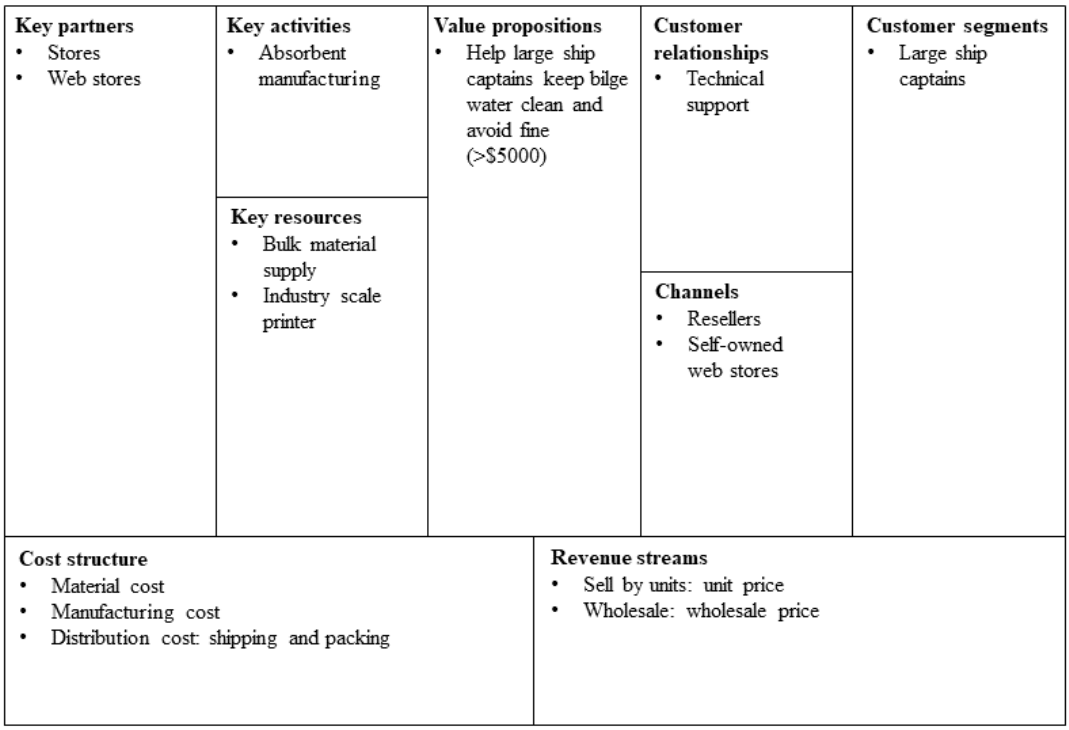

Fig. 6.9 Business model canvas after pivot during the training.

6.5.6 Closing phase

The final stage was a two-day closing workshop. The team summarized the progress and discussed with instructors to reach a final conclusion: a "go" (ready to commercialization) or a "no go" (need more research results and customer discoveries). My team reached the conclusion of "no go." This pivot to bilge water cleaner occurred one week prior to the closing workshop, so my team ran out of time to explore this market.

A 2-minute long *lesson learned video* was required at the closing workshop. The purpose of this video was to present the journey of the team exploring the commercialization process. To prepare the video, instructors recommended teams to review videos from previous cohorts. A majority of previous videos featured a common style: team members narrating the story in first person. I decided to reflect my personal taste by further exploring the story-telling nature of this video with a unique third-person fairy-tale narrative: a group of explorers (my team) was searching for a prize (commercialization opportunity) of a newfound treasure (my 3D printed oil absorbents). As a visual aid, I used a mix of photos to present real life elements (oil spill accidents, samples, and applications) and imaginary figures for story telling elements (story opening, ending, and plot twists) (full script in Appendix A).

6.5.7 Extension phase

The program also had an extended three months to explore commercialization opportunities. The follow-up customer discoveries after the training targeted a new group of customers: boat owners and boat manufacturers. I attended a boat show in Houston in June and found out that the timing was not ideal. Because my team's product was redefined as a spill prevention solution, the best season to present our product was before the start of boat season, the spring of each year. Therefore, the exploration of this spill

prevention market during late summer (June to September) put us at a disadvantage in terms of timing. In addition, my team further identified that large ships would greatly benefit from my team's products, which projected US Navy and cruise companies who own and operate large ships as a new customer segment.

6.5.8 Summary

Through this I-Corps program, I acquired new skills, experienced the entrepreneurial process first-hand, and gained an in-depth understanding of the commercialization prospect of my product. As a graduate student, I present my research mostly to the academic community, where the scientific values are most appreciated. During this program, my audience came from various industrial backgrounds with focus on the practical value of a product. I learned to substitute technological terms with common words in my speech and focused on the applications of my products rather than scientific features.

6.6 Reflection on Etsy project after I-Corps

After I-Corps training, I reviewed the failed Etsy business endeavor and applied the business model canvas to evaluate my Etsy store business (Table 6.1). The key failure was the lack of customer discoveries. I dreamed that the customers would love these amazing features of my products. However, I did not talk to customers before launching the shop. Customers do not need features (e.g., 3D printed, rigid). In contrast, they need solutions that either *solve a problem that has never been solved before* or *solve a solved problem through a cheaper way*. Unfortunately, my products could not solve problems that remained challenging for conventional oil diffusers. Furthermore, I invested so much effort in this project and was not willing to sell them at a cheap price. At the same time, I was wrong about the competitors. I assumed the competitors were other sellers on Etsy and

department stores that sell regular oil diffusers, so I copied their advertising style. However, compared these competitors, my products failed in offering a competitive price.

After this failure, I started to pay more attention to advertising strategies of other successful businesses. Since the selling point of my products was the cutting edge technology to produce them and a product that came from a scholarly laboratory directly, there was an urgent need to bridge the gap between the lab and the lay audience. To present my products as attractive pieces, I needed a narrative to help customers become familiar with my products. Because my products can drive away mosquitos, the pitch to promote these products can start with fighting against mosquitos and protecting people from the Zika virus. When I launched the store, I did not explicitly label my product as a virus prevention option and arrogantly assumed that every customer could see the importance of my products as a protection from the Zika virus. However, other fellow mosquito repellent related products all made a clear statement that they can repel mosquitos. A second point lacked was a personal touch. It would be good if my products could have an individual webpage/a stand-alone website to illustrate the manufacturing procedures of the products: photos of the printing process, machines, polishing tools, and so on. Furthermore, a product presentation would be a key element to add aesthetic value. My products photos were monotonic: a product on a slightly reflective black surface under natural light. Given the wearable nature of the bracelets, it would certainly become more appealing to customers to show photos of a person wearing the bracelet. Similarly, the diffuser products would show more features if they were photographed within a home environment. Although this business endeavor did not meet my expectations, I gained

valuable experience in planning a business and applied my I-Corps training to evaluate my failure.

6.7 Conclusions

I explored the commercialization possibilities of oil absorbents, bracelets, and diffusers through Etsy store and I-Corps program. Through these two attempts, I saw the gap between laboratory experiment inventions and market viable products. I also learned to change my market goal according to customers' opinions rather than my own assumptions. These experience taught me lessons that were not available within the academic environment. I am looking forward to applying my experience in further entrepreneurial effort should my other projects show potential for commercialization.

Table 6.1 Business model canvas analysis on the oil diffuser commercialization attempt.

Business canvas element	At the launch of Etsy shop	After I-Corps training
Value propositions	This section confused me the most during the I-Corps training because I mistook value propositions as features of my products. I listed value propositions as "rigid, biodegradable, customized, 3D printed oil diffusers." However, these were features of my products, not what customers might be willing to pay for.	From the perspective of customers, the value propositions include one-of-a-kind 3D printed oil diffuser to fit a personal need, serving as a conversation starter (e.g., "a home décor piece made with cutting-edge technology"), beautifying environment, and adding aroma into life.
Customer segments	For candle sleeves and oil diffusers, I assumed that my customers were interested in decorating their homes in an innovative way. For the repellent bracelet, my customers included everyone who wanted to avoid mosquito bites. My assumptions were too general.	Customer segments should be more specific. For example, one large segment of customers who might purchase the repellent bracelets is parents with young children who enjoy outdoor activities.

Table 6.1 Continued.

Business canvas element	At the launch of Etsy shop	After I-Corps training
Customer relationships	I considered including a video to demonstrate the oil loading process to attract potential customers. This plan was given up due to time conflict.	The "how-to" video is necessary to showcase the product. A Questions & Answers session with common questions listed and addressed will also clarify customers' confusion about the product. • Q1: What are 3D printed oil diffusers? • A1: 3D printed oil diffusers are rigid oil diffusers that gradually release aroma to rooms. Both the shape and releasing speed can be customized to your personal preference thanks to 3D printing. • Q2: Where can you enjoy 3D printed oil diffusers? • A2: A diffuser can be used wherever an aroma is needed. The diffusers release aroma naturally and do not require power to operate. • Q3: Are 3D printed oil diffusers easy to set up? • A3: Yes, using 3D printed oil diffusers is as easy as shown in the "How to" video. • Q4: Do 3D printed oil diffusers need special oil products? • A4: No. Regular essential oils are compatible with these diffusers.

Table 6.1 Continued.

Business canvas element	At the launch of Etsy shop	After I-Corps training
Channels	The channel was Etsy. I initially considered local and nearby handmade products trade shows, though did not pursue it due to time conflict. I attended a local trade show one year after closing my store and came across a booth selling another type of novel essential oil diffusers. This product had the same function and similar price range as mine.	A handmade product trade show can be a good choice. By attending the show, the customers have already shown their interest in handmade products. Person-to-person interaction with customers can provide me a chance to introduce my products thoroughly. Another option is a boutique store. Etsy has no clear threshold regarding the creativity and uniqueness and is open to any handmade ones. However, a boutique store has an operation team to evaluate the potential of a product and will give me an initial evaluation of the popularity of my products at their listing prices.
Key activities	Key activities were producing the oil diffusers with customizable options and sending them to customers.	The key activities are producing the oil diffusers and contacting selling platforms (trade shows and boutique stores).
Key resources	Key resources were the raw material, 3D printers, and packaging materials. I had all the resources.	Key resources are raw material, 3D printers, and packing materials. These resources are easy to obtain.
Key partners	None.	The key partners are providers of material and machine and selling platforms (trade shows and boutique stores).
Cost structures	The cost consisted of raw material, operation, packing, shipping, and listing.	Commission fees for trade shows and physical stores and labor cost also contribute to the overall cost.
Revenue streams	I did not consider this section.	The revenue streams include setting retail price and wholesale price.

CHAPTER VII

EMBEDDING HANDS-ON LABORATORY AND 3D PRINTING EXPERIENCES IN UNDERGRADUATE COURSES[1]

7.1 Overview

Hands-on experience are proven to be an effective approach to teach engineering. [170] They bridge the gap between textbook theories and real life problems, and then offer the opportunities of "learning by doing." However, embedding hands-on activities in undergraduate courses and K-12 education program faces a myriad of challenges: limited lecture time and classroom space, additional cost for equipment and supplies, and complicated activities that further confuse students rather than help them learn. There is a need for designing accessible and easy-to-implement hands-on activities for engineering students. Here I present my experience in design and execute hands-on activities in four projects: adding mini-lab experience to a core undergraduate fluidic mechanics course,[171] training undergraduate researchers in 3D printed oil absorbent application study through Aggie Challenge, teaching basic physics principles (capillary action) with 3D printing demonstration at local science events, and developing accessible hands-on activities enabled by 3D printing.

7.2 Mini-lab experience

7.2.1 Introduction

While serving as a teaching assistant for an undergraduate laboratory course in Spring 2013, I saw firsthand the value of hands-on experience in teaching engineering concepts.

[1] Part of results reported in this chapter was reprinted with permission from: Embedding Hands-on Mini Laboratory Experiences in a Core Undergraduate Fluid Mechanics Course: A Pilot Study by Han, D. et al. Chemical Engineering Education, Vol. 51, No. 3, Page 136-144, (2017). Copyright 2017 Chemical Engineering Division of the American Society for Engineering Education.

This experience sparked my interest to participate in laboratory course development, and eventually I enrolled in the Graduate Teaching Fellow program in College of Engineering during the Fall 2016 and the Spring 2017 semesters. This program provided the opportunity to actively participate in undergraduate level teaching with the help of a faculty mentor and a friendly environment for graduate students to share teaching experience. The student was expected to develop and teach a course under the guidance of a faculty mentor.

My project aimed to address the challenges associated with delivery of hands-on experiences in large classes, and my solution was embedding "mini-lab" experiments operated on pilot scale instruments directly into a junior-level core fluid mechanics course. My advisor and I piloted an adaptation of mini-labs that consisted of three 50-min laboratory sessions designed for the undergraduate core fluid mechanics class in the Department of Chemical Engineering at Texas A&M University as part of a three-course sequence covering momentum, heat, and mass transport. The course (CHEN 304) uses the textbook, *Fluid Mechanics for Chemical Engineers*, by J.O. Wilkes, and 155 students enrolled in fall 2015 (across three sections, one of which participated in the mini-lab pilot) and 28 students in spring 2016.

Three mini-labs were developed focusing on fluid mechanics concepts including friction losses in pipes, flow measurement, and centrifugal pump analysis. These topics dovetail with the dedicated senior-level unit operations laboratory course but are presented in a more focused and concise format (Table 7.1). Students were assigned to complete the mini-labs in the same manner as a typical homework assignment and were responsible for booking time on the experiment apparatus using an online scheduling tool. In addition to

reinforcing fundamental concepts, the mini-labs were structured to help students gain confidence in problem solving, establish self-identities as engineers, and obtain experience working in teams. I was the lab instructor.

Table 7.1 Comparison between mini-labs and dedicated unit operations laboratory courses. Reprinted with permission.[171]

	Mini-labs	**Dedicated unit operations laboratory course**
Curriculum schedule	Junior year, part of fluid mechanics course, lab completed within two weeks after concepts covered in lecture	Senior year, lab completed one or two semesters after concepts covered in lecture
Content scope	Fluid mechanics	Fluid mechanics
Prerequisite	Differential equations, material balances	Fluid mechanics course
Scheduling approach	Online scheduling tool deployed after the concepts are covered in lecture	Students register for a dedicated course
Attendance	Optional during fall 2015 pilot, mandatory as part of spring 2016 pilot, students unable to attend were given an alternate assignment	Mandatory
Level of participation	Groups of 1 to 4 students run lab and submit individual assignments	Groups of 4 students run lab and submit a single group report
Length of meeting time	Three 50-min sessions	Weekly 3-h sessions

Table 7.1 Continued.

	Mini-labs	Dedicated unit operations laboratory course
Level of in-lab instruction related to theory	Review of fundamental concepts and step-by-step demonstration of experiment procedures	Minimal
Lab report format	Assignment involving data analysis and answers to discussion questions, primarily evaluated for technical content	Formal written lab report including background, materials/methods, results/discussion, and conclusion sections, oral presentation
Lab report workload	1 to 2 h, comparable to typical homework assignment questions	Writing intensive, 4 to 5 h per student
Lab report focus	Basic data analysis and short answer questions to describe key phenomena	Thorough data analysis, technical writing emphasized
Learning objectives	Apply mass and momentum transport principles, analyze experiment data	Apply mass and momentum transport principles, acquire accurate data, analyze experimental results, prepare formal written reports, give oral presentations

7.2.2 Experiment courses in engineering education

The engineering profession involves applying fundamental scientific and mathematical concepts to solving problems involving real systems. These fundamentals are typically introduced in a theoretical context, making instructional laboratories vitally important to bridge the gap between concept and application.[172] In addition to introducing real-world scenarios,[173] laboratory experiences enable students to develop self-identities as engineers with relevant and valuable problem-solving skills.[174] Achieving an optimal

balance between theory and hands-on experience has been an important aim in engineering education since the nineteenth century. During this period, both military academies and civilian schools heavily underscored laboratory experience in the curricula by virtue of its focus on design and construction of machines and tools.[175] This practical focus continued until the mid-1950s when the Grinter report, issued by a committee formed under the American Society for Engineering Education (ASEE), advocated a shift from practice-oriented activities to basic science as part of an emphasis on solving problems by referring to fundamental principles.[176, 177] In the 1980s, the former Engineer's Council for Professional Development issued new criteria to evaluate engineering programs that brought renewed focus to laboratory courses,[178] and ASEE further reaffirmed the irreplaceable role of laboratory experiences.[179] At present, ABET criteria for accrediting engineering programs prominently include availability of laboratory facilities to support achievement of learning outcomes.[180] It is now widely accepted that laboratory courses effectively promote active and cooperative learning,[177, 181] both of which are proven to enhance engineering education and accommodate students with different learning styles.[182]

Unit operations laboratory courses play a critical role by allowing students to apply momentum, heat, and mass conservation principles in chemical engineering.[183] These laboratories are generally scheduled during the senior year, after fundamental instruction associated with these subjects has taken place in previous theory courses. This structure inevitably leads to a multiple-semester delay between the introduction in theory courses and the real-world applications, and reduces the effectiveness of laboratories to reinforce fundamental learning objectives.[184] Integrating laboratory experiences into a theory

course therefore offers an opportunity to link theory and application at the same stage of the curriculum.

Hands-on experiments, sometimes referred to as "learning by doing," have been explored as a method to capture student interest and enhance achievement of learning outcomes.[170] These activities have been broadly implemented across academic levels ranging from high school [185] to the undergraduate senior-level capstone design.[186] Beginning in high school, one example involved a one-week summer camp for students offering hands-on projects intended to attract the students to the engineering field (e.g., air pollutant measurement, water desalination). These activities were credited with contributing to the camp's success, with 28 out of 30 students indicating an interest in pursuing an engineering major as a consequence of participation.[185] At the undergraduate freshman level, a hands-on experiment exploring the science of carbonated soft drinks was incorporated into an introductory engineering course.[187] This activity enabled students to apply fundamental chemical engineering principles (gas absorption) toward a practical application at an early-stage of college study (e.g., how to keep soft drinks carbonated after their containers were opened), with the goal of increasing retention in the chemical engineering major. Although generally successful, some students found the open-ended nature of the project to be challenging. At the sophomore level, the Controlled Operation Mechanical Energy Transducer (COMETs) competition, was designed to expose students to a complete cycle of designing, building, and testing a product. This hands-on project was welcomed by students as learning "away from paper and theory," but strengthening the connection with the course material (i.e., energy balances) was cited as an area for improvement.[188] In the upper-level engineering curriculum, hands-on

experiments have been implemented in junior-level core courses, including fluid mechanics, heat transfer, and mass transfer. Students have, for example, been assigned tasks associated with design and scale-up of heat exchangers [189] and identifying leaks in a gas separation device.[190] These senior students gave positive feedback. However, the additional time commitment and operational costs involved imposed barriers against expanding implementation to other subjects.

Desktop-scale modules have been explored as a way to enable application of hands-on activities owing to their low cost and ability to be operated during regularly scheduled class time. For instance, inexpensive apparatuses (e.g., coffee cup warmers, metal rods, and CPU heat sinks) were used to assemble portable demonstration sets aligned with fundamentals of heat transfer.[191] Working in teams, students were able to study the apparatus at their own pace and actively engage with peers displaying different learning styles. In another adaptation of desktop-scale experiments, a pre-assembled see-through shell and tube heat exchanger was analyzed by students in teams.[192]

Virtual “weblabs” have also been explored because of their minimal space, staffing, scheduling, and safety requirements. For instance, students remotely operated a set of heat exchangers via a software interface.[193, 194] Students valued the opportunity to learn remotely through a hands-on experiment while practicing data collection and analysis. However, the lack of physical interaction with real equipment made it challenging for students to replicate the first-hand experience of troubleshooting and dealing with uncertainty, leading some students to view the instruments as virtual elements that are not likely to malfunction or generate imperfect data. Live, remote, and virtual labs each offer

their own unique benefits, and a balanced combination of each is therefore likely to deliver the most impactful student experience.

7.2.3 Methods

7.2.3.1 Organization and implementation

Mini-labs were scheduled concurrently with presentations of corresponding fundamental material in the theory course. Each student was asked to book a single 50-min session using the *SignUpGenius* service (www.signupgenius.com), an online scheduling tool. Time slots were assigned on a first come first served basis, and the signup tool remained open throughout the entire one to two-week period during which mini-labs were scheduled. Students were able to change their signup choices at any time prior to the start of their session. Preparatory materials were provided through the course website, as well as a guide to each experiment, assignments, and safety information.

The lab instructor provided an introduction to the experiment apparatus (a single Armfield C6-MKII-10 station), the associated theory concepts, and the operation procedure. Students were asked to work in groups of up to four to operate the apparatus and collect data. Instructions regarding the accompanying data analysis assignment were provided upon completion of the experiment. Students completed the assignments individually, and the instructor was available by appointment to answer questions. Anonymous assessment surveys were conducted using the online platform *Qualtrics* to gather student feedback about their pre-, in-, and post-lab experiences.

Student participation in the mini-lab pilot is detailed in Table 7.2. For lab 1 during the fall 2015 semester, the mini-lab and the alternate assignment were both optional. For lab 2 during the fall 2015 semester, the mini-labs were optional, but the alternate assignment

was mandatory. During the spring 2016 semester, mini-labs were mandatory, and the alternate assignment was mandatory for students who could not attend under circumstances accepted by institutional excused class absence policies. The alternate assignment included a video screencast describing the apparatus, theory background, operation procedure, and acquisition of a sample data set. Students were then asked to complete the same lab assignment as students who attended the mini-lab sessions using the provided sample data set. Examples of the screencasts are available online (friction loss in pipes - https://youtu.be/m3RuDhHLkt8; flow measurement - https://youtu.be/3KsgeiJHI10; a screencast for the centrifugal pump mini-lab was not prepared).

Table 7.2 Student participation in mini-lab pilot. Reprinted with permission.[171]

Semester	No. of students registered for fluid mechanics course	Mini-lab content	No. of students who participated in mini labs	No. of students who completed post-lab surveys
Fall 2015	47 Mini-lab not mandatory	Lab 1: flow measurement	26 attended 20 submitted lab assignment 4 submitted alternate assignment	Survey 1: 19 Survey given after completion of lab 1
	47 Either mini-lab or alternate assignment mandatory	Lab 2: friction losses in pipes	35 attended 33 submitted lab assignment 10 submitted alternate assignment	No survey
Spring 2016	28 Mini-lab mandatory	Lab 1: friction losses in pipes	28 attended 28 submitted lab assignment	Survey 2: 19 Survey given after completion of all 3 mini-labs
	28 Mini-lab mandatory	Lab 2: flow measurement	27 attended 26 submitted lab assignment 1 submitted alternate assignment	
	28 Mini-lab mandatory	Lab 3: centrifugal pump analysis	27 submitted lab assignment	

7.2.3.2 Course development cycle

A standard course development cycle framework was used in the instructional design process, as described below.

- **Analysis:** The purpose of the mini-labs is to embed fluid mechanics unit operations experiences into a lecture-based theory course to provide early exposure to hands-on activities, reinforce theory-oriented fundamental concepts, and offer opportunities to apply fluid mechanics principles to solve real-system problems.
- **Design:** Each mini-lab focuses on one concept and invites students to participate in a short lab session scheduled outside the regular class meeting time, after which students complete a data analysis assignment.
- **Develop:** The experiment procedure was developed by the instructor and tested with the help of an undergraduate honors program student.
- **Implement:** Students were asked to participate in mini-lab sessions and complete lab assignments.
- **Evaluate:** Student performance on lab assignments was assessed. Student feedback was collected and used to modify course design.

7.2.4 Results and Discussion

7.2.4.1 Teamwork

To foster teamwork, each mini-lab session was structured to allow up to four students to participate as a group. Around 60% of the sessions had three to four participants. Students were prompted to take turns performing different tasks (e.g., changing pressure sensor positions and flow rates, recording data, and operating the control software) and discuss their observations in the group setting. Communication among students was observed by the lab instructor. For example, in the flow measurement lab, one student who changed the pressure sensor position announced out loud the sensor positions. The student in charge of acquiring data also read the number aloud to confirm the measurement and

ensure that all participants could record the data. One student who was using crutches was also able to perform data recording tasks with the aid of other students in the group.

7.2.4.2 Assessment of learning objectives

The mini-lab learning objectives were structured to lead students toward the dedicated senior-level unit operations laboratory course, which emphasizes equipment operation, data recording and analysis, and communication of technical results via written and oral formats.[195] Assessment methods and results for the three mini-labs piloted are summarized in Tables 7.3, 7.4, and 7.5. An additional evaluative assessment question included in each mini-lab asked students to list at least two possible sources of error in the experiment.

Multiple students expressed positive impressions of mini-labs as a tool to reinforce the theory course learning objectives, with *visualization of real equipment* as a recurring theme. Representative positive responses to the question "are mini labs an effective use of your time to help reinforce the lecture material?" included the following.

- *"It helped me relate the lecture to the real world."*
- *"Being able to visualize the meters we were talking about was really helpful."*
- *"Seeing the actual equipment helps understanding material conceptually."*
- *"Definitely effective to help reinforce the material for me, since I am a pretty visual learner."*
- *"I believe the mini-labs were useful in the fact that they gave me more 'face time' with the material as well as that they allowed me to practice more problems with the different types of scenarios pertaining to fluids."*

Some negative comments were also expressed as follows.

- *"It was too long and repetitive to fill out the whole table."*
- *"Let us get a little more involve in the experiment. We just moved sensors to where were suppose. While I was fine doing them, I didn't feel like they added additional insight from what we were already discussing in lectures. Make use think a little more during the lab."*
- *"I think mini-lab 3 needs to have more to it. Simply plotting 5 points did not have much meaning to me. Otherwise mini-lab 1&2 need to somehow have less work. It would also help to do the labs earlier in the semester so they are not all back-to-back right before finals and projects."*

The mini-labs also helped students tie their visual impressions back to fundamental principles and link their experiences with real equipment back to the theory. As one student said, "*I worked with orifice plates in internship this summer, and it was very interesting to actually be able to do the calculations that accompany them."* The assessment survey also indicated that 73% of students reported feeling new confidence in their ability to solve real-world problems and were able to see themselves as future engineers.

Table 7.3 Learning objectives linked to mini-lab #1 (friction losses in pipes). Reprinted with permission.[171]

Learning objective	Level of learning	Assessment method	Assessment result
Measure pressure drops in pipe segments of different diameters and roughness at different flow rates	Remembering	Method: Instructor's observation Level of assessment: group Purpose of assessment: formative Object of assessment: behavior	Students were able to finish the tasks, either in a group or individually, without difficulties. This operation required changing pressure sensor positions. Students communicated effectively among each other about the parameters being measured.
Calculate friction factor with pressure drop data	Applying	Method: lab assignment Level of assessment: individual Purpose of assessment: formative Object of assessment: skill	91% of students answered the question correctly.
Compare friction factor with correlations (Moody chart)	Evaluating	Method: lab assignment Level of assessment: individual Purpose of assessment: formative Object of assessment: skill	68% of students answered the question correctly. Some students had difficulties working with logarithmic-scales and consequently plotted their data incorrectly.

Table 7.4 Learning objectives linked to mini-lab #2 (flow measurement). Reprinted with permission.[171]

Learning objective	Level of learning	Assessment method	Assessment result
Measure pressure at different positions across flow meters at different flow rates	Remembering	Method: instructor's observation Level of assessment: group Purpose of assessment: formative Object of assessment: behavior	Students were able to finish the tasks, either in a group or individually, without difficulties. This operation required changing pressure sensor positions. Students communicated effectively among each other about the parameters being measured.
Calculate the flow velocity at different positions	Understanding	Method: lab assignment Level of assessment: individual Purpose of assessment: formative Object of assessment: skill	88% of students answered the question correctly. Tables provided for students to record their data were revised in spring 2016 based on feedback from the previous semester.
Calculate the flow rate using the Venturi equation	Applying	Method: lab assignment Level of assessment: individual Purpose of assessment: formative Object of assessment: skill	88% of students answered the question correctly. This question could be self-checked by comparing with the apparatus' electronic flowmeter reading.
Calculate discharge coefficient and flow rate using the orifice plate equation	Applying	Method: lab assignment Level of assessment: individual Purpose of assessment: formative Object of assessment: skill	70% of students answered the question correctly. This question could be self-checked by comparing with the apparatus' electronic flowmeter reading.

Table 7.5 Learning objectives linked to mini-lab #3 (centrifugal pump analysis). Reprinted with permission.[171]

Learning objective	Level of learning	Assessment method	Assessment result
Measure discharge head at a fixed impeller speed at different flow rates.	Remembering	Method: Instructor's observation Level of assessment: group Purpose of assessment: formative Object of assessment: behavior	Students were able to finish the tasks, either in a group or individually, without difficulties. This was the third mini-lab performed, so students had developed deep familiarity with the procedures.
Plot a pump performance curve	Understanding	Method: Lab assignment Level of assessment: individual Purpose of assessment: formative Object of assessment: skill	All 27 students answered this question correctly.
Identify how discharge head changes with flow rate	Analyzing	Method: Lab assignment Level of assessment: individual Purpose of assessment: formative Object of assessment: skill	All 27 students answered this question correctly.

7.2.4.3 Scheduling

Some challenges were encountered in coordinating the students' schedules and the availability of the lab apparatus. Standard class periods are scheduled for either 50 minutes (Monday, Wednesday, and Friday) or 75 minutes (Tuesday and Thursday). To avoid overlap with multiple course periods and keep the lab material consistent, each lab session was structured so that it could be completed in 50 minutes. The time slots were arranged to

begin at the same time as regularly scheduled courses. Since the mini-labs share apparatus with the senior-level unit operations laboratory course, only limited four-hour periods in the mornings were available, allowing three time slots to be opened (Table 7.6). With groups of up to four per session, mini-labs scheduled during four consecutive weekdays (12 total sessions with capacity for 48 students) successfully accommodated all the enrolled students. Additional sessions were scheduled for individual students who could not attend during these time slots.

Table 7.6 Comparison between mini-lab schedule and regular course schedule. Reprinted with permission. [171]

Regular course schedule (Monday, Wednesday, and Friday)	Mini-lab schedule (Monday, Wednesday, and Friday)	Regular course schedule (Tuesday and Thursday)	Mini-lab schedule (Tuesday and Thursday)
9:10 – 10:00 am	9:10 – 10:00 am	8:00 – 9:15 am	8:25 – 9:15 am *
10:20 – 11:10 am	10:20 – 11:10 am	9:35 – 10:50 am	9:35 – 10:25 am
11:30 – 12:20 am	11:30 – 12:20 am	11:10 – 12:25 pm	11:10 – 12:00pm

*This session is postponed to match the end time of the first regularly scheduled course.

7.2.4.4 Student feedback survey results

7.2.4.4.1 Pre-lab experience

- **Sign-up:** All students who participated in the survey stated that the sign-up system was easy to use.
- **Lab preparation material:** The majority (92%) of students agreed that the materials posted on the course website were helpful.

7.2.4.4.2 In-lab experience

- **Time arrangement:** All students who participated in the survey stated that they had enough time to complete the experiments, either participating alone or in a group. The lab instructor agreed.
- **Worksheet for data recording:** The majority (92%) of students agreed that the worksheets provided were easy to use.
- **Introduction from the lab instructor:** All students agreed that the lab instructor was effective in giving background introduction about the theory and operation demonstration. The lab instructor was "*to the point on introduction*, *also tied everything to what we were learning in class."*

7.2.4.4.3 Post-lab experience

- **Homework load**
    - Survey 1 (fall 2015, lab 1: flow measurements)
        - Students spent an average of two to three hours on the lab assignment, and 50% agreed that the workload was higher than a typical homework assignment.
        - Student feedback toward the lab assignment calculations was mixed. Some reflected that "*the repetitive calculations also helped reinforce the course material*," whereas others responded that "*the write-up was very iterative and took a lot of time, about 50% of the time I spent learning and the other 50% was just changing numbers in my calculator and pressing enter*," and "*I should have done it all in Excel*."

        - We reduced the workload significantly in fall 2015, lab 2 (friction losses in pipes) from one and a half to one hour by decreasing the number of parameters tested.
    - Survey 2 (spring 2016: all labs):
        - Most students agreed that Lab 1 (friction losses in pipes) and Lab 2 (flow measurement) had a similar workload to a typical homework assignment, and Lab 3 (centrifugal pump analysis) has a lighter workload. The students spent 1.45, 1.57, and 0.72 hours on the lab assignment, respectively.
- **Lab assignment format and instructions**
    - In Survey 1, some students indicated that headers of the data tables were confusing. For example, students were confused about which flow rate should be chosen to calculate the Reynolds number.
    - To address this issue, data tables were revised (for example, to clearly state that the electronic flow meter readings should be used to calculate Reynolds number).
    - More instructions were also provided upon completion of the experiment, and students were encouraged to contact the lab instructor with any questions.
    - While grading the lab assignments in the fall 2015 semester, the lab instructor noted that several students plotted their data incorrectly. Then in the 2016 spring semester, the lab instructor gave additional instructions on reading logarithmic scale and notified the students that it was a common mistake in previous classes.

- Some students also expressed concern about scheduling labs during weeks close to final exams, with comments including" *Do the lab earlier in the semester*" and "*have them consistently*" along the course rather than "*all back-to-back right before final and projects.*"

7.2.4 Connection to theory course

We examined the course grades of the Spring 2016 cohort, for whom participation in the mini-labs was mandatory. This class of 28 students earned an average course grade of 3.233, which was over one standard deviation greater than the five-year average grade for the course in previous sections taught by the same instructor where no mini-labs were included (3.107 ± 0.058). Although these data are preliminary, they nevertheless provide encouraging evidence that the mini-labs enhance student mastery of the course learning objectives.

Student perspectives toward the fundamental concepts and their applications to real-world examples were quantified in terms of their level of confidence in solving problems associated with the mini-lab experiments at three different time points: after attending the lecture, after attending the mini-lab session, and after completing the data analysis assignment. Student responses were classified according to four different levels of problem solving skills. Each successive level includes the skills described in the preceding levels.

- **Level 1:** *I am unfamiliar with friction loss and unable to solve problems involving them*.
- **Level 2:** *I have a basic knowledge of the subject. I know enough to prepare for homework and exam problems*.
- **Level 3:** *I am able to apply textbook principles in a controlled laboratory environment*.

- **Level 4:** *I am able to solve real-world problems that I may encounter as an engineer.*

After classifying the student responses, their perceptions of mastery were interpreted in the context of the goals listed below.

- **Goal 1:** Reach skill level 2 after attending the theory course
- **Goal 2:** Reach skill level 3 after attending the mini lab
- **Goal 3:** Reach skill level 4 after completing the data analysis assignment

Goal 1 reflects a minimum level of mastery upon completion of classroom instruction and is asked to confirm that students are equipped with the fundamental knowledge needed to perform the mini-lab experiment. Goal 2 reflects the primary objective of the mini-labs, focusing on hands-on experience acquired simultaneously with the theory course instruction. Goal 3 reflects an additional level of mastery, as mini-labs are executed in a controlled environment that is less complicated than real systems. This goal captures the design of mini-labs as a vehicle to help students begin to develop self-identities as engineers.

7.2.4.1 Survey 1 (fall 2015, lab 1 (flow measurements))

Overall, 50% of students responded that they "learn more in a mini-lab than a typical homework assignment." Mini-labs offer experiences not available in conventional theory courses, such as exposure to the physical equipment and involvement in data collection and analysis. These unique experiences therefore likely contributed to impressions of "learning more." As to the level of confidence in solving problems involving flow meters (Fig. 7.1), 100% of students felt prepared for the mini-lab after attending the theory course (reached goal 1). With respect to higher-level goals, 88% of students perceived that they met the primary goal of the mini-lab (goal 2), and 47% perceived that they attained the

additional level of goal 3. It should be noted, however, that self-assessments of student mastery are often biased toward higher ratings than objective assessments.

7.2.4.2 Survey 2 (spring 2016, all labs)

In lab 1 (friction losses in pipes) and lab 2 (flow measurement), most students responded that they learned more in this lab than a typical homework assignment. In lab 3 (centrifugal pump analysis), most students responded that they learned less in this lab than a typical homework assignment. Lab 3 appeared to be slightly less effective regarding homework problem solving (goal 1), which might be partly attributed to the lack of homework problems focused on the same concepts to serve as a prior reference. Students also suggested adding more content to lab 3 regarding pump curve construction and/or merging lab 3 with other labs. The fact that all three labs shared the same apparatus possibly contributed to a feeling that lab 3 "seemed too simple and could go up another level" as students were familiar with the apparatus after the first two sessions. We interpreted this reaction positively as students gaining confidence in working with real equipment and solving engineering problems through mini-labs exercises.

As for the level of confidence in solving problems, students expressed similar responses regarding all three mini-labs with 100%, 93%, and 73%, indicating that students perceived that they met goals 1, 2 and 3, respectively. Achievement of goals 1 and 2 remained the same as in fall 2015, while goal 3 experienced a higher level of perceived attainment due to two factors. First, the mini-lab procedure was refined according to student feedback from the fall 2015 lab sessions and surveys. Second, many spring 2016 students had completed more junior level engineering courses and/or industry internships

than the fall 2015 students, thereby building more confidence and more clearly picturing their future engineering careers.

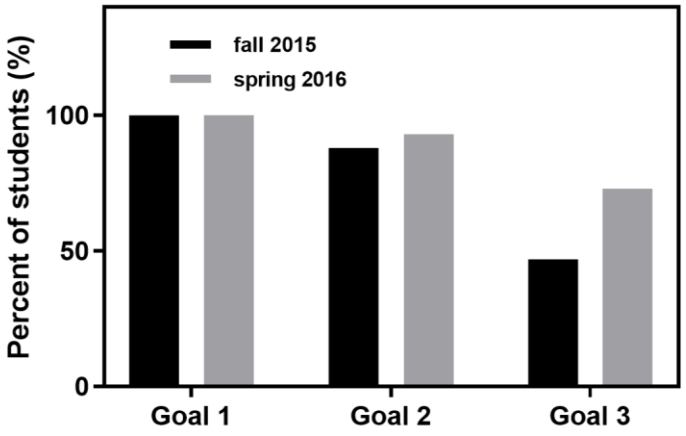

Fig. 7.1 Student feedback expressed perceptions toward reaching the three goals set for mini-labs for fall 2015 and spring 2016. Reprinted with permission. [171]

7.2.5 Using mini-labs to accommodate different learning styles

Felder and Silverman have expressed that there is a need to reach students of different learning styles when selecting teaching approaches. [182] Mini-labs can help achieve this goal by mixing multiple teaching approaches. The group experiment model and the individually completed lab reports are tailored toward active and reflective learners. The physical data gathering and data analysis through calculation suit the need for sensors and intuitors. The pilot-scale instrument experience with clearly defined steps to obtain a final result suits both global and sequential learners. In conclusion, this mini-lab model could accommodate all different learning styles.

7.2.6 Limitations

7.2.6.1 Mini-labs

The limited time available for scheduling the lab sessions was an issue because each session must be 50 minutes or less in order to accommodate the students' regular course

schedule. Operation instructions were given in detail by the lab instructor, and data recording sheets were provided with all parameters listed to save time. These approaches effectively accelerated the lab session but limited students' development of practical laboratory skills such as troubleshooting of the apparatus and experiment planning that are covered in dedicated laboratory courses of longer duration.[196]

7.2.6.2 Study approach

The number of students enrolled in this study was limited, and their willingness to voluntarily participate in the mini-labs and surveys was impacted by their regular semester schedule. The survey for all three labs in the spring 2016 semester was distributed after the final exam, and the response rate was only 68% (19 of 28). Scheduling constraints also made it difficult for us to designate a direct control group for our study. Since a cohort of students in the pilot section of the course during fall 2015 did not participate in the mini-labs, participation was not required. Thus, the fact that the students who participated had already demonstrated initiative by seeking out the experience may introduce bias. We are working to design future studies to include pertinent controls.

7.2.7 Instructor's experience

7.2.7.1 Prior teaching experience

In 2015 spring semester, I enrolled in the *Professional development for future faculty* course. The course was delivered in a *flip classroom* format, in which students read course material before classes and discussed them in classes with instructors. The course material included learning objectives, course development cycles, different learning styles, and teaching tools, which gave me the chance to learn to develop and deliver a course.

The highlight of this course was preparing a teaching philosophy, which is a statement describing one's perspective on teaching, and a personal touch is appropriate and encouraged. This assignment was different from routine writing tasks (e.g., recording experiment results, preparing journal manuscripts) for graduate students, so the instructors reviewed the draft twice and offered feedback at different phases of the writing process. I gained valuable feedback from both reviews and was able to improve my writing. Although my opinions on teaching kept developing as I participated in more teaching activities, this first teaching philosophy provided a strong base for me to develop my view on teaching. I appreciate the idea of "learning by doing," and engaging students through activities.

Another major project of this course was preparing and presenting a lecture for an undergraduate course. I presented my lecture at the junior-level CHEN 304 fluid mechanics course on the topic of "fluid flow of non-Newtonian fluids in pipes," which was suggested by my advisor, who was the instructor of this course. This topic was a follow-up session of a lecture "fluid flow of Newtonian fluid in pipes," which is a classic subject in the fluid mechanics course and given by my advisor one week prior to my lecture. This lecture also discussed non-Newtonian fluids, which were not intensively covered in the undergraduate fluid mechanics course except for a brief mention as part of the concept of viscosity. This topic gave me the chance to contribute new content to the course and relieved me from the pressure of introducing a totally new topic to students.

This lecture involved an intensive equation deduction process. To help my students follow the math work, I decided to prepare partial notes for students to fill in during the lecture. I wrote down half of all the deduction steps and distributed scanned hard copies

prior to the lecture. During the lecture, I explained the deduction process and wrote down the missing steps on my notes while projecting them onto a projector screen.

This course was scheduled as the first class of the day at 8 am. To grab students' interest at this early hour, I started my lecture with a demonstration experiment to illustrate different types of non-Newtonian fluids: cornstarch aqueous solution as shear thickening fluid and a video clip from a popular TV show that illustrated a similar idea. I also used a bottle of face lotion and a jar of peanut butter, as examples to illustrate the idea of shear-thinning fluids. At the end of the class, I sent out a survey to collect feedback from students about my teaching and gave out candy as a small gesture to show my appreciation of students' participation. I recorded myself during the lecture to evaluate my teaching later.

Upon reviewing the video record, I spotted my problems in delivering lectures: inconsistent voice volume and lack of interaction with students. My voice faded out after 30 minutes into the lecture. Luckily, the classroom was small, so students could still hear me without problems. As a new and nervous lecturer, I paid more attention to my notes rather than my students. This teaching experience exposed my shortcomings in delivering lectures.

7.2.7.2 Improvement in teaching

While preparing the course material for this mini-lab series, I reviewed my earlier teaching video record and decided to improve my teaching skills during these new teaching activities. This mini-lab activity was conducted in a small laboratory with three to four students in a group, and both my students and I were standing in a circle close to the experiment apparatus. Though I had to raise my voice to compete with the background

noise generated by the apparatus (pump, water flow, and fume hoods), I managed to speak loudly and clearly.

The next issue was to maintain eye contact with my students and get their feedback in real time. While preparing my lecture, I made specific notes to myself to pause my lecture after each important knowledge point, ask my students whether they could follow me, and encourage them to ask questions. With this small class size, I was able to get a verbal confirmation (or at least a nod) from each of my students as a green light to continue my lecture. Although this mini lab teaching environment was unique in its hands-on nature and small class size, these newly gained teaching experiences will certainly help me in traditional classroom teaching tasks.

7.2.7.3 Teaching philosophy

After completed mini-lab session, I revised my teaching philosophy, citing the mini-lab session as an example to illustrate my vision of how hands-on experience complements traditional engineering education.

"In my opinion, the fundamental goal of teaching is not making students learn but promoting learning. Learning takes place when the gap is filled between the previous experience and the new concepts or skills. An instructor's role is to show the connections between the known and unknown. Engineering major instructors are also responsible for helping students achieve "engineering literacy," which is more than just knowledge of engineering concepts, and also the ability to apply engineering knowledge to everyday problem-solving situations.

From my learning experience as a student, hands-on experience is an effective approach in teaching engineering, and a laboratory course is the most common format. The

unit operation laboratory course, one of core chemical engineering courses, is usually scheduled in senior year after the theories applied in these experiments are covered in junior year (momentum, heat and mass transfer course). Inevitably, there is a one to two semester's gap. It is not uncommon that senior students forget the theories while participating in these experiments, and junior students have no opportunity to see the connection between theory and application. To bridge the gap, I developed a series of lab sessions for a junior year fluid operation course with the help of my academic advisor. Three 50-minute lab sessions that covered basic fluid operations topics were scheduled within two weeks after the theory was covered. While the theories were still fresh in memory, students got the opportunity to apply theory knowledge in a pilot-scale apparatus. Students reflected that "being able to see the flowmeters and pipes" helped them visualize the concepts and learn better. Students were asked to sign up online individually at their convenience outside common lecture meeting time and each session allowed up to four students to participate. The flexibility of this arrangement also addressed the challenge of embedding hands-on activity to large class as a consequence of increasing student enrollment.

As an engineering major instructor, I am willing to utilize hands-on experience to help my students achieve "engineering literacy" that transfers learning from the classroom to the real world and provides creative solutions to existing problems."

7.2.8 Summary

Like many public universities, Texas A&M University is facing increasing enrollment trends, ultimately expecting to double the total number of engineering students over the next decade. This expansion makes it challenging to integrate active learning experiences

across large class sizes. Mini-labs offer an avenue to address these challenges by enabling hands-on activities to be easily inserted into traditional theory courses owing to their flexibility in scheduling and relatively short time commitment. Regarding broader implementation of mini-labs throughout the curriculum, 60% of students indicated that they would like to see more mini-labs in fluid mechanics and other courses. Most concerns from the students centered on the extra workload added by mini-labs, as indicated by sentiments such as "*it would be helpful to have mini-labs to replace homework assignments instead of at the same time*."

Early exposure to these sustainable high impact learning practices introduces students to real and non-ideal situations at the same time that fundamental concepts are introduced. The lab instructor experience also creates new opportunities for graduate students to gain teaching experience beyond traditional homework-focused grading roles by participating in a complete course development cycle.

7.3 Aggie Challenge

I held the role of a graduate student mentor of an Aggie Challenge team from September 2014 to May 2015. Aggie Challenge is a program organized by the College of Engineering at Texas A&M University to address the Grand Challenges for Engineering announced by the National Academy of Engineering (NAE). It actively engages undergraduate students through multidisciplinary teams in research projects. During this two-semester program, a team of engineering undergraduate students works in an engineering project under the guidance of a faculty mentor and a graduate student mentor. After two semesters, the team presents at the Engineering Project Showcase, which is open to the public.

My team's project was "Manufacturing Supersorbents for Oil Cleanup," which was an extension of my own research project (Chapter II). There were nine undergraduate students from four engineering majors (chemical engineering, industrial engineering, petroleum engineering, and ocean engineering) and different academic levels (freshman, sophomore, junior, senior, and fifth-year senior) on my team. Four of them participated for both semesters. My responsibilities included three parts: designing and monitoring experiment sessions, leading project discussions, and preparing final deliverables.

Part one of my task was designing and monitoring experiment sessions. Before conducting experiments, I gave team members a detailed lab safety training and prepared personal protection equipment for all participants. Students were split into groups of two or three members and met with me for two hours each week. The first session was a lecture introducing the oil absorbent project, a demonstration of a 3D printer operation, and a basic 3D model design tutorial. The students attended in small groups, so I was able to interact with students directly and answer their specific questions. Students' main task was designing new absorbent geometries and testing the corresponding oil absorption performance. I was responsible for the actual absorbent fabrication process as it took several hours, so students did not waste time waiting for printing. I stayed with students in the lab during all sessions to answer questions and provide technological support. In addition to lab experiments, I organized field tests with the help of my advisor. The test involved pairing the absorbents with a pool skimmer to test oil cleanup performance in an inflatable swimming pool. This experience gave the students an opportunity to test their ideas in a real-life scenario, which lab-oriented courses lacked.

Part two was leading project discussions. While this project had a well-defined industrial application (as a cleanup solution for oil spill accidents), we explored the commercialization process of these absorbent products. Students from industrial, petroleum, and ocean engineering showed great interest in this topic and were able to contribute based on their specific knowledge relating to the project. I, as the graduate student mentor, monitored the discussion process, encouraged students to brain-storm ideas, and helped them focus on the topic.

Part three was preparing final deliverables. The final presentation at the Engineering Project Showcase was a highly anticipated event, and we were competing with more than 160 teams. As the team members still had regular courses to attend to, I was responsible for the booth set up and material preparation with the help of my advisor. Our equipment was portable, so we moved all equipment to the presentation venue to present a live demonstration. With a 3D printer continuously demonstrating the manufacturing process of absorbents, our booth attracted heavy traffic from audiences. We also had hands-on sessions encouraging audience members to conduct simple oil absorption experiments by themselves. While the showcase could not support field tests on site, we set up a 40-inch LED screen to play clips of the field tests. In addition, we mounted the poster on a professional poster easel to attract audiences' attention. The poster content was also tailored to the general public's tastes, with more photos rather than text. Photos were a better choice to communicate ideas to the audience compared to text. Team members also provided verbal explanations to questions from the audience.

At the showcase, this project was also appreciated by judges and attendees from various backgrounds and was the only project that won two awards. My team won first

place in Multidiscipline/Vertically Integrated/Research voted by faculty and industry judges. My team also placed first in the inaugural High School Students' Choice Award category, which was voted by high school student attendees. The success of the project at the showcase encouraged the team members to return to future research projects. My team members also gave positive feedback. "Coming into college, I did not see the entire picture of engineering. Through this project, I was able to learn how to carry out a project and take an idea to new heights," said a freshman team member. "I learned how fun it can be to work on a team, explore new ideas and see all of your work become a success. We discovered something revolutionary, but we never forgot to have fun along the way."

7.4 Elementary school science event

My science, technology, engineering and math (STEM) outreach activity was presenting the 3D printed oil absorbent project at the two local elementary school science fairs organized by Rock Prairie Elementary School and Southwood Valley Elementary School in College Station, TX in April 2016. My task involved setting up a booth to demonstrate and explain a science experiment to attendees including elementary school students (age six to 12) and their parents.

The project I chose to present was 3D printed oil absorbent. The fundamental physics principle of the experiment was the capillary force that drew liquid upwards through thin tubes. This principle was easily related to the audience, as it had been explored in elementary school level science classes, usually in the forms of celery sticks drawing red ink into stalks or tissue papers transporting water between cups. The 3D printed oil absorbent project presented an innovative way to illustrate capillary forces through demonstrating the process of absorbents collecting oil. While traditional demonstrations only explored the capillary phenomenon with hydrophilic surfaces and water, my experiment introduced the interaction between oleophilic surfaces and oil, as well as oil/water selectivity. In addition, 3D printing presented a trending topic among the general public and thus a great tool to spark interest from audiences.

To keep the elementary school students engaged, my presentation booth included hands-on experiments, demonstrations, and simple schematics of the scientific principles. I chose a 3D printer as the centerpiece of my booth for demonstration purposes. It continuously printed a cube-shaped sample to vividly illustrate the layer-by-layer

manufacturing mechanism of 3D printing. This live demonstration attracted both parents and students.

The hands-on experiment had two parts. Part 1 demonstrated the oil absorption behaviors. The student attendees were instructed to wear a disposable nitrile glove for safety concerns, deposit a cube-shaped 3D printed oil absorbent into a shallow dish of colored non-toxic mineral oil, and observe the oil rising in the absorbent. This served as a teachable moment to introduce the concept of the capillary force. I explained to the attendees that capillary force draws the oil in. Part 2 explored the oil/water selectivity of the absorbents. The setup required two transparent plastic cups. Cup 1 was filled with 20mL of magenta dyed water and 20 mL clear mineral oil, and cup 2 was filled with 20 mL clear water and 20 mL red dyed mineral oil. The oil and water separated into two layers, and water was at the bottom because it has a higher density compared to oil. The student attendees were informed of the contents in the cup and were asked to dip a strip of absorbent to the bottom of the cup to reach both liquid layers. Then I asked the attendees to observe and describe the color of the absorbent. The absorbent picked up the clear mineral oil from cup 1, so it remained colorless. It had been in contact with the magenta color water but did not display the color of the water because it did not absorb water. The absorbent absorbed the red mineral oil from cup 2 and became red. I explained this phenomenon as *the sponge likes oil, so it picked up the color of the red oil; it does not like water, so it did not pick up the color from the magenta water*. Because these elementary school students have minimal science background, I avoided using the science terms such as “oleophilic” and “absorb” to convey the reasoning. The word absorbent was also replaced with sponge for the same reason.

Phase 2 was the advanced part of the hands-on experiments and was designed to expose the students to the concept of hydrophilicity for the first time. The schematic illustrations explained the capillary force and 3D printing, and a hard copy was displayed on the booth table. Upon the completion of the presentation, each attendee was given a souvenir of a 3D printed absorbent. The absorbent shapes available included English letters, a map of Texas, and a cartoon cactus. These souvenirs were specifically designed to please the attendees (elementary school students) and served as a take-home lesson: *this plastic piece can pick up oil like a sponge*. These activities successfully introduced the concept of capillary force to elementary school students. From my point of view as a graduate student, I was excited about this opportunity to present my research to the general public and contribute to the STEM education.

My booth reached 355 student attendees, counted by the absorbent consumption in hands-on experiments. The event organizers appreciated the combination of cutting-edge technologies and simple science principles of my demonstrations and invited me to return to the same events the following year (although I was not able to attend due to time conflict).

7.5 Accessible hands-on activities enabled by 3D printing

The mini-lab course, Aggie Challenge, and elementary school science all proved that hands-on activities were effective in engaging students in learning and improve their understanding of scientific concepts. These successes encouraged me to develop a series of accessible hands-on activity modules. This section discusses my experiment procedures and preliminary results and shared my vision of converting them to activities in undergraduate classrooms. 3D printing was heavily applied because of its flexibility in

creating custom shapes and intricate structures, which were valuable to create appealing demonstrations and explore structure-related material properties.

7.5.1 Evaporation through absorbents

7.5.1.1 Learning objectives

This module will demonstrate the correlation between evaporation rate and porosity. During this module, students will print samples for evaporation tests, measure sample weight change over time, and analyze the weight loss over time. At the end of this module, students will be able to recognize the relationship between fill and porosity, calculate evaporation rate, and identify the parameters that affect evaporate rate.

7.5.1.2 Experiment procedures and preliminary results

The absorbents had pores that allowed contact between absorbed oil and air. Mineral oil used in absorbent performance tests did not evaporate because there was no volatile compounds. Then, oil samples with volatile organic compounds were tested for their evaporation rate. This evaporation mass transfer process was governed by the porosity of the absorbents, which was determined by the infill. Absorbent samples with different infills were printed. The sample had two parts, a head (1 x 1 x 0.5 cm) and a tail (0.5 x 0.5 x 3 cm) (Fig. 7.2a). A glass vial was filled with natural orange oil (NOW Essential Oils 100% Pure Orange Oil), and a piece of paraffin film (Parafilm M PM996 All Purpose Laboratory Film) was used to cover the opening of the glass vial. The sample was inserted into the glass vial through the paraffin film, and the head part remained outside the glass vial (Fig. 7.2c). The paraffin film prevented oil from evaporating through the gap between the vial opening and the absorbent, so all evaporation occurred at the surface of the

absorbent. The weight of oil loss during the evaporation process was measured and plotted. An open glass vial filled with oil but without absorbent was set up as a control test.

The weight loss rate of the control test was 0.015 mg/min, which was significantly lower than the rate for tests with absorbents (0.073 to 0.680 mg/min), proving that the absorbent increased the evaporation rate by increasing the contact between volatile components and the environment. The weight loss and time followed a relatively linear relationship. A closer inspection of the data showed that the evaporation rate dropped after one hour, so the evaporation process was further analyzed as a two-phase process (Fig. 7.2b). Phase one was zero to one hour, and phase two was one to eight hours. The evaporation rate of the phase one ($K1$) was 1.5 to 2.5 times faster than the rate of the phase two ($K2$) for any absorbent design (Fig. 7.2d).

The key parameter affecting the evaporation rate was the infill of the head part (30%, 40%, 50%, 60%, 70%, 80%, or 90%) while the tail part was constant (80% infill). As the head part infill increased, the evaporation rate first increased then decreased and reached the peak value at 60%. This bell-shaped evaporation rate trend was determined by the equilibrium height of oil rise for different infill structures. The distance between the top surface of the head part and the oil surface at the beginning of the test was 2.5cm (Fig. 7.2c), which was same as the equilibrium height of oil rise in 60% infill structure. Oil filled the tail part first, then the head part. For samples with a head infill lower than 60%, the oil level did not reach 2.5 cm above the oil surface, then the head part was not saturated with oil. The higher the head infill, the easier for oil to be drawn to the head for evaporation. Consequently, evaporation became faster as the head part infill increased. For samples with a head infill of 60% or higher, oil always reached the head part, so the infill did not affect

the saturation of oil in the head part. Therefore, further increase of the infill from 60% to 90% did not improve the evaporation rate. Meanwhile, for a head part with a higher infill, there was less void space and less contact between oil and enviroment, and the evaporation rate dropped as the infill increased.

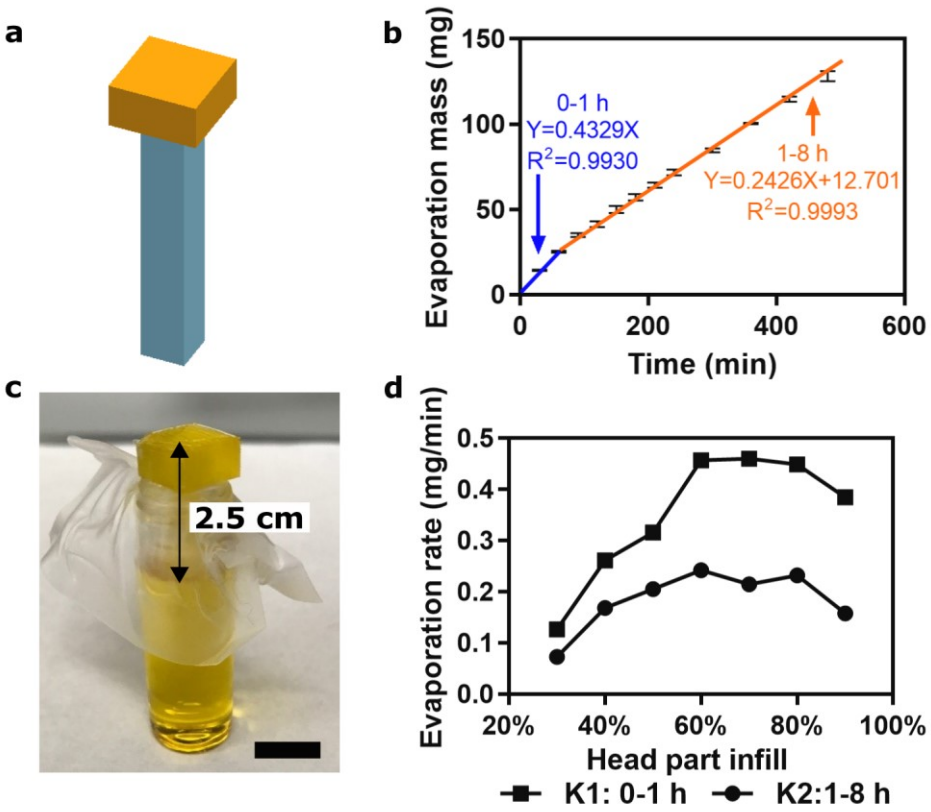

Fig. 7.2 Evaporation rate of volatile orange oil through absorbents. (a) Sample CAD model. **(b)** The oil mass evaporated over time. Phase one: zero to one hour. Phase two: one to eight hours. Each phase showed a linear relationship. Head infill: 60%. **(c)** Experiment setup. The sample was inserted into a glass vial filled with orange oil. Sample dimension: the head part, 1 x 1 x 0.5 cm; the tail part 0.5 x 0.5 x 3 cm. **(d)** Evaporation rate was determined by the head part infill. The peak evaporation rate was reached by samples with 60% head part infill. Scale bar, 1 cm.

7.5.2 Funnel shaped oil filters

7.5.2.1 Learning objectives

This module will demonstrate the correlation between infill and oil absorption performance of filters. During this module, students will print filter samples, perform water filtration, and evaluate the filtration results. At the end of this module, students will be able to describe the oil/water separation results and compare the performance of different filter designs.

7.5.2.2 Experiment procedures and preliminary results

The contact angle between water and a PLA surface was 76°, and the PLA substrate was made by melting PLA pellets. Although this contact angle measurement could not precisely represent the hydrophilicity of printed PLA absorbent structures, it led to possibilities of water passing through the absorbents and inspired the creation of a funnel-shaped water filter prototype. The filter had two parts: the top hollow part acted as a reservoir to store the unfiltered oil/water mixture; the bottom absorbent part had the structure of absorbents and absorbed oil (Fig. 7.3a). An oil/water mixture was poured into the opening at the top, and water was collected from the bottom. The goal was to absorb all oil from the mixture and produce clean water with minimum filter materials. The key parameter was the porosity of the absorbent part. A highly porous structure (infill < 60%) had more void volume, but the filtering efficiency was compromised. Oil droplets were observed floating on the surface of the filtered water. For example, a filter with a 20% infill absorbent part had a void volume of 11 cm^3, more than enough to absorb 5 mL of mineral oil from 50 mL of oil and water mixture. However, it did not produce clean filtered water (Fig. 7.3b). This failure was attributed to the large pore size in the absorbent part,

and both water and oil passed through the absorbent quickly, so the absorbent could capture the oil properly. The optimized structure was of 60% infill, in which 5 mL of mineral oil (mixed with 45 mL water) was completely absorbed into 5.3 cm^3 of void volume (Fig. 7.3c). Filters with higher than 60% infill did not further improve the oil/water separation, unnecessarily increased the production cost, and reduced oil uptake capacity. A single filter with 60% infill was able to process 50 mL of oil/water mixture within 10 minutes, cost less than one dollar to produce, and was ready to use after printing with no post processing required. It can serve as a preliminary step to remove oil from contaminated water and prepare the water for further treatment.

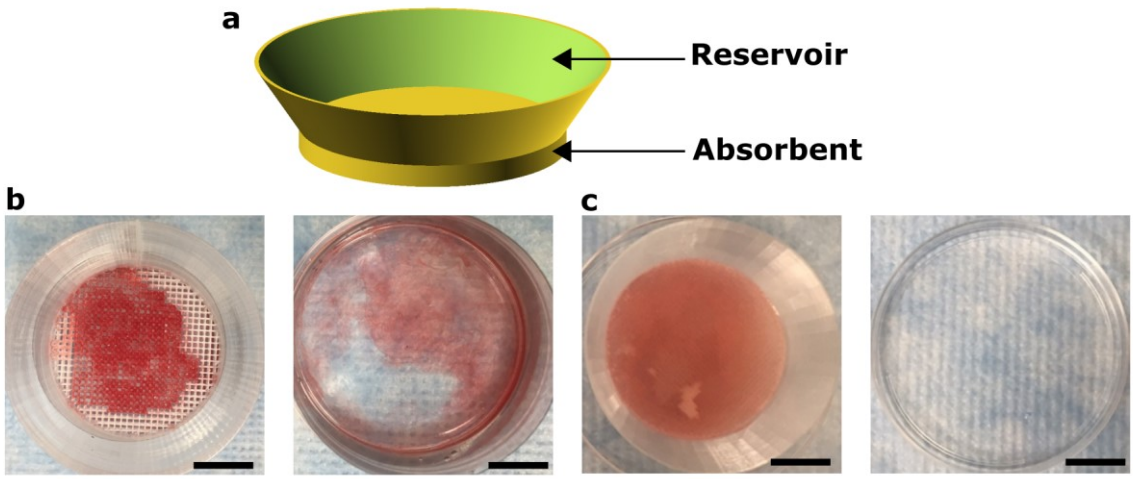

Fig. 7.3 Funnel-shaped filter captured oil from oil/water mixture. (a) CAD model. **(b)** Filter with 20% infill absorbent. Left: used filter. Right: filtered water with oil floating on surface. **(c)** Filter with 60% infill absorbent. Left: used filter. Right: no oil observed on water surface. Scale bar, 1 cm.

7.5.3 Starch-based absorbents

7.5.3.1 Learning objectives

This module will identify the two key characteristics of oil absorbents: oleophilicity and porous structures. During this module, students will produce or collect absorbent materials, perform oil absorption tests, and evaluate the absorption efficiency. At the end

of this module, students will be able to state the two key characteristics of oil absorbents and identify potential absorbents.

7.5.3.2 Experiment procedures and preliminary results

3D printed absorbents were designed with the purpose of reducing environmental footprint in mind, so they inspired me to search for other absorbents that produce minimum waste. The first object I chose was the packing peanut/foam peanut. This lightweight and porous packing material was usually disposed once the package was delivered, so functioning as an oil absorbent would give them a second chance to serve. Regular polystyrene white packing peanuts absorbed 11.9 g of mineral oil (Fisher BP 26291) per gram of material. Starch packing peanuts were available and absorbed 25.0 g of mineral oil (Fisher BP 26291), which doubled the performance of its polystyrene-made counterpart. Unfortunately, these starch packing peanuts were engineered originally as an environmentally-friendly alternative packing materials. They dissolved in water and could not be used for oil spill cleanup in water.

Nevertheless, starch packing peanuts proved the possibilities of starch-based materials as oil absorbents. Upon close inspection of the starch packing peanut, Cheetos sparked my interest because they had the shape and structures similar to a packing peanut. Cheetos did not perform well due to their high density. An average size piece of Cheetos (3 cm length, 1 cm diameter) absorbed more than 4 g of oil while it weighted 2 g, which led to 2.2 g of mineral oil (Fisher BP 26291) absorbed for each gram of Cheetos. Another starch-based food item, Corn Pops from Kellogg, absorbed 1.7 g of mineral oil (Fisher BP 26291) per gram of cereal. The last exploration in the realm of starch was starch plastic made with essential kitchen ingredients. The recipe had five items: 22.5 g (3 tablespoons) corn starch,

75 mL (5 tablespoons) water, 10 mL (2 tablespoons) white vinegar, 10 mL (2 teaspoons) glycerol, and s17 g (one tablespoon) to 51 g (three tablespoons) salt. These ingredients were cooked in a saucepan to a paste state; the paste was dried on aluminum foils and later broken into bits. The small pieces were immersed in water for 24 hours and dried for another 24 hours. The leaching and drying process leached out the salt in the paste and created pores in the structure. After increasing the salt amount from 17 g (one tablespoon) to 51 g (three tablespoons), the oil absorbing performance of each gram of starch plastic improved from 0.44 g of oil to 0.66 g. Increased use of salt led to starch plastic with more pores and void volume after leaching, thus a higher oil uptake capacity.

7.5.4 Shape memory property demonstration

7.5.4.1 Learning objectives

This module will demonstrate the shape transition process of shape memory polymers. During this module, students will print samples and perform shape transition tests. At the end of this demonstration, students will be able to identify the temporary shape and permanent shape of a shape memory element, describe the shape change phases, and name the temperature conditions required for the shape transition.

7.5.4.2 Experiment procedures and preliminary results

Four samples with complex geometries were designed: a tower (Fig. 7.4a), a five-petal flower (Fig. 7.4b), a letter logo (Fig. 7.4c, TAMU stands for Texas A&M University), and a compressed spring (Fig. 7.4d). Because the temperature required for the shape recovery process was 80 °C, the shape recovery process was executed either in an oven (tower, flower, and letter logo) or in hot water (spring). The shape change cycles were repeated three times, and the samples maintained their structural integrity.

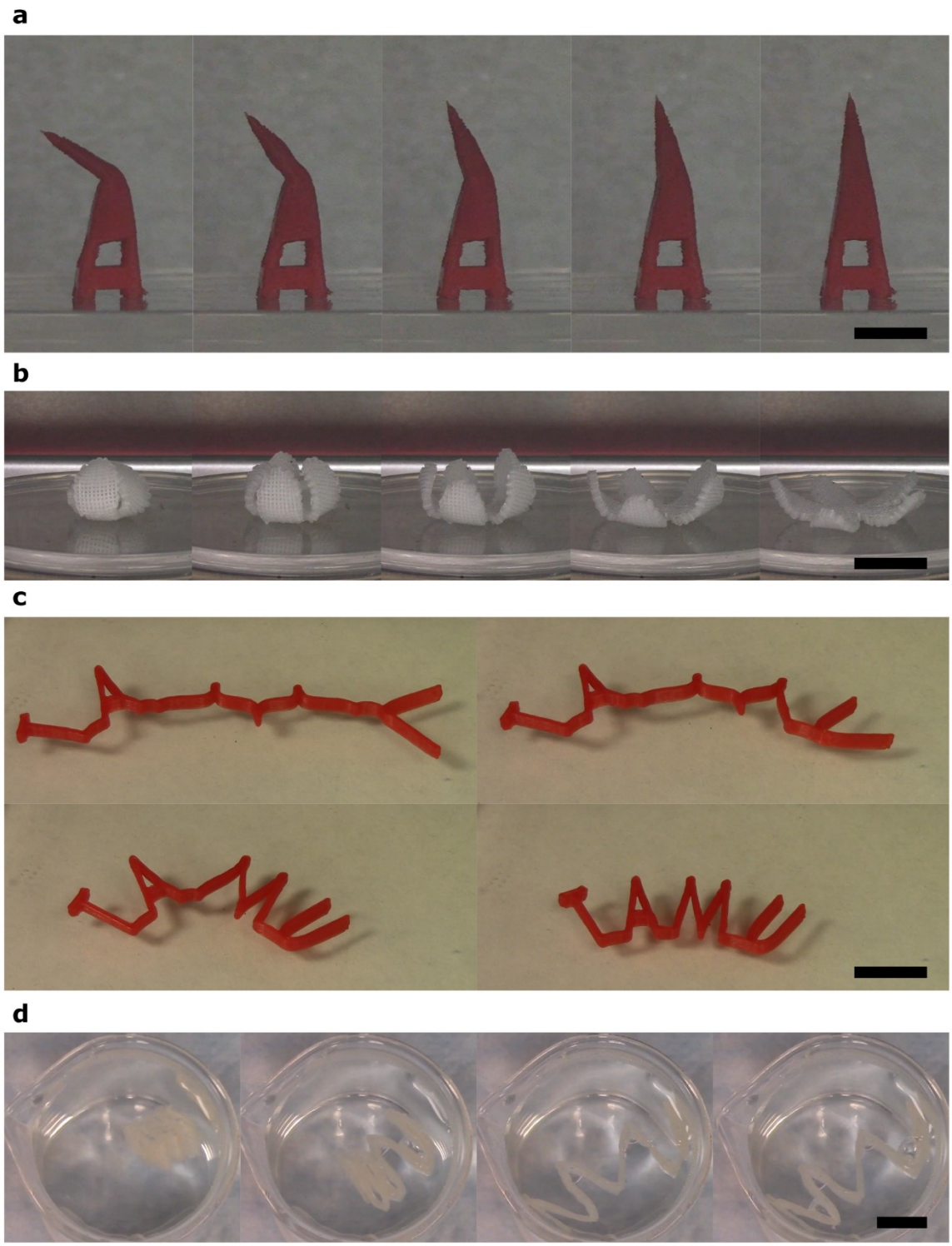

Fig. 7.4 Examples of 3D shape memory polymer structures, showing shape transition when exposed to heat. (a) (b) (c) Heat source: oven, 80 °C. **(d)** Heat source: hot water, 80 °C. Each sample started from a temporary shape and recovered its permanent shape. **(a)** Tower. Recovery time: 10 s. **(b)** Five-petal flower. Recovery time: 22 s. **(c)** Letter logo. Recovery time: 27 s. **(d)** A spring. Recovery time: 10 s. Scale bar, 1 cm.

7.5.5 Stirring stick

7.5.5.1 Learning objectives

This module will demonstrate the shape morphing of 3D printed samples from planar 2D to 3D structures at elevated temperature. During this module, students will print samples and perform shape morphing tests. At the end of this module, students will be able to identify the temperature condition required for shape morphing.

7.5.5.2 Experiment procedures and preliminary results

The bilayer warpage behavior, discussed in section 4.2.4, was further explored to produce a novelty stirring stick. It served the purpose of adding preloaded ingredients, mixing a hot beverage, and providing a unique user experience of a customizable shape morphing utensil. The stirring stick consisted of three parts: a handle, a shape morphing stem, and a loadable tip (Fig. 7.5a). The handle was a solid strip with 100%, 90°/0° infill and experienced minimum shape change at elevated temperature. The stem had bilayer structures that warped at a high temperature. The tip had a hexagon shape and a 40% hexagon pattern infill to mimic the honeycomb and was able to hold ingredients. Sugar syrup (1.5g sugar/ mL water, 75% saturation) was loaded into the tip and dried for six hours. The sugar solution was colored yellow to mimic honey.

A user held the handle, dipped the stirring stick into hot water, and swirled the stick (Fig. 7.5b). The sugar loaded in the tip dissolved immediately upon contact with water. By swirling the stick, sugar was distributed evenly within the hot water. The stem formed a wavy shape during the stirring process. The stem was removed from hot water and cooled down to room temperature after ten seconds, and the deformed shape was preserved. This novelty stirring stick can be produced with food grade PLA. There are food grade PLA

filaments (e.g., TRUE Food Safe PLA from Filaments.ca) readily available at a price of $45/kg, which is only slightly higher than regular PLA filaments ($39/kg for DeltaMaker filament used in my experiments).

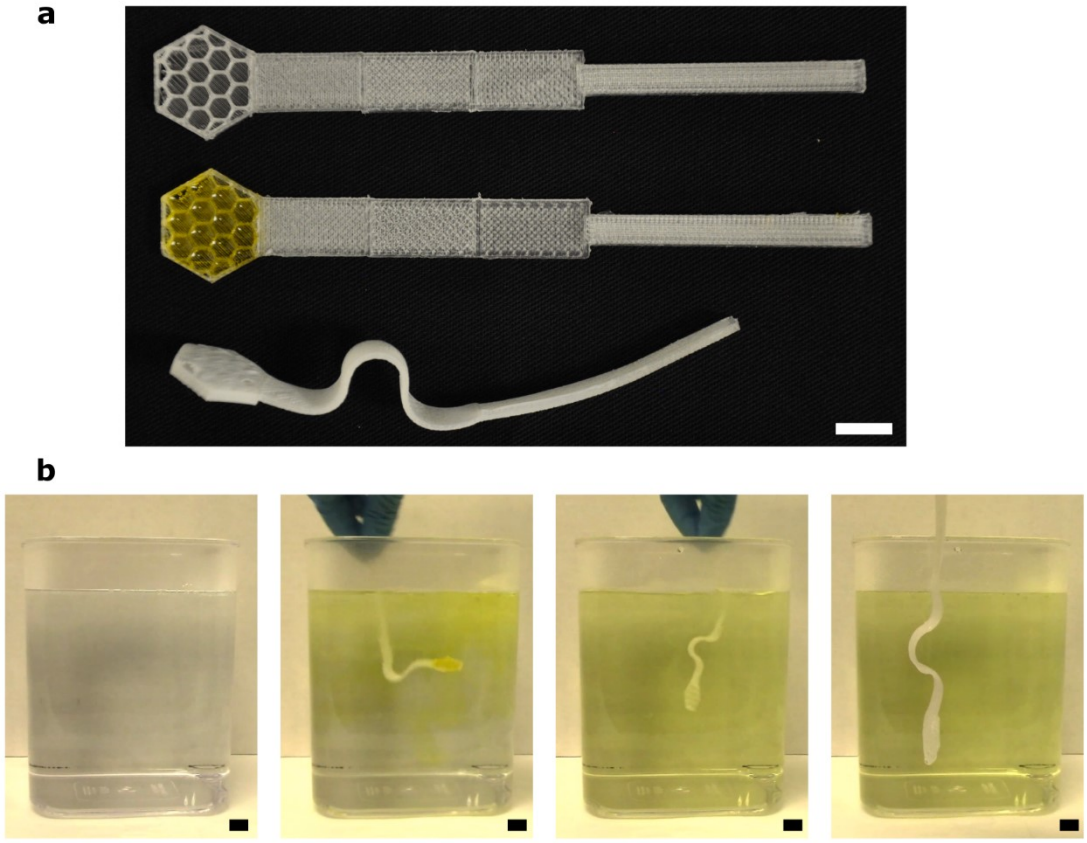

Fig. 7.5 A 3D printed stirring stick deformed into a wavy shape upon contact with hot liquid and released pre-loaded sugar content. (a) From top to bottom: Printed sample. Sample loaded with sugar solution. Sample after use, the sugar had been released, and the stem had changed shape. **(b)** Stirring stick in use. The container was filled with hot water of 80 °C. The stick was dipped into the container, and sugar started to dissolve and distributed in the water. The sugar was colored yellow to show its distribution. The stem part curled and formed a wavy shape. The stick maintained the shape after it was removed from water and cooled in room temperature. The shape morphing process was 25 s. Scale bar, 1 cm.

7.5.6 Self-assembled battery

7.5.6.1 Learning objectives

This module will demonstrate the production of a self-assembled battery. During this module, students will print samples and perform battery performance tests. At the end of this module, students will be able to describe the electrochemical reaction of an aluminum/air battery and compare the battery performance of different electrolyte concentrations.

7.5.6.2 Background: a brief history of batteries

Batteries are ubiquitous portable power sources in everyday life. Surprisingly, it took more than two centuries of transformation to develop the modern alkaline and lithium batteries. In 1749, Benjamin Franklin coined the word “battery” to describe a set of linked capacitors.[197] Half a century later, Alessandro Volta, the namesake of voltage, invented the voltaic pile, the first modern electrical battery.[198] This battery was made of zinc discs, copper discs, and pieces of brine-soaked cloth/cardboard that were arranged to form a circuit. Hydrogen ions from the electrolyte (brine) were reduced and formed hydrogen.

To reduce the release of hydrogen, John Frederic Daniell added a second electrolyte and created the Daniell cell in 1836.[199] Copper and zinc electrodes were immersed in solutions of copper sulfate and zinc sulfate, respectively. The Daniell cell also provided a contemporary definition of volt: a standard Daniell cell has a potential of 1.10 V at 25 °C.[200] Ever since then, the electrochemical battery has taken many different forms and utilized a myriad of materials, among which aluminum made a strong material candidate because of its low cost and accessibility. In 1855, aluminum made its first appearance in battery history by replacing the copper cathode in a zinc battery (the original

Daniell cell).[201] Two years later, aluminum was explored as the anode in the Buff cell.[202] A century later, aluminum was paired with air [203] and made its name among other metal/air batteries because of its high energy density (8.1 kW/kg) and theoretical voltage (2.71 V).[204] In addition to the electrode material, aluminum also serves as the package material for the modern dry alkaline battery. This invention eliminated the use of a water-based electrolyte and was patented in 1960.[205] It also defined the most popular batteries on the market today: a positive electrode of manganese dioxide paste and a negative electrode of zinc powder in potassium hydroxide gel assembled into a standardized cylindrical shape.

The bulky size and heavy weight of these alkaline batteries hindered their applications in small electronic devices (e.g., camera, cellphone) and inspired the search for other metals with a low density and a high electrochemical potential. This inquiry led to revisiting a metal studied by Gilbert Lewis in 1912 for its electrode potential: lithium.[206] The lithium battery made its market debut in the 1970s and became the focus of energy research [207, 208] targeting faster charging and discharging, a higher energy density, and a longer product lifespan. However, alkaline and lithium batteries are either made by industrial-scale productions or with sophisticated equipment in research labs. These production difficulties call for an easy-to-produce battery solution.

7.5.6.3 Battery assembly

A sample with bilayer structures (top layer: 40%, 45° and -45°; bottom layer: 100%, 90°) warped into a 360° roll instantaneously upon heat treatment. This phenomena was observed for samples of both 0.2 and 0.4 mm thickness. It led to an intriguing question: would two pieces of 0.2 mm sample stacked together form a roll as a 0.4 mm thick piece?

A preliminary test showed that the two-piece stack formed a roll in the same manner as a single piece. The heat-induced self-assembled process of two PLA pieces process inspired an innovative way to produce a self-assembling aluminum/air battery with the PLA pieces serving as the anode and cathode.

The battery consisted of two PLA sheets rolled together upon heating (80 °C, 1 minute) (Fig. 7.6a, c). The PLA sheet (20 x 20 x 0.2 mm) had a bilayer structure. One layer was 0.1 mm thick of 40%, 45° and -45° infill, and the other layer was 0.1 mm thick of 100%, 90° infill. The outer piece of the PLA sheet was painted with carbon conductive ink (MG chemicals 838AR) (Fig. 7.6b), then the ink was air-dried. The inner piece of the PLA sheet was covered with aluminum foil (Barnabas Blattgold, thickness 0.7 μm) (Fig. 7.6b). A section of 3 cm long tinted copper wire (Whitmore wirenectics BU2219344) was glued to aluminum foil with silver epoxy (MG Chemicals 8331). The two pieces were stacked and placed in an oven at 80 °C. Upon heating, both PLA sheets formed a tight roll. This assembled battery was immersed in Rain-X solution (Rain-X Anti-Fog) to increase the hydrophilicity of the PLA sheets, then air-dried. A pair of alligator clamps were used to connect the battery wire to a digital multimeter (Keithley 2100). Sodium hydroxide (NaOH, Sigma-Aldrich 221465) aqueous solutions of various concentrations was dropped onto the PLA samples. Voltage readings from the battery were recorded from the multimeter. The battery performance was evaluated by plotting voltage output as a function of time with different resistance loads (1 KΩ. 10 KΩ, 100 KΩ, or 1 MΩ) and electrolyte concentrations (0.01 mol/L, 0.1 mol/L, or 1 mol/L).

The PLA sheet served as the support material for the cathode and anode. The Rain-X treatment increased the hydrophilicity of the PLA sheet and made it more easily wetted by

NaOH solutions. Aluminum foil and carbon conductive ink were chosen as the anode and cathode because the thin foil or thin ink coating did not affect the formation of the roll. Aluminum foil provided electrons through its chemical reaction with NaOH, and carbon conductive ink served as the cathode to form a close circuit. The NaOH solution served as both an electrolyte and oxidizer to aluminum. This aluminum/air battery transferred chemical energy to electronic energy. At the anode, NaOH oxidized aluminum to aluminum hydroxide.

$$\mathrm{Al} + 4\mathrm{OH}^- \rightarrow \mathrm{Al(OH)}_4^- + 4\mathrm{e}^-, \mathrm{E}_{0\mathrm{anode}} = -2.35\ \mathrm{V} \quad (7.1)$$

At the cathode, oxygen was reduced to hydroxide ions.

$$O_2 + 2H_2\mathrm{O} + 4\mathrm{e}^- \rightarrow 4\mathrm{OH}^-, \mathrm{E}_{0\mathrm{cathode}} = 0.40\ \mathrm{V} \quad (7.2)$$

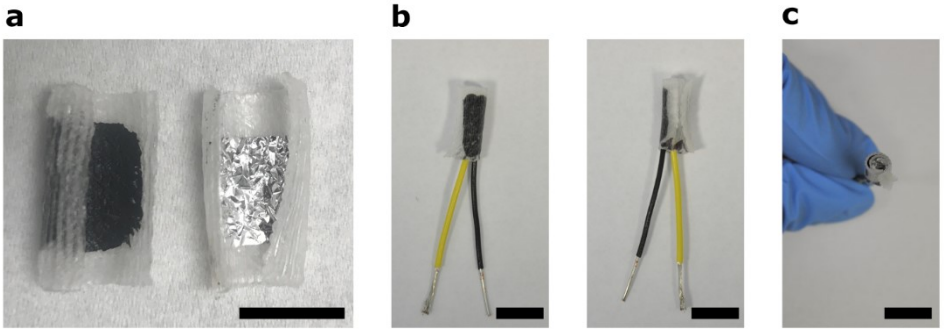

Fig. 7.6 A self- assembled battery included a conductive ink coated cathode and aluminum foil anode that formed one roll. (a) Warped PLA pieces. Left: the cathode piece, PLA with a layer of dried carbon conductive ink. Right: the anode piece, PLA with aluminum foil. This battery roll was disassembled to show the inside of the roll. **(b)** Side view, showing both sides of the roll and wires. The yellow wire was connected to the anode, and the black wire was connected to the cathode. **(c)** Top view, showing two layers of PLA formed a roll.

7.5.6.4 Battery performance

For tests with a resistance load, the battery was immersed in 25 mL of NaOH solution, and a resistor was added into the circuit. A higher resistance led to a lower current, a higher peak potential output, and a longer battery life, regardless of the electrolyte

concentration. NaOH solutions with a higher concentration reacted with the aluminum foil faster and generated a higher peak potential output but consumed the foil rapidly and led to a shorter battery life. It was worth noting that 1 mol/L NaOH concentration degraded the PLA piece and may have resulted in disintegration of the battery, which terminated the electrochemical reaction abruptly, generated a sudden potential output drop, and shortened the battery life significantly. These unexpected events explained the unusual potential output profiles for the 1 mol/L NaOH tests (Fig. 7.7a), in which the 1 MΩ test had a shorter battery life than others and the potential output dropped suddenly. Given the high NaOH concentration and large volume, the foil was consumed or broken down, and the potential dropped to zero at the end of reaction. In contrast, in the 0.1 mol/L (Fig. 7.7b) and 0.01 mol/L (Fig. 7.7c) NaOH groups, low NaOH concentration led to a slow reaction and could not consume the foil completely. The potential decreased to 0.1 - 0.3 V and maintained this voltage for over one hour.

For open circuit tests without a resistance load, a drop (2 mL) of NaOH solution was added to the battery roll. The concentration of the electrolyte was the key factor for the battery performance (Fig. 7.7d, e, f). A higher concentration of NaOH solution produced a higher peak voltage (1 mol/L, peak 1.36 V) than a lower concentration solution (0.1 mol/L, 0.95 V). For the 1 mol/L and 0.1 mol/L NaOH solution tests, there was enough hydroxide to react with all of the aluminum foil. In contrast, for the 0.01 mol/L NaOH scenario, all hydroxide was consumed, and some aluminum foil was left unconsumed. The potential output was expected to drop to zero upon completion of the reaction, which was signaled by either the disappearance of aluminum foil or discontinued bubble formation. However, regardless of the NaOH concentration, once the reaction was completed, the potential

output dropped to 0.4 V, and remained at this voltage for over one hour. One initial guess was that the zinc coat of the alligator clamps, which were used to connect the wires to multimeter, continued to react with NaOH after the aluminum foil disappeared and contributed to this output. Yet when the alligator clamps were immersed in fresh NaOH solution, no voltage output was detected. Consequently, 0.4 V was recognized as the base voltage output. A voltage reading of 0.4 V signaled the end of battery life. The foil was consumed fast in high concentration electrolyte scenarios, which caused the battery to last for a short period of time. For example, battery life increased from three to 56 minutes when the NaOH concentration dropped from 1 to 0.01 mol/L.

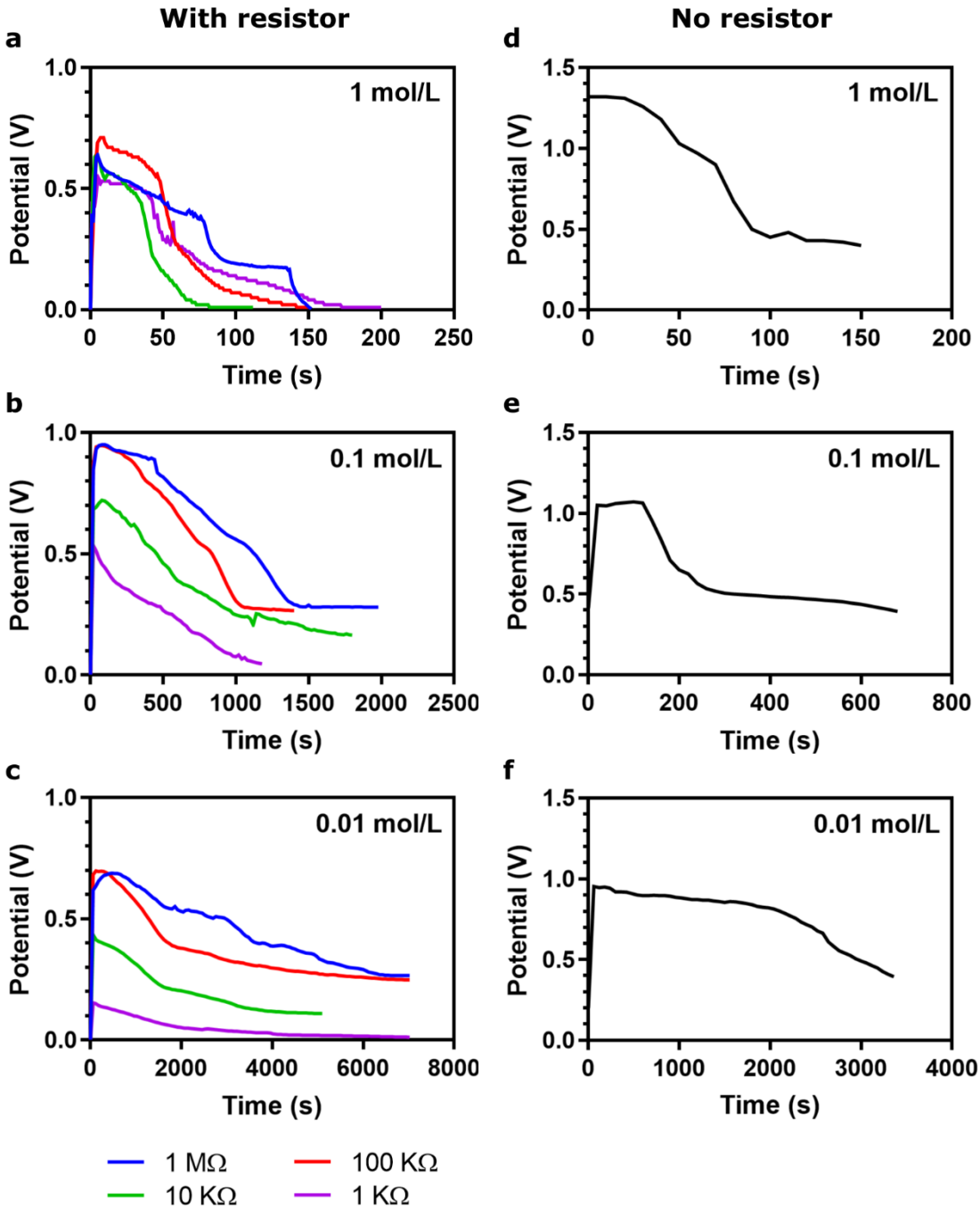

Fig. 7.7 The potential output of a battery was determined by the resistor load and electrolyte concentration. (a) (b) (c) With a resistor. **(d) (e) (f)** Without a resistor. NaOH concentration: **(a) (d)** 1 mol/L, **(b) (e)** 0.1 mol/L, **(c) (f)** 0.01 mol/L.

The battery was capable of powering a small electronic device. Three battery rolls connected in a series circuit were able to power a red light-emitting diode (LED), which

required a minimum of 2.5 V to operate. Battery rolls and the LED were connected using a breadboard to complete a circuit (Fig. 7.8). The battery rolls were immersed briefly in NaOH solutions to absorb approximately 1 mL of the solution. The electrochemistry reaction activated the LED, and the power lasted three minutes.

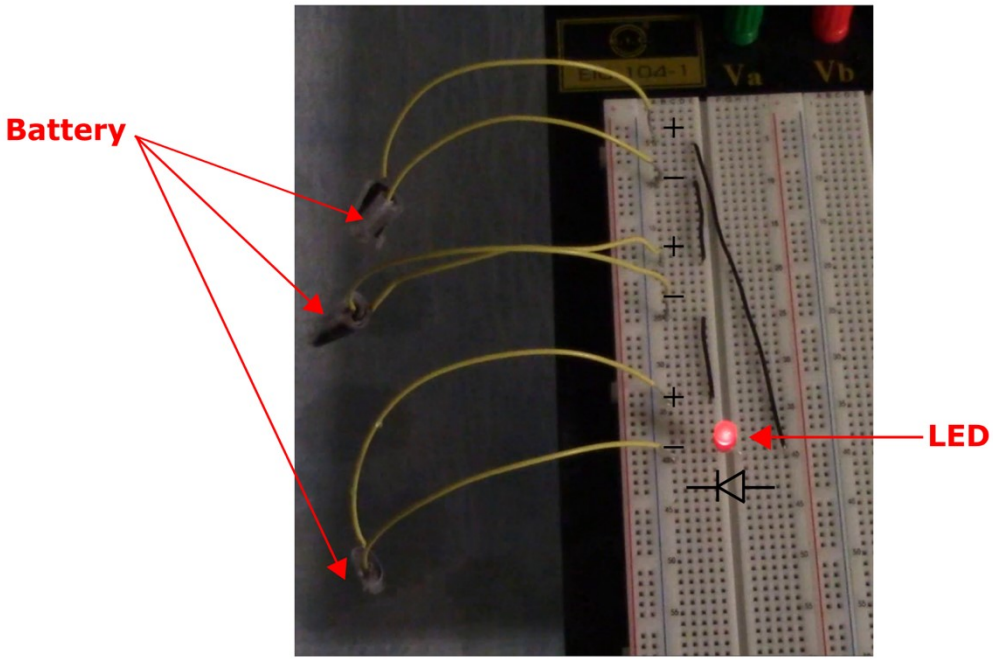

Fig. 7.8 Three batteries connected in a series circuit activated an LED. NaOH concentration: 1 mol/L. Aluminum foil size: 2 cm x 2 cm x 0.7 µm.

7.5.7 Glucose sensor

7.5.7.1 Learning objectives

This module will demonstrate the production of a self-assembled and self-powered glucose sensor. During this module, students will print samples and perform glucose detection tests. At the end of this module, students will be able to describe the electrochemical reaction of a glucose sensor.

7.5.7.2 Background: a brief history of glucose detection

Diabetes mellitus, an incurable disease, has inspired a plethora of studies in searching for its efficient diagnosis, monitoring, and treatment, among which the glucose measurement has been long identified as a critical link. The most common way to monitor one's glucose level is by pricking a fingertip with a lancet to measure the blood glucose level. However, this invasive process traumatizes patients and may lead to a delayed diagnose. In the United States, 7.2 million out of the 30.3 million (9.4% of US population) who have diabetes are undiagnosed.[209]

An alternate approach to diagnose diabetes is to use urine as an accessible biological fluid,[210] enabling a snap shot of the patients' glucose level in an accessible and safe manner. The name *Diabetes mellitus* suggested the sweet taste of glycosuria noticed in the urine of a diabetes patient. The history of detecting glucose in urine dates back to 1776,[211] as reported by English physician Matthew Dobson. A modern take of measuring glucose level relied on electrochemical reactions between glucose and glucose enzyme. Glucose enzyme electrodes were first introduced by Clark and Lyons in 1962 [212] (originally for monitoring open-heart surgeries patients, not for diabetes patients). Among a wide range of electrodes developed after this breakthrough, Prussian Blue (PB) modified-electrodes display strong and stable electrocatalytic activities.[213] A key advantage of this PB electrode is its colorimetric feature: blue $Fe(CN)_6^{4-}$ (PB) changing to colorless $Fe(CN)_6^{3-}$ (Prussian White, PW) (equation 7.3). This color change serves as an indicator and enables a visual readout. Recent excitement has been generated from a glucose sensor using a metal/air battery as the energy source to power the glucose oxidation process featuring a PB deposited indium-doped tin oxide (ITO) electrode.[214]

This study inspired the idea of implementing the self-assembled aluminum/air battery as the power source to create a low cost glucose sensor.

$$\text{Glucose} + 2\text{Fe(CN)}_6^{4-} + \text{H}_2\text{O} \xrightarrow{\text{glucose oxidase}} \text{Gluconic acid} + 2\text{Fe(CN)}_6^{3-} \quad (7.3)$$

7.5.7.3 Glucose sensor assembly

To make a PB-PLA sample, a drop (5 μL) of aqueous PB solution (1 mmol/L PB, Chemsavers 77510; 1 mmol/L iron (III) chloride, Alfa Aesar 12357; 5 mmol/L potassium chloride, Sigma-Aldrich P3911) was dropped on a PLA sample (Fig. 7.9a left). This sample was dried at room temperature, and the PB solution left a dot-shaped blue mark. To make a foil-PLA sample, a piece of aluminum foil was placed on top of a PLA sample (Fig. 7.9a right). A foil-PLA sample was stacked on top of a PB-PLA sample. Both pieces were placed in an oven at 80 °C for one minute, and the two samples formed a roll. Two ends of a segment of wire (10 cm long) were inserted into the hollow center of the roll and the gap between the PB-PLA sample and the foil-PLA sample, respectively (Fig. 7.9b, c). A drop of glucose oxidase solution (0.1 mL with 500U of glucose oxidase, Millipore Sigma 34538610KU, in 0.1 M phosphate buffer, pH = 7.0) was injected into the gap between the PB-PLA sample and the foil-PLA sample. Next, the roll was dried at room temperature. The glucose oxidation solution left a yellow mark on the PLA substrate. Next, the roll was briefly immersed in 3 mL of an artificial urine sample. The artificial urine solution included 170 mmol/L urea (Fisher Chemical U15) and 90 mmol/L sodium chloride (Sigma-Aldrich S9888). Urea and sodium chloride were chosen because they have the highest concentration among other compositions in human urine samples.[215, 216] Various concentrations of glucose (0.001 mol/L, 0.01 mol/L, or 0.1 mol/L, Acros Organics 41095) was added to mimic the urine of diabetes patients.

7.5.7.4 Glucose sensing performance

The first test was to verify the potential needed to facilitate the glucose oxidation reaction. A PLA sheet with PB and glucose oxidase dots was connected to a stable power source (DC power supply E3612A, HP) in 3 mL of artificial urine solution with glucose (0.01 mol/L). The power source supplied a potential of 0.5 V, 1.0 V, or 1.4 V. The PB dot served as the color indicator of the progress of glucose oxidation, and the disappearance of the PB dot signaled the completion of the oxidation process. Tracking the color change of the PB dot showed that the oxidation happened at a potential as low as 0.5 V. A high voltage input accelerated the oxidation process; increasing the potential from 0.5 to 1.4 V reduced the oxidation process from 190 to 40 minutes (Fig. 7.10).

The next step was to replace the external power source with an aluminum/air battery (Fig. 7.9d). Potassium chloride (3 mol/L, Sigma-Aldrich, P3911) was added to the artificial urine sample to increase the conductivity of the electrolyte solution, hence increasing the potential output of the battery to promote the progress of the electrochromic reaction of PB. Glucose was added to mimic the urine of a diabetes patient. The PB dot was the color indicator of the glucose oxidation process. The aluminum foil was consumed and provided electrons to the electrode, then the PB was reduced to colorless PW. After four hours, the blue color of the PB dot faded away (Fig. 7.9e, f), verifying the existence of glucose (0.001 mol/L) in the artificial urine sample, which could serve as a screening test for diabetes with a glucose detection limit was as low as 0.001 mol/L. In a glucose-free control group, the PB dot remained blue. This glucose sensor was significantly cheaper than the traditional indium-doped tin oxide (ITO) electrode (approximately $5). [214] Each PLA sample cost

as low as $0.01 and did not require electrodepositing process to load PB on an ITO electrode.

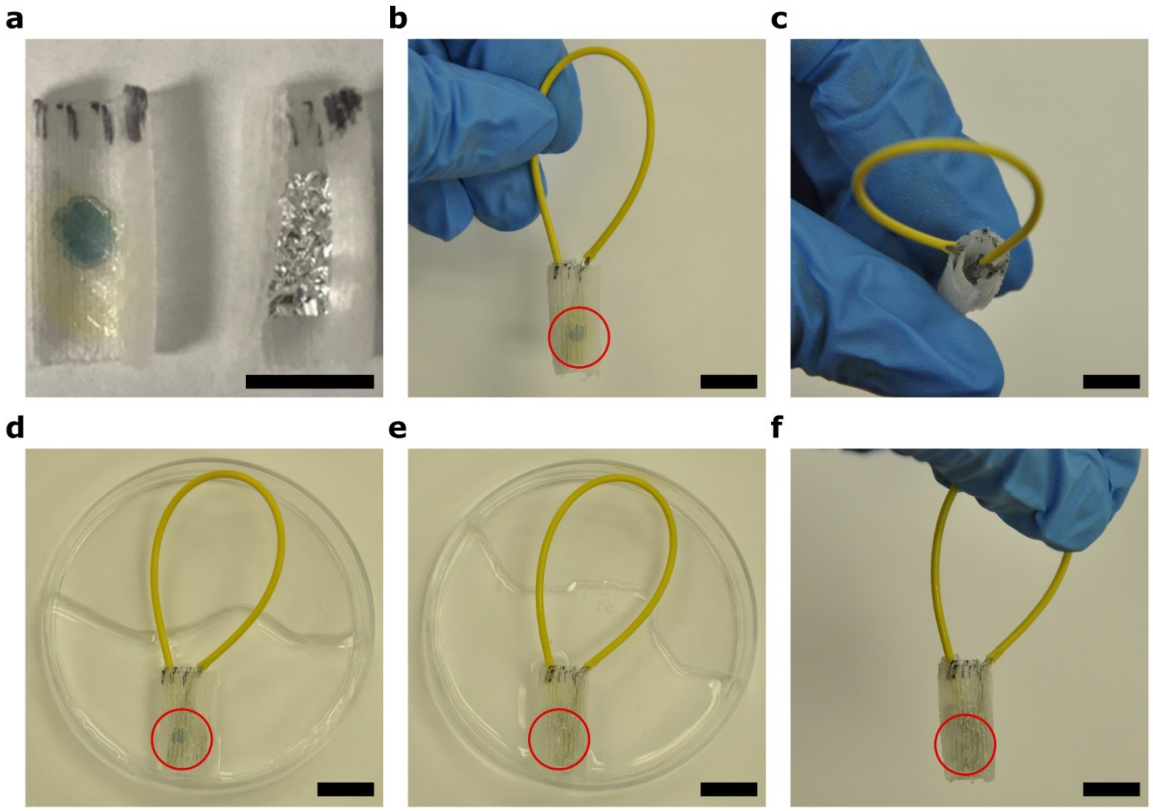

Fig. 7.9 Glucose sensor assembly and performance. (a) PLA pieces for a glucose sensor. Left: PB-PLA. The blue dot was PB, and the yellow dot was glucose oxidase. Right: foil-PLA. **(b)** Side view of an assembled glucose sensor showing the PB-PLA piece with PB and glucose oxidase dots. **(c)** Top view of the double-layer roll structure of the sensor. **(d)** Assembled sensor immersed in artificial urine solution at the start of the reaction. **(e)** After four hours, the blue color of the PB dot faded away. **(f)** The sensor was removed from the solution, showing no blue color. **(d)(e)(f)** The red circle showed the position of the PB dot. Scale bar, 1 cm.

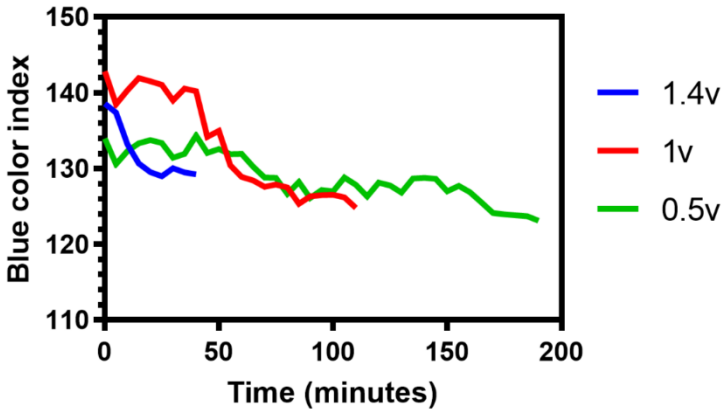

Fig. 7.10 The PB dot color gradually disappeared over time. The higher power input led to faster glucose oxidation reaction and faster reduction of PB. The end of the reaction was signaled by the disappearance of the blue color of PB, observed by naked eyes.

7.6 Conclusions

Accessible hands-on activities are valuable assets for engineering education. They stimulate learning in an engaging environment and help students remember textbook concepts as useful solutions to real life problems rather than equations and numbers. Through designing and implementing these activities, I was able to review scientific concepts from the viewpoint of an instructor, which complements my understanding of the knowledge as a student. I also tuned and polished my skills in communication, project planning, and time management, which all turned into precious aids for my graduate school study.

CHAPTER VIII

CONCLUSIONS AND FUTURE WORK

8.1 Conclusions

This dissertation has presented smart elements design and fabrication methods that allow production of 2D structures with programmed 3D shape morphing. The overarching goal of my research is not only to solve specific problems, either cleaning oil spills, producing shape memory mechanic actuators, simplifying the production of complex 3D morphologies, or fabricating microchannels without soft lithography, but also to present an approachable toolbox that can be embraced by users outside academic environments. Specific conclusions of each research project are described below.

8.1.1 3D printed oil absorbents

Remarkable progress in developing oil spill cleaning solutions is largely driven by the pressing environmental challenges triggered by oil spill accidents worldwide. Both physical (e.g., skimmers, absorbents) and chemical (e.g., in-situ burning, dispersants) methods have their limitations and present further environmental hazards. Chapter II discusses 3D printed PLA oil absorbents, which feature interconnected networks capable of selectively absorbing oil from an oil/water mixture and function as self-wringing sponges with self-cleaning properties. Unlike conventional manufacturing methods, 3D printing makes it possible to produce active absorbents in an on-demand manner that can be highly customized to suit the need for a specific application. Absorbents can be produced in virtually any shape and size to be deployed individually or as parts of an assembly. Individual absorbent pieces can be embedded with spatially variable internal microporous architectures that enable selective collection and sequestration of absorbed oil

and hydrocarbons. Compared to conventional industry-standard polypropylene pads and booms, the rigid printed absorbents are reusable, can be easily handled without releasing the absorbed oil, and can be disposed without adding environmental contamination by virtue of the biodegradability and starch-based nature of PLA.

8.1.2 PLA mechanical actuators

Shape memory polymers have demonstrated tremendous potential in soft robotics to perform mechanical tasks. Chapter III presents a new approach to harvest the inherent shape memory properties of PLA and implement them through fused deposition modeling, which enables easy and rapid fabrication of PLA parts. The shape deformation procedure is simplified to manual stretching rather than employing a machine, which greatly increases the accessibility of these parts. The development of multi-digit grippers and a self-tying knot capable of performing mechanical tasks promise to significantly increase adoption of 3D printing in soft robotics.

8.1.3 Shape morphing components

3D printed smart components respond to external stimuli via programmable shape morphing and have presented great potentials in various areas, including wearable devices, drug delivery, and soft robotics. However, the current methods employing specific composited inks and customized printing devices have limited their wide adaptation. Chapter IV presents a novel approach that harnesses inherent shape memory properties of PLA and its high compatibility with FDM. This approach makes PLA a suitable smart material candidate that responds to elevated temperature and displays programmable shape morphing from 2D substrates to 3D complex morphologies. The combination of PLA as a single material and a commercially available FDM machine provides an unprecedented

advance in simplifying the production procedure. FDM embeds prescribed internal stresses within a planar 2D PLA substrate; a heated environment with temperature higher than the glass transition point triggers the release of stresses and deforms the 2D substrate into a desired 3D shape. This controllable and programmable shape morphing enables construction of a library of active components, and arrangement of these components mimics hierarchical structures found in living systems.

8.1.4 Microchannel fabrication

Microfabrication approaches (e.g., soft lithography, electron beam etching) play a key role in expanding applications of microfluidic devices to multiple fields. However, these approaches face a number of drawbacks: consuming long hours to produce, requiring intensive training, and providing limited surface patterning possibilities. As discussed in Chapter V, the biodegradability of PLA introduces enzymatic etching as a novel tool to create channels with microscale depths. Coupled with tape masking, vacuum aided bonding, and 3D printing, enzymatic etching offers an unconventional procedure for microchannel fabrication. This lithography-free procedure elegantly addresses the growing need for microchannel devices. Paired with tunable crystal structures generated by isothermal crystallization, PLA channels are equipped with microscale and nanoscale embedded surface topographies, which function as built-in weirs to trap stationary phase, opening up possibilities to producing biomolecule separation devices.

8.2 Future work

8.2.1 Various microchannel features

Chapter V presented an accessible toolbox to produce microchannel devices without lithography. This procedure could be further exploited through the abundance of

combinatorial various enzyme/substrate libraries (e.g., poly(ethylene terephthalate) (PET)/lipase from *Candida Antarctica* [103] and polycaprolactone (PCL)/cutinase from *Fusarium solani* [118]), which provide unlimited potential to create surface crystal morphologies and etching profiles.

8.2.2 Biocompatible scaffolds

My oil absorbent study explored the physical principles of liquid absorption behaviors in uniform porous media driven by capillary action. These principles can be implemented to other combinations of liquid and surface hydrophilicity/oleophilicity provided by surface modification or changing absorbent material composition. One promising goal is to produce biocompatible scaffolds for medical implants, *in vitro* cell culture, and organ generation. A particular popular biocompatible material, poly (lactic-co-glycolic acid) (PLGA), has displayed the potential to be shaped as filaments for the FDM process.[217] An interconnected 3D matrix made from polycaprolactone (PCL) has been proven to support proliferation and differentiation of primary human fibroblasts and periosteal cells.[218] It is also worth noting that surface modification of PCL by various microorganism-sourced enzymes present new potentials of optimizing cell culture within PCL scaffolds.[114, 118]

8.2.3 Robust shape change behaviors

The shape memory and shape morphing behaviors were determined by sample dimensions, the spatially control of local structures, and thermal treatment. The sample dimension parameter has already been intensively explored in Chapter IV, which left the other two factors for future exploration. One robust way to gain more control of local structures is to design printing paths beyond the restriction of existed slicing engines

(Simplify 3D in this study) by creating new infill patterns (e.g., with Autodesk Dynamo Studio).

The thermal treatment used in this study was an oven set at a stable temperature with minimized temperature gradients surrounding the sample. This setting guaranteed that the entire sample experienced uniform thermal treatment. Consequently, all shape change occurred simultaneously. Other soft material studies introduced sequential shape change through controlling material profiles at different spatial positions. Unfortunately, the complexity of the material design and deposition limits the adaption of these procedures outside academic environments. However, a more versatile thermal treatment with customized isothermal profiles could enable sequential shape changes of a uniform material. In this controlled heat environment, shape change could be arranged in steps and regions, under the hypothesis that temperature affects the activation time of shape morphing.

8.2.4 Fluidic control element and device

The shape recovery behavior of the spring (section 7.5.4, Fig. 7.4d), triggered by an elevated temperature, could potentially perform mechanical tasks and inspired three designs of fluidic control elements. A spring can actuate controlled metering and delivering of liquids by leveraging the spring's linear displacement to push or pull the plunger of a syringe to dispense or withdraw liquid. An eyedropper ring can squeeze the rubber bulb to initiate the flow of liquid in the bulb. A pinch valve can squeeze a tube and clamp it to terminate the flow passing through the tube.

Initial fluidic control element tests used an oven as the heat source, which requires electricity and limits the application of these elements. An individual heating block can

provide an alternative heating source via hot water/hot air to activate them. These blocks can be assembled into a device to activate multiple fluid control elements in a time sequence. This section documents my proof-of-concept effort to create these fluid control elements and devices. The future work mainly focuses on quantifying the correlation between element/device design, heating condition, and fluidic control specifications (volume and rate).

8.2.4.1 Spring

A spring was printed in its permanent shape, heated at 80 °C for one minute, and compressed to its temporary shape (Fig. 8.1a, b). The spring was aligned with the plunger of a syringe and both placed in an oven. Once the spring was heated at its glass transition temperature, it expanded to its permanent length and pushed the plunger at the same time. The syringe can dispensed liquid in this setup. To refill the syringe, the spring was stretched to its temporary shape and attached to the end of a syringe plunger. While the spring recovered to its permanent shape, it retracted and pulled the plunger. Then liquid can be drawn into the syringe. The future work is to quantify and control the rate of length changing of the spring to achieve desired fluid flow rates in dispensing the liquid and refilling the syringe.

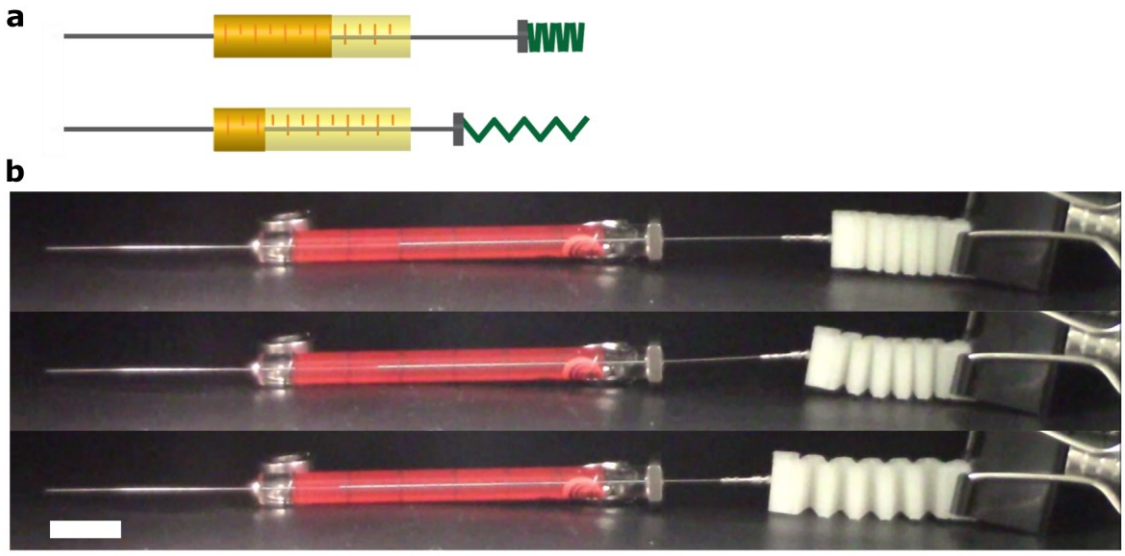

Fig. 8.1 A compressed spring recovered its permanent length and pushed the plunger of a syringe. (a) Schematics of the spring and syringe. Top: spring in its temporary shape. Bottom: spring expanded to its permanent shape and pushed the plunger. **(b)** Top to bottom: The spring expanded from the temporary shape to the permanent shape and pushed the syringe plunger. Scale bar, 1 cm.

8.2.4.2 Eyedropper ring

The eyedropper ring was printed in its permanent shape, heated at 80 °C for one minute. A metal rod was inserted into the hole to stretch it to its temporary shape (Fig. 8.2c). The ring was mounted on the rubber bulb of an eyedropper. Once the ring was heated at its glass transition temperature, it shrank to its permanent shape (Fig. 8.2d) and squeezed the bulb. The eyedropper can potentially dispense the liquid inside the bulb and initiate a flow. The future work is to establish correlations between the ring specification (dimension and its position on the bulb) and the volume/rate of fluid being released.

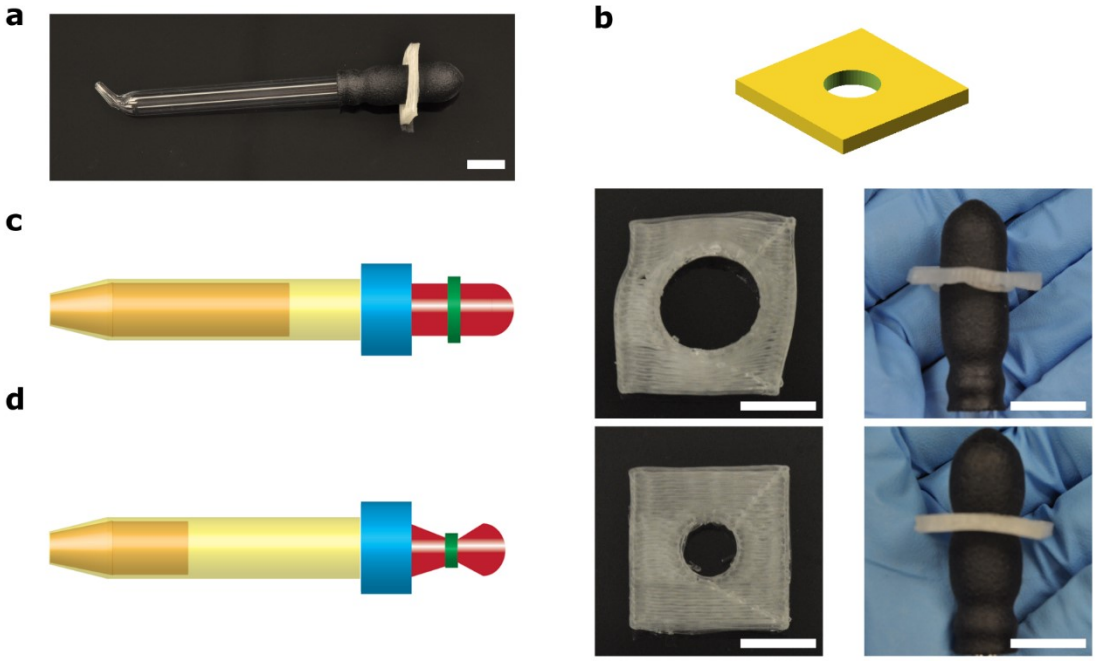

Fig. 8.2 A stretched eyedropper ring recovered its permanent shape and squeezed the rubber end of an eyedropper. (a) An eyedropper ring mounted on the rubber bulb of an eyedropper. **(b)** CAD model. **(c)** Stretched eyedropper ring. Left: Schematics. Middle: The ring was stretched to its temporary shape. Right: With eyedropper. The rubber bulb did not have shape deformation. **(d)** Recovered eyedropper ring. Left: Schematics. Middle: Without eyedropper. Right: The eyedropper ring recovered to its permanent shape. The rubber bulb was squeezed, and the cross section was reduced. Scale bar, 1 cm.

8.2.4.3 Pinch valve

The pinch valve was printed in its permanent shape, heated at 80 °C for one minute, and stretched to its temporary shape with a metal rod (Fig. 8.3b). The valve was mounted on a segment of a latex tube. Once the valve was heated at its glass transition temperature, it shrank to its permanent shape (Fig. 8.3c) and squeezed the tube, then reduced the cross-section of the tube. Therefore, this valve can stop the flow from passing through the tube. The future work is to design valves to accommodate a boarder range of tubes (e.g. rubber tubes, latex tubes with a larger diameter).

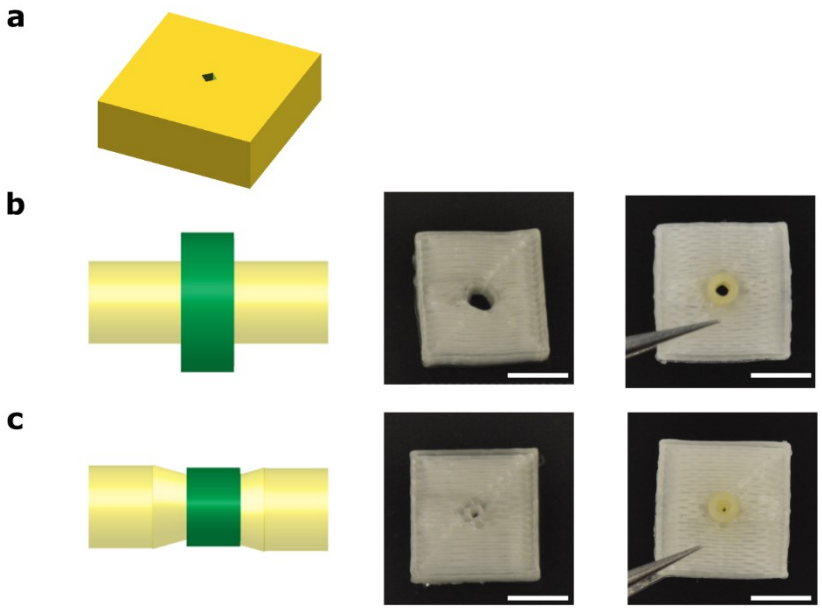

Fig. 8.3 A stretched pinch valve recovered its permanent shape and squeezed the tube. (a) CAD model. **(b)** Stretched pinch valve. Left: Schematics. Middle: The valve was stretched to its temporary shape. Right: With latex tube. The tube did not have shape deformation. **(c)** Recovered pinch valve. Left: Schematics. Middle: Without tube. Right: The pinch valve recovered to its permanent shape. The tube was squeezed, and the cross section was reduced. Scale bar, 1 cm.

8.2.4.4 Individual heating block

The use of an oven to activate fluidic control elements limit their application in areas where electricity power is not guaranteed.. Hot water serves as an excellent heat source because it can be attained via solar energy, natural hot spring, or fire. However, immersing elements in hot water might not always be applicable if the fluid being transported is sensitive to heat, and water may bring unnecessary humidity to the working environment. To address these issues, an individual heating block used hot water to produce hot air to activate the elements, which had no direct contact with water and were cased in a dry environment.

An individual heating block had a water reservoir and a unit to hold the fluid control element (Fig. 8.4a). The unit was embedded in the wall of the reservoir but not connected

to the reservoir (Fig. 8.4b). Hot water was poured into the reservoir and covered the unit. The air in the unit was heated up by the hot water surrounding it. After 23 seconds, the air temperature raised from room temperature to 65 °C, the glass transition temperature of PLA, which was adequate to start the shape change of the element. The temperature stayed above 65 °C for 80 seconds, providing ample time for the element to recover to its permanent shape (Fig. 8.4c). The future work is to design blocks that can create customized temperature profile within the unit (e.g., maintaining the 65 °C temperature for a longer period of time by adding insulation to the block).

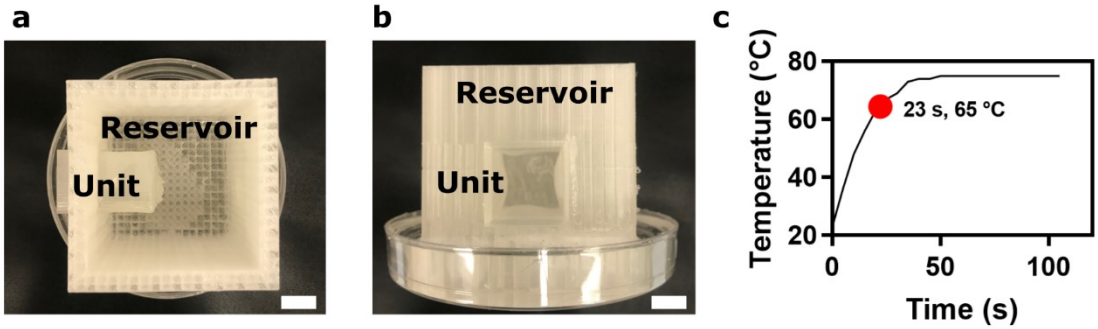

Fig. 8.4 An individual heating block heated up the air in the unit after water was added to the reservoir. (a) Top view. The unit was embedded in the reservoir wall. **(b)** Side view. The unit was not connected to the reservoir, so water would not flow into the unit. The block was placed in a petri dish, and the bottom was sealed with silicone gel to prevent water leakage. **(c)** Temperature profile inside the unit. The temperature reached 65 °C (glass transition temperature of PLA) in 23 seconds and stayed above 65 °C for 80 seconds.

8.2.4.5 Fluid control device

An assembly of heating blocks can control multiple fluidic control elements and activate them in a time sequence to establish flow. This example showed the design and operation principle of a two- step sequential activation of an eyedropper ring and a pinch valve (Fig. 8.5a, b). There was one water reservoir connecting to chamber A and B through port A and B, respectively. Each chamber had a unit to house a fluid control element. Hot

water was poured into the water reservoir (Fig. 8.6b), and the water level rose in the reservoir. The water level reached port A (lower position than port B) then water overflowed to chamber A, and unit A was immersed in water (Fig. 8.6c). Next, the water level reached port B, water overflowed to chamber B (Fig. 8.6d, e), and unit B was immersed in water (Fig. 8.6f). Unit A and unit B had an opening to host and activate a functional fluidic element.

A future experiment is to verify the design of this device. A tube is connected to two fluidic elements: the inlet is connected to a liquid-filled eyedropper in Unit A and the outlet to a pinch valve in Unit B (Fig. 8.5b). After the chamber A is filled with water first, unit A is filled with hot air, and the eyedropper squeezes out the liquid; the flow is initiated. Then unit B is heated by the hot water, the pinch valve is activated, and the tube cross-section reduces; the flow is terminated. The initiation and termination of the flow is programmed by the hot water flow.

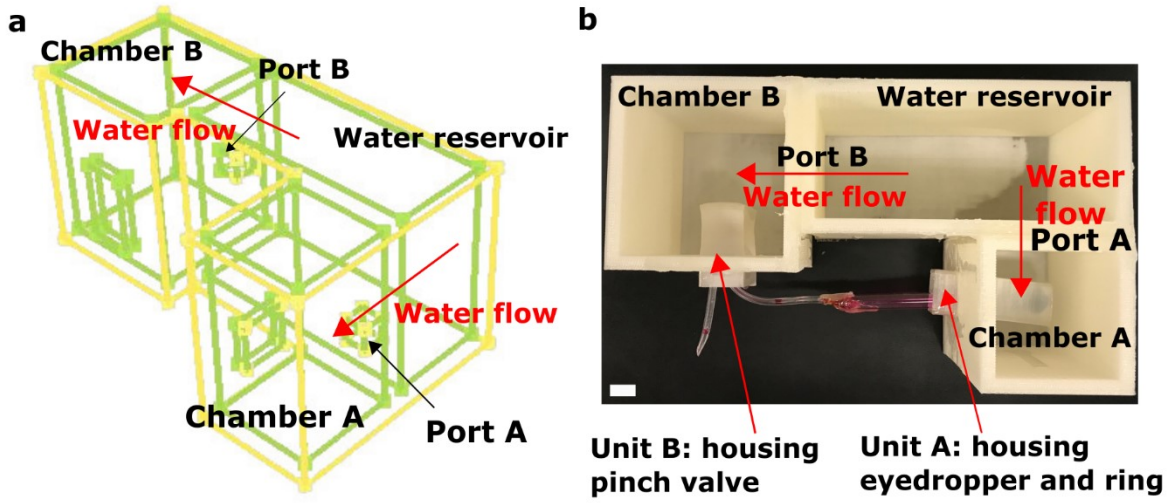

Fig. 8.5 An assembled fluid control device and its CAD model. (a) CAD model in framework view showing ports for water flow and windows to mount units. The water reservoir was connected to chamber A and B through port A and B, respectively. The water in reservoir overflowed to chambers through the ports. The position of port A was lower than port B, so the water first overflowed to chamber A then to chamber B. Unit A and B were not shown in this view. **(b)** Top view of assembly with flow control elements: eyedropper and ring (flow initiation), pinch valve (flow termination). Scale bar, 1 cm.

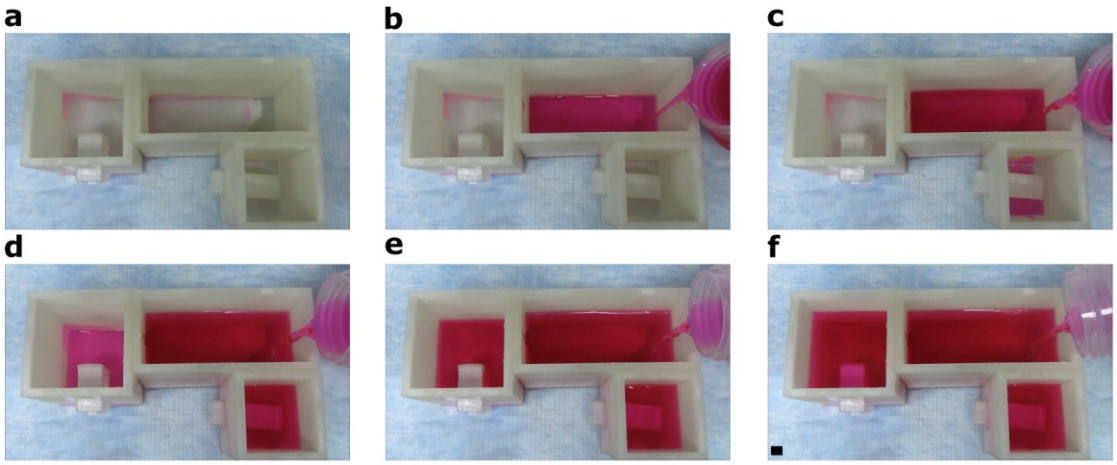

Fig. 8.6 Water flow sequence in an assembled fluid control device.
(a) An empty assembled fluid control device. **(b)** Hot water was poured into the water reservoir. **(c)** The water level rose in the reservoir and reached the port A, then water overflowed to chamber A. **(d)** Water level in chamber A rose, and unit A was immersed in water. The water level in the reservoir reached the port B, water overflowed to chamber B. **(e)** Water level kept rising in chamber B. **(f)** Water level in chamber B rose, and unit B was immersed in water. Scale bar, 1 cm.

The future work is to achieve precise control of the fluid sequence (e.g. volume and rate of the flow, time gap between each step) by tailoring the device design (e.g. chamber and reservoir dimension) and expanding the device to accommodate more complex fluid sequence (e.g. more chambers). The overarching goal of this fluidic control system is to release a desired amount of liquid at a given time, powered purely by hot water, and eliminated the use of electricity. Programmed flow control is prevalent in bioanalysis instruments. The existing approaches face the challenges of dispensing precisely measured quantities of liquid reagents and driving their transport through microfluidic networks. These barriers are addressed by either sacrificing system complexity for zero electrical power consumption (passive methods, e.g., capillary wicking in paper-based systems) or requiring mechanical pumps. Now, 3D printed fluidic control elements show potentials to resolve these issues as they can be operated by exposure to heated water, owing to its shape memory response within a specific temperature range. They do not rely on electricity power and permit operation by personnel with minimal training. The 3D printed fluidic control device has sufficient portability to be deployed in resource-limited situations and can offer a simple, inexpensive, and robust alternative to conventional bioanalysis instruments.

REFERENCES

1. Palleau, E., Morales, D., Dickey, M.D., and Velev, O.D., *Reversible patterning and actuation of hydrogels by electrically assisted ionoprinting.* Nature communications, 2013. 4: p. 2257-2263.
2. Zhao, X., Kim, J., Cezar, C.A., Huebsch, N., Lee, K., et al., *Active scaffolds for on-demand drug and cell delivery.* Proceedings of the National Academy of Sciences, 2011. 108(1): p. 67-72.
3. Graham, B., Reilly, W., Beinecke, F., Boesch, D., Garcia, T., et al., *Deep water: the gulf oil disaster and the future of offshore drilling. report to the president. national commission on the BP deepwater horizon oil spill and offshore drilling*. 2011, Washington, DC: Government Publishing Office (GPO).
4. Smith, L.C., Smith, M., and Ashcroft, P., *Analysis of environmental and economic damages from British Petroleum's Deepwater Horizon oil spill.* Albany Law Review, 2011. 74(1): p. 563-585.
5. Allen, A.A., Jaeger, D., Mabile, N.J., and Costanzo, D. *The use of controlled burning during the Gulf of Mexico Deepwater Horizon MC-252 oil spill response*. in *International Oil Spill Conference Proceedings (IOSC)*. 2011. American Petroleum Institute.
6. Ifelebuegu, A.O., Nguyen, T.V.A., Ukotije-Ikwut, P., and Momoh, Z., *Liquid-phase sorption characteristics of human hair as a natural oil spill sorbent.* Journal of Environmental Chemical Engineering, 2015. 3(2): p. 938-943.
7. Mullin, J. and Champ, M., *Introduction/overview to in situ burning of oil spills.* Spill Science & Technology Bulletin, 2003. 8(4): p. 323-330.

8. Li, F., Duggal, R., Oliva, O., Karki, S., Surolia, R., et al., *Heme oxygenase-1 protects corexit 9500A-induced respiratory epithelial injury across species.* PloS one, 2015. 10(4): p. e0122275.

9. Knap, A., Turner, N.R., Bera, G., Renegar, D.A., Frank, T., et al., *Short-term toxicity of 1-methylnaphthalene to Americamysis bahia and 5 deep-sea crustaceans.* Environmental toxicology and chemistry, 2017. 36(12): p. 3415-3423.

10. Kleindienst, S., Seidel, M., Ziervogel, K., Grim, S., Loftis, K., et al., *Chemical dispersants can suppress the activity of natural oil-degrading microorganisms.* Proceedings of the National Academy of Sciences, 2015. 112(48): p. 14900-14905.

11. Broje, V. and Keller, A., *Improved mechanical oil spill recovery using an optimized geometry for the skimmer surface.* Environmental Science & Technology, 2006. 40(24): p. 7914-7918.

12. Sakthivel, T., Reid, D.L., Goldstein, I., Hench, L., and Seal, S., *Hydrophobic high surface area zeolites derived from fly ash for oil spill remediation.* Environmental science & technology, 2013. 47(11): p. 5843-5850.

13. Zang, D., Liu, F., Zhang, M., Gao, Z., and Wang, C., *Novel superhydrophobic and superoleophilic sawdust as a selective oil sorbent for oil spill cleanup.* Chemical Engineering Research and Design, 2015. 102: p. 34-41.

14. Wang, P., Zhong, T., Jing, C., and Chen, L., *An ultralight, elastic, cost-effective, and highly recyclable superabsorbent from microfibrillated cellulose fibers for oil spillage cleanup.* Journal of Materials Chemistry A, 2015. 3(16): p. 8772-8781.

15. Abdullah, M., Rahmah, A.U., and Man, Z., *Physicochemical and sorption characteristics of Malaysian Ceiba pentandra (L.) Gaertn. as a natural oil sorbent.* Journal of hazardous materials, 2010. 177(1-3): p. 683-691.

16. Srinivasan, A. and Viraraghavan, T., *Removal of oil by walnut shell media.* Bioresource technology, 2008. 99(17): p. 8217-8220.

17. *Pollution prevention for Washington state marinas*. Available from: http://wsg.washington.edu/wordpress/wp-content/uploads/marina-handbook.pdf.

18. *Oil pollution volume by sources*. Available from: http://seawifs.gsfc.nasa.gov/OCEAN_PLANET/HTML/peril_oil_pollution.html.

19. Nguyen, D., Tai, N., Lee, S., and Kuo, W., *Superhydrophobic and superoleophilic properties of graphene-based sponges fabricated using a facile dip coating method.* Energy & Environmental Science, 2012. 5(7): p. 7908-7912.

20. Pham, V. and Dickerson, J., *Superhydrophobic silanized melamine sponges as high efficiency oil absorbent materials.* ACS Applied Materials & Interfaces, 2014. 6(16): p. 14181-14188.

21. Zhu, Q., Pan, Q., and Liu, F., *Facile removal and collection of oils from water surfaces through superhydrophobic and superoleophilic sponges.* The Journal of Physical Chemistry C, 2011. 115(35): p. 17464-17470.

22. Liu, Y., Ma, J., Wu, T., Wang, X., Huang, G., et al., *Cost-effective reduced graphene oxide-coated polyurethane sponge as a highly efficient and reusable oil-absorbent.* ACS Applied Materials & Interfaces, 2013. 5(20): p. 10018-10026.

23. Peng, L., Yuan, S., Yan, G., Yu, P., and Luo, Y., *Hydrophobic sponge for spilled oil absorption.* Journal of Applied Polymer Science, 2014. 131(20).

24. Choi, S., Kwon, T., Im, H., Moon, D., Baek, D., et al., *A polydimethylsiloxane (PDMS) sponge for the selective absorption of oil from water.* ACS Applied Materials & Interfaces, 2011. 3(12): p. 4552-4556.

25. Zhang, A., Chen, M., Du, C., Guo, H., Bai, H., et al., *Poly (dimethylsiloxane) oil absorbent with a three-dimensionally interconnected porous structure and swellable skeleton.* ACS Applied Materials & Interfaces, 2013. 5(20): p. 10201-10206.

26. Liu, Y., Huang, G., Gao, C., Zhang, L., Chen, M., et al., *Biodegradable polylactic acid porous monoliths as effective oil sorbents.* Composites Science and Technology, 2015. 118: p. 9-15.

27. Cheng, Y., Xu, P., Zeng, W., Ling, C., Zhao, S., et al., *Highly hydrophobic and ultralight graphene aerogel as high efficiency oil absorbent material.* Journal of Environmental Chemical Engineering, 2017. 5(2): p. 1957-1963.

28. Barry, E., Mane, A., Libera, J., Elam, J., and Darling, S., *Advanced oil sorbents using sequential infiltration synthesis.* Journal of Materials Chemistry A, 2017. 5(6): p. 2929-2935.

29. Hai, J., Bai, B., Ding, C., Wang, H., and Suo, Y., *Removal of oil from water surface by novel composite NSM-g-P(MMA-co-BA) super oil-absorption resin.* Polymer Composites, 2016. 39(4): p. 1051-1063.

30. Na, J.H., Evans, A.A., Bae, J., Chiappelli, M.C., Santangelo, C.D., et al., *Programming reversibly self-folding origami with micropatterned photo - crosslinkable polymer trilayers.* Advanced Materials, 2015. 27(1): p. 79-85.

31. Stuart, M., Huck, W., Genzer, J., Müller, M., Ober, C., et al., *Emerging applications of stimuli-responsive polymer materials.* Nature Materials, 2010. 9(2): p. 101-113.

32. Gladman, A., Matsumoto, E., Nuzzo, R., Mahadevan, L., and Lewis, J., *Biomimetic 4D printing.* Nature Materials, 2016. 15(4): p. 413-418.

33. Erb, R., Sander, J., Grisch, R., and Studart, A., *Self-shaping composites with programmable bioinspired microstructures.* Nature Communications, 2013. 4(1): p. 1-8.

34. Chluba, C., Ge, W., de Miranda, R.L., Strobel, J., Kienle, L., et al., *Ultralow-fatigue shape memory alloy films.* Science, 2015. 348(6238): p. 1004-1007.

35. Gómez-Cortés, J.F., Nó, M.L., López-Ferreño, I., Hernández-Saz, J., Molina, S.I., et al., *Size effect and scaling power-law for superelasticity in shape-memory alloys at the nanoscale.* Nature nanotechnology, 2017. 12(8): p. 790-797.

36. Jochum, F. and Theato, P., *Temperature-and light-responsive smart polymer materials.* Chemical Society Reviews, 2013. 42(17): p. 7468-7483.

37. Lendlein, A., Jiang, H., Jünger, O., and Langer, R., *Light-induced shape-memory polymers.* Nature, 2005. 434(7035): p. 879-882.

38. Kim, Y., Yuk, H., Zhao, R., Chester, S.A., and Zhao, X., *Printing ferromagnetic domains for untethered fast-transforming soft materials.* Nature, 2018. 558(7709): p. 274-279.

39. Pikul, J., Li, S., Bai, H., Hanlon, R., Cohen, I., et al., *Stretchable surfaces with programmable 3D texture morphing for synthetic camouflaging skins.* Science, 2017. 358(6360): p. 210-214.

40. Fusco, S., Sakar, M.S., Kennedy, S., Peters, C., Bottani, R., et al., *An integrated microrobotic platform for on‐demand, targeted therapeutic interventions.* Advanced Materials, 2014. 26(6): p. 952-957.

41. Zarek, M., Layani, M., Cooperstein, I., Sachyani, E., Cohn, D., et al., *3D printing of shape memory polymers for flexible electronic devices.* Advanced Materials, 2015. 28(22): p. 4449-4454.

42. Wehner, M., Truby, R.L., Fitzgerald, D.J., Mosadegh, B., Whitesides, G.M., et al., *An integrated design and fabrication strategy for entirely soft, autonomous robots.* Nature, 2016. 536(7617): p. 451-455.

43. Yuan, C., Roach, D.J., Dunn, C.K., Mu, Q., Kuang, X., et al., *3D printed reversible shape changing soft actuators assisted by liquid crystal elastomers.* Soft Matter, 2017. 13(33): p. 5558-5568.

44. Kotikian, A., Truby, R.L., Boley, J.W., White, T.J., and Lewis, J.A., *3D printing of liquid crystal elastomeric actuators with spatially programed nematic order.* Advanced Materials, 2018. 30(10).

45. Ambulo, C.P., Burroughs, J.J., Boothby, J.M., Kim, H., Shankar, M.R., et al., *Four-dimensional printing of liquid crystal elastomers.* ACS applied materials & interfaces, 2017. 9(42): p. 37332-37339.

46. Ware, T.H., McConney, M.E., Wie, J.J., Tondiglia, V.P., and White, T.J., *Voxelated liquid crystal elastomers.* Science, 2015. 347(6225): p. 982-984.

47. Lum, G.Z., Ye, Z., Dong, X., Marvi, H., Erin, O., et al., *Shape-programmable magnetic soft matter.* Proceedings of the National Academy of Sciences, 2016. 113(41): p. E6007-E6015.

48. Bakarich, S.E., Gorkin, R., and Spinks, G.M., *4D printing with mechanically robust, thermally actuating hydrogels.* Macromolecular rapid communications, 2015. 36(12): p. 1211-1217.

49. Han, D., Lu, Z., Chester, S.A., and Lee, H., *Micro 3D printing of a temperature-responsive hydrogel using projection micro-stereolithography.* Scientific reports, 2018. 8(1): p. 1-10.

50. Kim, J., Hanna, J.A., Byun, M., Santangelo, C.D., and Hayward, R.C., *Designing responsive buckled surfaces by halftone gel lithography.* Science, 2012. 335(6073): p. 1201-1205.

51. de Marco, C., Alcântara, C.C., Kim, S., Briatico, F., Kadioglu, A., et al., *Indirect 3D and 4D printing of soft robotic microstructures.* Advanced Materials Technologies, 2019. 4(9).

52. Ma, M., Guo, L., Anderson, D.G., and Langer, R., *Bio-inspired polymer composite actuator and generator driven by water gradients.* Science, 2013. 339(6116): p. 186-189.

53. Li, W., Li, F., Li, H., Su, M., Gao, M., et al., *Flexible circuits and soft actuators by printing assembly of graphene.* ACS applied materials & interfaces, 2016. 8(19): p. 12369-12376.

54. Kokkinis, D., Schaffner, M., and Studart, A.R., *Multimaterial magnetically assisted 3D printing of composite materials.* Nature communications, 2015. 6(1): p. 1-10.

55. Kim, J., Chung, S.E., Choi, S.-E., Lee, H., Kim, J., et al., *Programming magnetic anisotropy in polymeric microactuators.* Nature materials, 2011. 10(10): p. 747-752.

56. Liu, Y., Boyles, J.K., Genzer, J., and Dickey, M.D., *Self-folding of polymer sheets using local light absorption.* Soft matter, 2012. 8(6): p. 1764-1769.

57. Adebajo, M.O., Frost, R.L., Kloprogge, J.T., Carmody, O., and Kokot, S., *Porous materials for oil spill cleanup: a review of synthesis and absorbing properties.* Journal of Porous materials, 2003. 10(3): p. 159-170.

58. Gupta, S. and Tai, N.-H., *Carbon materials as oil sorbents: a review on the synthesis and performance.* Journal of Materials Chemistry A, 2016. 4(5): p. 1550-1565.

59. Liu, H., Geng, B., Chen, Y., and Wang, H., *Review on the aerogel-type oil sorbents derived from nanocellulose.* ACS sustainable chemistry & engineering, 2016. 5(1): p. 49-66.

60. Li, J.-J., Zhou, Y.-N., and Luo, Z.-H., *Polymeric materials with switchable superwettability for controllable oil/water separation: A comprehensive review.* Progress in Polymer Science, 2018. 87: p. 1-33.

61. Bell, J.M. and Cameron, F., *The flow of liquids through capillary spaces.* The Journal of Physical Chemistry, 1906. 10(8): p. 658-674.

62. Lucas, R., *Rate of capillary ascension of liquids.* Kolloid Z, 1918. 23(15): p. 15-22.

63. Washburn, E., *The dynamics of capillary flow.* Physical Review, 1921. 17(3): p. 273-283.

64. Ichikawa, N. and Satoda, Y., *Interface dynamics of capillary flow in a tube under negligible gravity condition.* Journal of colloid and interface science, 1994. 162(2): p. 350-355.

65. Fries, N. and Dreyer, M., *The transition from inertial to viscous flow in capillary rise.* Journal of Colloid and Interface Science, 2008. 327(1): p. 125-128.

66. Buryakovsky, L., Aminzadeh, F., and Chilingarian, G.V., *Petroleum geology of the south Caspian Basin* 2001, Ch.10, p.303: Elsevier.

67. Fries, N. and Dreyer, M., *An analytic solution of capillary rise restrained by gravity.* Journal of colloid and interface science, 2008. 320(1): p. 259-263.

68. Figliuzzi, B. and Buie, C., *Rise in optimized capillary channels.* Journal of Fluid Mechanics, 2013. 731: p. 142-161.

69. Södergård, A. and Stolt, M., *Properties of lactic acid based polymers and their correlation with composition.* Progress in polymer science, 2002. 27(6): p. 1123-1163.

70. Daniels, A., Chang, M.K., Andriano, K.P., and Heller, J., *Mechanical properties of biodegradable polymers and composites proposed for internal fixation of bone.* Journal of applied biomaterials, 1990. 1(1): p. 57-78.

71. Lendlein, A. and Langer, R., *Biodegradable, elastic shape-memory polymers for potential biomedical applications.* Science, 2002. 296(5573): p. 1673-1676.

72. Isayev, A. and Crouthamel, D., *Residual stress development in the injection molding of polymers.* Polymer-plastics technology and engineering, 1984. 22(2): p. 177-232.

73. Reiter, G., Hamieh, M., Damman, P., Sclavons, S., Gabriele, S., et al., *Residual stresses in thin polymer films cause rupture and dominate early stages of dewetting.* Nature materials, 2005. 4(10): p. 754-758.

74. Jacques, M.S., *An analysis of thermal warpage in injection molded flat parts due to unbalanced cooling.* Polymer Engineering & Science, 1982. 22(4): p. 241-247.

75. Aou, K., Kang, S., and Hsu, S.L., *Morphological study on thermal shrinkage and dimensional stability associated with oriented poly (lactic acid).* Macromolecules, 2005. 38(18): p. 7730-7735.

76. Postawa, P. and Kwiatkowski, D., *Residual stress distribution in injection molded parts.* Journal of Achievements in Materials and Manufacturing Engineering, 2006. 18(1-2): p. 171-174.

77. Liang, H. and Mahadevan, L., *Growth, geometry, and mechanics of a blooming lily.* Proceedings of the National Academy of Sciences, 2011. 108(14): p. 5516-5521.

78. Nath, U., Crawford, B.C., Carpenter, R., and Coen, E., *Genetic control of surface curvature.* Science, 2003. 299(5611): p. 1404-1407.

79. Amass, W., Amass, A., and Tighe, B., *A review of biodegradable polymers: uses, current developments in the synthesis and characterization of biodegradable polyesters, blends of biodegradable polymers and recent advances in biodegradation studies.* Polymer International, 1998. 47(2): p. 89-144.

80. Bastioli, C., *Handbook of biodegradable polymers*. 2005: iSmithers Rapra Publishing.

81. Davis, G. and Song, J., *Biodegradable packaging based on raw materials from crops and their impact on waste management.* Industrial crops and products, 2006. 23(2): p. 147-161.

82. Ahmed, J. and Varshney, S.K., *Polylactides—chemistry, properties and green packaging technology: a review.* International journal of food properties, 2011. 14(1): p. 37-58.

83. Siracusa, V., Rocculi, P., Romani, S., and Dalla Rosa, M., *Biodegradable polymers for food packaging: a review.* Trends in Food Science & Technology, 2008. 19(12): p. 634-643.

84. Domb, A.J. and Kumar, N., *Biodegradable polymers in clinical use and clinical development*. 2011: John Wiley & Sons.

85. Ulery, B.D., Nair, L.S., and Laurencin, C.T., *Biomedical applications of biodegradable polymers.* Journal of polymer science Part B: polymer physics, 2011. 49(12): p. 832-864.

86. De, A., Bose, R., Kumar, A., and Mozumdar, S., *Targeted delivery of pesticides using biodegradable polymeric nanoparticles*. 2014: Springer.

87. Kasirajan, S. and Ngouajio, M., *Polyethylene and biodegradable mulches for agricultural applications: a review.* Agronomy for Sustainable Development, 2012. 32(2): p. 501-529.

88. Benninga, H., *A history of lactic acid making: a chapter in the history of biotechnology*. Vol. 11. 1990: Springer Science & Business Media.

89. Williams, C. and Hillmyer, M., *Polymers from renewable resources: a perspective for a special issue of polymer reviews.* Polymer Reviews, 2008. 48(1): p. 1-10.

90. Masutani, K. and Kimura, Y., *Poly(lactic acid) Science and Technology: Processing, Properties, Additives and Applications*. 2014. Ch.1, p.1-36.

91. Williams, D., *Enzymic hydrolysis of polylactic acid.* Eng. Med., 1981. 10(1): p. 5-7.

92. Garlotta, D., *A literature review of poly (lactic acid).* Journal of Polymers and the Environment, 2001. 9(2): p. 63-84.

93. Lim, L., Auras, R., and Rubino, M., *Processing technologies for poly (lactic acid).* Progress in polymer science, 2008. 33(8): p. 820-852.

94. Lim, L. and Tsuji, H., *Poly (lactic acid): synthesis, structures, properties, processing, and applications*. Vol. 6. 2010: Wiley.

95. Jimenez, A., Peltzer, M., and Ruseckaite, R., *Poly (lactic acid) science and technology: processing, properties, additives and applications*. 2014: Royal Society of Chemistry.

96. MacDonald, R., McCarthy, S., and Gross, R., *Enzymatic degradability of poly (lactide): effects of chain stereochemistry and material crystallinity.* Macromolecules, 1996. 29(23): p. 7356-7361.

97. Gan, Z. and Abe, H., *Temperature‐induced polymorphic crystals of poly (butylene adipate).* Macromolecular Chemistry and Physics, 2002. 203(16): p. 2369-2374.

98. Zhao, L., Wang, X., Li, L., and Gan, Z., *Structural analysis of poly (butylene adipate) banded spherulites from their biodegradation behavior.* Polymer, 2007. 48(20): p. 6152-6161.

99. Zhao, L. and Gan, Z., *Effect of copolymerized butylene terephthalate chains on polymorphism and enzymatic degradation of poly (butylene adipate).* Polymer degradation and stability, 2006. 91(10): p. 2429-2436.

100. Witt, U., Müller, R., and Deckwer, W., *Biodegradation behavior and material properties of aliphatic/aromatic polyesters of commercial importance.* Journal of environmental polymer degradation, 1997. 5(2): p. 81-89.

101. Kleeberg, I., Welzel, K., VandenHeuvel, J., Müller, R., and Deckwer, W., *Characterization of a new extracellular hydrolase from Thermobifida fusca degrading aliphatic-aromatic copolyesters.* Biomacromolecules, 2005. 6(1): p. 262-270.

102. Shah, A., Hasan, F., Hameed, A., and Ahmed, S., *Biological degradation of plastics: a comprehensive review.* Biotechnology advances, 2008. 26(3): p. 246-265.

103. Müller, R., Schrader, H., Profe, J., Dresler, K., and Deckwer, W., *Enzymatic degradation of poly (ethylene terephthalate): rapid hydrolyse using a hydrolase from T. fusca.* Macromolecular rapid communications, 2005. 26(17): p. 1400-1405.

104. Nagata, M., Kiyotsukuri, T., Minami, S., Tsutsumi, N., and Sakai, W., *Enzymatic degradation of poly (ethylene terephthalate) copolymers with aliphatic dicarboxylic acids and/or poly (ethylene glycol).* European polymer journal, 1997. 33(10): p. 1701-1705.

105. Đorđević, D., Petronijević, Ž., and Cvetković, D., *Polyester fabric modification by some lipases.* Chemical Industry and Chemical Engineering Quarterly, 2005. 11(4): p. 183-188.

106. Cheng, H. and Gross, R., *Green polymer chemistry: biocatalysis and biomaterials*. 2010: American Chemical Society New York, NY, USA.

107. Mueller, R., *Biological degradation of synthetic polyesters—enzymes as potential catalysts for polyester recycling.* Process Biochemistry, 2006. 41(10): p. 2124-2128.

108. Nowak, B., Pająk, J., Łabużek, S., Rymarz, G., and Talik, E., *Biodegradation of poly (ethylene terephthalate) modified with polyester "Bionolle®" by Penicillium funiculosum.* Polimery, 2011. 56(1): p. 35-44.

109. Vertommen, M., Nierstrasz, V., Veer, M., and Warmoeskerken, M., *Enzymatic surface modification of poly (ethylene terephthalate).* Journal of biotechnology, 2005. 120(4): p. 376-386.

110. Potts, J., Clendinning, R., Ackart, W., and Niegisch, W., *The biodegradability of synthetic polymers*, in *Polymers and ecological problems*. 1973, Springer. p. 61-79.

111. Goldberg, D., *A review of the biodegradability and utility of poly (caprolactone).* Journal of Polymers and the Environment, 1995. 3(2): p. 61-67.

112. Oda, Y., Oida, N., Urakami, T., and Tonomura, K., *Polycaprolactone depolymerase produced by the bacterium Alcaligenes faecalis.* FEMS Microbiology letters, 1997. 152(2): p. 339-343.

113. Gan, Z., Liang, Q., Zhang, J., and Jing, X., *Enzymatic degradation of poly (ε-caprolactone) film in phosphate buffer solution containing lipases.* Polymer degradation and stability, 1997. 56(2): p. 209-213.

114. Baker, P., Poultney, C., Liu, Z., Gross, R., and Montclare, J., *Identification and comparison of cutinases for synthetic polyester degradation.* Applied microbiology and biotechnology, 2012. 93(1): p. 229-240.

115. Sanchez, J., Tsuchii, A., and Tokiwa, Y., *Degradation of polycaprolactone at 50° C by a thermotolerant Aspergillus sp.* Biotechnology Letters, 2000. 22(10): p. 849-853.

116. Pastorino, L., Pioli, F., Zilli, M., Converti, A., and Nicolini, C., *Lipase-catalyzed degradation of poly (ε-caprolactone).* Enzyme and microbial technology, 2004. 35(4): p. 321-326.

117. Benedict, C., Cameron, J., and Huang, S., *Polycaprolactone degradation by mixed and pure cultures of bacteria and a yeast.* Journal of Applied Polymer Science, 1983. 28(1): p. 335-342.

118. Murphy, C., Cameron, J., Huang, S., and Vinopal, R., *Fusarium polycaprolactone depolymerase is cutinase.* Applied and environmental microbiology, 1996. 62(2): p. 456-460.

119. Oda, Y., Asari, H., Urakami, T., and Tonomura, K., *Microbial degradation of poly (3-hydroxybutyrate) and polycaprolactone by filamentous fungi.* Journal of fermentation and bioengineering, 1995. 80(3): p. 265-269.

120. Dave, P., Gross, R., Brucato, C., Wong, S., and McCarthy, S., *Biodegradation of blends containing poly (3-hydroxybutyrate-co-valerate)*, in *Biotechnology and Polymers*. 1991, Springer. p. 53-61.

121. Fields, R., Rodriguez, F., and Finn, R., *Microbial degradation of polyesters: polycaprolactone degraded by P. pullulans.* Journal of Applied Polymer Science, 1974. 18(12): p. 3571-3579.

122. Berkane, C., Mezoul, G., Lalot, T., Brigodiot, M., and Marechal, E., *Lipase-catalyzed polyester synthesis in organic medium study of ring− chain equilibrium.* Macromolecules, 1997. 30(25): p. 7729-7734.

123. Kumar, A. and Gross, R., *Candida antartica lipase B catalyzed polycaprolactone synthesis: effects of organic media and temperature.* Biomacromolecules, 2000. 1(1): p. 133-138.

124. Cook, W., Cameron, J., Bell, J., and Huang, S., *Scanning electron microscopic visualization of biodegradation of polycaprolactones by fungi.* Journal of Polymer Science Part C: Polymer Letters, 1981. 19(4): p. 159-165.

125. Benedict, C., Cook, W., Jarrett, P., Cameron, J., Huang, S., et al., *Fungal degradation of polycaprolactones.* Journal of Applied Polymer Science, 1983. 28(1): p. 327-334.

126. Mochizuki, M., Hirano, M., Kanmuri, Y., Kudo, K., and Tokiwa, Y., *Hydrolysis of polycaprolactone fibers by lipase: effects of draw ratio on enzymatic degradation.* Journal of applied polymer science, 1995. 55(2): p. 289-296.

127. Becker, H. and Locascio, L.E., *Polymer microfluidic devices.* Talanta, 2002. 56(2): p. 267-287.

128. Becker, H. and Gärtner, C., *Polymer microfabrication technologies for microfluidic systems.* Analytical and bioanalytical chemistry, 2008. 390(1): p. 89-111.

129. Becker, H. and Heim, U., *Hot embossing as a method for the fabrication of polymer high aspect ratio structures.* Sensors and Actuators A: Physical, 2000. 83(1): p. 130-135.

130. Becker, H. and Dietz, W. *Microfluidic devices for μ-TAS applications fabricated by polymer hot embossing*. in *Micromachining and Microfabrication*. 1998. International Society for Optics and Photonics.

131. Su, Y., Shah, J., and Lin, L., *Implementation and analysis of polymeric microstructure replication by micro injection molding.* Journal of Micromechanics and Microengineering, 2003. 14(3): p. 415-422.

132. Attia, U., Marson, S., and Alcock, J., *Micro-injection moulding of polymer microfluidic devices.* Microfluidics and Nanofluidics, 2009. 7(1): p. 1-28.

133. Xia, Y. and Whitesides, G., *Soft lithography.* Annual review of materials science, 1998. 28(1): p. 153-184.

134. Whitesides, G., Ostuni, E., Takayama, S., Jiang, X., and Ingber, D., *Soft lithography in biology and biochemistry.* Annual Review of Biomedical Engineering, 2001. 3(1): p. 335-373.

135. Roberts, M., Rossier, J., Bercier, P., and Girault, H., *UV laser machined polymer substrates for the development of microdiagnostic systems.* Analytical chemistry, 1997. 69(11): p. 2035-2042.

136. Romoli, L., Tantussi, G., and Dini, G., *Experimental approach to the laser machining of PMMA substrates for the fabrication of microfluidic devices.* Optics and Lasers in Engineering, 2011. 49(3): p. 419-427.

137. Romanato, F., Tormen, M., Businaro, L., Vaccari, L., Stomeo, T., et al., *X-ray lithography for 3D microfluidic applications.* Microelectronic Engineering, 2004. 73: p. 870-875.

138. Tormen, M., Businaro, L., Altissimo, M., Romanato, F., Cabrini, S., et al., *3D patterning by means of nanoimprinting, X-ray and two-photon lithography.* Microelectronic Engineering, 2004. 73: p. 535-541.

139. Huang, J., Jayaraman, A., and Ugaz, V., *Enzymatic sculpting of nanoscale and microscale surface topographies.* Angew Chem Int Ed Engl, 2012. 51(38): p. 9619-9623.

140. Kikkawa, Y., Fukuda, M., Ichikawa, N., Kashiwada, A., Matsuda, K., et al., *Tuning the enzymatic hydrolysis of biodegradable polyesters and its application to surface patterning.* Journal of Materials Chemistry A, 2013. 1(15): p. 4667-4670.

141. Khan, I., Dutta, J., and Ganesan, R., *Enzymes' action on materials: Recent trends.* Journal of Cellular Biotechnology, 2016. 1(2): p. 131-144.

142. Clausen‐Schaumann, H., Grandbois, M., and Gaub, H., *Enzyme‐assisted nanoscale lithography in lipid membranes.* Advanced Materials, 1998. 10(12): p. 949-952.

143. Ionescu, R., Marks, R., and Gheber, L., *Nanolithography using protease etching of protein surfaces.* Nano Letters, 2003. 3(12): p. 1639-1642.

144. Ionescu, R., Marks, R., and Gheber, L., *Manufacturing of nanochannels with controlled dimensions using protease nanolithography.* Nano Letters, 2005. 5(5): p. 821-827.

145. Piner, R., Zhu, J., Xu, F., Hong, S., and Mirkin, C., *"Dip-pen" nanolithography.* science, 1999. 283(5402): p. 661-663.

146. Li, H., He, Q., Wang, X., Lu, G., Liusman, C., et al., *Nanoscale-controlled enzymatic degradation of poly(L-lactic acid) films using dip-pen nanolithography.* Small, 2011. 7(2): p. 226-229.

147. Nakamura, C., Miyamoto, C., Obataya, I., Takeda, S., Yabuta, M., et al., *Enzymatic nanolithography of FRET peptide layer using V8 protease-immobilized AFM probe.* Biosensors and Bioelectronics, 2007. 22(9): p. 2308-2314.

148. Moraille, P. and Badia, A., *Enzymatic lithography of phospholipid bilayer films by stereoselective hydrolysis.* Journal of the American Chemical Society, 2005. 127(18): p. 6546-6547.

149. Luo, X., Pedrosa, V., and Wang, J., *Enzymatic nanolithography of polyaniline nanopatterns by using peroxidase‐modified atomic force microscopy tips.* Chemistry‐A European Journal, 2009. 15(21): p. 5191-5194.

150. Riemenschneider, L., Blank, S., and Radmacher, M., *Enzyme-assisted nanolithography.* Nano letters, 2005. 5(9): p. 1643-1646.

151. Jackman, R., Wilbur, J., and Whitesides, G., *Fabrication of submicrometer features on curved substrates by microcontact printing.* Science, 1995. 269(5224): p. 664-666.

152. Guyomard-Lack, A., Delorme, N., Moreau, C., Bardeau, J., and Cathala, B., *Site-selective surface modification using enzymatic soft lithography.* Langmuir, 2011. 27(12): p. 7629-7634.

153. Huo, F., Zheng, Z., Zheng, G., Giam, L., Zhang, H., et al., *Polymer pen lithography.* Science, 2008. 321(5896): p. 1658-1660.

154. Ganesh, M., Nachman, J., Mao, Z., Lyons, A., Rafailovich, M., et al., *Patterned enzymatic degradation of poly (ε-caprolactone) by high-affinity microcontact printing and polymer pen lithography.* Biomacromolecules, 2013. 14(8): p. 2470-2476.

155. Mao, Z., Ganesh, M., Bucaro, M., Smolianski, I., Gross, R., et al., *High throughput, high resolution enzymatic lithography process: Effect of crystallite size, moisture, and enzyme concentration.* Biomacromolecules, 2014. 15(12): p. 4627-4636.

156. Huang, J., Han, D., Ruggles, M., Jayaraman, A., and Ugaz, V., *Characterization of enzymatic micromachining for construction of variable cross-section microchannel topologies.* Biomicrofluidics, 2016. 10(3).

157. Kutter, J., *Liquid phase chromatography on microchips.* Journal of Chromatography A, 2012. 1221: p. 72-82.

158. Ceriotti, L., de Rooij, N., and Verpoorte, E., *An integrated fritless column for on-chip capillary electrochromatography with conventional stationary phases.* Analytical Chemistry, 2002. 74(3): p. 639-647.

159. Thurmann, S., Mauritz, L., Heck, C., and Belder, D., *High-performance liquid chromatography on glass chips using precisely defined porous polymer monoliths as particle retaining elements.* Journal of Chromatography A, 2014. 1370: p. 33-39.

160. Nagy, A. and Gaspar, A., *Packed multi-channels for parallel chromatographic separations in microchips.* Journal of Chromatography A, 2013. 1304: p. 251-256.

161. Oleschuk, R., Shultz-Lockyear, L., Ning, Y., and Harrison, D., *Trapping of bead-based reagents within microfluidic systems: on-chip solid-phase extraction and electrochromatography.* Analytical Chemistry, 2000. 72(3): p. 585-590.

162. Tsuji, H. and Miyauchi, S., *Enzymatic hydrolysis of poly (lactide) s: effects of molecular weight, L-lactide content, and enantiomeric and diastereoisomeric polymer blending.* Biomacromolecules, 2001. 2(2): p. 597-604.

163. Tantra, R., Tompkins, J., and Quincey, P., *Characterisation of the de-agglomeration effects of bovine serum albumin on nanoparticles in aqueous suspension.* Colloids and Surfaces B: Biointerfaces, 2010. 75(1): p. 275-281.

164. Lee, S., Mativetsky, J., Loth, M., Anthony, J., and Loo, Y., *Quantifying resistances across nanoscale low-and high-angle interspherulite boundaries in solution-processed organic semiconductor thin films.* ACS Nano, 2012. 6(11): p. 9879-9886.

165. *Vector borne diseases key facts*. Available from: https://www.who.int/en/news-room/fact-sheets/detail/vector-borne-diseases.

166. *Etsy annual revenue*. Available from: https://www.statista.com/statistics/409371/etsy-annual-revenue/.

167. *Etsy active buyers*. Available from: https://www.statista.com/statistics/409375/etsy-active-buyers/.

168. Osterwalder, A. and Pigneur, Y., *Business model generation: a handbook for visionaries, game changers, and challengers*. 2010: John Wiley & Sons.

169. Blank, S. and Dorf, B., *The startup owner's manual: The step-by-step guide for building a great company*. 2012: BookBaby.

170. Carlson, L.E. and Sullivan, J.F., *Hands-on engineering: learning by doing in the integrated teaching and learning program.* International Journal of Engineering Education, 1999. 15(1): p. 20-31.

171. Han, D. and Ugaz, V., *Embedding hands-on mini laboratory experiences in a core undergraduate fluid mechanics course: a pilot study.* 2017. 51(3): p. 136-144.

172. Feisel, L.D. and Rosa, A.J., *The role of the laboratory in undergraduate engineering education.* Journal of Engineering Education, 2005. 94(1): p. 121-130.

173. Ma, J. and Nickerson, J.V., *Hands-on, simulated, and remote laboratories: A comparative literature review.* ACM Computing Surveys (CSUR), 2006. 38(3).

174. Edward, N.S., *The role of laboratory work in engineering education: student and staff perceptions.* International Journal of Electrical Engineering Education, 2002. 39(1): p. 11-19.

175. *U.S. National Archives,* . Available from: www.archives.gov/research_room/federal_records_guide.

176. Grinter, L.E., *Report on the evaluation of engineering education.* Journal of Engineering Education, 1955. 46(1): p. 25-63.

177. Froyd, J.E., Wankat, P.C., and Smith, K.A., *Five major shifts in 100 years of engineering education.* Proceedings of the IEEE, 2012. 100(Special Centennial Issue): p. 1344-1360.

178. ABET, *Criteria for accrediting engineering programs 2000-2001.* 2001.

179. *The undergraduate engineering laboratory, final report of the quality of engineering education project (QEEP)*. 1986, American Society for Engineering Education: Washington, D.C. p. 125-145.

180. ABET, *Criteria for accrediting engineering programs 2016–2017.* 2016.

181. Felder, R.M., Woods, D.R., Stice, J.E., and Rugarcia, A., *The future of engineering education II. Teaching methods that work.* Chemical Engineering Education, 2000. 34(1): p. 26-39.

182. Felder, R.M. and Silverman, L.K., *Learning and teaching styles in engineering education.* Engineering education, 1988. 78(7): p. 674-681.

183. Peterson, K.L., Compere, M.D., Allam, Y.S., and Van Wie, B.J. *A fluid flow characterization device for an educational desktop learning module*. in *ASME 2012 International Mechanical Engineering Congress and Exposition*. 2012. American Society of Mechanical Engineers.

184. Doughty, G., Magill, J., Pollock, M., Truman, A., Wilkinson, J., et al., *Experimentation: how it reinforces self-learning.* Innovative Methods in Enging Educ, 1992. 43: p. 264-269.

185. Yilmaz, M., Ren, J., Custer, S., and Coleman, J., *Hands-on summer camp to attract K–12 students to engineering fields.* IEEE Transactions on Education, 2010. 53(1): p. 144-151.

186. Dutson, A.J., Todd, R.H., Magleby, S.P., and Sorensen, C.D., *A review of literature on teaching engineering design through project‐oriented capstone courses.* Journal of Engineering Education, 1997. 86(1): p. 17-28.

187. Hohn, K.L., *The chemical engineering behind how pop goes flat: a hands-on experiment for freshmen.* Chemical Engineering Education, 2007. 41(1): p. 14-18.

188. Prausnitz, M.R., *COMET: An open-ended, hands-on project for ChE sophomores.* Chemical Engineering Education (CEE), 1998. 32(1): p. 20-23.

189. Rajala, J.W., Evans, E.A., and Chase, G.G., *Heat exchanger lab for chemical engineering undergraduates.* Chemical Engineering Education, 2015. 49(4): p. 208-214.

190. Hoare, T., *Toward" reality-based" integrative laboratories in ChE: introducing real-time, hands-on troubleshooting.* Chemical Engineering Education, 2015. 49(2): p. 118-126.

191. Minerick, A.R., *Versatile desktop experiment module (DEMo) on heat transfer.* Chemical Engineering Education, 2010. 44(4): p. 274-279.

192. Golter, P.B., *Combining modern learning pedagogies in fluid mechanics and heat transfer*. 2006, Washington State University.

193. Selmer, A., Kraft, M., Moros, R., and Colton, C., *Weblabs in chemical engineering education.* Education for Chemical Engineers, 2007. 2(1): p. 38-45.

194. Colton, C.K., Knight, M., Khan, R.-A., Ibrahim, S., and West, R., *A web-accessible heat exchanger experiment.* INNOVATIONS 2004: World Innovations in Engineering Education and Research, 2004: p. 93-106.

195. Drake, B.D., Acosta, G.M., Wingard, D.A., and Smith, R.L., *Improving creativity, solving problems, and communicating with peers in engineering and science laboratories.* Journal of chemical education, 1994. 71(7): p. 592-596.

196. De Jong, T., Linn, M.C., and Zacharia, Z.C., *Physical and virtual laboratories in science and engineering education.* Science, 2013. 340(6130): p. 305-308.

197. Franklin, B. and Collinson, P., *Experiments and observations on electricity, made at Philadelphia in America... To which are added, letters and papers on philosophical subjects. The whole corrected, methodized... and now first collected into one volume, etc. Edited by Peter Collinson*. 1774.

198. Volta, A., *XVII. On the electricity excited by the mere contact of conducting substances of different kinds. In a letter from Mr. Alexander Volta, FRS Professor*

of Natural Philosophy in the University of Pavia, to the Rt. Hon. Sir Joseph Banks, Bart. KBPR S. Philosophical transactions of the Royal Society of London, 1800. 90: p. 403-431.

199. Daniell, J.F., *X. On voltaic combinations. In a letter addressed to Michael Faraday, DCL, FRS, Fullerian Prof. Chem. Royal Institution, Corr. Memb. Royal & Imp. Acadd. of Science, Paris, Petersburgh, &c. By J. Frederic Daniell, FRS, Prof. Chem. in King's College, London.* Philosophical Transactions of the Royal Society of London, 1836. 126: p. 107-124.

200. Spencer, J.N., Bodner, G.M., and Rickard, L.H., *Chemistry: structure and dynamics*. 2010: John Wiley & Sons. Page 564.

201. Hulot, M., *Comptes rendus hebdomadaires des séances de l'academie des sciences.* Comptes Rendus, 1855. 40: p. 15-24.

202. Tomassi, D., *Traits' des piles Electriques, Georges*. 1889: Car& Paris.

203. Zaromb, S., *The use and behavior of aluminum anodes in alkaline primary batteries.* Journal of The Electrochemical Society, 1962. 109(12): p. 1125-1130.

204. Doche, M., Novel-Cattin, F., Durand, R., and Rameau, J., *Characterization of different grades of aluminum anodes for aluminum/air batteries.* Journal of Power Sources, 1997. 65(1-2): p. 197-205.

205. Marsal, P.A., Karl, K., and Urry, L.F., *Dry cell*. 1960, Google Patents.

206. Hildebrand, J.H., *Gilbert Newton Lewis.* Biographical memoirs National Academy of Sciences, 1958. 31: p. 210-235.

207. Tachi, T., Kaji, N., Tokeshi, M., and Baba, Y., *Simultaneous separation, metering, and dilution of plasma from human whole blood in a microfluidic system* Analytical Chemistry, 2009. 81(8): p. 3194-3198.

208. Yoshio, M., Brodd, R.J., and Kozawa, A., *Lithium-ion batteries*. Vol. 1. 2009: Springer.

209. *Centers for Disease Control and Prevention. National Diabetes Statistics Report, 2017. Atlanta, GA: Centers for Disease Control and Prevention, US Department of Health and Human Services; 2017.*

210. Bruen, D., Delaney, C., Florea, L., and Diamond, D., *Glucose sensing for diabetes monitoring: recent developments.* Sensors, 2017. 17(8).

211. Dobson, M., *Nature of the urine in diabetes, Medical Observations and Inquiries.* vol, 1776. 5: p. 298-310.

212. Clark, L.C. and Lyons, C., *Electrode systems for continuous monitoring in cardiovascular surgery.* Annals of the New York Academy of sciences, 1962. 102(1): p. 29-45.

213. Wang, J., *Electrochemical glucose biosensors.* Chemical reviews, 2008. 108(2): p. 814-825.

214. Liu, H. and Crooks, R.M., *Paper-based electrochemical sensing platform with integral battery and electrochromic read-out.* Analytical chemistry, 2012. 84(5): p. 2528-2532.

215. Martinez, A.W., Phillips, S.T., and Whitesides, G.M., *Three-dimensional microfluidic devices fabricated in layered paper and tape.* Proceedings of the National Academy of Sciences, 2008. 105(50): p. 19606-19611.

216. Brooks, T. and Keevil, C., *A simple artificial urine for the growth of urinary pathogens.* Letters in applied microbiology, 1997. 24(3): p. 203-206.

217. Feuerbach, T., Callau-Mendoza, S., and Thommes, M., *Development of filaments for fused deposition modeling 3D printing with medical grade poly (lactic-co-glycolic acid) copolymers.* Pharmaceutical development and technology, 2019. 24(4): p. 487-493.

218. Hutmacher, D.W., Schantz, T., Zein, I., Ng, K.W., Teoh, S.H., et al., *Mechanical properties and cell cultural response of polycaprolactone scaffolds designed and fabricated via fused deposition modeling.* Journal of Biomedical Materials Research: An Official Journal of The Society for Biomaterials, The Japanese Society for Biomaterials, and The Australian Society for Biomaterials and the Korean Society for Biomaterials, 2001. 55(2): p. 203-216.

APPENDIX A

FULL SCRIPT OF LESSON LEARNED VIDEO

Once upon a time, three explorers embarked on an adventure searching for a prize of their new findings: 3D printed rigid biodegradable oil absorbents. They observed the uncleaned oil sheen in marinas. It was a sign of small scale oil spills. Solutions were labor intensive and designed for large spills so they were economically inefficient.

They have all marinas in the plan, from their camping site in San Diego to hometown Texas. Their journey would cover all the coastline and the only limit was the end of the sea. Like everyone who spends the whole life on the land, our explorers had their dreams retold by the first boat they boarded.

Boat owners fueled their small boats at a gas station for a cheaper price, so there were not many spills at fuel docks near the water. And gasoline evaporated at a blink of an eye, so did not need clean up. Then our explorers met Mr. Spill Contractor who offered a tour of his castle filled with different absorbents and an unexpected greeting from the kitty litter. These products were cheap and performed well. The customers lived a life happily ever after.

The customers had no pain. Our explorers had no gain. They left with a sinking heart. Then a gentleman named Mr. Boatowner showed them the right path to the gold mine. Every boat had a bilge. Every bilge had a leaked engine. Every oil leak contaminated the bilge water. Every bilge pump discharged oily water into the sea. The oil solution was a bilge sock who failed its mission.

The explorers' absorbents could make a perfect fit. The bilge felt like a home and the explorers can finally enjoy a break.